Université de Neuchâtel, Suisse
Centre d'hydrogéologie

GENERATION AND EVOLUTION OF HYDRAULIC UNDERPRESSURES IN A MARL-SHALE AQUITARD AT WELLENBERG, CENTRAL SWITZERLAND

Thèse

Présentée à la Faculté des Sciences
pour obtenir le titre de docteur ès sciences
par

Pascal H. Vinard

Directeur de thèse: ***Prof. L. Kiraly***
Co-rapporteurs: ***Prof. G. de Marsily***
Dr. C. Neuzil
Prof. J. Tóth
Prof. F. Zwahlen

Neuchâtel, avril 1998

IMPRIMATUR POUR LA THÈSE

Generation and evolution of hydraulic underpressures in a marl-shale aquitard at Wellenberg, central Switzerland

de M. Pascal Vinard

UNIVERSITÉ DE NEUCHÂTEL

FACULTÉ DES SCIENCES

La Faculté des sciences de l'Université de Neuchâtel sur le rapport des membres du jury,

MM. L. Kiraly (directeur de thèse), F. Zwahlen, G. de Marsily (Paris), C. Neuzil (Reston, USA) et J. Toth (Edmonton, Canada)

autorise l'impression de la présente thèse.

Neuchâtel, le 16 avril 1999

Le doyen:

F. Stoeckli

ACKNOWLEDGEMENTS

At this point I would like to express my gratitude to John McCord and Tom Doe both of whom – independently from each other – made me aware of the importance of subnormal pressure phenomena in general and at Wellenberg in particular, and who strongly supported my project to write a doctoral thesis on that specific topic. Without John's inestimable support, and his suggestions of various avenues of investigation to explore, this work would probably not exist. It would not have existed either if Emil Kowalski, at that time a member of Nagra's board of directors, had not believed in me and supported me in this enterprise. Thank you very much, Emil, for your steady and kind support through thick and thin.

Contributions by George Aristorenas, Antonio Bobet, Prof. Herbert Einstein (hydraulic-mechanical coupling); Stefan Finsterle (two-phase flow), Werner Klemenz (Quaternary geology and geomorphology), Alfonso Rivera (hydraulic-mechanical coupling), Rainer Senger (hydraulic-mechanical coupling, two-phase flow), Joe Pearson (geochemical effects) and Ulrich Kuhlmann (coupled flow) paved the way to my own contribution in the field of abnormal pressure hydrology. I would like to express my thanks to them all.

Fruitful discussions with and review comments from François Pasquier, Andrea Baumann, Samuel Kappeler, Walter Müller, Martin Huber, Peter Hufschmid, Stratis Vomvoris, Laurent Tacher and Pierre Perrochet also contributed to an improvement in the understanding of processes and the argumentation for the proposed conceptual models.

I owe a lot to the director of this thesis, Prof. Laszlo Kiraly, who risked taking on board a student from outside his alma mater and who patiently guided me with well-posed questions and a clear methodology. My special gratitude goes, of course, to Chris Neuzil who agreed to support this study and who shared with me some of his invaluable experience. I would like also to thank here the other co-referees, Profs. Jozsef Tóth, Ghislain de Marsily and François Zwahlen, who all – despite heavy work loads – unhesitatingly accepted to become members of the evaluation board and provided me with a series of pertinent comments and suggestions, which I tried to duly take into account in this final version.

Victoria Atchison and later on Linda McKinley carefully reviewed the different versions of the manuscript and indefatigably improved my desperately poor English syntax and grammar. I hope that in editing the final version of this text, I did not murder Shakespeare's language too badly! Thank you very much, dear ladies.

Numerical simulations cannot be performed without adequate computers and appropriate codes. Both, as well as a great deal of time, were generously supplied by Ulrich Kuhlmann and Jürg Trösch, who accommodated me and my (never-ending) wishes, even without any contractual frame and despite the fact that they were already overloaded with many other studies. I will never forget their solicitude and empathy!

Finally, this thesis could only have been realised thanks to the patience and understanding of my wife and children. For many months they accepted a sometimes unbearable husband and often unavailable father.

SUMMARY

This doctoral thesis is about the abnormally low hydraulic pressures as observed in various deep boreholes drilled on behalf of Nagra[1] in order to evaluate the suitability of the Wellenberg site (Canton Nidwalden, Central Switzerland) for disposal of short-lived radioactive wastes.

The subhydrostatic pressures are characteristic of an aquitard composed of consolidated marls and schists, which thickness amounts almost 1'000 m. In terms of hydraulic head, the absolute lowest values were monitored in the centre of the aquitard and are, therefore, incompatible with a hydraulic system in equilibrium with its surroundings. As a matter of facts, the mechanism which produced underpressures is of transient nature. This, consequently, poses the question of persistence of this phenomenon. This observation provoked a process of reflection and investigation, leading to various studies reflected for in this thesis.

Among the various mechanisms envisaged in order to explain this hydraulic anomaly, and based on a series of studies and models organised in concert, including comparison with world-wide occurrences of abnormal pressure, the decompaction of the aquitard rock as a response of glaciations and/or phases of active erosion is clearly privileged with respect to alternative hypotheses based on two-phase flow (water and gas) or on rock-water interactions (osmosis, swelling). Furthermore, the performed simulations tend to show that – whatever tha sequence of geological and/or climatic processes may have been - it is essentially the most recent among them which impacts most on the abnormal hydraulic pressures as we know them today. Therefore, it will never be either possible nor necessary to reconstruct the full sequence of past hydraulic pressures in order to achieve a sensible forecast for the next millenniums. Beginning with the last glaciation which terminated between 12'000 and 10'000 years ago, it seems likely that the distribution of hydraulic underpressures in the aquitard corresponds to a vast concentric body – a so-called underpressure zone – which will probably survive at least the next thousands of years, providing therefore an efficient trap for the radionuclides released progressively from an underground disposal built in its vicinity. Consequently, taking this phenomenon duly into account in the site characterisation will result in a reasonable level of long-term safety assurance for an underground disposal, especially if a dedicated observation network and further studies will improve current understanding of the phenomenon.

---

[1] Nagra: Swiss National Cooperative for the Disposal of Radioactive Waste

RESUME

La présente thése de doctorat traite des pressions hydrauliques anormalement basses telles qu'observées dans divers forages profonds foncés sur mandat de la Cédra[1] afin d'évaluer l'aptitude du site du Wellenberg (Canton de Nidwald, Suisse centrale) pour y stocker des déchets radioactifs à vie courte.

Les pressions subhydrostatiques sont le fait d'un aquitarde composé de marnes et schistes consolidés d'une épaisseur verticale de près de 1'000 m. En termes de potentiel hydraulique, les valeurs les plus basses, au centre de l'equitarde, avoisinent le niveau actuel de la mer et sont de ce fait inconciliables avec un systéme hydraulique en équilibre avec son environnement. De toute évidence, le processus ayant causé les pressions anormales est de caractére instationnaire, ce qui pose les questions de durée et de rémanence de ce phénomène. Cette observation a déclenché un processus de réflexion et d'investigation conduisant á diverses études dont cette thèse est le reflet.

Parmi les différents processus envisagés pour expliquer l'anomalie hydraulique du Wellenberg et sur la base d'un faisceau concerté d'études et de simulations, incluant une comparaison avec des occurrences de même type de part le monde, la décompaction du massif rocheux suite aux glaciations et/ou à des phases actives d'érosion est l'explication privilégiée par rapport à des hypothéses alternatives se basant sur des flux biphasiques eau – gaz ou sur des interactions roche – eau (osmose, gonflement des argiles). Les simulations indiquent en outre que quel que soit la succession possible des événements géologiques et/ou climatiques ayant produit les pressions anormales, c'est avant tout le plus récent d'entre eux qui laisse l'empreinte que nous observons actuellement. Ainsi, il ne sera jamais ni possible, ni nécessaire de reconstituer la séquence complète des pressions hydrauliques ayant prévalu par le passé pour estimer leur évolution dans les prochains milliénaires. En partant de la demiére glaciation s'étant terminée entre 12'000 et 10'000 ans AD, on peut considérer que les pressions anormales, formant probablement une vaste zone concentrique au sein de l'aquitarde – une zone de pressions anormales - vont encore perdurer au-moins plusieurs milliers d'années formant en cela un piége efficace pour les radionucléides relâchés progressivement d'un dépôt souterrain construit dans sa périphérie. En conséquence, une caractérisation de site tenant pleinement compte de ce phénoméne est á même de fournir des garanties appréciables de sûreté à long terme d'un dépôt et cela d'autant mieux que le réseau d'observation et les futures études amélioreront l'état actuel des connaissances.

---

[1] Cédra: Coopérative nationale (suisse) pour le stockage des déchets radioactifs

TABLE OF CONTENTS

LIST DF FIGURES

LIST OF TABLES

1 CONTEXT AND SCOPE OF THIS STUDY

1.1 Context, basic statements and hypotheses

The Wellenberg site has been selected by Nagra as a potential site for disposal of short-lived low and intermediate-level radioactive waste. The target marl-shale aquitard is an extensive mass of strongly deformed and overconsolidated[1] Cretaceous marls and Tertiary shales, characterised by low to very low permeability, and referred to in this thesis as the "marl-shale aquitard".

From 1991, when Nagra began its first drilling campaign at Wellenberg, subnormal hydraulic pressures were inferred from packer tests performed in five deep exploration boreholes traversing large sections of the marl-shale aquitard. The underpressuring was confirmed a few months later by long-term pressure measurements performed in isolated straddle intervals of multipacker systems installed in most of the wells at the end of the drilling and testing operations. The discovery of strongly subnormal pressures within the aquitard has brought into question many preconceived ideas about hydrogeological conditions at the site and has led to initiation of a project aimed at identifying all possible causes for the observed anomalous phenomenon.

Although unexpected, the occurrence of abnormal pressures gave a feeling of "déjà vu" to the geoscientists who had participated in the exploration of the Oberbauenstock site, another potential repository site located only 16 km to the east, in the same lithologies and tectonic setting as Wellenberg. In the case of Oberbauenstock, the sole explanation for underpressuring was based on gas shows and was perhaps too hastily believed to be free gas resident in the formation, either flowing naturally upwards or induced by the excavation of the nearby Seelisberg highway tunnel. At Wellenberg, in contrast with Oberbauenstock, only sparse indications of the presence of free gas could be identified in the first borehole SB4. After review and investigation of a large range of mechanisms which potentially generate hydraulic underpressures, two were considered to be more likely in the preliminary investigation phase: the mechanical rebound of the aquitard system and gas flow. Most of the effort invested since then was therefore devoted to modelling studies of different scenarios based on this pair of preferred hypotheses. The results of these preliminary studies indicated that, although free gas can theoretically produce significant underpressuring, there is no evidence for its presence in large volumes nor for according geological events, and that it is most likely that mechanical rebound is the actual driving force providing the strongest contribution to the hydraulic underpressuring as we observe it today. This thesis attempts to give an overview of the studies performed in this respect and analyses this preferred hypothesis in more detail.

For the first geologic dataset used as input for performance assessment studies (NAGRA, 1993a), hydraulic underpressures were ignored in most groundwater flow models, because Nagra considered underpressures at best as a safety reserve. It was once boreholes SB4a/v and SB4a/s definitely confirmed the large extent of the pressure anomaly within the aquitard that hydraulic underpressures were recognised as an integral component of the hydrodynamic system. From then on, all abstraction schemes[2] (conceptual models) and hydrodynamic models based on the existence and evolution of an "underpressure zone"[3] (UPZ) represented as a three-dimensional body, based on head data from five deep boreholes (NAGRA, 1997). For deriving geological data as input to performance assessment, the "conservative" assumption was taken that the mechanism that generated

---

1 overconsolidated: state of a rock that has been consolidated previously under a lithostatic pressure much higher than currently existing

2 for definition, refer to Subsect. 6.3.1

3 referred to as UPZ, for definition refer to Sect. 1.4.3

the pressure anomaly was no longer active, and that hence only the dissipation of the UPZ is relevant. Consequently, most transient numerical simulations used the assigned UPZ as an initial condition (NAGRA, 1997). This modelling approach did not impede research work dedicated to identifying the causes of abnormal pressures (VINARD, 1998). Model calculations were carried out up till 1998 with the aim of improving the understanding of the generation and dissipation mechanisms controlling the evolution of the hydraulic pressure anomaly at Wellenberg. The rationale for this work is based on four fundamental hypotheses which are established in this study:

1. Hydraulic underpressures exist within the marl-shale aquitard at Wellenberg.
2. The underpressures observed in five boreholes most probably appertain to a single, contiguous UPZ.
3. Hydraulic underpressures have been, or are being, generated essentially by two geological processes: differential erosion and glacier unloading, both driven by past climatic changes.
4. It is almost impossible to assess the specific contribution of a given geological process. If glacier rebound is the main driving force, then hydraulic underpressures are currently in a dissipation stage. If, on the contrary, ongoing erosion plays the governing role, generation and dissipation of underpressures occur concomitantly which implies that geologic forcing[1] needs to be considered for prediction of the future evolution of subnormal pressures.

This thesis is dedicated primarily to identifying and exploring conceptual models and corresponding modelling scenarios based on the preferred hypothesis of mechanical rebound of the marl-shale aquitard. It is also explained why alternative mechanisms, i.e. mechanisms which are presumed to participate only marginally in underpressuring, are considered so.

1.2 Scope of the study

The objectives are:

1. to identify, on the conceptual level, all mechanisms likely to produce significant underpressuring under realistic conditions and, if possible, to find appropriate mathematical expressions which can reproduce them
2. to test these potential mechanisms by means of state-of-the art analytical or numerical solutions in order to produce a plausible classification of mechanisms in terms of their probability and contribution to underpressuring
3. to compare the Wellenberg occurrence with abnormal pressure occurrences world-wide in order to identify similarities with, and differences from, Wellenberg
4. to identify time frames and geological evolution scenarios which correspond to the preferred generation mechanism
5. to propose likely material properties and parameter ranges (hydraulic conductivity, specific storage, Young's modulus, etc.), which are consistent with measurements, and which are likely to produce subnormal pressures in the observed order of magnitude

[1] for definition, refer to Subsect. 7.2.1

6. to propose a consistent conceptual model of the generation and evolution of underpressures at Wellenberg which is supported by relevant data without contradicting others.

In this study, the fundamental assumption is that the observed head condition in the marl-shale aquitard results primarily from mechanical rebound of the rock in response to glacial unloading and/or to erosion. Other mechanisms, like two-phase flow, are considered as possible minor contributions, which, if neglected, will not significantly affect the simulated magnitude of underpressuring and may therefore be disregarded at this stage.

1.3 Organisation of the thesis

This study is structured into five main blocks.

In the first block, the geographic setting, the geological as well as hydrological and hydrochemical conditions are presented with focus on findings and data related to the observed phenomenon (Chaps. 2 to 4).

In the second block, a brief excursion is made in abnormal pressure occurrences throughout the world (Chap. 5) with the aim to identifying important similarities and relevant differences between world-wide occurrences and Wellenberg.

The third part sets out the directory of the investigations presented in this thesis: Chapter 6 defines the procedure for the identification and treatment of the overall conceptual model of mechanical rebound and derived abstraction schemes. Chapter 7 summarises the basic principles of the physical processes considered in the modelling studies, including essential mathematical formulations, and addresses the associated conditions and limitations as well as the problem of identifying appropriate parameters and moduli for time and size scales often far beyond testing feasibility. The basic features of the applied computer codes as well as the way in which physical processes are accounted for are summarised, including a brief discussion of the inherent capabilities and limitations.

The fourth section consists of the description of the abstraction schemes and associated model scenarios which are all based on the coupled hydraulic-mechanical approach introduced in the previous part. While Chapter 8 summarises preliminary model studies and studies on subordinate mechanisms with the aim of providing background information for the reader, Chapters 9 and 10 present in greater detail those abstraction schemes which all derive from the preferred hypothesis of underpressure generation. To work out these abstraction schemes, the most recent literature available on tectonic and geomorphologic evolution of the Alps and the Swiss plateau as well as state-of-the art numerical treatment of coupled hydraulic-mechanical processes were used. The model scenarios result from different approaches and cover different time ranges. The first set of abstraction schemes considers the restricted time window from the Pleistocene to today and treats the erosional and glacial events in great detail (Chap. 9). The second set considers the longer-lasting evolution of the marl-shale aquitard from the end of the Miocene to today in a very schematic way, and with emphasis on material properties (Chap. 10).

Owing to the large variety of evolution scenarios and processes to be tested and to the availability of competent personnel, computer capacity and appropriate codes, the actual modelling work was carried out at MIT by Dr. A. Bobet, under the supervision of Prof. H. Einstein, and at TK Consult Inc. by Dr. U. Kuhlmann and myself.

The last part of the thesis is dedicated to synthesising and critically reviewing working hypotheses and results. Furthermore, open issues are identified and possible areas of

further investigation are proposed (Chap. 11). Chapter 12 presents a draft contribution to the potential use of underpressuring in designing and managing a radioactive waste repository.

1.4 Definitions

1.4.1 Abnormal hydraulic pressure

HUBBERT & RUBEY (1959) gave the first rigorous definition of normal and abnormal states of hydraulic pressure in the subsurface, which they simply relate to nominal hydrostatic conditions. Therefore, *formation pressures*, i.e. *pore pressures*, can be abnormally high or low with respect to the standard hydrostatic pressure gradient, defined by the increment of 0.01 MPa/m, i.e. 1 m of fresh water at 25°C per m of depth. For practical purposes, "... abnormal formation pressures are defined as any departure from normal hydrostatic pressure at any given depth..." (FERTL ET AL., 1994). Some authors even require "... large departures from a hydrostatic gradient..." (BELITZ & BREDEHOEFT, 1988), while for NEUZIL (1993, 1995) abnormal subsurface fluid pressures exist when they differ from hydrostatic by more than 100 m of hydraulic head. This latter definition has been adopted in this study, especially for the case of *underpressures*, which have been defined by PARKS & TÓTH (1995) as "fluid pressures that are less than hydrostatic..."

Abnormally high pressures or *overpressures* are very widespread around the world and occur in several different geological environments and depth intervals, often associated with petroleum provinces (MOUCHET & MITCHELL, 1989; FERTL ET AL., 1994; LEFTWICH & ENGELDER, 1994). *Abnormally low pressures*, also referred to as *subnormal pressures* or *underpressures* are more seldom, probably because they usually show up in connection with tight formations, although according to BELITZ & BREDEHOEFT (1988) this is not a necessary condition. Moreover, NEUZIL (1995) identifies many types of geologic forcing for overpressure but only few for underpressure.

1.4.2 Equilibrium and disequilibrium pressures

Abnormally high or abnormally low hydraulic pressures occur in flow regimes that are either equilibrated (i.e. adjusted to the geological and hydrological conditions) or disequilibrated. *Disequilibrium pressures* result from geological processes which have provoked fundamental changes in the geological environment. These geological changes can result from a large variety of processes, as for example compaction, diagenesis or erosion (NEUZIL, 1995). TÓTH (1979a, 1990a,b; 1986 in TÓTH & CORBET) defines abnormal pressures in terms of "dynamic pressure increments".

The notion of *disequilibrium pressure* was introduced by CORBET & BETHKE (1992), and is defined as "the amount by which fluid pressure differs from the pressure that would exist if the flow system were equilibrated with land surface." This definition clearly discriminates between *apparent underpressures* resulting from equilibrated flow and *true underpressures* due to disequilibrium flow.

ORR & KREITLER (1985) distinguish between *regionally underpressured conditions* and *apparently underpressured conditions* due to measurements in different locations of the aquifer (Denver basin described by BELITZ & BREDEHOEFT, 1988). Heterogeneities in the flow domain may affect hydraulic gradients and do not necessarily imply transience, since such conditions are compatible with flow conditions in equilibrium with topography (TÓTH, 1963). Fig. 1.4-1 shows two schematic cases.

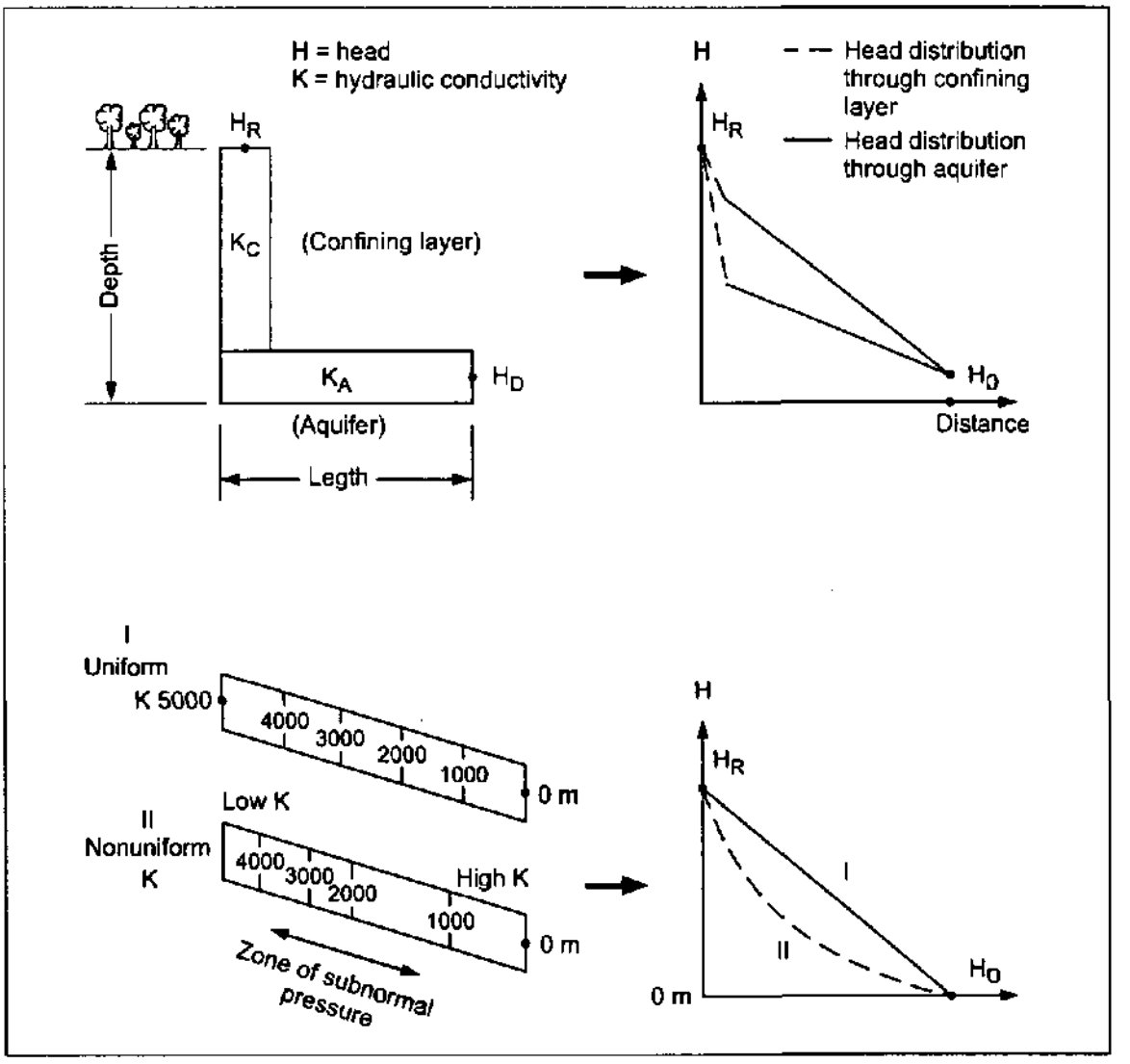

Fig. 1.4-1: Schematic representation of apparent underpressuring (after BELITZ & BREDEHOEFT, 1988)

Disequilibrium pressures may be generated even without unloading or cooling. In or below thick sedimentary sequences, changes in boundary conditions can produce underpressures which derive from delayed adaptation to changes in topographic relief (TÓTH, 1979a; BELITZ & BREDEHOEFT, 1988; TÓTH & MILLAR, 1983). CORBET & BETHKE (1992) name the resulting disequilibrium pressures "memory effect". An example is the Palo Duro Basin, Texas, as reported by SENGER & FOGG (1987). However, such cases are probably overemphasised in the literature of the early eighties, because it was difficult to imagine at that time that small changes in overburden pressure might produce significant underpressuring in aquitards. NEUZIL & POLLOCK (1983) and NEUZIL (1985, 1986) were pioneers in this field. Using simple model calculations, they demonstrated that anomalous pore pressures can be generated by changes in overburden stress. In his reply to TÓTH & MILLAR (1983), NEUZIL (1985) shows that mechanical rebound is often necessary to explain inwards oriented flow. His statements were supported a few years later by TÓTH & CORBET (1986) and CORBET & BETHKE (1992) who provided a detailed description of inwards flow towards the centre of an UPZ. A recent work by PARKS & TÓTH (1995) treats subnormal

pressures in the same way.

1.4.3 Definitions which apply to the Wellenberg case

The restrictive definition of disequilibrium pressure, implying modifications of the applied stress field or changes in temperature as defined by CORBET & BETHKE (1992) corresponds best to the hydraulic conditions of the marl-shale aquitard at Wellenberg. This notion is equivalent to NEUZIL's (1993) definition of "naturally transient flow" (NTF), which occurs "...when a groundwater regime fails to accommodate geologic changes." The corresponding "lagging hydrodynamic response to mechanical rebound...", as it is postulated for the Pierre shale, probably also applies to Wellenberg.

All the above definitions refer to hydraulic pressure, but, in order to avoid possible confusion between apparent and true underpressures, the conversion to *hydraulic head* (subnormal head conditions), and more specifically to *freshweter head*, is appropriate, provided density and salinity contrasts are not a salient feature of the flow field. The hydraulic head is defined as (HUBBERT, 1940):

$$h = z + \frac{p}{\rho \cdot g}$$

where
- z: elevation of point of measurement expressed in metres above an arbitrary datum, generally sea level [m a.s.l.]
- p: fluid pressure [Pa]
- ρ: reference fluid density [kg/m^3]

Hydraulic heads are expressed as equivalent freshwater heads, which are obtained by converting hydraulic heads based on the estimated density of the formation water into equivalent heads for freshwater with a density of 1 (specific mass: 1'000 kg/m^3). Therefore, the equivalent of subnormal pressure is *abnormally low head*.

Abnormally low heads at Wellenberg clearly result from disequilibrium flow (i.e. natural transient flow). In this thesis, abnormally low heads refer to head values clearly below any value possible in an equilibrated flow system. In other words, underpressures exist whenever the lowest head level observed in a borehole interval or piezometer is notably below the level of any known or potential exfiltration zone. This definition implies naturally transient flow directed towards the absolute head minimum much below an exfiltration zone; it is somewhat more restrictive than the one usually given in the literature, which refers to subnormal pressures or to abnormally low hydraulic heads when the pressure is significantly below hydrostatic (or more specifically below the head that can reasonably be expected for the specific position of the observation point in the topographically driven flow system, see Subsect. 1.3.1).

From the observation of radially inwards flow, it follows that zones of abnormally low heads must exist (see Subsect. 1.3.2). Such zones are defined as *hydraulic underpressure zones* (UPZ) and correspond to closed potentiometric volumes, i.e. sub-elements of an aquitard in which all head values are abnormally low and decrease from the isopotential envelope to the absolute lowest head at its centre. A two-dimensional (2D) cross-section through a UPZ will consequently exhibit a closed potentiometric surface defined by closed head isolines.

In practice, the term UPZ is used only in the case where:

i enough evidence supports the assumption that a closed head volume may exist and no evidence speaks against it (large-scale water-conducting features, high-permeability inclusions, etc.)

ii an interpolation between (or extrapolation from) individual head observations is deemed reasonable.

As a rule, since head data are fairly limited in most cases, any geometry of an UPZ represents a best guess among several possible configurations. This best guess can result from an educated manual interpolation or from one or several numerical models. Therefore, based on the same dataset, a variety of UPZ's are possible which individual configuration depends on the assumed generation process(es) and on the type and magnitude of critical parameters. Fig. 1.4-2 represents the geometry of the UPZ used for dissipation calculations in Nagra's groundwater models (NAGRA, 1997). Note that this configuration corresponds to a minimal extension of the UPZ, provided all observations belong to a single UPZ.

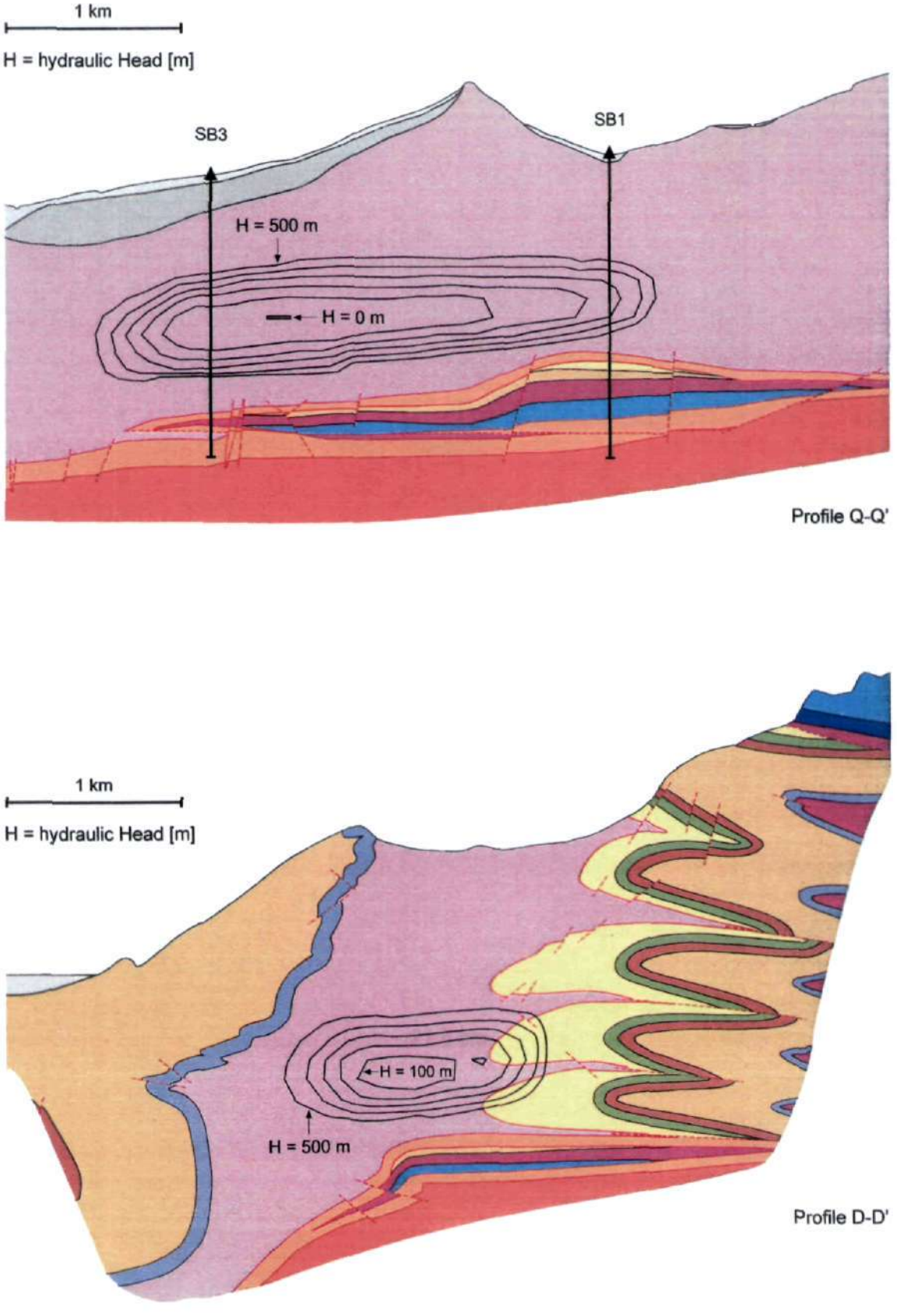

Fig. 1.4-2 Geometry and extension of the UPZ used for dissipation calculations in NAGRA (1997)

2 GEOGRAPHIC AND GEOLOGICAL SETTING

2.1 Location and geographic conditions

The Wellenberg site is located in the central part of Switzerland, only a few kilometres south of Lake Lucerne (Vierwaldstättersee), between the smooth U-shaped lower Engelberger Aa valley and the steep and narrow Secklisbach valley. The site forms part of the Central Alps and is named after the hill marking the water-divide between the two valleys. The name "Wellenberg" stems from the small "waves" (Wellen in German), i.e. narrow folds, marking the eastward flank of the Wellenberg hill when observed from Oberrickenbach.

Fig. 2.1-1 shows the position of the Wellenberg site in Switzerland (top left), and in Central Switzerland (main picture). Represented on the map are the topographic relief, the main towns and rivers, as well as roads and railway tracks. The investigated area is characterised by a very sharp topographic relief as illustrated by Fig. 2.1-2. All vertical cross-sections illustrated in this thesis have therefore an aspect ratio of 1:1. The smooth and relatively wide Engelberger Aa valley is at an average elevation of 540 m a.s.l. (metres above sea level), while the Secklisbach valley ranges from the same altitude at the confluence of the Engelberger Aa river and the Secklisbach stream to more than 1'000 m at the foot of the steep escarpments of the Walenstöcke mountains, culminating locally at more that 3'000 m as shown on the right-hand side of the picture. The marl-shale aquitard is encompassed by the limestone mountains of the Walenstöcke in the south and the lower elevation limestone mountains, which also form the Wellenberg (in the foreground of Fig. 2.1-2), in the north.

Fig. 2.1-2 is a perspective view of the site taken from the southwest. The marl-shale aquitard forms a narrow stretch of land encapsulated on both sides by mountain ridges and masked almost completely by Quaternary deposits. Outcrops exist only locally on topographic saddles (Eggeligrat, Sinsgäuer Schonegg at the eastern border of the investigation area). Valley bottoms are formed essentially by glacier tills (ground and subglacial moraines) and by debris from landslides and collapses. The main part of the aquitard is masked by the extensive landslide mass of Altzellen, forming most of the southwest limb of the Eggeligrat (central part of the picture) and dipping towards the Engelberger Aa valley (in the foreground of the picture).

2.2 Geological setting and regional tectonic situation

The various phases of alpine orogeny have resulted in a complex tectonic deformation style on every scale. The Central Alps underwent various episodes of strong crustal shortening, uplift of the crystalline basement and transportation and overthrusting of huge sediment stacks far away from their original depositional environments. Figs. 2.1-2 & 2.2-1 provide a rough impression of the huge tectonic forces that acted on the Helvetic domain, which is comprised of a huge stack of nappes (kilometre-scale tectonic units), on which erosion accentuated relief. Fig. 2.2-1 shows two schematic vertical cross-sections of the various tectonic units represented in the Central Alps. The relative position of Wellenberg is highlighted in profile 3. Note also the relatively shallow level of the tectonic projection (this profile was drawn before Nagra boreholes provided insight into deeper-seated tectonic structures). Fig. 2.2-2 provides an overview of the tectonic situation of the Central Alps, including a definition of the perimeter of the investigation area and the position of the cross-sections represented in Fig. 2.2-1.

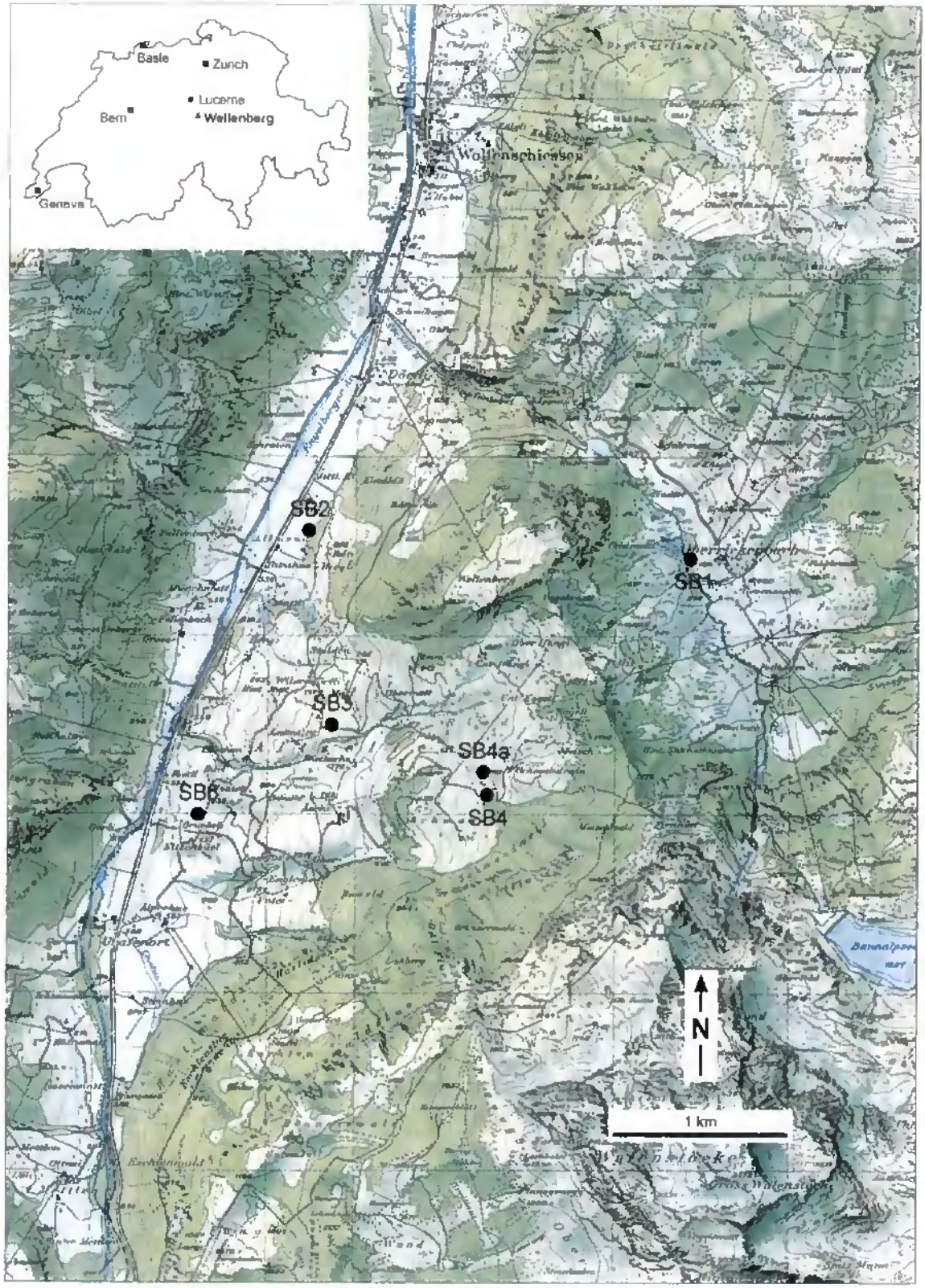

Fig. 2.1-1: Location of the investigated area

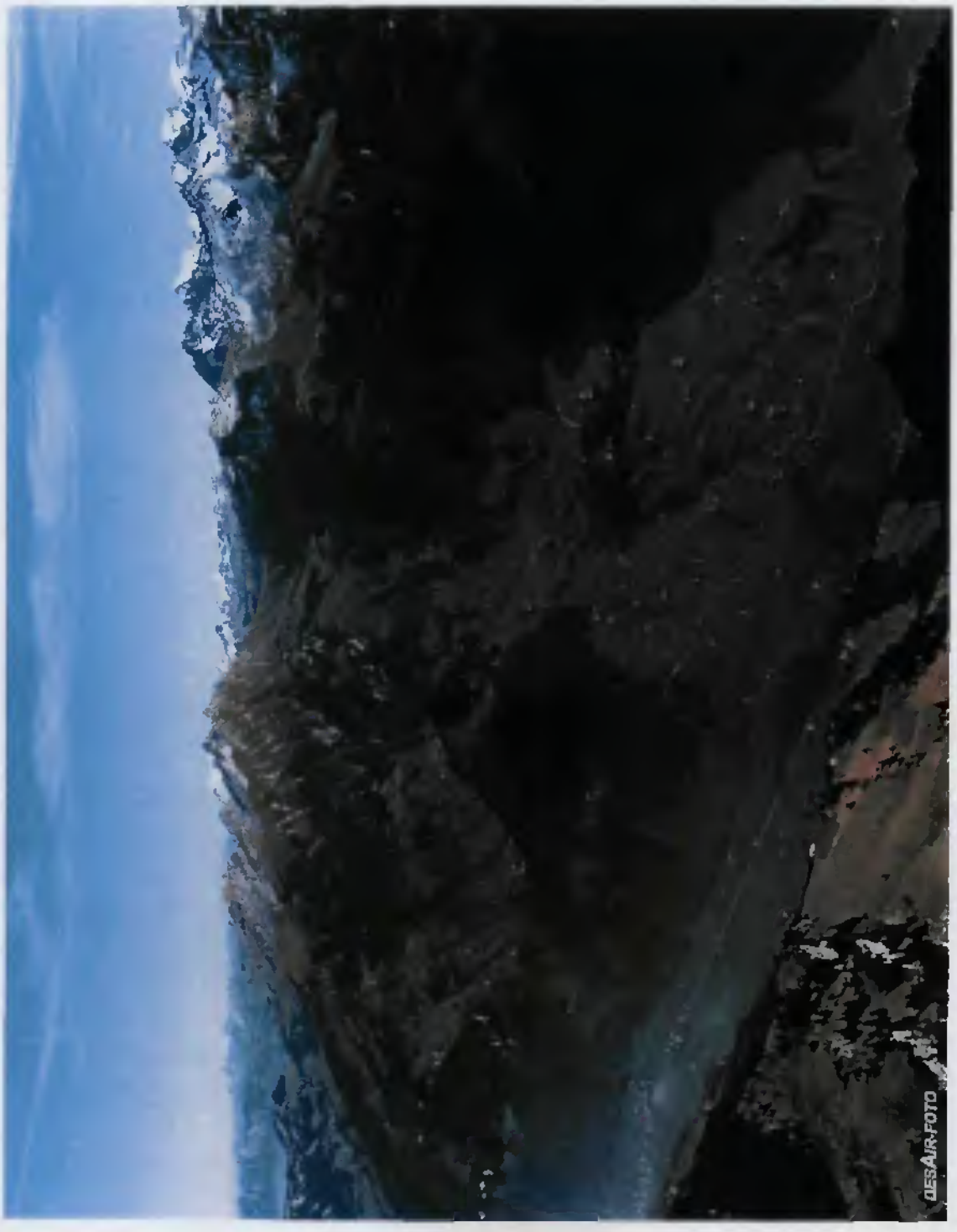

Fig. 2.1-2: Aerial photography of the Wellenberg site taken from the southwest towards the northeast. The Engelberger Aa valley is located in the foreground, Lake Lucerne in the upper right corner and the background is formed by the Swiss plateau (in the mist)

Within the investigated perimeter, the Helvetic nappes of importance are the Drusberg nappe (Cretaceous and Cenozoic sediments), and the Axen nappe (Jurassic, Cretaceous and Cenozoic sediments). Both tectonic units lie on top of a stack of Parautochthonous and Autochthonous sediments of Triassic and Jurassic age, themselves forming the cover of the crystalline basement of the Aar Massif.

The marl-shale aquitard consists of Lower Cretaceous sediments of the Drusberg nappe (Palfris Formation and Vitznau Marls, formerly designated using the collective term "Valanginian Marls"; NAGRA, 1993a) and of minor amounts of Tertiary sediments of the Axen nappe (Globigerina Marls and Schimberg Shales), together with interhelvetic mélanges which appear within the above formations or between them. All these lithologies have in common a characteristically low to very low permeability.

Based on a literature review, extensive surface mapping of the in situ geological features and on examination of borehole cores, a set of 11 geological profiles covering the investigated area were produced. These profiles represent the best-guess tectonic position and geometry of all geological formations present up to a depth of 1'000 m below sea level. Based on these profiles, a deterministic three-dimensional (3D) geological model was constructed (TACHER, 1994). This model was further used to set up the 3D Finite Element (FE) mesh of the regional-scale hydrodynamic model (SCHRODER et al., 1994; Subsect.. 4.2.3, Sects. 9.3 & 9.4).

2.3 Overview of field investigations and studies

From 1990, when Nagra began its first drilling campaign, up to 1996, when the last borehole was equipped with a multipacker system, seven exploration boreholes totalling more than 6'000 m have been drilled with a high rate of core recovery. All boreholes were investigated using state-of-the art petrophysical and hydraulic testing methods. Cores were analysed in detail for porosity determination, mineralogical and petrographic analysis, gas extraction, rock mechanics testing, etc. Two seismic reflection campaigns helped identifying structural discontinuities, and a seismic refraction campaign in the Engelberger Aa valley provided basic data to determine the level of the bedrock. Detailed geological mapping was performed to try to identify potential fractures, supported by soil gas surveys. Hydraulic and standard hydrogeological measurements have been carried out periodically in a large number of streams, natural and artificial exfiltrations (springs, wells) as well as in various piezometers drilled specially for investigation of the shallow groundwater systems.

Chapter 3 provides a summary of relevant borehole data with emphasis on hydrogeological, hydrochemical, and geomechanical data. The existence of hydraulic underpressures could be evidenced beyond doubt and the relevant rock characteristics determined within an acceptable bandwith of uncertainty.

The quality, variety and amount of relevant geoscientific data as well as the level of the corresponding geological synthesis (NAGRA, 1997) represent probably the best characterisation of an occurrence of subnormal pressures, which does not imply that the datasets and analyses are comprehensive and irreproachable in all respects. However, based on this exceptional dataset, some confidence could be gained in the proposed hypothesis for the generation and maintenance of underpressures.

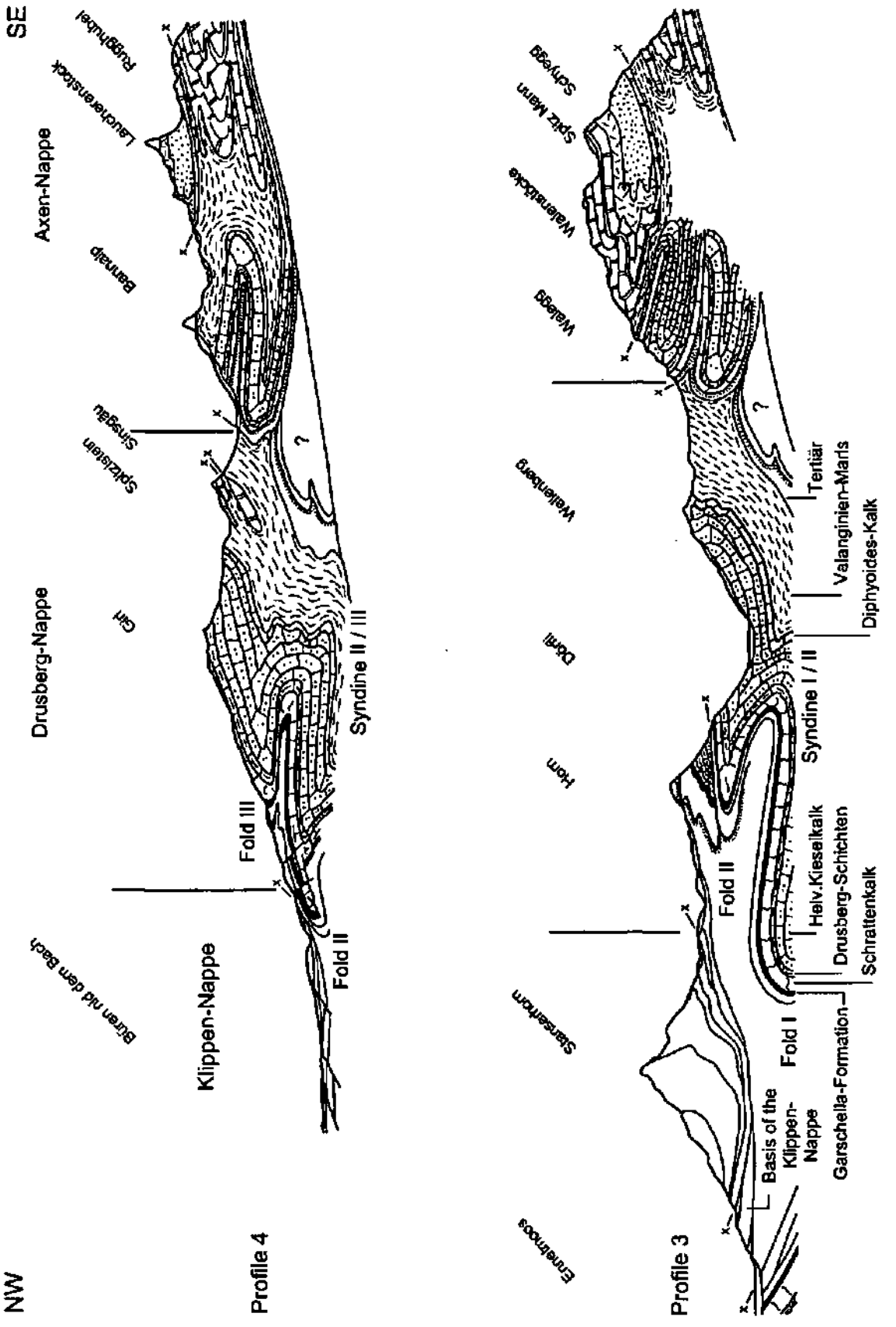

Fig. 2.2-1: Schematic cross-sections of the main tectonic units in the Central Alps (after HANTKE, 1961 in NAGRA, 1997)

Fig. 2.2-2: Location of the geological profiles and model domain for the setup of the regional model used in scenarios Q2 and Q3

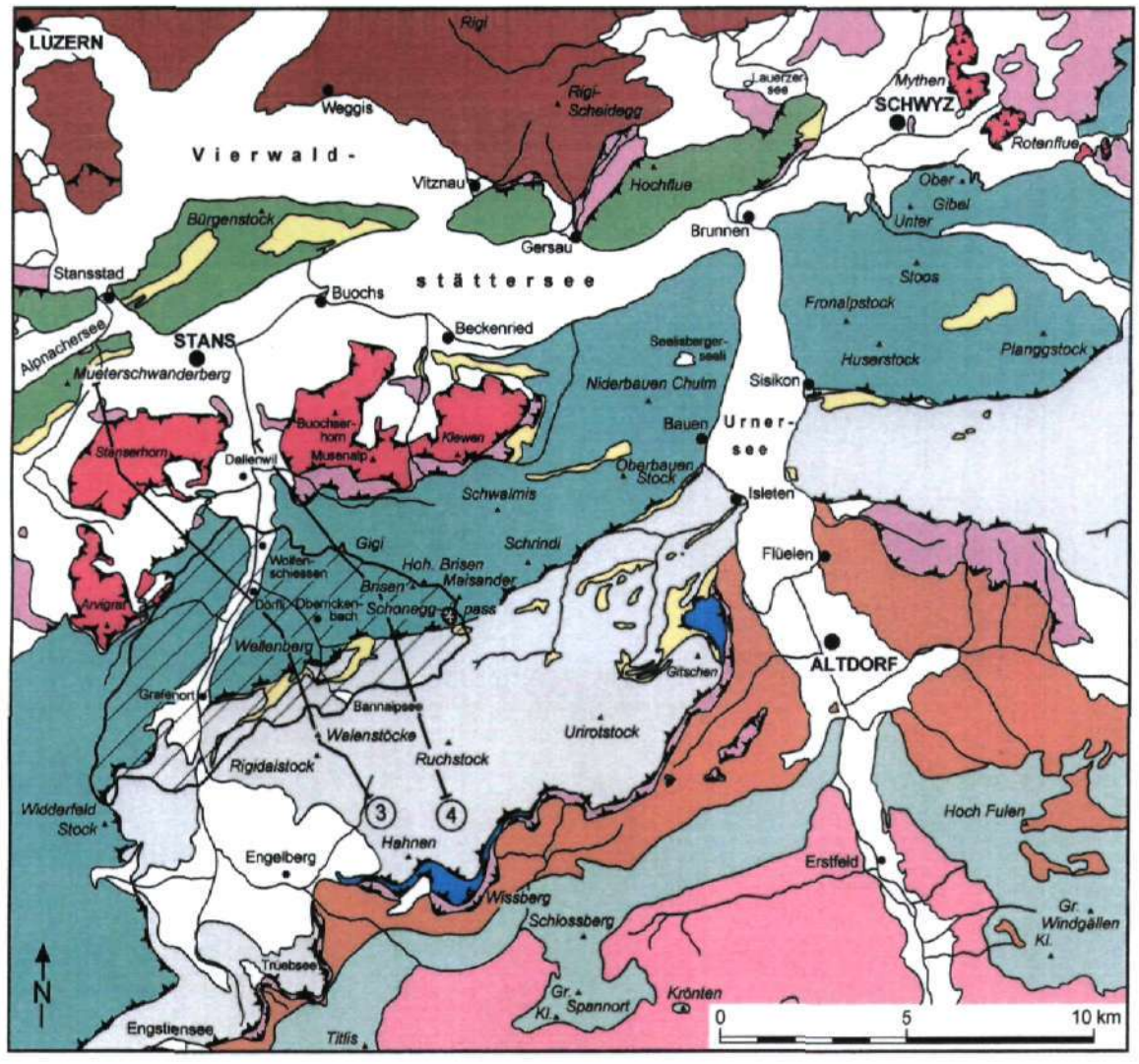

LEGEND

- Subalpine Molasse
- "Subalpiner Flysch" (Upper Cretaceous-Eocene) Mélange, Complex basis of the Klippen-Nappe
- Klippen-Nappe
- Eocene of the Helvetic Nappes
- Helvetic Randkette
- Drusberg-Nappe
- Axen-Nappe
- Subhelvetic Elements (Gitschen-/Wissberg-Scholle)
- North-Helvetic Flysch (Altdorfer-Sandstone)
- Autochthonous sediment cover of the Aar-Massiv
- Aar-Massiv
- Main thrust planes
- Investigation area Wellenberg
- Traces of the profiles in Fig. 2.2-1 (HANTKE 1961)

Fig. 2.2-3: Tectonic overview with traces of the profiles represented in Fig. 2.2-1 and delimitation of the investigation area

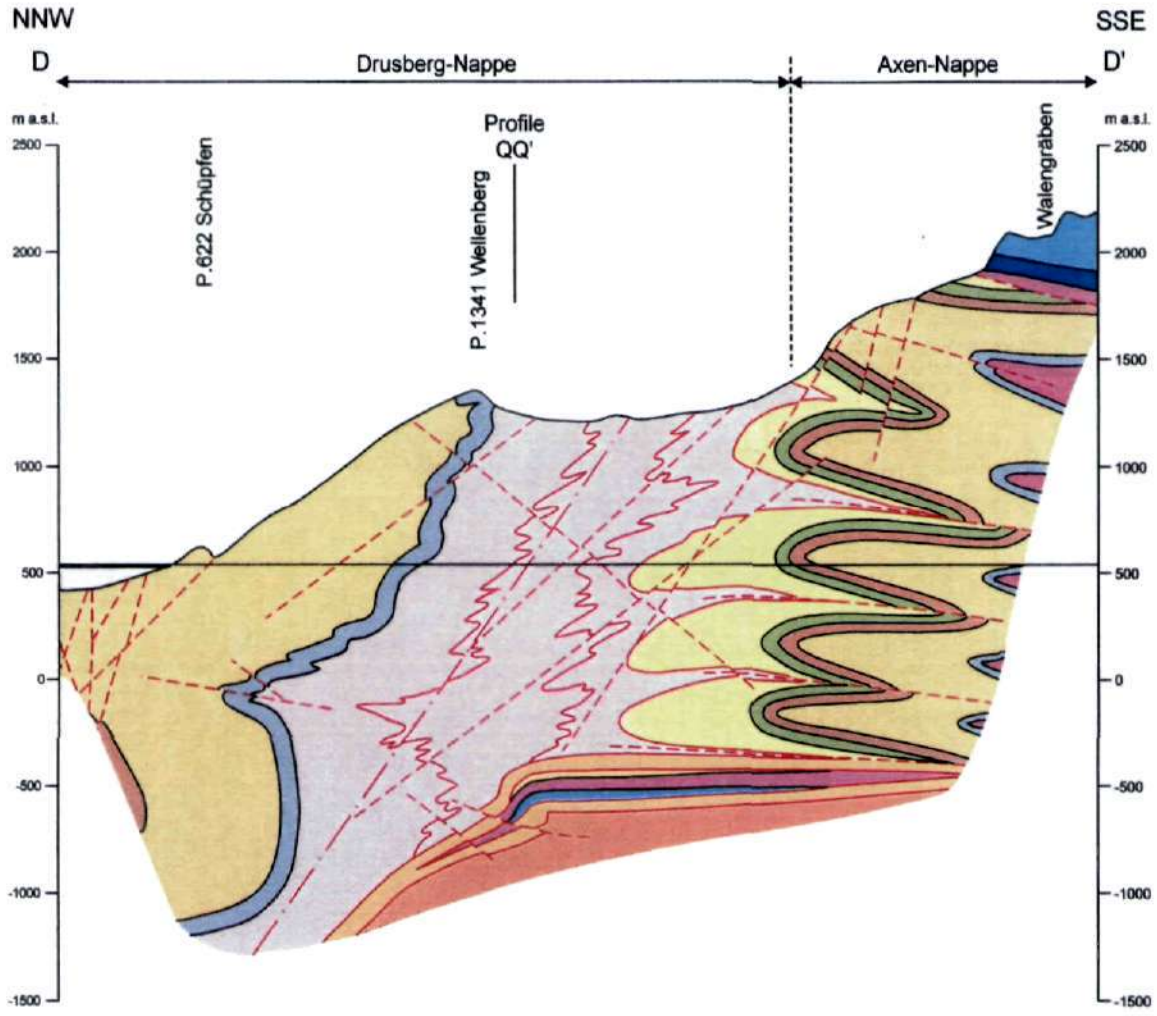

Fig. 2.2-4a: Geological profile D - D' (for location see Fig. 2.2-2), (after NAGRA, 1997)

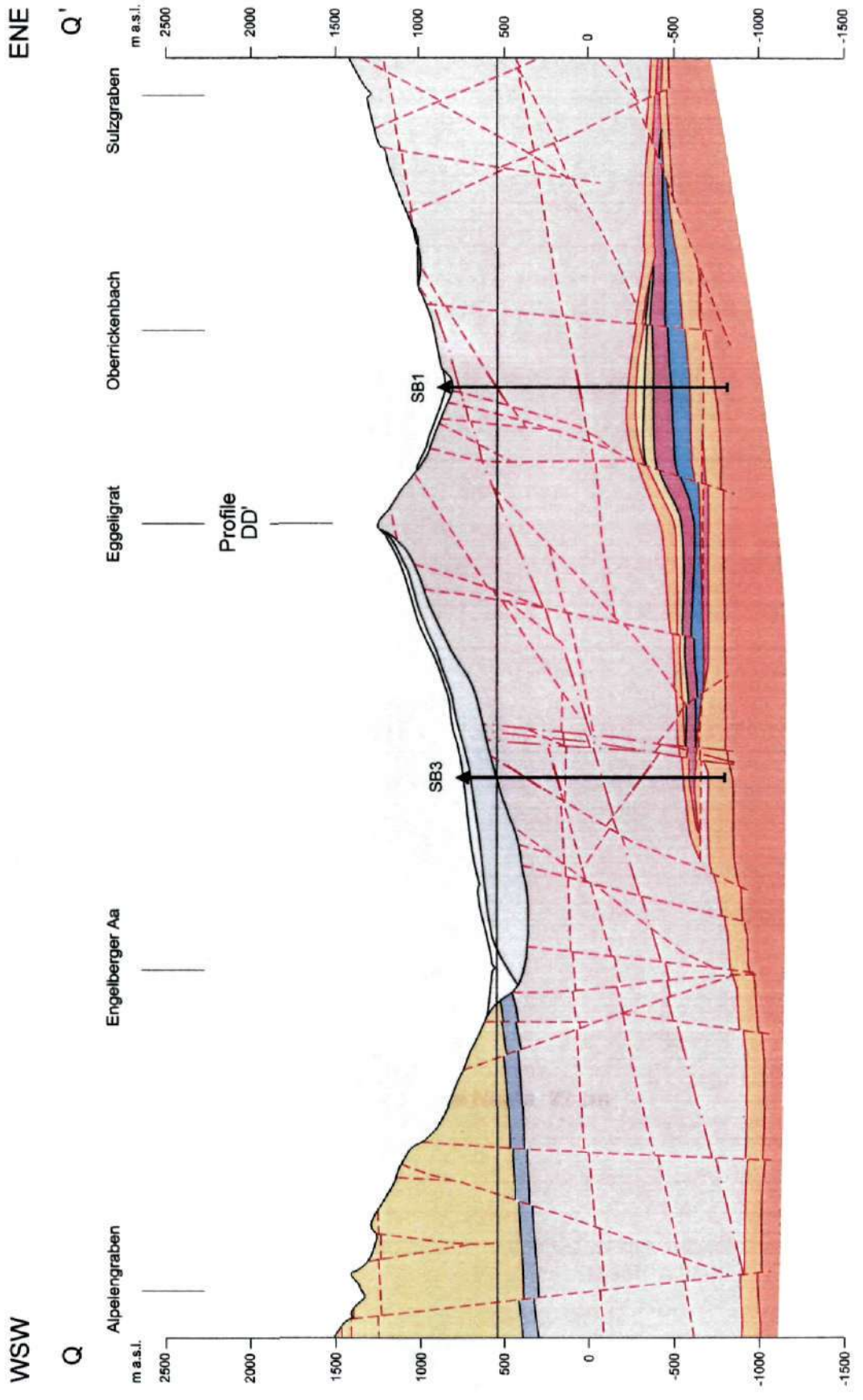

Fig. 2.2-4b: Geological profile Q - Q' (for location see Fig. 2.2-2), (after NAGRA, 1997)

Fig. 2.2-4c: Legend of tectonic and stratigraphic information on geological profiles (after NAGRA, 1997)

3 RELEVANT GEOSCIENTIFIC DATA

3.1 Scope and application of data

Data on the specific characteristics (on various scales) of either rock properties or forces acting on the marl-shale aquitard are summarised below. Addressed first are geological and petrographic data, because they describe the framework in which flow occurs; this is followed by geomechanical data, which provide essential information on rock deformability and failure, and stress data which reveal the strongly anisotropic stress field prevailing at depth. Further, hydrochemical and isotopic data provide indirect evidence for the long-lasting hydraulic isolation of the aquitard with respect to the surrounding geological formations. Finally, hydraulic data from hydrotests are reviewed. The combination of all data results in a consistent picture of the hydrogeological conditions at Wellenberg.

3.2 Geological and petrographic data

3.2.1 Scope and definition

Lithology and stratigraphy are fundamental elements in the definition of the marl-shale aquitard. In this respect, it is important to identity the common denominators and the main differences between the various lithologic types entering the definition of the aquitard. The proportion of clay minerals in relation to other minerals, the porosity and the degree of metamorphism play a significant role in this connection.

Small-scale structural and petrographic data are obtained both from analyses of core material and from interpretation of petrophysical logs. Both methods are necessary to characterise discontinuities which represent potential permeable zones, as revealed by fluid logging (Sect. 3.5), and the more or less undisturbed "rock matrix" in between. Groundwater flow is concentrated to a large extent in permeable or potentially permeable discontinuities, which are defined as "water-conducting features" (WCFs). Four main types of WCFs were identified, based on their particular structural and mineralogical habitus. Detailed field mapping as well as crosshole petrographic correlation studies were also carried out in order to estimate the extent, geometry and internal heterogeneity of WCFs at aquitard scale. Finally, all this work provided the necessary deterministic and, particularly, statistical input data for generating a fracture network block model. This hectometric block model simulates networks of WCFs which, associated with realistic transmissivity distributions, was used to estimate effective hydraulic conductivity distributions.

Moreover, petrographic and structural data also provided the necessary basis for understanding the evolution of groundwaters and gases, as well as for estimating total porosity and flow porosity both within the undisturbed matrix blocks as well as within the different types of water-conducting features.

3.2.2 Lithologic and stratigraphic description of the relevant rock formations

All lithologic types fitting into the definition of the marl-shale aquitard are characterised by relatively large amounts of clay minerals, independent of their stratigraphic position or tectonic situation. These lithologies behave as soft material with respect to limestone, which manifests itself clearly in the topography: marl-shale lithologies form characteristic depressions beneath Quaternary cover (e.g. landslide of Altzellen) and, locally, topographic

saddles (Eggeligrat and Sinsgäuer Schonegg, see Fig. 2.2-3 and Sect. 9.5). The few outcrops, located principally on the saddles themselves, are strongly weathered. Geological mapping of structural features in the Palfris Formation was possible only at one location in a small stream Valley (Haldibach), a few kilometres away from the site.

The description of the elements of the aquitard follows a stratigraphic guideline.

3.2.2.1 Stratigraphy

The lithologic types which belong to the marl-shale aquitard are, in stratigraphic order: the *Vitznau Marls* formation (Valanginian age), which consists of relatively thin cycles of limestones and marls (about 50 m), followed by the *Palfris Formation* (Berriasian age), which forms most of the aquitard rock. The latter formation consists in the first order of dark, silty to sandy and clayey marls alternating with limy marls and limestone beds of variable magnitude. The sedimentary thickness of the Palfris Formation is estimated to be about 200 - 250 m. The thickness observed in the boreholes is often more than four times this amount, which indicates tectonic folding and thrusting.

The *Globigerina Marls* formation (Bartonian - Priabonian age) constitutes the uppermost level of the Tertiary formations of the Axen nappe. It consists of dark, clayey marls with remarkable amounts of micaceous minerals. In the same tectonic unit, but in a stratigraphically lower position, the *Schimberg Shales* formation (Priabonian age) consists of massive accumulations of grey, micaceous and sandy marls.

The *interhelvetic mélange* formation is a mixture of all lithologies and results from intensive stripping and thrusting. It appears in cores as a black, clayey schist, with minor calcite veins and components of quartzose sandstones.

3.2.2.2 Petrographic, mineralogical and petrophysical properties of the aquitard rocks

The evolution of mineralogical and petrographic conditions dictates the evolution of the in situ fluids. Starting from sedimentation, through diagenesis and Neoalpine metamorphism, up to brittle deformation phases, the marl-shale aquitard has experienced a large variety of pressure and temperature conditions, which led to strong rock-water interaction.

As can be seen from Tab. 3.2-1, the total amount of clay minerals is nearly 30 %, with essentially illite and illite-smectite mineral associations. From the perspective of discussing potential effects of osmosis, this type of clay is far from providing a suitable semi-permeable membrane.

Clay content and typology

The clay content is determined indirectly by X-ray diffractometry. The different formations of the aquitard are chiefly composed of carbonates (calcite, dolomite, ankerite), clays (illite, illite-smectite layers, chlorite) and quartz.

Tab. 3.2-1: Average clay weight-percentage in the lithologies of the marl-shale aquitard (after Tab. 4.3-1 in NAGRA, 1997)

Tectonic unit	Lithology	total %	illite %	illite-smectite %	chlorite %	kaolinite %
Drusberg nappe	Vitznau Marls	17	6	6	4	1
	Palfris: clayey marls	40	16	14	9	1
	Palfris: limestone marls	17	7	5	4	1
	Palfris: total average	34	14	12	8	-
Axen nappe	Globigerinenmergel	34	12	12	10	-
	Schimberg-Schiefer	30	10	11	9	-
	Mélange	44	21	10	13	-
	Average of all probes	29	11	10	8	-

Porosity and density

Porosity is a key parameter since it enters into the definition of hydraulically relevant parameters (e.g. specific storage), determines the residence time of groundwaters, controls two-phase flow conditions (dual porosity model, Subsect. 8.5.4) and indicates if rather advective or diffusive type of flow prevails. Hg injection is considered the most reliable determination method, porosity estimates based on seismic velocities are, however, not reliable, as explained below.

The sum of the micro- and macroporosity of the rock and of the fault gouges is the open Hg-porosity of the rock. The total porosity is the sum of the latter and of the porosity corresponding to isolated pores disseminated in the rock matrix (essentially geodes). The total porosity exceeds the open porosity only by an insignificant fraction represented by millimetric to centimetric isolated geodes present exclusively in carbonate veins. The flow porosity corresponds to the fracture porosity, i.e. the pore space in which advective transport actually takes place. Tab. 3.2-2 below summarises key information on porosity as well as density values of the main lithologies of the marl-shale aquitard.

Tab. 3.2-2: Average porosity values in the marl-shale aquitard (based on Palfris Formation and Vitznau Marls data), (after NAGRA, 1997)

Type of Hg-porosity [% -vol.]	Undeformed rock (undifferentiated)	Undeformed clay-rich rock (Palfris Formation)	Strongly deformed rock (undifferentiated)	Fault gouges
Open macroporosity	0.28	0.35	1.04	2.48
Open microporosity	1.15	2.51	2.68	7.76
Open total porosity	1.43	2.81	3.72	10.24
Density [kg/m^3]	2.88	2.89	2.87	2.10

As can be seen from Tab. 3.2-2, the open microporosity is many times larger than the open macroporosity, which can be attributed to the large amount of extremely small pores (pore

radii ≤ 0.01 µm). This distribution suggests the predominance of diffusive transport in the aquitard as a whole or at least in its matrix. The open microporosity is, as expected, larger in clayey sections, due to the lower degree of cementation of inter-plate micropores. Secondary porosity due to brittle daformation is noticeable locally (microcracks, pressure-solution of carbonates) and contributes to flow porosity where connected with fault gouges.

Petrophysical data

A comprehensive suite of logging techniques was applied to all boreholes. Of interest for this study are determinations of clay content (e.g. gamma-gamma measurements), porosity (neutron porosimetry) and density. The different methods are related to some extent, since in clay-rich rocks the neutron measurements must be corrected due to the high clay content.

Porosity values derived from petrophysical measurement techniques differ greatly from laboratory determinations (Hg) and are strongly affected by variable clay content (bound water). Therefore, the correlation between subnormal pressures along hole and corresponding local increases in porosity suggested in VINARD et al. (1993) cannot be confirmed here, due to the lack of accuracy of in situ porosity determinations (ALBERT, 1994). However, in situ determination of density and clay content are - within a reasonable range - consistent with laboratory data.

Carbonate veins

The Palfris Formation, the Vitznau Marls and, to some extent, the Tertiary shales of the Axen nappe are traversed by disseminated carbonate veins. These veins are of importance to the study of underpressures in two respects:

1. Carbonate veins were generated at different evolution stages of the rock when brine fluids were temporarily mobile. The veins therefore stored relevant information on past pressure and temperature conditions (geochemical and isotopic composition of fluid inclusions).

2. Geodes are isolated macropores which exist exclusively in carbonate veins. Dedicated measurements show that geodes are filled with gas. Geodes have been sometimes erroneously considered as a major contribution to macroporosity; this led to a model study that, however, produced interesting results (Subsect. 8.5.4).

Geodes represent only an insignificant amount of the macroporosity and do therefore not play any significant role in the generation of underpressures. Moreover, the presence of gas within the voids does not necessarily imply that the aquitard is a dual-phase medium (water and free gas). Free gas in large isolated voids is absolutely consistent with a single-phase system, where the wetting fluid, i.e. water, contains a large amount of dissolved gas.

3.2.3 Water-conducting features

3.2.3.1 Types of water-conducting features

By combining the 160 inflow zones detected by fluid logging (116 - 119 in the aquitard, Subsect. 3.5.3) and analyses of core material, four types of water-conducting features (WCFs) could be defined (MAZUREK, 1997), which all result from brittle deformation:

Type 1: cataclastic shear zones (fractures)

Type 2: thin discrete shear zones (reactivated shear veins)

Type 3: calcareous marl/limestone layers with drusy veins

Type 4: joints in clayey marls and marls

Definition-wise, WCFs comprise both features that indeed exhibit flow and features of similar characteristics that do not. However, in order to come up with the above definition, only those features correlating with inflow zones were used. In practice, there were several difficulties to overcome, for instance when more than one candidate feature exists within the resolution of fluid logging, when salinity and temperature contrasts at large depth are poor and do not allow recognition of inflows, or when core material is of insufficient quality or simply lacking. In spite of these difficulties, the identification was possible to a large extent.

Particularly relevant for flow are types 1 and 3, types 2 and 4 being subordinate. Cataclastic shear zones (type 1) show up in clayey parts of the marl-shale aquitard. They typically contain fault breccias and fault gouges (magnitude ranging from 4 to 400 cm) indicative of shearing, and are surrounded by a damaged zone, also of variable thickness. Interestingly, cataclastic shear zones and fault breccias dip to a large extent towards NNW and NW with dip-angles ranging from 20 to 60°, more or less in concordance with the orientation of the regional schistosity. Cataclastic deformation strongly influences porosity, as shown by the porosity values for the damaged zone, which are 3 to 4 vol.-%, compared to about 1.5 vol. % for the undeformed matrix.

Type 3 WCFs result from extensional fracturing of limestone layers due to the rheologic contrast between the competent layers and the surrounding incompetent argillaceous material. WCFs of this type represent the oldest circulation pathways for formation fluids in the Palfris Formation and the Vitznau Marls (type 3 does not exist in Tertiary marls) since they hosted flow during Neoalpine metamorphism. However, their overall importance is limited, since flow paths are restricted to the limestone strata themselves.

Type 2 WCFs, i.e. thin discrete shear zones, are 0.5 to 2 cm thick planar shear veins that were reactivated in late phases of Neoalpine deformation; they are subordinate and often associated with cataclastic zones.

3.2.3.2 Depth-dependency of water-conducting feature properties

Hydraulic tests show that transmissivity decreases with increasing depth in all five boreholes representative of the marl-shale aquitard. VINARD & LAVANCHY (1994) addressed the question whether the decrease in hydraulic conductivity with depth is related to either the density of WCFs or their internal structure. After careful review and statistical analysis, MAZUREK (1997) found out that frequency and macroscopic structure of major WCFs (type 1) is independent of depth, but that flow porosity decreases with increasing depth. Therefore, the connectivity of WCFs decreases with increasing depth, which explains why transmissivity also decreases.

Furthermore, MAZUREK (1997), based on field mapping in the Haldibach stream valley, notes that the internal structure of the WCFs is heterogeneous, implying channelled flow. Channelling contributes to decreasing connectivity between WCFs; it might explain why only a subset of WCFs actually conducted flow to the boreholes during testing. Therefore, the transmissivity distribution is independent of the frequency of brittle discontinuities, in

line with the pervasive deformation of the whole stacking of tectonic units in the Central Alps.

3.3 Geomechanical data and in situ stress

3.3.1 Scope and limitations

Geomechanical investigations were conducted essentially for engineering purposes, i.e. to provide rock mechanics parameters for underground construction and, to a lesser extent, to characterise the mechanical properties of all types of discontinuities. Therefore, geomechanical data stemming from the depth interval of the planned repository are strongly over-represented. Most geomechanical data are derived from standard rock mechanical laboratory experiments, complemented by specific experiments to test the potential for inelastic time-dependent strain.

Obviously, the scale and duration of standard rock mechanics tests is not representative for larger volumes of rock and for long-duration deformation (Subsect. 7.4.5). As mentioned by HETTKAMP & RUMMEL (1996), significant differences in estimated static Young's modulus E_{stat} from triaxial tests appear for the same material, just because the sample sizes were different! Furthermore, the results from time-dependant experiments carried out by HETTKAMP & RUMMEL (1996) are very difficult to put into the context of small incremental strain as experienced by the aquitard during uplift, erosion and glacial rebound. Additional problems result from core extraction and handling, which strongly affect the original conditions. Bearing in mind these weaknesses, the parameter ranges were applied in different studies, e.g. those reported in Chapters 8, 9 and 10.

In situ stress data, on the other hand, reveal a stress field which is consistent with measurements in the alpine belt. Deviatoric stress is important due to the still active tectonic stress.

3.3.2 Relevant laboratory results

Uniaxial and triaxial compression tests were carried out to investigate the short-term deformability of the rock (HETTKAMP & RUMMEL, 1996). Lithology was taken into account to some extent by classifying the samples with respect to the amount of clay, carbonates or quartz. Anisotropy was also taken into account by classifying the samples into three categories: P samples in which foliation is parallel to the longitudinal axis of the test core, S samples which are normal to the longitudinal axis and Z samples which are oriented 45°. The results show that the Young's modulus increases only marginally with the amount of clay, but that the orientation of the sample with respect to the foliation plays the major role. Correlation of σ_{max} with $E_{stat.}$ as well as correlations between seismic velocity and $E_{stat.}$ tend to indicate that the anisotropic behaviour is due to microcracks mostly parallel to the main foliation present in the cores.

3.3.3 In situ measurements

In situ experiments consisted exclusively of dilatometer tests applied on selected borehole wall sections. Here also a strong anisotropy is noticeable. The dynamic E modulus (obtained from seismic wave propagation) ranges between 16 - 52 GPa. When considering additionally the directional component, this range increases to 7 - 135 GPa. The dynamic Young's modulus inferred parallel to the borehole longitudinal axis shows a range between 30 and 50 GPa. A strong depth dependency is also observed in the upper 500 m, which is considered as the response to surficial decompaction (see also Chap. 9.5 for implications).

It is usually expected that E moduli derived from in situ dilatometer tests will be lower than their counterparts measured in the laboratory, i.e. they exhibit larger bulk rock compressibility values due to the larger volumes of rock involved. However, the clayey marls behave exactly the opposite way, as can be seen in Figure 3.3-1. The best agreement between the two types of Young's modulus is achieved when the E moduli were derived from samples oriented parallel to the foliation. My interpretation of this is that dilatometer tests are also affected by systematic error due to mud cake and especially to strong degassing as observed from aquitard borehole sections when the hole was open to atmospheric pressure conditions. Degassing provokes rapid dessication of the borehole wall, which, in turn, favours formation of microcracks and hardening. Moreover, an unexplained decrease in the E modulus at shallow depths (< 10 MPa overburden stress) was observed.

Tab. 3.3-1: Rock mechanics data for clay-rich materials classified following the orientation of the samples with respect to foliation (after NAGRA, 1997)

ARGILLACEOUS MARLS									
	∝ (SAMPLES ALONG P)			∠ (SAMPLES ALONG Z)			⊥ (SAMPLES ALONG S)		
	Data	Amount	STA or R^2	Data	Amount	STA or R^2	Data	Amount	STA or R^2
uniaxial tests (shear tests)									
Density [g/cm³]	2.71	244	0.02	no anisotropic tests					
E [GPa]	33	15	10.6	16	8	8.4	13	15	3.6
σ_c [MPa]	57	17	26.3	24	22	14.8	59	21	26.2
ν	0.26	10	0.07	0.20	10	0.09	0.20	13	0.06
σ_t [MPa]	3.6	30	1.6	no anisotropic tests					
triaxial tests with σ_3 between 25 MPa and 90 MPa									
c_{peak} [MPa]	32	24	(0.46)	22	21	0.57	47	17	(0.35)
ϕ_{peak} [°]	25	24	(0.46)	12	21	0.57	11	17	(0.35)
c_{rest} [MPa]	24	24	(0.43)	11	21	0.81	18	17	(0.79)
ϕ_{rest} [°]	17	24	(0.43)	17	21	0.81	22	17	(0.79)
triaxial tests with σ_3 between 0 and 25 MPa									
c_{peak} [MPa]	17	24	(0.35)	13	27	0.44	11	22	(0.65)
ϕ_{peak} [°]	36	24	(0.35)	19	27	0.44	36	22	(0.65)
c_{rest} [MPa]	9	26	(0.87)	7	31	0.74	5	22	(0.91)
ϕ_{rest} [°]	36	26	(0.67)	19	31	0.74	33	22	(0.91)
abrasivity- Index [CAI]	1.3	4	0.2	-	-	-	1.9	8	0.5
swelling heave [%]	1.2	33	0.72	no anisotropic tests					
swelling pressure [MPa]	0.66	8	0.29	no anisotropic tests					

∝ σ_1 in degrees from 0° to 30° with respect to foliation, mostly 0° (P samples)
∠ σ_1 in degrees from 30° to 60° with respect to foliation, mostly 45° (Z samples)
⊥ σ_1 in degrees from 60° to 90° with respect to foliation, mostly 90° (S samples)
R^2 = linear regression coefficient (values in brackets)
STA = standard deviation
E = static Young's modulus
ν = Poisson ratio
c_{peak} = cohesion
c_{rest} = residual cohesion
N = number of probes
σ_c = uniaxial strength
σ_t = shear resistance
ϕ_{peak} = friction angle
ϕ_{rest} = residual friction angle

Tab. 3.3-2: Rock mechanics data classified in terms of their quartz and carbonate content (anisotropy is not considered) (after NAGRA, 1997)

	QUARTZ-RICH MARLS			CARBONATE-RICH MARLS		
	Data	Amount	STA or R^2	Data	Amount	STA or R^2
Density [g/cm³]	2.71	50	0.02	2.71	52	0.02
E [GPa]	30	5	10.6	29	5	18.9
σ_c [MPa]	66	5	40.9	86.4	10	39.8
ν	0.21	3	0.04	0.16	9	0.05
σ_t [MPa]	8.9	4	1.2	4.1	16	1.9
c_{peak} [MPa]	33	28	(0.38)	18	33	(0.59)
ϕ_{peak} [°]	25	28	(0.38)	32	33	(0.59)
c_{rest} [MPa]	8	30	(0.78)	8	42	(0.87)
ϕ_{rest} [°]	30	30	(0.78)	28	42	(0.87)
swelling heave [%]	0.23	2	0.2	0.92	8	0.45
swelling pressure [MPa]	-	-	-	0.65	4	0.27

explanation of abbreviations, see Tab. 3.3-1

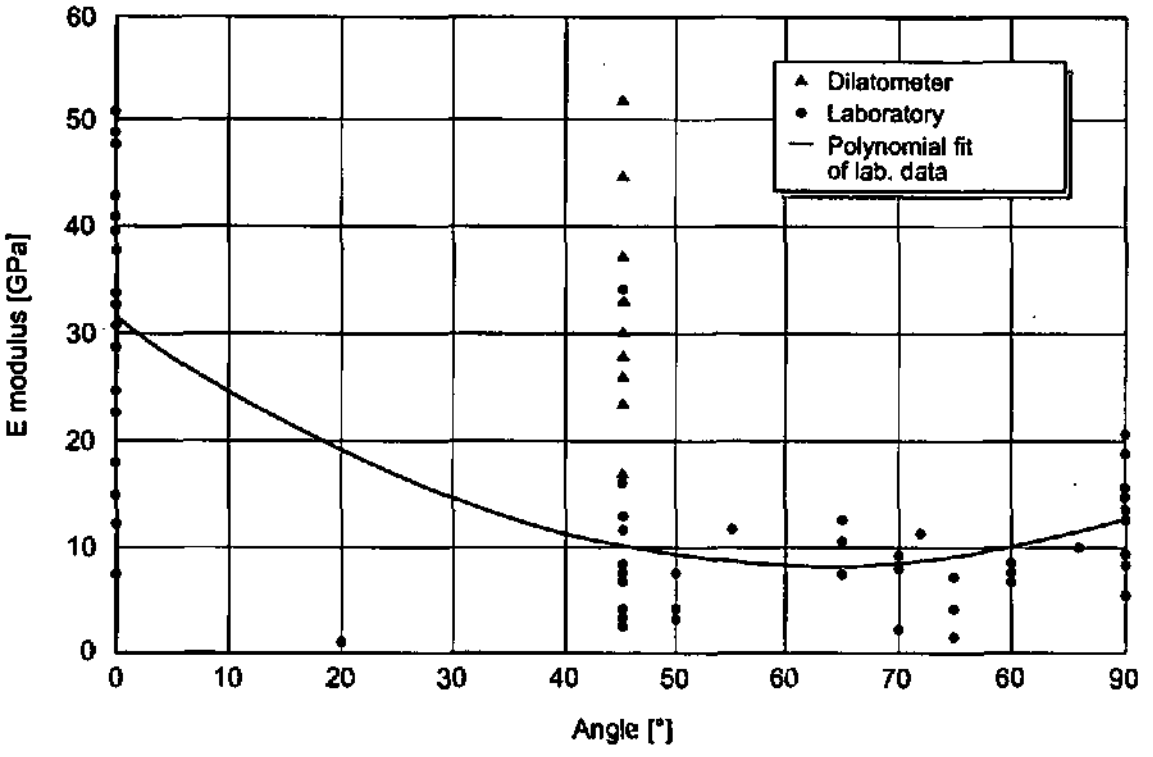

Fig. 3.3-1: Comparison between Young's moduli for clayey marls determined in the laboratory and in situ. Note that the dilatometer test data are not oriented with respect to foliation and are plotted by default at an angle of 45° (after NAGRA, 1997)

3.3.4 Long-term deformation behaviour and material law

Three types of long-term experiments were carried out: deformation tests with constant deformation rate, relaxation experiments with constant deformation and creep experiments with constant differential pressure ($\sigma_1 - \sigma_3$). For triaxial experiments carried out by monitoring the volumetric strain under confining pressures between 5 and 90 MPa, the results show that the rock always reacts with brittle failure, even if the deformation rate $\dot{\varepsilon}$ is reduced from $4 \cdot 10^{-5}$ s^{-1} to $2 \cdot 10^{-8}$ s^{-1} and for confining pressures not exceeding 30 MPa. The inelastic behaviour is controlled by the formation of microcracks. Moreover, as shown by creep experiments, the inelastic deformation rates are not stationary but proportional to the logarithm of time. However, below the strength threshold, inelastic deformation is subordinate, which implies that an elastic approximation is valid in such case.

As already stated, the rock anisotropy is dictated by microcracks preferentially oriented parallel to the foliation. This inelastic response to applied strain rates seems to be controlled by the orientation and density of already present (and not induced) microcracks. It is surprising, finally, to note that a rock containing such a high amount of clay minerals exhibits a relatively pronounced brittle behaviour. The rock strength depends strongly on the applied confining pressure. As a rule, tha Palfris Formation exhibits a higher strength than originally expected for this type of rock.

3.3.5 In situ stress state determination

3.3.5.1 Application and methodology

Only two methods allow the determination of in situ stress; of these, hydraulic fracturing is the only method which provides stress direction and stress magnitude together. The other method is limited to defining stress directions as indicated by borehole wall breakouts or induced fractures, which are visualised from logging data (televiewer, formation microscanner or dipmeter).

Hydraulic fracturing consists of applying a high hydraulic pressure to an isolated (vertical) borehole interval up to the stage where extensional shearing occurs. The lecture of the characteristic pressure evolution (breakdown, refrac and shut-in pressures) provides the magnitude of maximum and minimum horizontal stress, while the orientation of the induced fracturing provides information on the orientation of the stress field. It is assumed that the axis of the borehole represents the principal vertical stress, which is not necessarily the case at Wellenberg due to induced effects of the abrupt topography.

Hydraulic fracturing was applied in boreholes SB1, SB2, SB3 and SB4a/v. Except for the latter, all measurements were carried out below the level of 540 m a.s.l.

3.3.5.2 Main results

For the relevant boreholes SB1, SB3, SB4a/v, the combined results from hydraulic fracturing and breakout orientation (BLÜMLING & GLAWE, 1996) can be summarised as follows (Tab. 3.3-3).

Tab. 3.3-3: Combined results of stress orientation and stress magnitudes in the deep boreholes SB1, SB3, SB4a/v (after NAGRA, 1997)

Borehole	Depth b.g. [m]	S_H [MPa]	S_h [MPa]	Orientation S_H [° N]	Method HF: hydrofrac BO: breakout	ratio S_H / S_h	Stress regime
SB1	350 - 530	12 - 23	10 - 13	35 ± 10	HF	1.2 - 1.8	$S_h \leq S_v < S_H$
	550 - 600	18 - 20	9 - 10	65 ± 10	HF	2	$S_h < S_v < S_H$
	610 - 935	24 - 42	12 - 21	135 ± 10	HF	1.8 - 2.0	$S_h < S_v < S_H$
	600 - 1'500	—	—	145 ± 25	BO	—	—
SB3	590 - 915	32 - 38	16 - 20	135 ± 10	HF	1.9 - 2.0	$S_h \leq S_v < S_H$
	450 - 1'050	—	—	124 ± 15	BO	—	—
	550 - 1'420	—	—	125 ± 20	BO	—	—
SB4a/v	199 - 727	9.4 - 29.5	4.4 - 15.4	142 ± 25	HF	—	$S_h \leq S_v < S_H$
	600 - 730	—	—	124 ± 12	BO	—	—

With the exception of the rotation of the orientation of the principal horizontal stresses above 500 b.g. in SB1 which is probably due to topographic effects, this compilation reveals a remarkably constant orientation around north 130° east, which corresponds perfectly with the Middle European stress field (MÜLLER et al., 1992). Note that this orientation in nearly normal to the front of the Axen nappe.

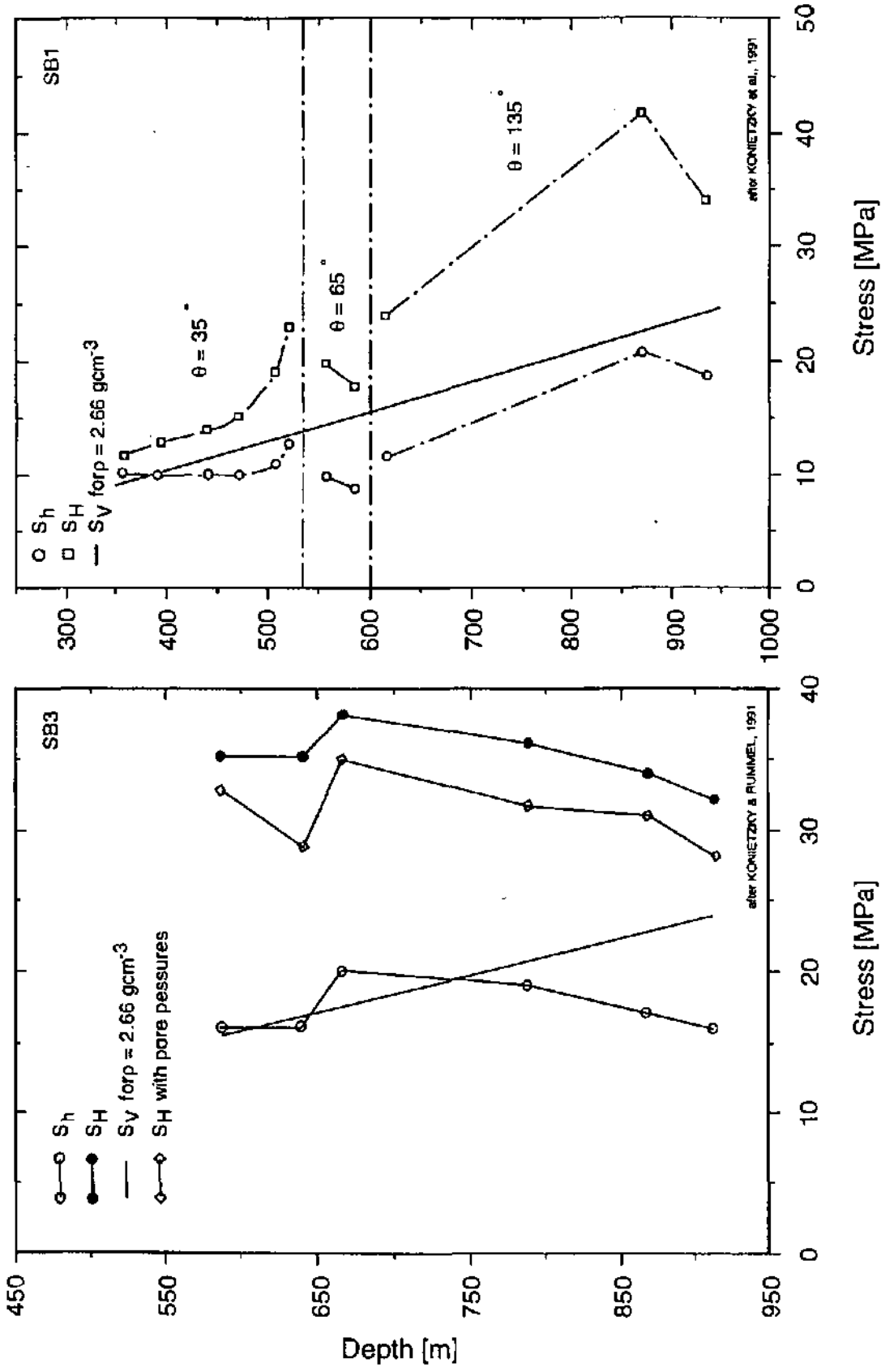

Fig. 3.3-2 Horizontal stress magnitudes with depth in boreholes SB1 and SB3

3.4 Hydrochemical and isotopic data

3.4.1 Role of hydrochemical and isotopic data in the hydrogeological data-set

The hydrochemical and isotopic characterisation of the marl-shale aquitard is based on a limited set of groundwater and porewater samples (obtained via vacuum extraction) which are available up to the periphery of the levels at which hydraulic underpressures were noticed. However, the analysis of these samples and of the groundwaters in the neighbouring formations contributes decisively to the understanding of the hydrogeological conditions. The most important results which were obtained, sometimes with a fairly high degree of confidence, provide information on:

- residence times of groundwaters
- climatic conditions during infiltration of meteoric water
- geochemical evolution of groundwater in response to rock-water interactions
- likelihood evaluation of flow pathways and mixing rates between groundwaters of different origin.

State-of-the-art interpretation techniques were applied to the sampled groundwaters and gases, including standard hydrochemical equilibration (by means of geochemical modelling) and determination of isotopic composition and ratios. More information on results and applied techniques can be found in NAGRA (1997).

3.4.2 Hydrochemical characterisation and classification of groundwaters in the marl-shale aquitard and surrounding formations

By combining hydrochemical and isotopic data, ten main groundwater types could be identified in the investigated region. When classified in terms of hydrochemical composition, these 10 groundwater types fit into 5 main categories, which are summarised in Tab. 3.4-1 and represented in Fig. 3.4-1 (boreholes projected horizontally on profile D - D') and Fig. 3.4-2 (profile Q - Q').

Tab. 3.4-1: Groundwater categories and sampling depth (after NAGRA, 1997)

Chemical category	Sampling depth (m b.g.)	Sampling location	Geological classification	Type[1]
Ca-HCO_3- type	down to about 70 m	Springs, piezometer boreholes, SB4a/v[2], SB4a/s[2]	Quaternary deposits Kieselkalk aquifer	I,II, VIII
Shallow Na-HCO_3-type	from ~70 m to ~ 360m	SB1, SB3, SB4, SB4a/v, SB6	Palfris Formation and Vitznau Marls (marl-shale aquitard)	III
Na-Cl-type	> 400 m	SB1, SB3, SB4a/s[2]	Palfris Formation and Vitznau Marls (marl-shale aquitard)	IV[2], V
deep Na-HCO_3-type	~ 1180 m - 1475 m	SB1, SB3	equivalent of the Wissberg slab	VI, VII
other groundwaters	~ 100 m - 1420 m	SB2	limestone units of the Drusberg nappe	IX, X

[1] the roman numerals refer to the groundwater types represented in Figs. 3.4-1 and 3.4-2

[2] intermediate type between two groundwater types

Isotopic analyses of groundwaters are used, among other things, to determine residence times by comparing ratios of isotopes. Mixing of groundwaters of different origin make such determinations difficult.

As seen in Figs. 3.4-1 and 3.4-2, the sampled groundwaters in the marl-shale aquitard are mainly of the Na-HCO_3 type in its upper part, and of the Na-Cl type at deeper levels. It is therefore assumed that this latter groundwater type is representative of rather tight conditions. If the above assumption holds, the hydrochemical contrast between aquitard and underlying formations (Na-HCO_3 type) is sharp, as is the head difference (Fig. 3.5-3), while there is a smooth transition from recently infiltrated shallow Ca-HCO_3 waters, sampled in the Quaternary deposits (Altzellen landslide mass and surface deposits), through the Na-HCO_3 type at the interface between landslide and shallow Palfris Formation and down to the deep-seated Na-Cl brines.

Laterally, as suggested by borehole SB2 data in Fig. 3.4-1, geological boundaries between limestone units and the marl-shale aquitard reflect in an equivalent boundary between different types of bicarbonate waters (Types VIII, IX, and X) and the Na-Cl (type V) groundwater. Even though no data are available for the limestone units of the Axen nappe, this may also apply there, since the lithologies are similar to those of the Drusberg nappe.

The evolution of these groundwaters is discussed in Section 4.3.

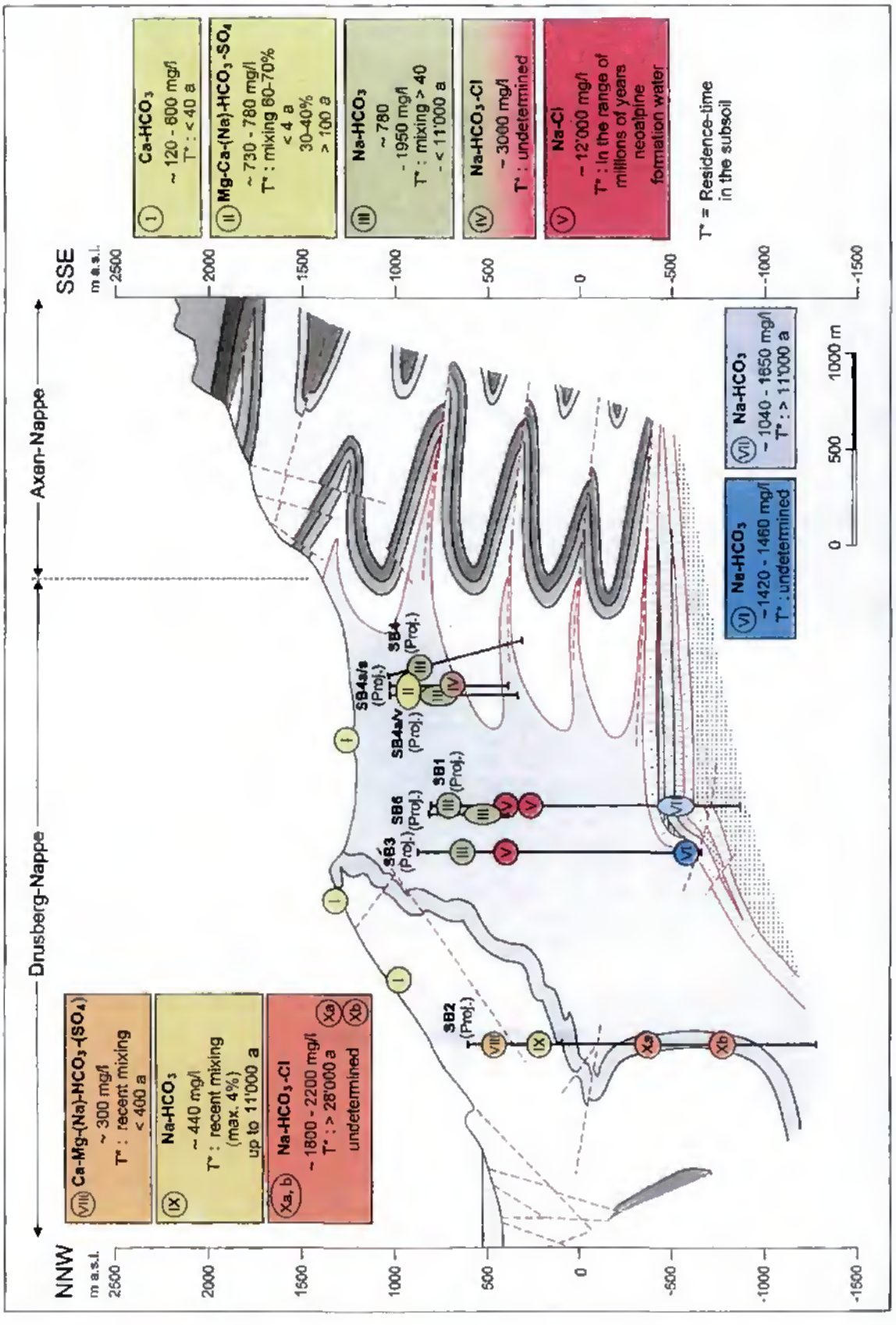

Fig. 3.4-1: Hydrochemical characterisation of groundwaters projected on cross-section D - D' (oriented NNW - SSE), (after NAGRA, 1997)

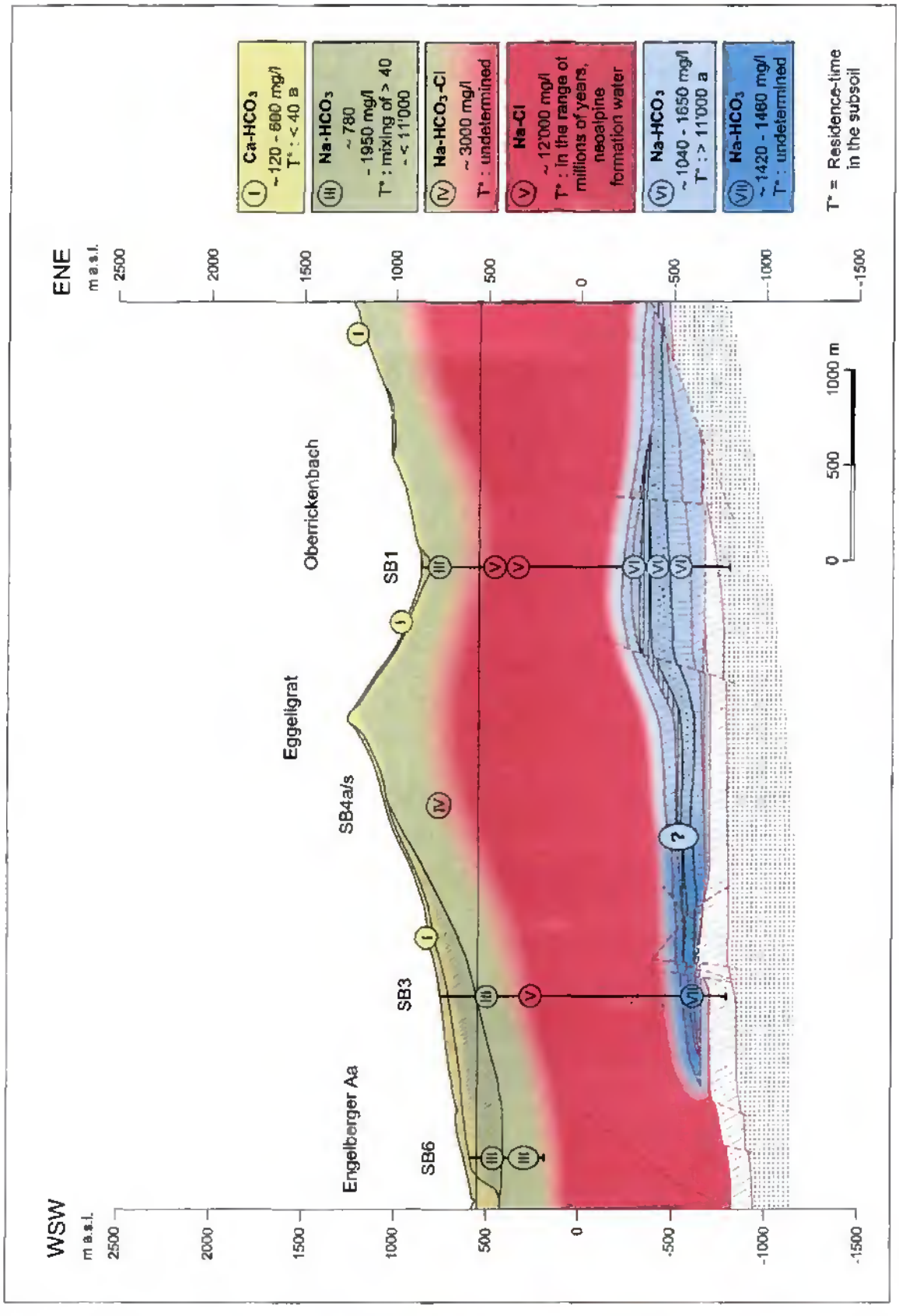

Fig. 3.4-2: Schematic distribution of the groundwater types in cross-section Q-Q' (oriented WSW - ENE), (after NAGRA, 1997)

3.5 Hydrogeological data

3.5.1 Scope and test procedures

Hydrogeological data combine by definition all types of geological, hydrochemical, isotopic and hydraulic data. The present overview is restricted to hydraulic data. Hydraulic tests are performed to characterise hydrogeological units, i.e. lithostratigraphic formations exhibiting similar hydrogeological properties. Given this definition, the marl-shale aquitard, characterised by low to very low hydraulic conductivity, represents a hydrogeological unit. The application and limitations of hydraulic testing are best defined per method:

Packer tests

1. comprehensive distribution of overall hydraulic conductivity along hole
2. distribution of hydraulic head (expressed as freshwater head) along hole
3. determination of the flow model (radial flow, linear flow, etc.) and radius of investigation or of visibility of the test into the formation
4. sampling of groundwaters for hydrochemical and isotopic analysis
5. determination of potential two-phase flow characteristics of a given interval (either rock properties for gas injection using threshold pressure measurements or detection and possibly quantification of potential free gas under natural conditions using ad hoc packer test sequences).

Fluid logging

1. identification of discrete inflow zones
2. local transmissivity values

Long-term monitoring

1. direct measurement of formation pressure
2. if conditions are appropriate, sampling of uncontaminated groundwater.

3.5.2 Hydraulic testing methods

Most hydrogeological data were derived from hydraulic tests performed in deep boreholes (VINARD & LAVANCHY, 1994; LAVANCHY & MARSCHALL, 1997). Classic shallow groundwater surveys provide little helpful information on the hydrogeological conditions in the marl-shale aquitard. For example, only 3 % of all investigated springs and drainage systems suggest a contribution of deep groundwaters, and this only in the adjacent rock formations. Therefore, almost all relevant hydrogeological information is obtained from boreholes. Three main hydraulic investigation methods were applied:

- single and double packer tests
- fluid logging
- long-term hydraulic pressure measurements in multipacker systems.

Description of testing procedures and interpretation techniques is well beyond the scope of this thesis and the interested reader is referred to ERLOUGHER (1977) and GRINGARTEN (1982) for the theoretical basis of packer testing, to TSANG et al. (1990) for fluid logging and to PASQUIER (1996) for long-term monitoring. Interpretation procedures and results are

described in detail IN VINARD & LAVANCHY (1994) and LAVANCHY & MARSCHALL (1997).

3.5.2.1 Fluid logging

Two main steps are carried out. In the first step, the drilling fluid is replaced by a flushing fluid (usually low-salinity freshwater) in order to obtain a strong salinity and temperature contrast with formation waters. In the second step, pumping is applied to significantly lower the freshwater head in the borehole, which forces formation water to flow into the well. The electrical conductivity and temperature logs measured dynamically by a probe travelling at a constant speed along the well materialise in the form of characteristic peaks. These peaks identify the locations of inflow zones and, if quantitative analysis is possible, they also provide the transmissivity distribution of inflow zones along the hole. Identification of inflow zones is dependent on the applied drawdown as well as on the hydraulic head of the inflow zone. The detection threshold is therefore variable from borehole to borehole, and even within a single borehole. A threshold in the order of $T = 10^{-10}$ to 10^{-9} m^2/s can be reasonably expected when borehole conditions are favourable, less if not. Inflow zones are identified with a precision of ± 1 m along hole (a.h.) for appropriate well conditions, ± 2 to 4 m otherwise.

3.5.2.2 Packer testing

Single and double packer tests were routinely used as a state-of-the-art hydraulic measurement technique in all boreholes. As a rule, single packer tests or "bottom-hole" tests were applied at the end of every drilling step, whereas double packer tests were chiefly used for specific investigations after completion of drilling activities. Packer testing is the basic method used for hydraulic characterisetion of a borehole and for providing a basis for the hydrogeological classification.

Packer tests are performed by isolating a given borehole section between bottom hole and e packer or between two packers. Before testing, the interval of interest is carefully flushed to remove drilling fluid and mud cake. At this point, the packer(s) is/are inflated and a first phase of static pressure recovery is applied to overcome pressure disturbance due to drilling (borehole pressure history). This sequence is followed by the active testing phase, which sequences depend on the test objectives. A dedicated sequence of test procedures is applied in the isolated interval; these tests are performed either by instantaneously applying strong pressure differences, followed by immediate shut in (pulse tests), or by withdrawing water over longer periods of time. In low permeability environments, these techniques almost never result in full re-equilibration of formation pressure during the duration of the test itself. The pressure evolution is therefore extrapolated from the existing data. Head, permeability, flow model and other relevant information on the flow system are derived using analytical and numerical techniques and assuming ideal rock properties (homogeneous region, radial flow, etc.).

3.5.2.3 Long-term monitoring

Long-term monitoring is performed in selected borehole intervals isolated by ad hoc multipacker systems which are installed after completion of all drilling and active well testing operations. In principle, this method is very simple and is the only absolutely reliable method for obtaining direct and unbiased equilibrated formation pressures. At Wellenberg for instance, long-term monitoring confirmed beyond doubt the reality of hydraulic underpressures and of artesian head conditions below the marl-shale aquitard. In some cases, especially for artesian intervals and provided the hydraulic conductivity is high

enough, "uncontaminated"[1] groundwaters may be sampled for hydrochemical and isotopic identification. An attempt has also been made to use long-term pressure data for estimation of larger-scale storage coefficients. The results are, however, mitigated (PASQUIER, 1995). Technically, the completion of multipacker systems is all but easy, particularly in environments where strong vertical hydraulic gradients exist between isolated intervals, as is the case at Wellenberg (PASQUIER & VINARD, 1994; PASQUIER, 1996). Hydraulic communication occurred between some adjacent zones, making the pressure data useless.

The confidence in transmissivity data was increased by the generally good agreement between fluid logging and packer test data (best-guess for both methods lay within half of an order of magnitude). The integrated transmissivity profiles for each borehole, as shown in Fig. 3.5-1, result from a combination of packer test and fluid logging data. With respect to hydraulic head estimates, the agreement between extrapolated values from packer tests and pressure readings from the multipacker systems is also remarkably good, with a discrepancy not exceeding 0.5 MPa.

3.5.3 Interpreted hydrogeological data

3.5.3.1 General observations

The main result of hydraulic testing was the demonstration that groundwater flow within the aquitard is concentrated in WCFs, whereby the rock matrix only plays a significant role in the deep and extremely low-permeability levels of the aquitard. A second important result is that, as mentioned already in Subsection 3.2.3, no depth dependency of the frequency[2] of inflow points could be identified. Based on boreholes SB1, SB3, SB4, SB6, SB4a/v, and SB4a/s, which are deemed representative of central aquitard conditions, an average frequency of 3.3 inflows per 100 m borehole section was found.

3.5.3.2 Flow model and radii of visibility

Diagnostic analysis of packer test results revealed that linear flow boundaries almost never exist in the tested volume. Therefore, the radius of visibility of each test could be defined, depending on the diffusivity ratio. As expected, tight sections have low to extremely low radii of visibility (down to < 1 m). Of 105 analysed packer tests, only 17 exhibited radii > 10 m and these were all concentrated in the medium-transmissivity sections of the boreholes. In tight sections of the aquitard, the values deemed representative of undisturbed conditions do not exceed a few centimetres around the test interval, which poses the problem of representativity of the inferred permeability values.

The flow model providing the best fits is infinitely acting radial flow (IARF). Surprisingly, dual porosity models which currently apply to fractured systems could be applied only in a few cases.

3.5.3.3 Transmissivity and hydraulic conductivity

Introductory remark: Commonly, in hydrogeological science, the ability of rocks and fluids to conduct flow is expressed in terms of hydraulic conductivity. However, in discontinuous

---

[1] uncontaminated refers to groundwaters, which are representative for the formation, withoutsignificant amounts of drilling water, notoriously mixed with different tracers

[2] the frequency of inflows corresponds to the number of inflow points divided by the length of the borehole sections tested by means of fluid logging

systems, tested hydraulically at the level of individual inflow zones, it is convenient to express flow properties in terms of transmissivity as a two-dimensional state variable at metric scale. The upgrade to hydraulic conductivity, which applies to a three-dimensional volume, explicitly requires an appropriate conceptualisation step, which differs in nature depending on the observation scale, i.e. on the representative elementary volume (REV). For this study, on the regional (i.e. hectometre to kilometre) scale, it is probably justified to consider the fracture network system as an equivalent porous medium (EPM). All groundwater or coupled hydraulic-mechanical models dealt with in this study are based on this fundamentel hypothesis. Therefore, the conversion of transmissivity to equivalent hydraulic conductivity (K_{eff}) is based on this assumption. This T to K conversion, as well as the concept of the K-model based on it, are explained briefly in Subsection 9.5.4 and particularly in MARSCHALL et al. (1997).

The hydraulic characterisation of the aquitard and of the neighbouring formations is based on so-called "interval transmissivity" derived for each packer interval. These data were combined with the locations of inflow zones within the packer test interval and - if available - with the inflow zone transmissivity. Interval transmissivity was then distributed to the corresponding inflow zones, resulting in discrete transmissivity profiles. Generally, interval transmissivity and inflow zone transmissivity are in good agreement. Results are shown for all relevant boreholes in Fig. 3.5-1. Note that for borehole sections for which no inflow zone transmissivity could be obtained, a per default transmissivity over the packer test interval is plotted (dotted vertical lines). The individual error estimetes are represented by horizontal dotted lines. For comparison purposes, the boreholes are represented with respect to absolute depth levels below ground (i.e. not along hole).

Hydraulic conductivity values for the "rock matrix" were determined by selecting packer test intervals in which no inflow zone was detected (i.e. the domain can readily be considered as an EPM, although it is obvious that inflow zones do exist in the rock matrix but below the detection threshold). The inferred range of hydraulic conductivities is 10^{-14} - 10^{-12} m/s.

The landslide of Altzellen is characterised by relatively high transmissivity values, spread over a wide range ($T = 10^{-8}$ - 10^{-5} m²/s). The underlying formations must be differentiated into the "Wissberg Scholle" (tectonic slab), the neighbouring mélange layers with relatively large transmissivity values ($T = 10^{-8}$ - 10^{-6} m²/s) and the infrahelvetic mélange with very low values ($T = 10^{-11}$ - 10^{-10} m²/s).

3.5.3.4 Hydraulic head

All hydraulic pressure values were uniformly converted to hydraulic head (for definition refer to Subsect. 1.3.3), expressed in terms of freshwater head. As for transmissivity, hydraulic head was attributed wherever possible to individual WCFs. Fig. 3.5-2 shows the head evolution for all boreholes together.

The Quaternary deposits are characterised by subartesian to hydrostatic heads. Within the marl-shale aquitard, the characteristic head depression which motivated the present study can be observed in all relevant boreholes. The shallow zone of the aquitard exhibits hydrostatic or slightly artesian conditions. With increasing depth and decreasing hydraulic conductivity, however, hydraulic heads decrease to an absolute minimum (reached only in SB1 and SB3), to finally increase again towards the bottom of the aquitard, attaining up to artesian conditions. This minimum head is encountered in SB3 around the current sea level. It is theoretically possible that unsaturated conditions exist at this level (NEUZIL & POLLOCK, 1983). Unfortunately, this could not be explored with current technology. Also interesting is the strong artesian head of about 1'000 m a.s.l. measured consistently in SB1 and SB3 in the equivalent of the Wissberg Slab. This is remarkable considering that these boreholes are more than 1'600 m apart.

Finally, it is worth mentioning that almost all head measurements in the 19 (of initially 25) still working monitoring zones of the multipacker systems lay within the bandwith of packer test head interpretation. Zones Z3 and Z5 in borehole SB1 and zone Z2 in SB4 in particular confirm the subnormal hydraulic heads in the marl-shale aquitard. With the exception of the latest boreholes (SB4a/v and SB4a/s), for which subnormal pressures are extrapolated, all head measurements are based on stabilised head versus time profiles.

Fig. 3.5-3 focuses on the transmissivity and head profiles of the most important boreholes for this study, i.e. SB1 and SB3. The good agreement between packer test results and long-term monitoring measurements are explicitly shown in this plot.

3.5.3.5 Free gas in the aquitard

At least as constituent of groundwater, gas (dissolved gas) is ubiquitous in the aquitard for the reasons explained in Section 4.3. Gas was observed previously in the same lithologies at the Oberbauenstock site and relatively large amounts of gas were produced from below the marl-shale aquitard in SB3. Given also that gas flow was considered first as the mechanism generating underpressures, or - due to its high compressibility - as being capable of invalidating the mechanical rebound hypothesis, it is only logical that a lot of effort was invested in evaluating whether free gas exists in the aquitard and then in identifying and quantifying its occurrence.

In the Palfris Formation, only few packer tests indicate the potential for free gas occurrence (12 of 141 interpreted packer tests). This is an important observation, even though most packer tests were not specifically designed for the identification of free gas. In order to increase understanding of potential two-phase flow processes, a specifically designed "gas evidence test" was performed in SB4a/s. An interval of about 10 m at 450 m depth was selected because gas was detected in it during the standard test phase. Detailed interpretation of this gas evidence test indicated that an average content of 3 % free gas was indeed present in the pore space (at most 9 %). This result shows that locally free gas exists. However, this does not alter the generally accepted statement that free gas is subordinate and limited to small isolated zones disseminated within the aquitard. This can be affirmed based on the lack of spatial correlation of potentially gas bearing zones in the different boreholes and also based on the lack of depth dependency of gas shows (NAGRA, 1997).

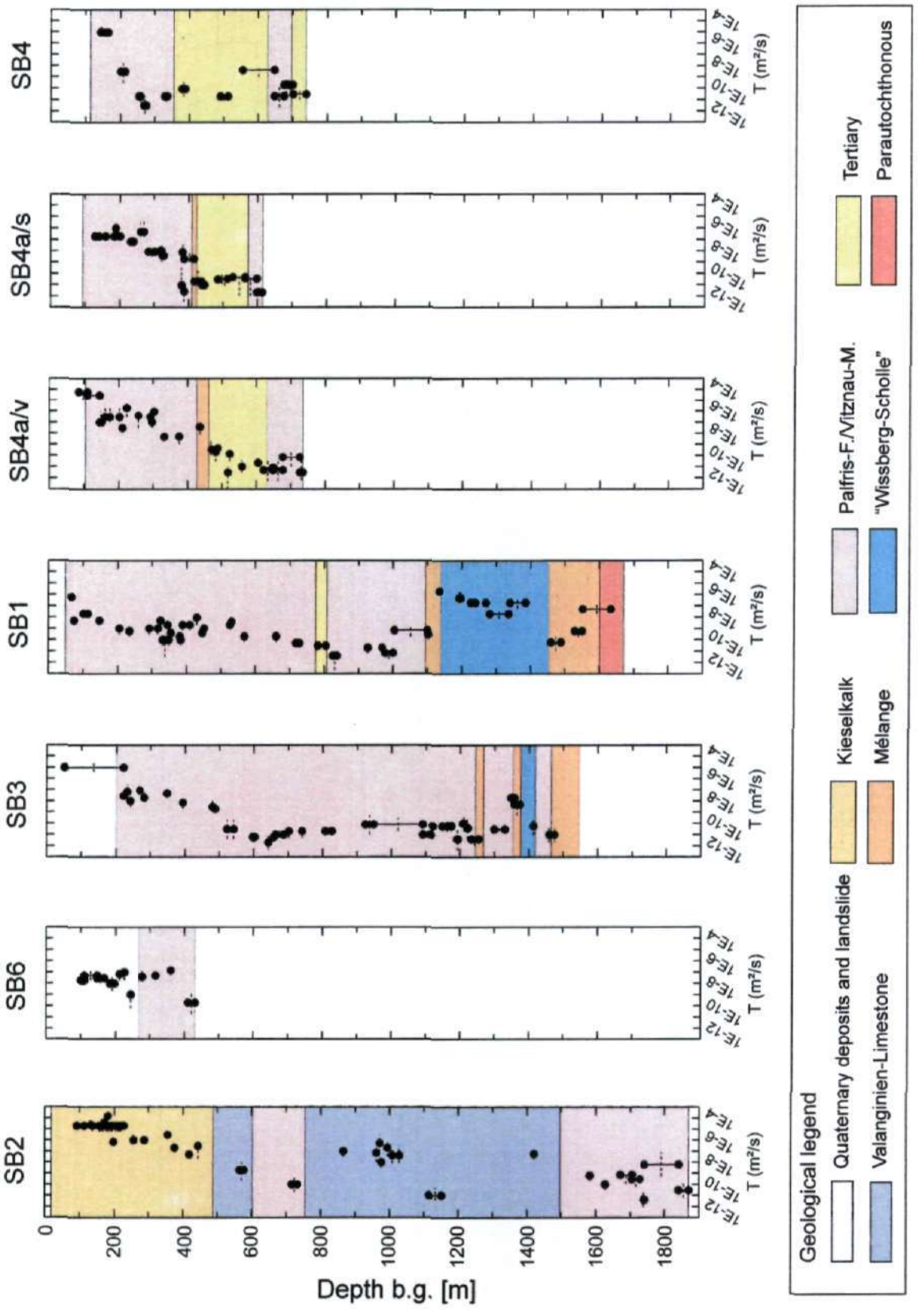

Fig. 3.5-1 Transmissivity of the water-conducting features in boreholes SB1 to SB6 (for discrete inflow zones or interval transmissivity for sections below detection limit), (after NAGRA, 1997)

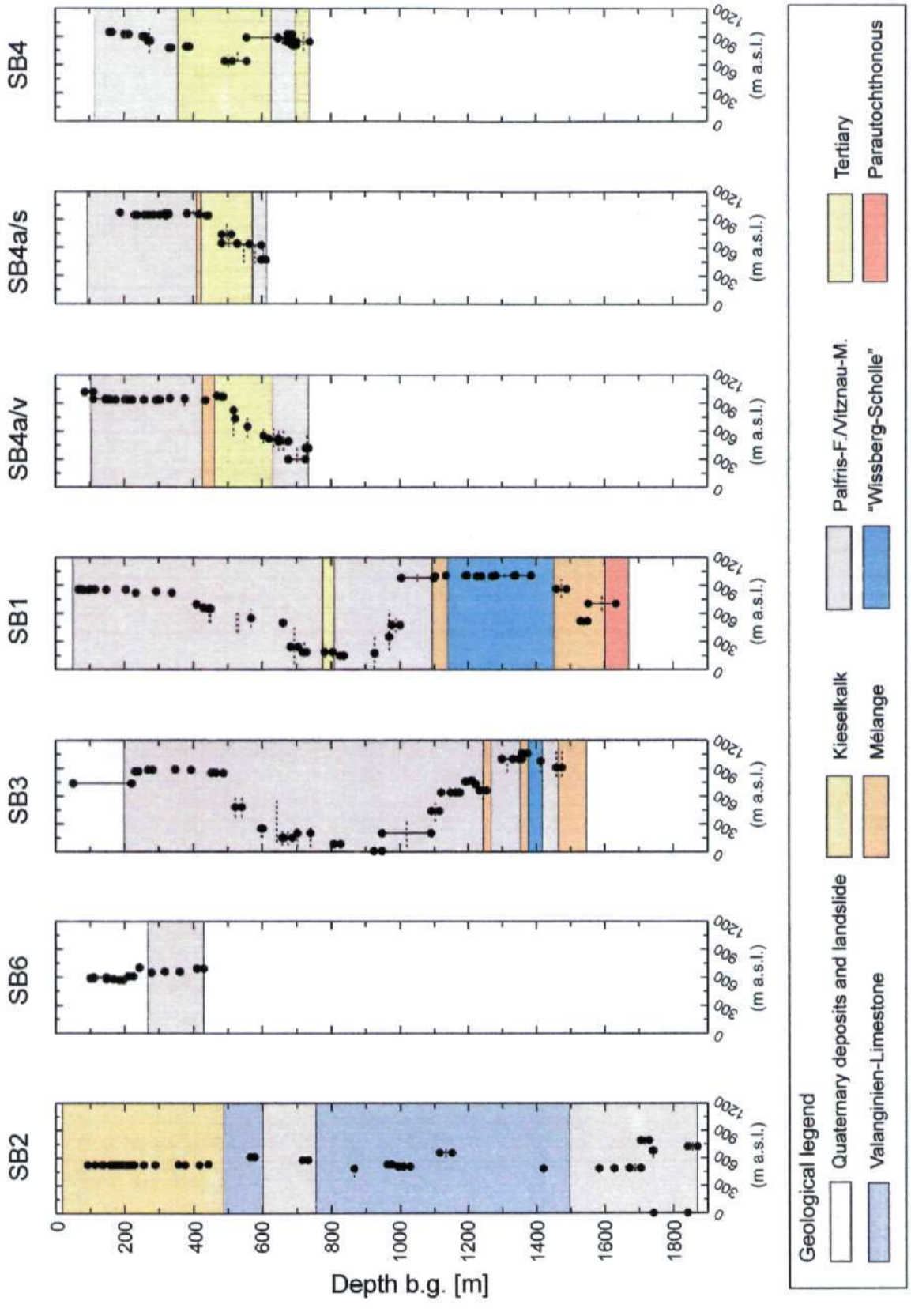

Fig. 3.5-2: Hydraulic heads (packer test results) in boreholes SB1 to SB6 (after NAGRA, 1997)

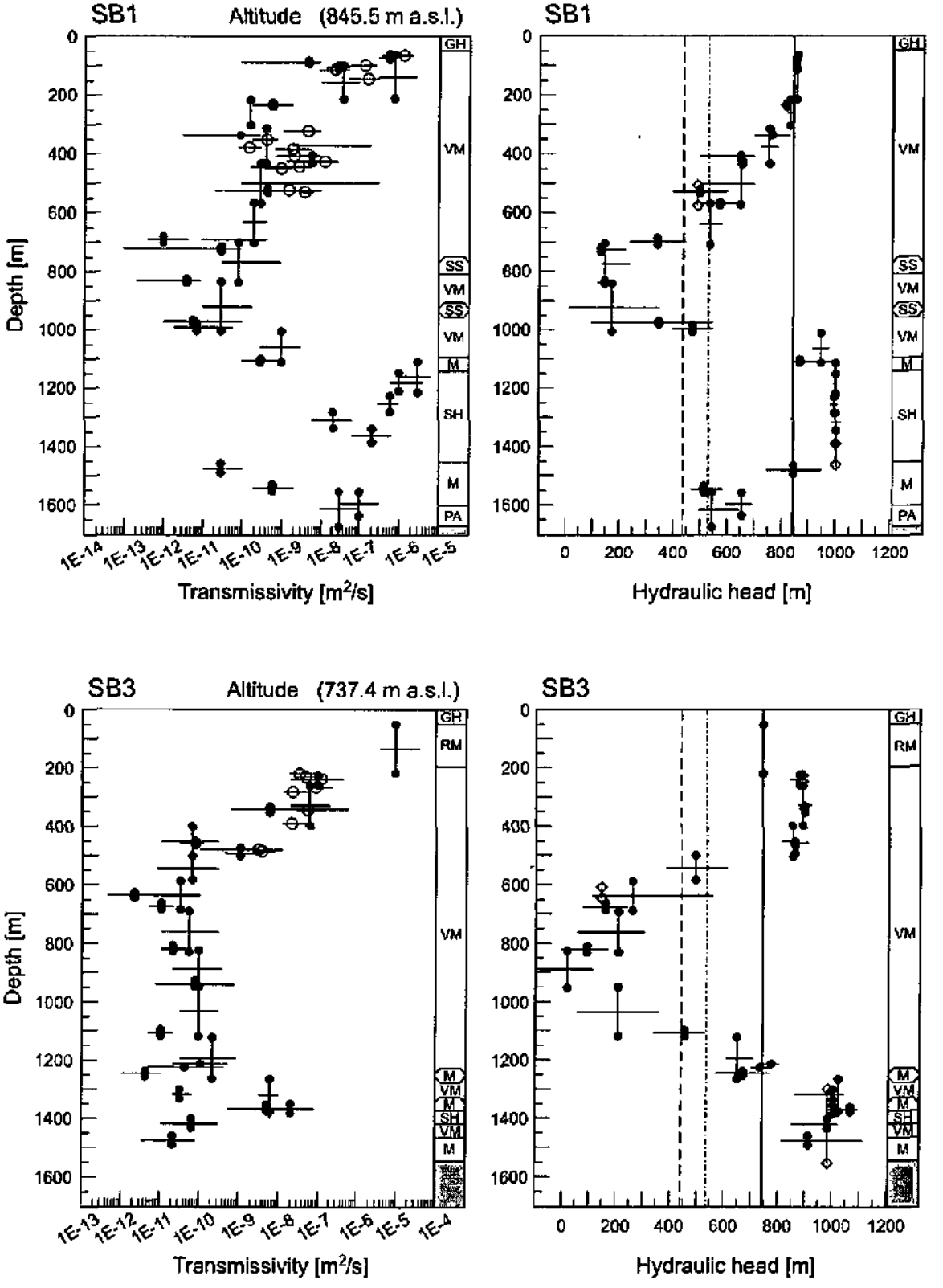

Fig. 3.5-3: Interpreted head and transmissivity profiles of SB1 (above) and SB3 (below), (after NAGRA, 1997)

3.5.4 Discussion of the results and outlook

As mentioned previously, the representativity of transmissivity profiles centred on individuel boreholes for the entire aquitard can be questioned. The only direct way to increase confidence in transmissivity values and thus in the derived hydraulic conductivity data, would be to drill a large number of boreholes and to perform cross-hole tests between them, which is of course impracticable. Due to the current lack of additional data from the underground, the only way to obtain "representative" hydraulic conductivities for the aquitard (K_{eff}) is to apply a conceptuel model which shall encompass the sparse transmissivity data and a representation of the distribution of WCFs (including their properties) in three-dimensional space.

Nagra (NAGRA, 1997) invested a great deal of effort in defining a procedure for upgrading from local transmissivity to equivalent hydraulic conductivity representative of the hectometre scale. The first step consists in converting the local T values to equivalent K values representative of hectometre scale. This was done by generating hectometric fracture network blocks centred on each borehole. In a second step, once the vertical K-profiles for individual boreholes had been simulated satisfactorily, a generally valid description of the K depth-dependency was approximated by an error function where each K-profile in a borehole is considered as a "realisation". The last step is to generate K-distributions, based on this generally valid depth-dependency and on correlation distances. The smoothest K-distribution, but at the same time not the most realistic one, is produced by *kriging*. Additionally, *in order to take the influence on K of decompaction at shallow* depth into account, the kriging response was weighted by a depth-dependency function provided by a gravitative stress model. Furthermore, in order to take the assumed spatial variability of hydraulic conductivity into account, geostatistical modelling applying the turning band algorithm was performed. The output takes the form of equally probable realisations of the hydraulic conductivity field, according to the basic model assumptions.

The K-model is of course subjective, since it depends on the various hypotheses and choices made during its elaboration (e.g. vertical and horizontal correlation length, link to a modelled stress field, assumptions on geostatistical properties of fracture networks, etc.). It is, however, probably the best method to date, since it is open to additional data, tractable and flexible. The 3D models presented in Sections 9.6 and 9.7 are based on this conceptualisation, but make use of the possibility to scale down K values. More information on this topic is provided in Section 9.5 and in condensed form in NAGRA (1997) or JAQUET & al. (1997).

4 GEODYNAMIC EVOLUTION OF THE WELLENBERG SITE

4.1 Scope, relevant processes and time frames

The Alps are a geologically dynamic system. From the first compressional movements which led to the closure of the original sedimentary basins (Tethys sea) at the beginning of the Tertiary era, some 67 million years ago, up to today, tectonic stress has been continuously active and is still active today as shown by the current uplift rate of 1.5 mm/a in the Central Alps with respect to the Swiss plateau. Tectonic stress is therefore one of the two main driving forces acting on geological and hydrogeological systems. The other driving force is climate or, more precisely, climatic fluctuations, which provoke ice ages and a variety of geomorphologic changes (scouring, erosion, landfall, etc.).

Both forces in conjunction with each other continuously alter boundary conditions and rock properties. The most obvious manifestations are superficial denudation and erosion, which are activated by glacial events. Erosion, thus, both modifies the geometry of the hydrogeological body itself and, by unloading the rock framework, also modifies the internal stress state, which in turn modifies rock properties, especially the distribution of hydraulic conductivity and specific storage.

Therefore, in order to understand the past evolution of the rock framework of the marl-shale aquitard itself and of its groundwaters, and possibly to provide qualitative predictions of its future evolution, the entire time span over which substantial climatic changes occurred must be understood. However, although understanding is of primarily importance for setting up an appropriate conceptualisation, it is even more relevant to understand that primarily the most recent Quaternary events control the system to the largest extent. For this reason, this period of geological time is addressed in more detail.

4.2 Orogenic evolution

4.2.1 Scope

The Central Alps are formed by stacking of large-scale tectonic nappes. A large part consists of Helvetic nappes, which sediments initially were deposited in different basins. During the alpine orogeny, the Helvetic nappes were progressively transported (and strongly deformed) northwards over more than 50 km from their initial emplacements. Basic knowledge of tectonic processes is necessary in order to understand the present fabric, properties and thickness of the marl-shale aquitard. At depth, most of the boundaries between the marl-shale aquitard and neighbouring geological formations are not well known. They are estimated essentially by observing the tectonic style and interpolating between the few deep boreholes which actually reached boundaries.

4.2.2 Regional-scale tectonic evolution

EMILE ARGAND and ALBERT HEIM were the pioneers of modern tectonic theories on the alpine orogeny. Since then, a large number of regional and local studies have been performed and there is a wide consensus on the general evolution of the alpine belt. Debate and controversy relate only to details, which do not seriously affect the basic assumptions underlying this study.

When exactly the surrection of the Alps began is unclear. TRÜMPY (1980), for example, considers that an early "eoalpine" phase began already during the Cretaceous era (Albian up to Turonian). This phase was followed by a comparatively low-activity period during the

Palaeocene (around 66 to 58 Ma BP[1]). The main deformation phase took place during the early Eocene (around 58 to 52 Ma BP), which is subdivided into an early mesoalpine and a late neoalpine sequence (JEANRICHARD, 1972,SCHAER & JEANRICHARD, 1974).

Fig. 4.2-1 summarises the most important stages of the evolution of the Helvetic nappes, while Fig. 4.2-2 shows the schematic evolution of the Central Alps with indication of the position of the study area. This latter scenario depicts how the sediments forming the present marl-shale aquitard were progressively overthrust by a large mass of allochthonous sediments and how, in favour of thrust planes originated inside the Drusberg nappe itself, the initial sediment thickness was multiplied by at least a factor of 4.

Of importance to the study of underpressures is the evolution of the aquitard rock, starting at the middle Oligocene (34 to 30 Ma BP). This period corresponds to the onset of the neoalpine phase, which culminated with a metamorphic peak between 24 and 18 Ma BP. The estimated temperatures are in the order of 190 to 245° C, an interval which corresponds to a maximum overburden of 8 km, assuming a geothermal gradient of 25° C/km. At that time, deformation was ductile, i.e. dominated by plastic creep, and was fully penetrative, which means that the continuity of the rock framework is conserved (schistosity and foliation). In this stage, the already deformed thrust plane between the Axen and Drusberg nappes was further folded, resulting in the deformation style we observe today (Fig. 2.2-4a). In the middle Miocene (16.5 to 10.4 Ma BP), the shortening of the crust was further enhanced and resulted in a marked rise in the sediment accumulation above the uplifting crystalline basement. At the same time, erosion was acting at an average denudation rate of 0.3 to 0.4 mm/a. As a consequence, the overburden was reduced by about 3 to 4 km, leaving an overburden of about 4 to 5 km at the end of this phase (GUDMUNDSSON, 1994).

During the Pliocene and Pleistocene, the deformation style evolved from ductile to brittle (Fig. 4.2-2g). Brittle deformation occurs when the rock strength is exceeded and is characterised by a loss of material cohesion, leading to open fissures and fractures. Note the relatively great depth of the sketch profiles in Fig. 4.2-2, which was rendered possible by the deep boreholes SB1, SB2 and SB3. For instance, it is thanks to these boreholes that the steep dip of the Parautochthonous and overlying units, including the marl-shale aquitard in the northern part of the site, was identified, for it was not reached in SB2.

The great sediment accumulation of the Palfris Formation and Vitznau Marls is explained by the subdivision of the original strata into sub-units, so-called "Sinsgäu-units", probably originating in the early Miocene and piled up by thrust planes and intensive faulting and large-scale folding, as the reversed position of some sediment elements suggest. The relatively thick accumulation of interhelvetic mélange is explained by several shear horizons at the contact zone between tectonic nappes (Axen nappe to Drusberg nappe).

All sediments belonging to the definition of the marl-shale aquitard, except for the Tertiary shales, are cyclothems of clay-rich sediments and intercalated limestone banks. The ductile phase produced large-scale folds as shown on outcrops by the competent limestone banks, which mark the deformation thanks to their rheologic contrast with the clayey material. Later on, all the Lower Cretaceous sediments were affected by faults and fractures, thus impeding to a large extent the continuity of the limestone banks.

---

1 Ma BP: million years before present time

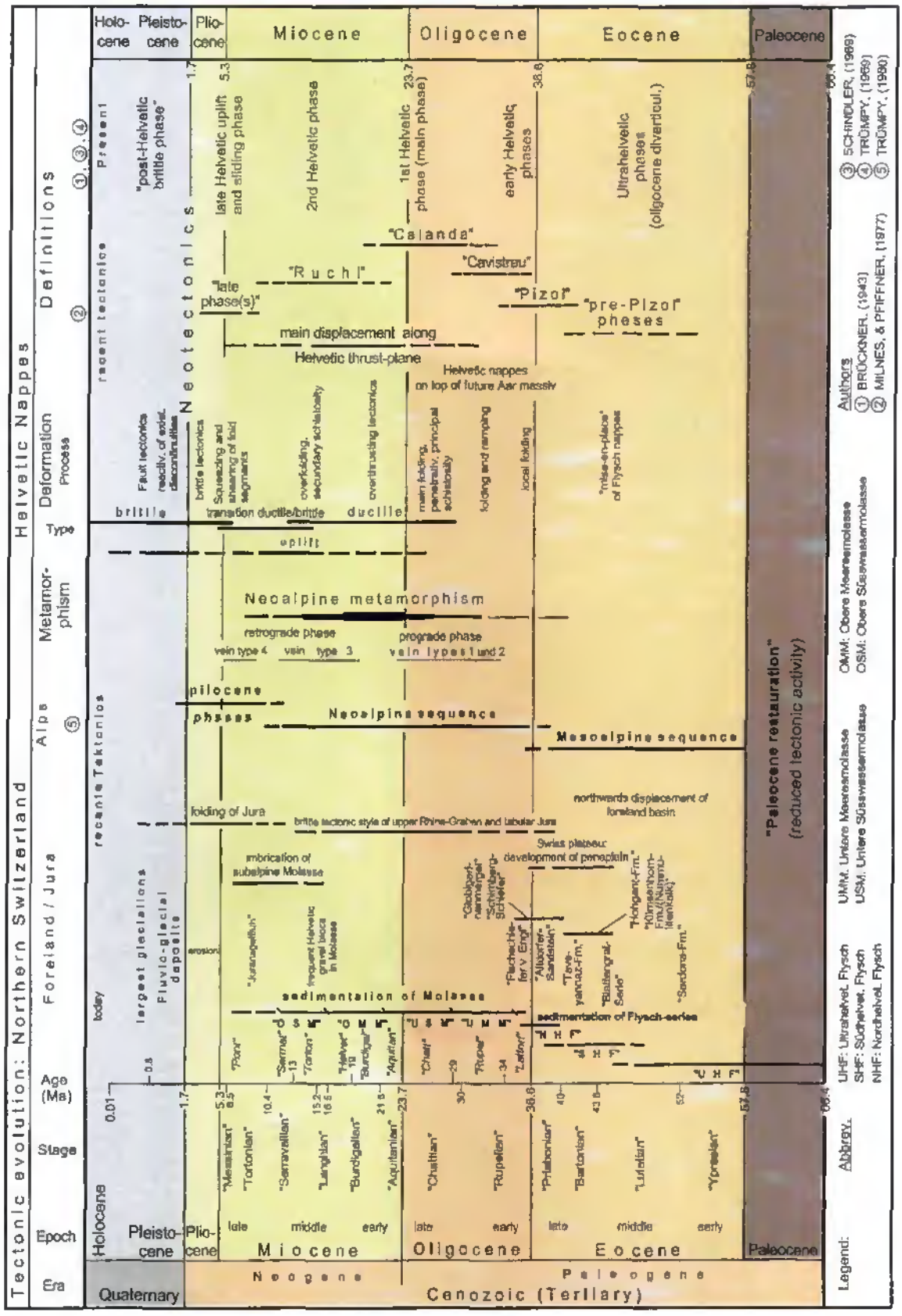

Fig. 4.2-1: Geological and tectonic evolution of the Helvetic nappes from the beginning of the Tertiary era (after NAGRA, 1997)

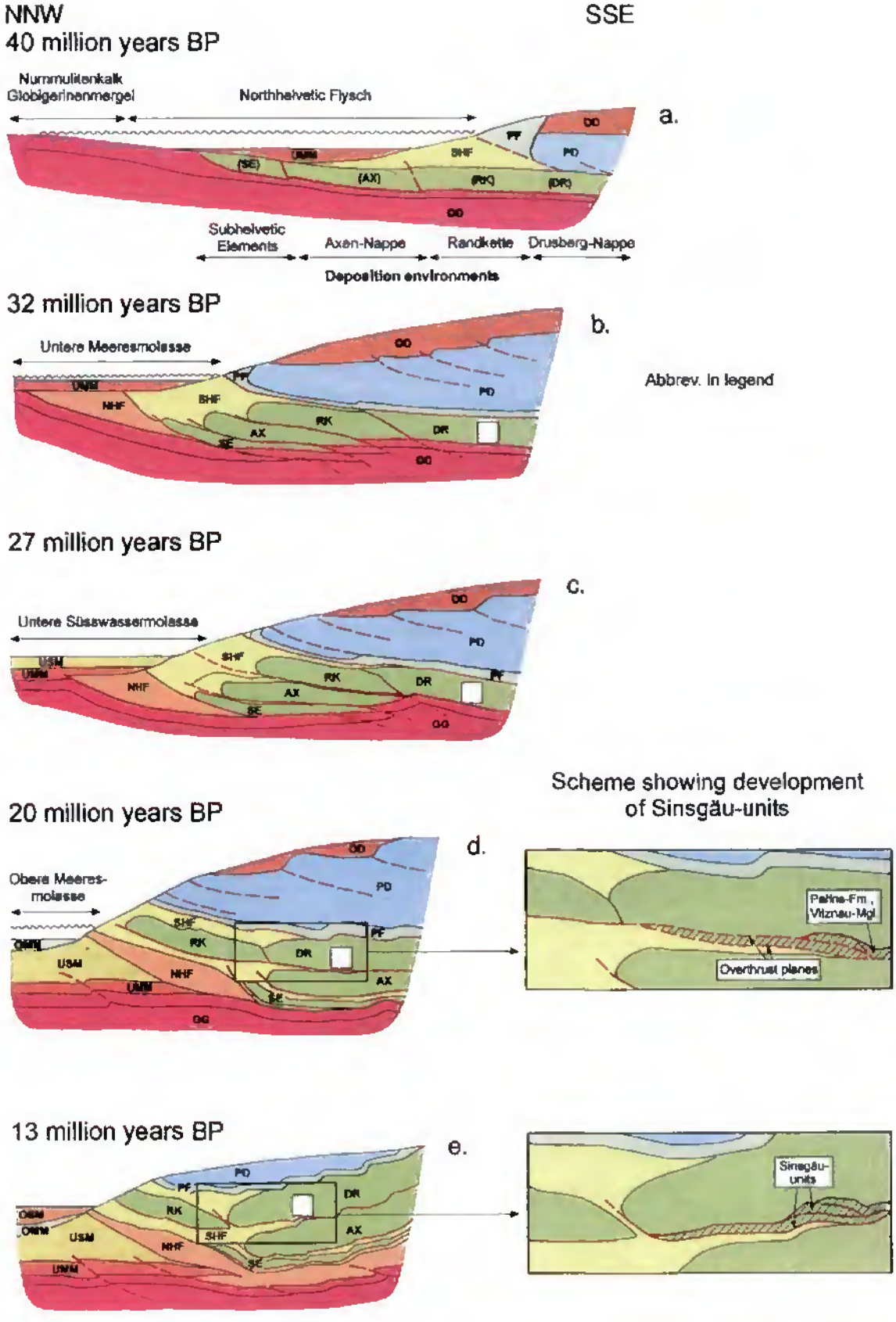

Fig. 4.2-2: Schematic evolution scenario of the most important tectonic units in the Central Alps (for details refer to NAGRA, 1997)

NNW SSE

7 million years BP

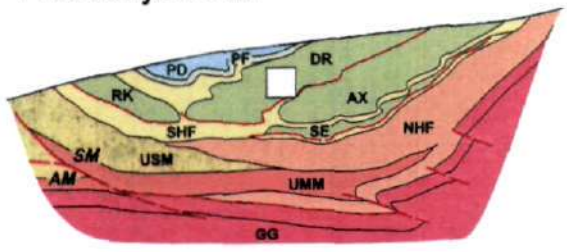

f.

today

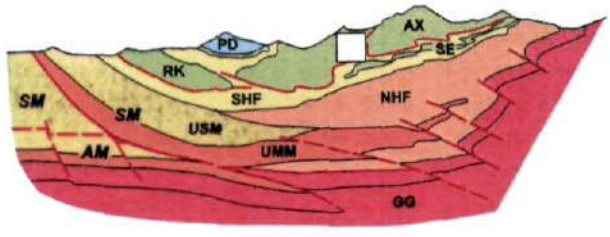

g.

without scale

Legend

- Obere Süsswassermolasse (OSM)
- Obere Meeresmolasse (OMM)
- Untere Süsswassermolasse (USM)
- Untere Meeresmolasse (UMM)

AM: Autochthone Molasse
SM: Subalpine Molasse

- Helvetic Nappes

RK: Randkette
DR: Drusberg-Nappe
AX: Axen-Nappe
SE: Subhelvetic Elements

- Northhelvetic Flysch (NHF)
- Southhelvetic Flysch (SHF)
- Pennine Flysch / Mélange (PF)
- Pennine Nappes (PD)
- Eastalpine Nappes (OD)
- Basement rocks (GG)
- Autochthonous sediment cover
- Crystallin
- Structural feature
- Location of the investigated aera

Fig. 4.2-2: continued

4.2.3 Current geological conditions at site-scale

The geological profiles in Section 2.2 (Fig. 2.2-4) reveal the strong anisotropy of the aquitard geometry and the complex tectonic structure of the Wellenberg site: While the WSW - ENE cut suggests an extent of the marl-shale aquitard of at least 15 km, the lateral extent is restricted to about 1 km only. This aspect ratio is perfectly consistent with the regional horizontal stress field (S_H oriented ± N 130°, as shown in Subsect. 3.3.5). The vertical thickness of the aquitard is between 1'000 m and almost 2'000 m, of which approximately 1/3 is below current sea level.

4.3 Petrogenesis and evolution of the groundwaters

4.3.1 Sedimentation and diagenesis

Most rocks were deposited in the Lower Cretaceous sea and during the Cenozoic era. Subsequent diagenesis led to compaction and lithification, the main effects of which were to reduce pore volume and to squeeze out connate porewater of marine origin. The first carbonatation originated during these times as a consequence of pressure solution (ankerite vein generation). Microfossils show that diagenesis did not fully recrystallise the rock matrix. Transport of dissolved matter occurred to a large extent within the formations of interest themselves.

4.3.2 Neoalpine metamorphism

Different geothermometers in combination (evolution of mineral parageneses, vitrinite reflection, microthermometry on fluid inclusions, etc.) allow determination of the pressure and temperature conditions prevailing during the peak of metamorphism. DIAMOND & MARSCHALL (1994) suggest a temperature range between 190 - 245° C and a corresponding pressure range of 40 to 270 MPa. Fluid inclusions (taken from carbonate veins) reveal large pressure differences fluctuating between lithostatic and subhydrostatic conditions. This large range has been explained by episodic deformation phases of a closed system, leading to opening veins and corresponding mineral precipitation. The fluid inclusions further reveal the co-existence of two immiscible fluid phases in the system: a methane-saturated, saline fluid and a CO_2 and methane gas phase; this is further confirmed by fluid analysis of geodes. It seems that both fluids originated within the rock matrix itself. This statement is of primary importance with respect to potential methane gas flow in the system.

4.3.3 Late neoalpine and post-neoalpine processes

After the culmination of neoalpine metamorphism, brittle deformation began. The corresponding cataclastic deformation produced tectonic discontinuities which overprinted the previous neoalpine, mostly ductile, features. The time sequence of brittle deformation is not well understood; it ranges from the early retrograde metamorphism up to the end of the Cenozoic era, probably occurring in multiple phases. However, to our concern, and based on isotopic analysis of carbon and oxygen isotopes in the latest calcite generation (carbonate veins), even brittle deformation could produce noticeable invasion by meteoric waters.

A lower estimate for the age of the first uplift movements of the Drusberg nappe and the "mise-en-place" of the limestone formations is of the order of 15 to 11 Ma BP. This corresponds to kinematic reconstructions by PFIFFNER et al. (1996). This age range clearly postdates neoalpine metamorphism and implies that the very old Na-Cl formation

groundwaters sampled in the vicinity of today's underpressure zone are at least 11 to 15 million years old. Other methods, for example analysis of fluid inclusions (MULLIS, 1996), also come to the conclusion that the Na-Cl groundwater type is composed to a large extent of fossil neoalpine (metamorphic) fluid, originally sea water, and modified by strong rock-water interactions. These brines are characterised by heavy water isotopes (^2H, ^{18}O), and their δ^2H - $\delta^{18}O$ pairs lie outside the GMWL (global mean water line). Interestingly, porewaters extracted from undisturbed core material of borehole SB4a/s by vacuum extraction show an increasing trend of δ^2H and $\delta^{18}O$ concentrations with increasing depth. This confirms the high degree of equilibration between water in the matrix and water sampled from water-conducting features. Furthermore, porewater samples are particularly important since they provide the only source of information for the conditions prevailing inside the underpressure zone.

The highest concentrations in Cl^- were obtained from SB1 samples: 7 to almost 17 g/l (about 0.2 - 0.47 molal). Dewatering of clay minerals as indicated by the reduction in δ^2H values is deemed responsible for the reduction in salinity of the groundwaters with respect to the original sea water.

Na-Cl groundwaters were also identified at Oberbauenstock in the same aquitard rock, and at one other location within the Helvetic domain, also in low permeability rocks (Amdener Marls, and Globigerina Marls in Sachseln, less than 10 km southwest of Wellenberg). These observations tend to confirm that the Na-Cl groundwater type is a hallmark of tight environments, at least for lithologies of the Helvetic domain.

Gas analysis also can be used to show isolation of the aquitard, since there is a positive correlation between gas concentration and residence time of groundwater. Although gas production in a deep-seated mother rock cannot be fully ruled out, it is, however, not very likely since free-flowing gas and gas inside the fluid inclusions exhibit the same isotopic composition, which indicates a common origin. Most gases were created during the Neoalpine metamorphic phase as indicated by their thermocatalytic origin (and temperature ranges above the oil-window). CH-type gases were produced by disaggregation of organic matter under anaerobic conditions. The increasing methane concentration with increasing depth is related to the greater solubility of gas with increasing formation pressure and to the lack of advective transport of the gas in low permeability environments (only diffusive transport possible). The same applies to Helium, which does not show production outside the aquitard. Even noble gases exhibit residence times of more than one million years. Another important indication is given by equilibration calculations. Assuming endogenous gas production, methane should be present today almost exclusively in dissolved form, which is - according to packer test results - the rule rather than the exception.

Younger deformation phases are postulated to reach within the time span of the last 6 million years BP. This time interval corresponds to the surrection of the Jura mountains, the last imbrication thrusting of the foreland Molasse basin and possibly to the last generation of calcite veins.

4.3.4 Evolution of groundwaters and gases

The transition from shallow young Ca-HCO_3 groundwaters, mixed with gas of predominantly atmospheric origin, to various intermediate types, of which the Na-HCO_3 is the most important, occurs within few years by cation-exchange. Therefore, the presence of Na-HCO_3 groundwater, representing a mixture of young and older waters, as sampled in the shallow part of the aquitard is indicative of advective flow which has contributed to the initial Na-Cl groundwater being substituted by invading Na-HCO_3 groundwater. This process is consistent with the depletion of methane and noble gases observed at these depth levels.

The deep Na-HCO_3 groundwaters below the aquitard show a distinct evolutionary process (infiltration 11'000 a BP, at the end of the last glaciation). From the isotopic data it can be excluded that contribution of Na-Cl water occurred. Therefore, the aquitard plays the role of a confining layer, not only hydrodynamically but also hydrochemically.

4.4 Quaternary evolution

4.4.1 Denudation, climatic changes and glaciations

4.4.1.1 Overview

During the last few million years, neotectonic movements are negligible when compared to uplift and tilting of entire tectonic units from the early Pliocene to the Cenozoic era. However, erosion has been enhanced during the Quaternary, especially because of the periodically recurrent ice ages. Each ice age excavated and widened valleys a step further, prograding from the Swiss foreland into higher levels of the alpine valleys as illustrated by the typical U-shaped valleys, of which the lower Engelberger Aa valley is a typical example.

4.4.1.2 Effects of glaciations on topographic relief and pore pressures

The Quaternary is well known in comparison to Miocene and Pliocene and comprises a high diversity of geomorphological events that potentially have altered the hydrogeological conditions in the marl-shale aquitard. 780'000 a BP (years before present) is defined by SCHLÜCHTER (oral comm.) as the "Mid-Pleistocene turning-point". Before this period, erosion was characterised by deep scouring into the foreland Molasse basin; after this period, the former topography is concealed by sediment accumulation. Glacier advances and retreats cause a direct change in pore pressure in the very low permeability ground and also amplify erosion, which contributes significantly to the removal of overburden and hence to a decrease in pore pressure.

Differential erosion[1] occurred primarily during the early glaciations, as illustrated in Fig. 4.4-1, and was concentrated essentially in the foothills of the Alps and along their edge. During later glacial events, the initially small narrow alpine valleys (located along structural weaknesses) were progressively widened and deepened by each glacier progradation. This evolution progressed from the exterior of the mountain range to more and more interior domains. Most glaciers removed deposits in the valley bottoms, often down to the bedrock, additionally provoking slope instabilities and thus numerous landslides during the Pleistocene.

A dramatic example of differential erosion is the extensive landslide of Altzellen on the western flank of the Eggeligrat, which, according to KLEMENZ (1995), collapsed downwards almost immediately after the retreat of the Engelberger glacier at the end of the penultimate glaciation. It seems, however, that the last glaciation did not noticeably affect the landslide structure and glacial tills of the previous glaciation, as indicated by careful inspection of the Quaternary intervals of borehole SB6 (SCHLÜCHTER, 1995). The reason for this "gentle behaviour" of the glacier is probably that the Engelberger Aa valley, in this specific section,

---

[1] differential erosion or retrogressive erosion are terms which address the process by which erosion progresses preferably on smooth rocks along valley floors, and from the exterior of a mountain chain to more and more interior domains

had already reached an equilibrated topographic profile (which is still not the case upstream, south of Grafenort, where the valley becomes extremely steep).

Based on recent findings (using modern radiocarbon dating methods, see SCHLÜCHTER & MÜLLER-DICK, 1996), it can be taken as understood that both advances and retreats of glaciers took place within a few centuries. For instance, the last glacier retreat was so sudden that the retreat of the local glaciers at Davos-Clavadel (altitude around 2'000 m a.s.l.) was synchronous with the retreat at Zurich (about 500 m a.s.l.).

It is also generally recognised that, in the alpine region, during the different glaciations most valley glaciers were so-called temperate glaciers, which means that bottom drainage of groundwater (at the interface between the rock surface and the sole of the glacier) was provided for most of the time during which an ice cap covered the valley floors and flanks (BOULTON & CURLE, 1997). The investigated region is situated at a short distance from the accumulation zone of the Engelberg and Bannalp-Sinsgäu glaciers. Therefore, the progression of the glaciers into the valleys occurred extremely rapidly, which rendered the development of a pervasive permafrost base impossible before arrival of the ice tongue. Locally, and especially during interglacial periods when the ice cap was lowered or even removed in some places, permafrost zones could develop and be maintained temporarily. Permafrost was extensive only in the Firn zone (above the level of permanent ice, i.e. higher than 1'400 m a.s.l. as stated by HAEBERLI, 1994).

Hence, acknowledging the presence of temperate glaciers, it can be deduced from the above statements that both glacier melting water and groundwater could drain freely at most locations and over most of the duration of the ice ages. Consequently, the overpressures generated in the ground by the glacier load could dissipate to a large extent even during the presence of the ice cap.

The old nomenclature (Würm, Riss, etc.) of the glacial and interglacial periods was completely revised by SCHLÜCHTER & MÜLLER-DICK (1996; Fig. 4.4-1). This new nomenclature has been adopted and supplemented wherever necessary for modelling purposes (Chap. 9).

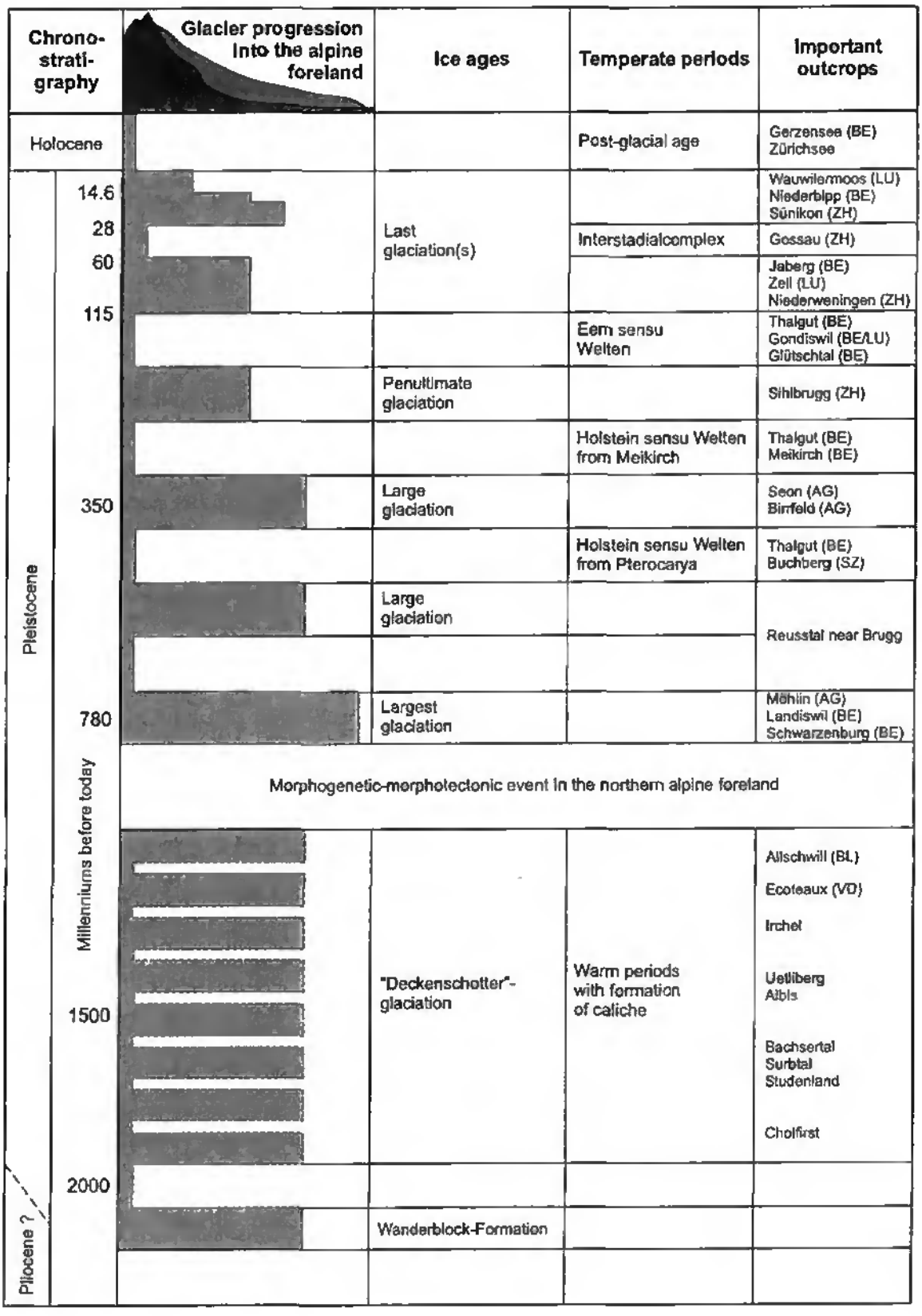

Fig. 4.4-1: Time table of glacier events

4.4.3 Future evolution

Qualitative statements regarding possible evolution of the hydraulic underpressures depend strongly on the postulated generation mechanism. If the glacial hypothesis is assumed, the hydraulic pressures in the ground will change dramatically with respect to today. On the other hand, if ongoing erosion is considered more likely, hydraulic underpressures will still be temporarily affected by the glacial loading, but to a lesser extent than in the former case. These aspects will be discussed more in detail in Chapter 11 and to some extent also in Chapter 12.

Forecasting the evolution of hydrogeological conditions in the aquitard depends strongly on the climate variability during the estimated time interval and the evolution of tectonic forces. The currently observed uplift rate of about 1.5 mm/a in the Alps with respect to the Swiss plateau will probably remain constant in the next 100'000 a.

Climatic conditions control erosion, but erosion also depends on the regional erosion basis. For the Engelberg region, as for almost all of Central Switzerland, erosion is controlled by a hard rock threshold on the river Reuss at Lucerne. Assuming an uplift rate of 0.55 mm/a for Wolfenschiessen, and relating this rate to the rate measured in Luceme, i.e. 0.35 mm/a, the uplift difference between the controlling erosion level and the investigated site is only of the order of 0.2 mm/a, which is deemed negligible for a period of 100'000 a.

KLEMENZ (1993) derived five basic potential climatic evolution scenarios for the Wellenberg site, which are summarised in Tab. 4.4-1. These scenarios do not consider likely climatic trends but try to identify hazardous (i.e. conservative) climatic conditions for a potential repository, and therefore also for the integrity of the corresponding aquitard rock.

These scenarios aim at covering all possible future climatic conditions. For all cases, the threshold at Lucerne is the factor which governs local erosion. Therefore, the evolution of the sedimentation in Lake Luceme (deltas), and the potential for filling the Lake with sediments, is of primary importance because, from then on, the threshold on the Reuss river itself will become eroded. This in tum will shift and lower the base-level for erosion towards the north, i.e. towards Basel on the River Rhine.

Addressing the details and postulated effects of each of these five erosion scenarios is well beyond the scope of this thesis. However, the following processes and parameter evolutions should be kept in mind for discussion in Chapter 12:

1. Local erosion will preferentially affect valley floors of the Engelberger Aa and Secklisbach valleys and the soft rock formations such as the marl-shale aquitard. Consequently, the relief and, therefore, the hydraulic gradient between (eroded) aquitard rock and comparatively hard rock outcrops (chiefly limestone formations of the Axen and Drusberg nappes) will increase, sometimes considerably.

2. Almost independently of the climatic evolution scenario considered, erosion will continue to promote the inwards expansion of the decompaction layer existing in the upper levels of the aquitard. Decompaction is a process acting essentially on rock discontinuities and on pre-existing microfractures by progressively widening the pore space and therefore enhancing permeability. The more the decompaction zone progresses downwards, the more the volume and duration of the UPZ will be reduced as a result of two parallel processes: the increase in diffusivity and the decrease of the distance to a high permeable boundary.

3. In the likely case of a forthcoming glaciation, possibly shifted by several thousand years due to human influence on climate, hydraulic underpressures will be buffered in general and temporarily compensated or reversed locally by the pressure due to the increasing ice load on top of the aquitard. However, at the beginning of the next interglacial era, underpressures will develop again.

4. Strong erosion due to humid climate or differential uplift movements are rather unlikely in view of the past climatic fluctuations.

Tab. 4.4-1: Long-term evolution scenarios (after NAGRA, 1997)

Scenario	Climatic conditions, duration (at most 100'000 a)
1	Same climatic conditions as today
2a [2]	Ice age of the magnitude of the last glaciation, duration 60'000 a case 1 – no excavation up to bedrock in the Engelberger Aa valley and in the landslide of Altzellen during the next glaciation[1] – position of the lacustrina delta in Buochs/Stansstad unaffected by next glaciation case 2 – excavation of the Engelberger Aa valley up to Stans during the next glaciation – deep erosion of the valley bottom up to 50 m below the basis of the landslide of Altzellen case 3 – excavation of the Engelberger Aa valley during the next glaciation up to Buochs/Stansstad – deep erosion of the valley bottom up to 50 m below the basis of the Altzellen landslide
2b [2]	Postglacial period as today, after completion of scenario 2a, duration: 40'000 a
3	semi-arid climate only seasonal vegetation with strong rainfalls
4	arid climate evaporation above Lake Lucerne > inflows → decrease of Lake level
5a/b	tropical climate with strong precipitation scenario 5a: natural vegetation scenario 5b: vegetation disturbed by human activity

1) SCHLÜCHTER (1995), based on evaluation of basal moraine core material in borehole SB6, concludes that these sediments have been overridden by the ice mass of the last glaciation and preconsolidated. However, the last glaciation disturbed the sequence only negligibly, i.e. did not produce significant valley excavation.

2) this scenario is still based on the classical Würm ice age (it was elaborated before the new nomenclature), which is of negligible consequence with respect to duration of ice-free and glacial periods.

5 HYDRAULIC UNDERPRESSURES WORLD-WIDE: COMPARISON WITH THE WELLENBERG SITE

5.1 Treatment of abnormal pressure in the literature

The topic of abnormal pressure has been an active area of research from the moment the first scientific basis for petroleum exploration was set up at the turn of the century. The definition given by DOMENICO & SCHWARTZ (1990) - "Abnormal pressure study is a study of competing rates of pressure production and dissipation." - summarises perfectly the challenge geoscientists face when dealing with this phenomenon[1].

Rock formations exhibiting abnormal hydraulic pressure conditions have been observed increasingly world-wide in the dynamic upper crust of the lithosphere. Reported cases of hydraulic overpressures are far more frequent than those of underpressures, due to the fact that overpressures represent a key issue for oil and gas exploration (overpressures make pumping of oil or gas superfluous, but also represent a major hazard for drilling operation if not detected early enough or if the mud density is too low to prevent blowouts (PERRODON, 1983; POWLEY, 1984; MOUCHET & MITCHELL, 1989; FERTL et al., 1994).

In comparison, fewer cases of hydraulic underpressures, which are to some extent comparable with the situation at Wellenberg, are described in the specialist literature. This does not mean that hydraulic underpressures are a rarity by definition. It shows rather that, since subnormal pressure is often a hallmark of low to very low permeability sediments, economic interest in exploring tight rocks is far more limited than oil and gas exploration. It is only in the last two to three decades that advances have been made in this field, primarily for the investigation of potential sites for toxic or radioactive waste disposal (BRADLEY, 1975, 1985; BREDEHDEFT & HANSHAW, 1968; JIAO et al., 1997). The oil industry has only recently shown growing interest in characterising tight units using direct methods in order to obtain better control over reservoir characteristics and especially reservoir boundaries and leakage.

The common classification relates overpressures to young, actively subsiding basins (Gulf Coast, South Caspian basin), while underpressures are rather restricted to older, uplifted basins or continental interiors (Denver basin, Southern Alberta) without active subsidence for tens or hundreds of million years (DEMING, 1994). NEUZIL (1995) notes that "the most extensive low-permeability regions are associated with Cretaceous shales in the foreland basins of the Rocky Mountains." He also ascertains that "relatively few disequilibrium pressure regimes have been reported in environments where permeable units are rare or absent." Among exceptions to this statement, NEUZIL (1995) cites the Pierre Shale and Wellenberg[2].

The great majority of reported over- or underpressures are extrapolated data from drill stem tests performed in borehole sections with comparatively high permeabilities (sand lenses in tight clayey formations, reservoirs or high permeability formations immediately beneath an aquitard) or are inferred from indirect borehole geophysical methods (NEUZIL, 1994). Consequently, it is not surprising that most of the world-wide surveys on abnormal pressure relate to oil and gas fields, i.e. to more or less actively subsiding sedimentary basins and to non-metamorphic or very low grade metamorphic rocks of Tertiary age or younger (DEJU,

---

1 agree to this definition those scientists that consider that abnormal pressures are transient. For those who believe in "permanent" or almost permanent pressure seals, this definition is of course unacceptable.

2 obviously, Wellenberg follows the rule rather than the exception

1973, cited by DOMENICO & SCHWARTZ, 1990). However, these studies are of interest to scientists dealing with underpressures because most of the authors did not restrict their curiosity to recording case studies. They also tried to find explanations for the observed pressure anomalies. Among the postulated mechanisms, some are also of interest for this study of underpressures. Even information on geological processes and environments which can be excluded or considered very unlikely for the generation of underpressures might reveal interesting aspects. By examining the common denominators and also the differences between overpressure and underpressure situations, conceptual models of the problem at hand can be progressively improved.

Another important issue is the duration of the pressure anomaly which, according to many authors, may survive "and be in transient state for hundreds to millions of years, thus appearing anomalous at the time of observation..." and "... may be considered therefore as slowly attenuating relicts from bygone geological times" (TÓTH & MILLAR, 1983). It is, however, difficult to believe in that large time ranges, unless geologic forcing is acting. On the other hand, specific characteristics of overpressured rocks such as undercompaction (overburden effect), clay mineral, sulphate and evaporite diagenesis, petroleum genesis (organic matter transformation), carbonate compaction, most osmotic phenomena and, particularly, porosity reduction due to burial metamorphism may be disregarded since they are obviously specific to abnormally high formation pressure, i.e. they do not have a counterpart during erosional exhumation (NEUZIL, 1986; HAXBY & TURCOTTE, 1976). While mechanical effects produce hydraulic pressure anomalies which are to a large extent reversible, heating of the rock skeleton produces expansion by opening microcracks and fractures, which enhance porosity and permeability in an irreversible way. Cooling is not the exact reverse of heating since it will not dramatically affect the rock framework as heating does, which means that its effects are reversible. Therefore, cooling essentially produces contraction of the pore fluid, contributing to the generation or maintenance of underpressures (Chap. 7).

5.2 Review of underpressured rock formations

The review of occurrences of underpressured formations presented here does not pretend to be comprehensive. The only objective is to briefly describe some relevant settings in order to prepare for comparison with the Wellenberg case discussed in Section 1.3. To classify abnormal pressure occurrences with respect to the type of abnormal pressuring is virtually impossible in most cases, because either a single site may involve different types of abnormal pressures or the abnormal pressure type itself may result from a combination of sometimes competing processes, which particular effects cannot be assessed (NEUZIL, 1995). Most even apparently simple pressure anomalies may result from a complex interaction of mechanisms and of geological events. Not infrequently, the evolution history is extremely complicated, consisting of alternating periods of quiescence, uplift and deformation or erosion and/or competing processes acting simultaneously. The sometimes perplexing patterns of both high and low abnormal pressures probably originate from these complexities. At Wellenberg, for instance, hydraulic underpressures and overpressures both occur in the deep boreholes SB1 and SB3. Even if the hydraulic overpressures can be explained by regional groundwater flow, there is absolutely no certainty that this simple model applies (NAGRA, 1997).

DICKEY & COX (1977) reviewed some underpressured reservoirs. Amongst others, they cite the Hugoton Gas Field (Texas). This field has been analysed by JIAO et al. (1997) to evaluate the potential for injection of liquid wastes. HUNT (1990) provides a relatively long

list of similar and additional occurrences. LAW et al. (1989) describe underpressures in the Piceance basin, a coal-rich formation. BELITZ & BREDEHOEFT (1988) cite the San Juan basin in New Mexico, the Denver basin (Colorado and Nebraska), the Alberta basin in Canada, the Arkoma basin in Arkansas, the Appalachian region, the Anadarko basin in Oklahoma, the Palo Duro basin, studied intensively by SENGER & FOGG (1987), and even the southern Siberian platform below the permafrost layer.

Of all these contributions, the papers by NEUZIL (1993, 1995) on the Pierre Shale formation, the contribution of TÓTH & CORBET (1986) on the Taber area in southern Alberta and the recently performed study by PARKS & TÓTH (1995) are probably the most valuable for comparison with Wellenberg for two main reasons: the described underpressured formations are - to our knowledge - the only ones for which direct and reliable pressure measurements exist and, in these formations, the underpressures are of a similar order of magnitude to that at Wellenberg. For instance, PARKS & TÓTH (1995) provide interesting data for comparison:

- the zone of strongest underpressuring is located 500 - 1'000 m b.g.
- the head deficit is around 6 MPa
- denudation has removed between 1'600 m and 3'000 m of sediment overburden in the last 60 million years, which results in erosion rates of the order 0.3 - 0.7 mm/a.
- fluid flow seems to be directed towards the area of greatest erosional removal.

SENGER & FOGG (1987), studying the deep brine aquifer in the Palo Duro Basin (Texas), note that this basin was uplifted and tilted during the Cenozoic (10 - 15 Ma BP). The maximum head deficit (with respect to hydrostatic) is 6.89 MPa (nearly 700 m), of which 250 m head deficit is attributed to the erosion of a caprock escarpment. However the major mechanism is considered to be epeirogenic movements, with only a minor contribution from erosional unloading.

Hydraulic underpressures were found also in Switzerland and on the German border. These cases are reported in Section 5.4. Underpressure phenomena are not restricted solely to deep geological formations. Subnormal pressures may also exist in shallow terrain, as exemplified by the clayey hill of Bisaccia in Southern Italy. At this site, periodically occurring shallow slides provoke disequilibrium pressures (FENELLI & PICARELLI, 1990). Similar cases have been reported by KOPPULA & MORGENSTEIN (1984) in the United States and Canada, by BROMHEAD & DIXON (1984) and VAUGHAN & WALBANCKE (1973) in coastal cliffs of London Clay. Finally, abnormal pressure is not restricted to natural rocks only, as exemplified by abnormal pressures temporarily measured inside the concrete wall structure of a retention dam as a response to changes in the level of the reservoir lake (KLEMENZ, *oral. comm.*).

NEUZIL (1995) summarises his observations on abnormal pressure by stating that abnormal pressures occur "in flow regimes that are both equilibrated and disequilibrated hydrodynamically". By "equilibrated", he means flow regimes which are adjusted to geological and hydrogeological surroundings and in which pressures result from topographically driven flow or non-hydraulic gradients, as resulting from osmosis for instance. This type of situation has been described in great detail by TÓTH (1979a) and by BELITZ & BREDEHOEFT (1988). The Wellenberg is most probably a typical case of disequilibrium pressure, i.e. a non-adjusted flow regime, that is why this hypothesis is treated preferentially in the following.

Finally, as shown by literature review, the few descriptions of occurrences in the Alps or discussions of potential abnormal pressures in the alpine belt describe or predict

overpressures, for the Po plane for instance (DEJU, 1973). With the notable exception of Nagra's investigations, no reported case of underpressures could be identified in the Alps or in any other orogenically active region of the world (e.g. Japan, New Zealand, Himalayas).

5.3 Similarities with and differences from Wellenberg

A comparison of the occurrences described in the literature reveals interesting similarities with, and differences from, Wellenberg.

5.3.1 Similarities

1. Rock formations exhibiting underpressures systematically show little to very little hydraulic conductivity on larger scales (hectometre to kilometre), which does not exclude local inhomogeneities (e.g. highly permeable sand lenses, isolated or poorly connected fractures, etc.).
2. Underpressures are usually encountered in relatively large sedimentary basins and thick stratigraphic sections under comparatively high thickness of overburden. A remarkable lithologic feature is the large proportion of clay minerals in most formations. However, the presence of clays does not seem to be an absolute condition, as shown by the case of Bois de la Glaive (Subsect. 5.4.2).
3. Where hydrochemical data are available, the hydraulic underpressures correlate with very long residence times of the groundwater.
4. Along boreholes, the magnitude of the hydraulic underpressures correlate negatively with the transmissivity or inferred hydraulic conductivity distribution.
5. The observed sections show, in sufficiently deep boreholes, a clearly noticeable head minimum that, for instance, lies around the middle of the corresponding geological formation (aquitard). This was the case at Wellenberg, as well as in the Pierre Shale (South Dakota, USA) and in the Red Earth Region (Central Alberta, Canada; MAGARA, 1981).
6. Most authors cite the decrease of overburden caused by either denudation (superficial erosion) or differential erosion (enhancement of valley relief) as the governing mechanism for the origin of subnormal pressures.

5.3.2 Differencas

1. Except for the occurrences explored by Nagra at Wellenberg, Oberbauenstock, and Bois de la Glaive, almost all other underpressure occurrences are situated in tectonically calm regions of the world, where the stress field is dominated by the weight of the overburden ($S_v > S_H > S_h$). Strong horizontal compressive stress components like those at Wellenberg are virtually absent. If any horizontal effects are noticed, they are due rather to lateral expansion of the basin. Basins are often referred to as "intracratonic basins" as opposed to actively subsiding basins, for example the Gulf of Mexico, which tend rather to exhibit overpressures (LEFTWICH & ENGELDER, 1994).
2. The sites of underpressures referred to in the specialist literature as "aquitards" (NEUZIL, 1995) or exaggeratedly as "aquicludes" are mostly overlain by massive overburden strata. At Wellenberg, however, the marl-shale aquitard is partially eroded and forms several outcrops (Eggeligrat, Sinsgäuer Schonegg) of weathered rock.

3. In the case of Wellenberg and Oberbauenstock, highly conductive rock units (limestone formations) form the lateral boundaries to the marl-shale aquitard, which is actually sandwiched between them. As a result, high aspect ratios of aquitard geometries prevail. In the case of large sedimentary basins, the lateral boundaries are most often not recognised directly but assumed to lie at a greater distance away (at least several tens of kilometres from the borehole locations). Instead of lithologic discontinuities, it is assumed that structural features (faults, etc.) cause the interruption of the continuity of both aquitard and UPZ (NEUZIL, 1986, 1995). The distance between available reference boreholes and the probable exfiltration zones is often in the order of several tens to hundreds of kilometres.

5.4 Underpressure occurrences in Switzerland

5.4.1 Oberbauenstock

In 1987, Nagra investigated the Palfris Formation and the Vitznau Marls of the Drusberg nappe as a possible marl-shale aquitard at the potential repository site of Oberbauenstock (Canton Uri). Oberbauenstock is only about 16 km east of Wellenberg and is located in more or less the same lithologic and structural setting as the latter. Oberbauenstock was the first location where Nagra observed subnormal pressures in boreholes (KENNEDY & DAVIDSON, 1989). Three exploration boreholes were drilled underground from a ventilation gallery, close to a recently excavated motorway tunnel. Abnormally low pressures were measured in the deepest borehole, about 300 m below the level of the gallery, in which - locally - gas and water inflows were observed. This discovery was explained primarily by gas flow into the borehole and depletion of a high-permeability zone of limited extent. Two distinct conceptual and numerical two-phase flow models (groundwater and natural gas) were set up (NAGRA, 1988). Model B attempted to explain the underpressures by regional gas flow, while the preferred model A considered the degassing of methane as a consequence of the excavation of the Seelisberg highway tunnel in the first half of the seventies as the most plausible explanation. The pressure drawdown, caused by the underground opening, was believed to be strong enough to produce the exsolution of initially dissolved gas in the groundwater. The underpressures would be a consequence of the higher mobility of gas with respect to water, since gas would escape easily while the wetting phase took some time to refill the pore space left by the gas (MISHRA et al., 1993).

The circumstances at Wellenberg are comparable in many respects with those at Oberbauenstock since the same tectonic units occur in approximately the same position. The main difference is that, at Wellenberg, the deep boreholes were drilled from ground level, whereas at Oberbauenstock shallow boreholes were drilled from an underground ventilation shaft. Therefore, the pressure data inferred from packer tests at the latter site are much more likely to have been affected by transient effects associated with the underground openings. The lower concentrations of free gas (i.e. not dissolved in groundwater under the prevailing pressure conditions) noticed at Wellenberg, in comparison with Oberbauenstock, are probably due to the absence of artificial disturbance at the former site.

Finally, the head minima at Wellenberg (SB1: approx. 140 m a.s.l.; SB3: approx. 0 m a.s.l., NAGRA, 1997) are so dramatically low that no corresponding exfiltration region can exist. The same situation had already been observed at Oberbauenstock, although the local head minimum of 357 m a.s.l. is somewhat higher than at Wellenberg (NAGRA, 1988); it

cannot, however, be explained by exfiltration into the nearby Umersee, which is an arm of Lake Lucerne (Vierwaldstättersee, middle lake mirror at 434 m a.s.l.).

5.4.2 Bois de la Glaive

Besides Oberbauenstock and Wellenberg, Nagra also measured underpressures at Bois de la Glaive on the north rim of the lower Rhone valley, some 5 km upstream of Lake of Geneva (NAGRA, 1993b). The target rock for radioactive waste disposal at this site was anhydrite under a continuous alteration cover of gypsum between 10 and more than 100 m thick. From the floor of the lower Rhone valley, two "deep" piezometers were installed in cored boreholes. In one of these piezometers (AN13), approx. 130 m deep, anhydrite was encountered at 45 m b.g. below a gypsum cap rock about 17 m thick, itself covered by 26 m of Quaternary deposits (essentially glacial tills and fluvio-lacustrine sediments). The water level of the anhydrite interval equilibrated itself at a level of 287 m a.s.l., which is significantly below the level of Lake of Geneva (372 m a.s.l.). However, the same observation could not be repeated in the 300 m deep piezometer (ON 9), owing to the very low hydraulic conductivity of the anhydrite. At the end of the measurement period, the equivalent freshwater level had still not stabilised and was decreasing slowly but steadily. The last measurements indicated a groundwater level only few metres above lake level. It is therefore likely that underpressures exist there also.

The interpretation of this occurrence ranges from perfect isolation of the anhydrite from the shallow groundwater level in the gypsum and the Quaternary deposits (which by itself is not an explanation) to invasion of low salinity borehole fluid into the fissures and voids of the anhydrite aquitard, thus causing dissolution of rock and widening of pore space. Since no further analysis was possible, the question remains open. It is, however, likely that this hydrodynamic system still lags behind the pore pressure release due to the melting of the Rhone glacier some 12'000 years ago.

5.4.3 Other occurrences

Nagra also recorded and re-interpreted borehole information from the northeastern part of Switzerland and the German border, focusing essentially on sediments from the Muschelkalk to the Malm, in preparation for the Opalinus Clay (part of the Dogger era) drilling campaign (EHRMINGER et al., 1995). The re-interpretation of the database, comprised of packer tests performed in the sedimentary sections of Nagra's own boreholes at Riniken, Schafisheim and Weiach and of drill stem tests conducted in four oil and gas exploration boreholes, tends to indicate that very low heads may exist in the Dogger. The best estimate for the corresponding hydraulic conductivity in the Opalinus Clay varies between $8 \cdot 10^{-14}$ m/s and $4 \cdot 10^{-13}$ m/s. To explain these anomalous heads, EHRMINGER et al. (1995) - based on the very low hydraulic conductivity and the typical mineralogical characteristics of this clay (very small pore size, cation exchange capacity) - consider that the Opalinus Clay may give rise to non-hydraulic flow phenomena[1], i.e. effects that cannot be explained by Darcy's flow equations.

---

[1] non-hydraulic phenomena are meant in the terminology of NEUZIL (1986) and are described by MARINE & FRITZ (1981), TÓTH & MILLAR (1983), and HORSEMAN et al. (1991).

5.5 Inferences

From the observed similarities and differences it can be deduced, with due caution, *that only a few geological conditions must be met for hydraulic underpressures to result.* The following are required:

1. Relatively thick sediment accumulations, which have been consolidated or even overconsolidated into a rock mass whose mechanical behaviour under further loading or unloading can be validly approximated by (linear) elastic deformation.
2. A succession of geological events that produce an unloading of the rock mass and consequent rebound of the rock skeleton.
3. Complex geological conditions (tectonic folding and overthrusting) and compressive tectonic fields seem to be no obstacle to the generation of hydraulically subnormal pressures, as the examples of Wellenberg, Oberbauenstock and Bois de la Glaive in the Alps and Prealps show.
4. All authors recognise that, in order to maintain anomalous heads over significant periods of time, a certain "isolation" of the formation in which the head enomaly has been observed is necessary (e.g. NEUZIL, 1995). Where opinions clearly diverge is in the interpretation of the term "isolation" (see Sect. 5.6).

5.6 Static or dynamic conceptualisation of abnormal pressures

Authors can be divided grosso modo into two categories according to BREDEHOEFT et al. (1994):

- the *static school* represented almost exclusively by petroleum geologists such as POWLEY (1984), BRADLEY (1975), HUNT (1990) and GRETENER (1993), who uses the term "geopressures" to define abnormal pressures
- the *dynamic school* comprising leading hydrogeologists such as TÓTH, BREDEHOEFT, NEUZIL.

Up till now, for many petroleum geologists the origin of isolation is due to so-called "pressure seals". They consider that HUBBERT's (1940) theory of groundwater motion is not applicable at great depth or that if Darcy's law is applicable, hydraulic conductivity is close to zero as exemplified by HUNT's statement (HUNT, 1990): "fluid pressures were discovered that were either too high or too low to be attributed to fluid flow to or from the surface". The pressure seals are considered as more or less impervious boundaries delimiting flow domains. DEMING (1994) defines a pressure seal as a "rock layer capable of confining anomalous pressure over geologic time" and HUNT (1990) as "a zone of rocks capable of hydraulic sealing, that is, preventing the flow of oil, gas and water." Commonly, a seal is supposed to be tight for at least one million years. HUNT further states that "even a very slow drainage mechanism would eliminate overpressure differences over short geological time periods for most rocks". Pore pressures are thus "relict features" of a remote past, commonly referred to also as "paleopressures". The underground at great depth is constituted of pressure seals delimiting fluid compartments of different relative formation pressures. The alternation of highly pressured and subnormally pressured sequences in deep oil exploration wells is explained by this static paradigm of pressure compartmentalisation.

The opposite opinion is defended by the great majority of hydrogeologists, who are, by definition, confronted with groundwater flow, i.e. with flow dynamics. They consider that

almost no natural rock is absolutely tight, except pure halite (BREDEHOEFT et al., 1994; NEUZIL, pers. comm.). The fact that formations exhibiting contrasting pore pressures co-exist or that subnormal or supernormal pressures exist in some formations is considered not as proof that flow conditions remain invariable, but as evidence for strong hydraulic gradients. By definition, hydraulic gradients are representative of flow and flow (for example cross-formational flow) will tend to compensate anomalous pressures up to reaching pressure head conditions that are conform to contemporaneous topographic and/or tectonic conditions (which is not necessarily synonymous of hydrostatic). In the early eighties, this group formed a movement which considered that most abnormal pressure phenomena are due to differences in topography or to regional groundwater flow patterns (BREDEHOEFT, TÓTH) and a movement for which changing boundary conditions or heterogeneities in the flow domain cannot account for most observations without additionally considering the rebound of the rock skeleton. This approach was advocated by various hydrogeologists, among them essentially NEUZIL and CORBET, who based modelling on coupled hydraulic-mechanical processes. The increasing number of hydrogeologists who apply hydraulic-mechanical coupled models when studying abnormal pressure phenomena speaks for the efficiency of this approach.

However, only the standard diffusion equation is needed in those cases where the generating mechanism can be considered as being terminated, i.e. the driving force must no longer be considered. The time required for dissipation of positive or negative excess pore pressure is a function of the rock intrinsic diffusivity and the distance to the nearest drainage boundary. For very low permeability thick aquitards, the dissipation of anomalous heads will take up to millions of years. This in turn constitutes a serious problem, since it is seldom possible to determine if the generating mechanism is still acting or not. NEUZIL (1995) considers that hitting a time window in which the geologic forcing has vanished, but in which the decaying abnormal pore pressures are still noticeable, is very lucky. This statement is of course meant in a broad sense and in the context of a conceptual model assuming long-lasting erosion of sedimentary basins. At Wellenberg, however, it is likely that the current observations reflect a dissipation stage, especially if the dominant mechanism is glacier rebound (see Chap. 9).

AS PARKS & TÓTH (1995) demonstrate, strong hydraulic gradients from the interior of an UPZ towards its envelope imply flow in the opposite direction, and flow is irreconcilable with pressure compartments. However, it is necessary to point out that the fluxes involved are extremely small, even for strong underpressuring. This aspect deserves consideration, since strong hydraulic gradients are often misunderstood and erroneously considered as proof of high flow rates and rapid replenishment of an underpressure zone. This applies to petroleum geologists, as seen from the above discussion, but also to performance assessors. Therefore it makes sense to explain at length that underpressure zones are indeed able to sequester water and solutes effectively for long periods of time and that, as indicated by NEUZIL (1995), the rate of fluid transport is, in many cases, "comparable to - or indistinguishable from - that of diffusive solute transport in porous media."

6 APPROACH TO THE INVESTIGATION OF HYDRAULIC UNDERPRESSURES

6.1 Fundamental considerations on the origin of underpressures

The differences in two-phase flow characteristics at Oberbauenstock and Wellenberg, as well as the divergent explanations for the observed underpressuring between the two sites, gave rise to an investigation programme aimed specifically at trying to explain the reasons for the observed pressure anomaly at Wellenberg. Different working hypotheses, considered with the same priority at the start of the investigation, were identified and explored sequentially (VINARD & MCCORD, 1991). The arguments for or against each individual hypothesis were tested and compiled by specialised scientists. Their conclusions were reviewed by internationally recognised experts (VINARD & MCCORD, 1994). The extent of this examination and the procedure followed are shown in Fig. 6.1-1. The basic findings and conclusions are as follows:

1. The hydraulic underpressures measured in situ correspond to the effective physical state of the groundwater in the marl-shale aquitard. They are only slightly influenced by measurement errors. This conclusion was later supported by independent long-term measurements of the head levels in selected isolated straddle intervals (multipacker systems installed in the wells at the end of the investigation programme; NAGRA, 1997).
2. The origin of the more frequent occurrences of overpressures observed world-wide can be explained by rapid loading of a tight and compressible rock mass saturated with a fluid, e.g. water, oil (artesian pressure conditions in confined aquifers are not considered here). A thick sedimentary water-saturated stratum that becomes compressed through rapid strong accumulation of sediments in a subsiding basin can serve as an exemplary geological model. Its interstitial water (porewater) cannot leak out (or only very slowly) because of the low hydraulic conductivity (and in that case the great distance to the nearest water-conducting feature) and it therefore supports the overburden by taking on an appreciable amount of the normal stress (NAGRA, 1997).
3. The most plausible process at Wellenberg is coupled hydraulic-mechanical rebound due to the elastic behaviour of the water-saturated rock. After compaction and lithification, decompaction of the marl-shale framework occurred, manifesting itself by dilation of the (water)-saturated pores. Decrease of the external stress under assumed elastic conditions results in a departure from equilibrated (often hydrostatic) pressure in the pore space. In most soils and rocks, relaxation of disequilibrium pressure is almost instantaneous. However, in low to very low permeability environments, the re-equilibration of the pore pressure will be delayed, sometimes considerably. Such a conceptual model is compatible with all previous direct and indirect observations and measurements at Wellenberg and provides a comprehensive and plausible explanation for the existence of subnormal pressures (Chap. 7).
4. Other possible explanations for the phenomenon, such as free gas flow or chemico-physical effects (osmosis, swelling i.e. dilation of clay minerals) are too insignificant or even counteract underpressures. They are therefore either disregarded or are considered - at best - as modest contributions, which, if neglected, do not strongly influence the model results.

6.2 Procedure for inspection of the different working hypotheses

In view of the long and complex geological history of the Central Alps, it must be acknowledged that the marl-shale aquitard was subject to numerous loading and unloading

cycles. For conceptual and numerical models, this implies that, as far as possible, representative and well quantifiable events have to be selected within defined periods.

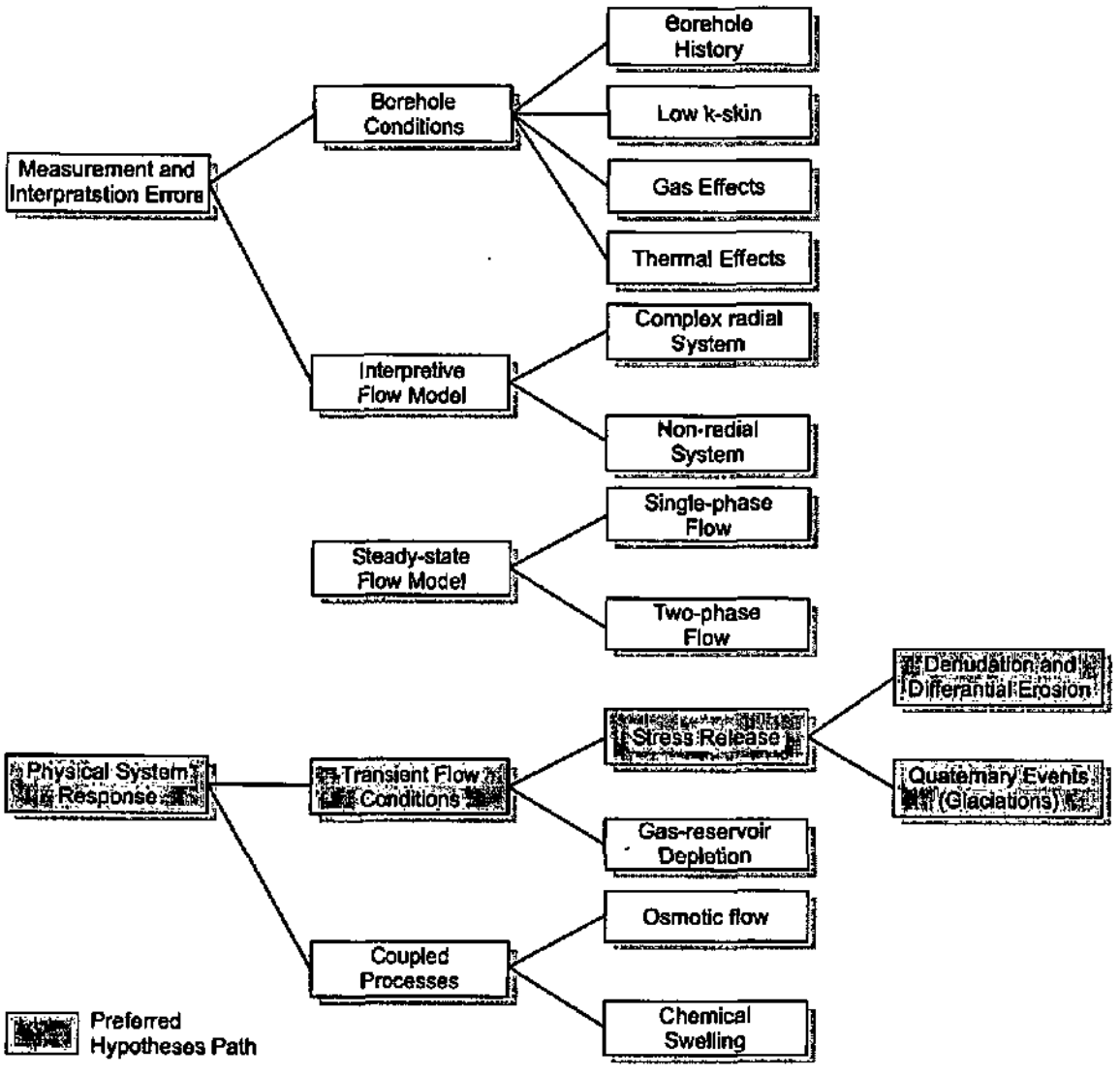

Fig. 6.1-1: Schedule of the different working hypotheses checked in order to explain the generation of underpressures

Of all potential geological events, the Quaternary ice ages are best investigated and documented. This is the reason why in VINARO & MCCORD (1991) the hypothesis of mechanical unloeding was tested primarily on the basis of glacier rebound scenarios of the Late Pleistocene. The corresponding climatic change is relatively recent (less than 14'000 a BP), and can therefore be considered as the shortest-term event potentially able to generate subnormal pressures. It is thus the most "conservative model". The mathematical basis is addressed in Section 7.4.

The analytical approaches of TERZAGHI (1943) and OLSON (1977) were applied for computation of the loading/unloading events (VINARD & MCCORD, 1991; RIVERA & SENGER, 1993). The shape and magnitude of the simulated head profiles match observations well. Later on, numerical coupled hydro-mechanical models were also applied (ARISTORENAS & EINSTEIN, 1993) as well as two-phase flow models (schedule in Fig. 6.1-1).

6.3 The overall conceptual model, abstraction schemes and modelling scenarios

In order to study the hydrogeological conditions at any site, the investigator needs an a priori mental picture of the problem at hand. This means that, before the technical part of modelling can start, a schematic representation of all aspects of the overall problem must be elaborated. This is the conceptual model, which - in order to become applicable - needs to be organised into a logical framework comprised of different hypotheses addressing specific issues. Since it is impossible to test all likely processes simultaneously with one single model, a set of manageable "abstraction schemes" is needed, each of which addresses a specific case.

6.3.1 Definitions

An *abstraction scheme* of reality is an organised framework of hypotheses, which, taken together, describe how a particular system or process operates. An abstraction scheme contains the main physical processes, expressed in terms of equations, that are supposed to act on the groundwater flow system, the geometry and size of the domain to be considered, the magnitude and ranges of relevant parameters and the description of initial[1] and boundary conditions. The abstraction scheme is a partial conceptual model, restricted to processes supposed to act on the real system and defined in such a way that it is amenable to analysis by means of a numerical and/or analytical model. The abstraction scheme is, by definition, only a schematic representation of the complex reality and results from a deliberate choice that does not require to be justified or defended against other possible interpretations. Its role is to provide a logical "language", a clear link between the inherently unknown reality, the schematic representation in the abstraction scheme and the (multiple) realisations of the abstraction scheme provided by running mathematical models.

The *numerical (or analytical) model* is comprised of the computer code, the input data, the simulated results and their graphical representation in terms of equipotentials, flux vectors, advective flow pathways, etc. Each numerical or analytical model represents one single realisation of the abstraction scheme and should therefore not be confounded with reality. A model realisation can be compared with some information from reality but is not a genuine representation of this reality. A *model scenario* describes the evolution pathway of a transient model, without carrying all model specifications described in the abstraction scheme.

Elaborating an abstraction scheme is a dynamic and iterative process. An initial model is constructed beforehand, followed by model realisations. These model realisations are compared with reality. In ideal cases, new data help to improve the abstraction scheme and the corresponding mathematical model by confirming or invalidating model predictions. The different elements of an abstraction scheme, as well as their interaction, are illustrated in Fig. 6.3-1 (KIRALY, 1994). Fig. 6.3-1 represents the case of standard numerical simulations of regional groundwater flow, but is readily applicable to coupled models, etc.

---

[1] for transient processes

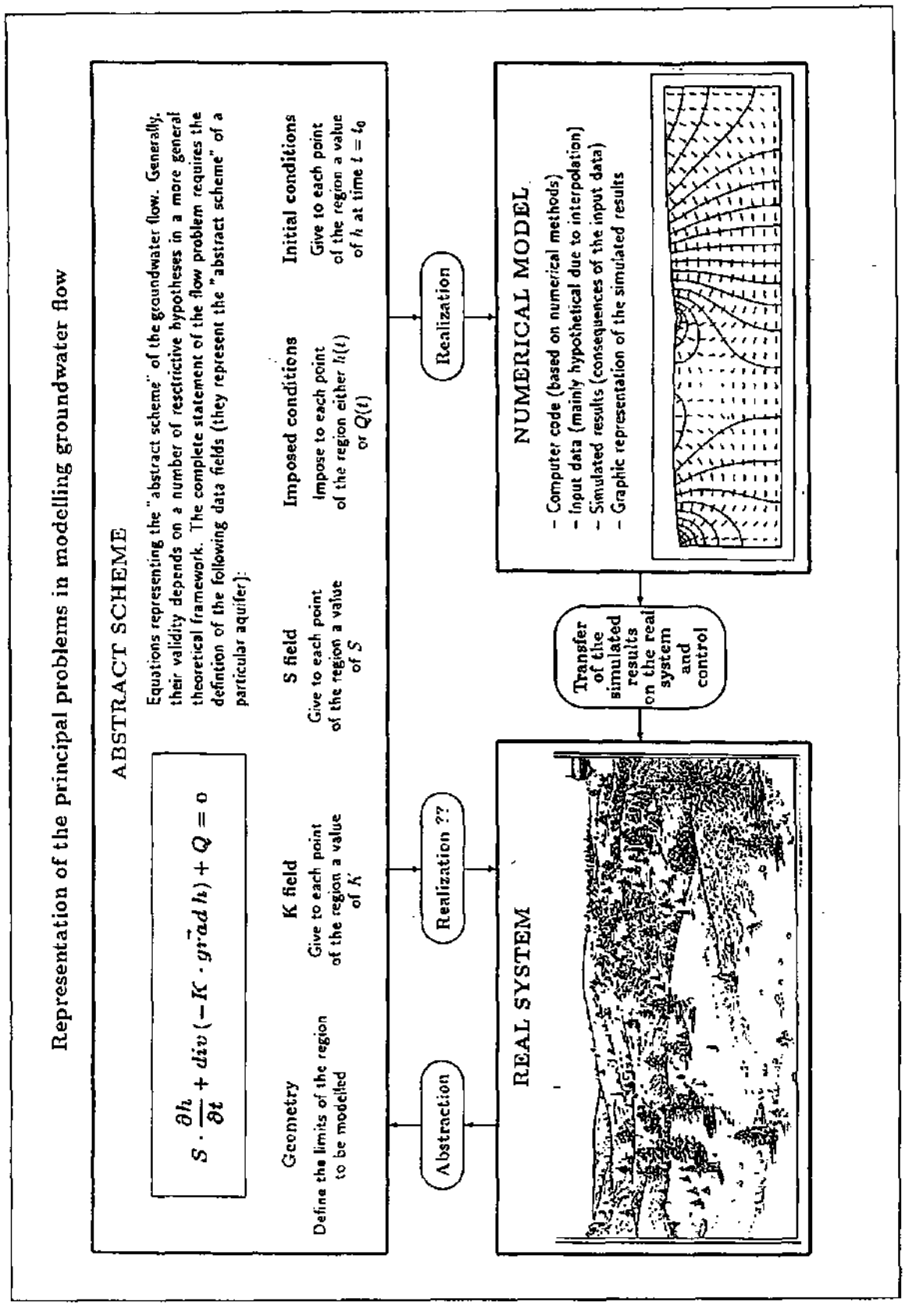

Fig. 6.3-1: Relationships between "real system", "abstraction scheme" of the real system and "numerical model" (after KIRALY, 1994)

6.3.2 Organisation of the model studies and use of abstraction schemes

All model studies described in this thesis are based on abstraction schemes as described above. This approach provides the following advantages:

1. It avoids overinterpretation or misinterpretation of model results i.e. confusion between model realisation and the real world because the results are brought back into the appropriate context
2. It highlights the choices made by the modeller. Since the choices are clearly noted, the investigator does not need to justify his approach
3. It halps identifying an aspect or a point of disagreement
4. It provides a clear terminology and a clear reference, i.e. avoids confusion between statements conceming reality and those concerning models.

None of the models in this thesis pretends to provide a comprehensive explanation for the multiple phenomena that are represented in reality. All models aim at approaching the problem of disequilibrium hydraulic pressure from a different angle: some models assume simple elastic material properties and, at the same time, are based on rather complex 3D geological evolution scenarios; some others include sophisticated treatment of material properties and stress-strain relationship but neglect the 3rd dimension and are based only on schematic geological features. Most of them assume constant parameter properties with time or assume strong stress dependency.

Statements and predictions made in this thesis have to be understood in this context. Currently, most information that would be necessary to really provide reliable predictions is lacking. BREDEHOEFT et al. (1994) state that "Most geological problems have too many degrees of freedom to reach unique conclusions; one must accept the non-uniqueness of the results. Our attempt is to test one hypothesis." This statement is supported by NEUZIL (1986) when he states that "the nature of the problem is such, however, that significant uncertainty is likely to remain a component of most analysis encompassing large spans of time."

7 MECHANISMS APT TO PRODUCE HYDRAULIC UNDERPRESSURES

7.1 Scope

Hydraulic underpressures at Wellenberg result from a disequilibrium in groundwater flow conditions, itself due to the rebound of the marl-shale aquitard as described by NEUZIL (1995): "Heuristically, fluid pressure decreased because expansion of the porous matrix and the resulting increase in porosity occurred more rapidly than pore fluid could flow in", provoking therefore a pressure disequilibrium which - in low diffusivity environments - will take significant time to dissipate. This mechanism is the basic premise for this work.

This Chapter is aimed at describing the involved mechanisms, their limitations and consequences, and the way they are accounted for in the applied computer codes.

7.2 The concept of geologic forcing

7.2.1 Use and definition

All cases of disequilibrium pressure are related to geologic changes, among which "burial and denudation are perhaps the most ubiquitous and significant geologic processes affecting flow in low permeability environments" (NEUZIL, 1986).

In low-diffusivity environments, disequilibrium flow regime will result because of the inability of the hydrodynamic system to evolve rapidly enough to accommodate the natural changes imposed upon it. *Geologic forcing* corresponds, therefore, to the mechanical and thermal time-varying terms acting on pore pressures as well as on the fluid source term (e.g. fluid expelled during lithification or metamorphism), (NEUZIL, 1995).

Disequilibrium pressure starts to form instantaneously when the corresponding generating process begins, is reinforced for as long as the process continues, and persists some time after the process stops. Many model calculations suggest that disequilibrium pressure can persist for geological significant periods of time after the generating process stopped. Hence, the observation of disequilibrium pressure may reflect processes acting in the present or in the past, or both, since the pressure changes resulting from all current and past processes are superimposed (CORBET & BETHKE, 1992; NEUZIL, 1986). NEUZIL (1995) states that it is almost impossible to distinguish between a "decaying remnant of a once geologically active system formed by processes that are no longer active" and a regime which is subject to current geologic forcing. This applies particularly well to Wellenberg, where different types of geologic forcings are possible covering distinct time ranges.

If geologic forcing is active, pore pressures are dictated by "a balance between ongoing geologic processes that perturb the pressure and fluid fluxes that tend to dissipate the perturbations" (NEUZIL, 1995). Consequently, the generating mechanism must be taken into account in conceptual and mathematical models. If, on the contrary, the generating mechanism can be considered as terminated, the problem considerably simplifies itself, since only the dissipation process of disequilibration pressure is to be considered as used by NAGRA (1997).

NEUZIL (1995) considers that most occurrences of underpressures are driven by ongoing geologic forcing (".... observing a disequilibrium system as it decays to an equilibrium state would imply rather lucky timing."). Although erosion is acting at Wellenberg, it cannot be ignored that the most recent geological event that contributed to the unloading of the marl-shale aquitard is the melting of the ice cap at the end of the last ice age. Therefore, from

the conceptual point of view, both types of geologic forcing, i.e. continuous and discontinuous, are equally likely at Wellenberg. Their effects on pore pressures are to a large extent indistinguishable, due to the location of the few observation boreholes, which do not allow discrimination. However, and since these types of geologic processes are relatively amenable to analysis, their respective impact on pore pressures can be estimated quantitatively.

In order to focus on the most important governing physical processes, i.e. to rule out negligible contributions, which would tremendously complicate the treatment of the problem, NEUZIL (1995) proposes a list of conditions that define the frame of interpretation work of underpressures and that may be summarised in the following way:

- no large deformation of the porous matrix
- coupling between changes in pore pressure and 3D deformation of the solid matrix is described by the theory of poroelasticity
- only fluid transport is of importance (neglects transport of heat and of dissolved solids, i.e. density driven flux)
- the geologic fluid sources are present throughout a volume of rock but their strength rate of fluid production may vary spatially.

These conditions rule most of the physical statements used in this study.

7.2.2 A small review of geologic forcings proposed in the literature

Definitions and statements made in Section 7.2 above can be summarised as follows: In order to generate and maintain hydraulic underpressures over long periods of time (some tens of thousands of years) in an aquitard, two basic conditions are required:

1. a driving force (i.e. geologic forcing), which acts on the hydrodynamic system
2. a significant delay in re-equilibration of pore pressures to equilibrated ("hydrostatic") pressures prevailing in the neighbouring, more permeable, formations or water-conducting features. This delay being controlled by the low hydraulic diffusivity of the aquitard and the large distance to drainage boundaries.

Many different mechanisms have been evoked in order to explain abnormal positive or negative pore pressures in the ground (FERTL, 1994; MOUCHET & MITCHELL, 1989; BREDEHOEFT & HANSHAW, 1968; BRADLEY, 1975; DICKEY & COX, 1977). TÓTH & MILLAR (1983) probably provide the most complete review to date:

1. active but possibly decaying endogenous sources of energy, i.e. osmosis
2. phase changes of minerals (and more specifically hydration/dehydration of clay minerals or evaporitic minerals)
3. changes in fluid volume due to heating or cooling
4. deformation of the rock framework by tectonic compression/decompression
5. sediment compaction/decompaction
6. erosional unloading or melting of a glacier ice mantel
7. changes in water table at outcrop areas of confined aquifers as a result of long-term changes in precipitation or epeirogenic movements.

Additionally, some authors propose also variations in the magnitude of tectonic stress, as for example BELL & MCCALLUM (1990). Studying the in situ stress patterns in the Peace

River Arch aree (Western Canada), they come to the conclusion that, possibly, time lag for adjustment of pore pressures to a decrease in the horizontal stress magnitude might explain "why some 'tight sands' in the area are underpressured."

Still other authors, for instance, TÓTH & MILLAR (1983) and ENGLAND & FREEZE (1988) concentrated their attention primarily on process (7) above. Their objective was "to evaluate the likely orders of magnitude of change in heads due exclusively to changes in the boundary conditions without the masking effects of other possible factors..." This means that only the downward movement of the surface boundary is permitted to affect fluid pressures at depth. Beyond doubt, previously established pressure patterns can survive a certain time, changes in the boundary conditions, as well as pressure patterns far away from exfiltration areas may appear as underpressured, due to cross-formational flow. NEUZIL (1985) criticised this approach because it does not account for the deformation of the rock framework in response to erosional unloading and also because the simulated pressure patterns do not consistently reproduce observations. Coupling hydraulics with mechanics succeeds far better as proven by the orientation taken by most contributions in this field (TÓTH & CORBET, 1986; SENGER et al. 1987; SENGER & FOGG, 1987; CORBET & BETHKE, 1992; PARKS & TÓTH, 1995; VINARO et al. 1993, etc.).

The basic assumption made for the studies presented in this thesis is that mechanical forces acting on the rock skeleton are the actual driving force leading to subnormal pore pressures. Rebound is due to the fact that the pore space is slightly more compressible than the solid framework (i.e. the bulk rock is more compressible than individual grains). The contraction of pore fluid due to cooling plays a comparatively small role because of the long time spans involved and the fact that cooling during the Quaternary is negligible when compared to the 15 million years since the culmination of the metamorphic peak. Assuming isothermal conditions is, therefore, deemed appropriate.

7.2.3 Mechanical unloading: application and limitations

The basic constitutive equations that are used for unloading of aquitards were originally derived for consolidation of soils as proposed by TERZAGHI & FRÖHLICH (1936), and few years later by BIOT (1941), who established the general theory of three-dimensional consolidation. Extend the domain of application of these equations to the reversal mechanism of consolidation, i.e. unloading, and to (over)consolidated hard rocks was not self-evident. However, there is general agreement among hydrologists to consider that these equations are – with due caution – applicable to tight and hard rocks (Sect. 7.3).

Knowledge of the deformation history of the aquitard rock and of its geomechanical properties is essential to perform appropriate simulations. Several problems arise, some of which are listed below:

1. The mechanical effects of rebound are less well known than those of consolidation (NEUZIL & POLLOCK, 1983)
2. Rates of erosion (removal) are much more difficult to estimate than rates of deposition (NEUZIL & POLLOCK, 1983)
3. Theoretically, unloading might result in absolute negative pore pressures (NEUZIL & POLLOCK, 1983; based on WHITMAN et al., 1961)
4. Plenty of complex formulations of mechanical and thermal processes are not warranted, because the long-term variations of the boundary conditions are nearly always unknown (NEUZIL & POLLOCK, 1983)
5. The mechanical behaviour of rocks, i.e. the time-dependency of critical geomechanical parameters and non-linearities of strains, is to a large extent unknown when considering

geological time scales.

7.2.4 Possible types of geologic forcing at Wellenberg

Three different abstraction schemes linked to geologic forcings, all describing mechanical rebound processes, were originally considered. They are in brief:

- Erosion of the alpine stacking of tectonic nappes, also termed "orogenic erosion" or "denudation", starting in the Miocene or early Pliocene
- Differential erosion, becoming significant during Pleistocene
- Periodically returning glaciations, with focus on the upper Pleistocene, with and without significant erosive events.

Scoping calculations (Sects. 10.3 and 10.4) tend to indicate that significant rock decompaction and resulting hydraulic underpressures may be due to long-lasting erosion (denudation of cap-rocks), starting in the Pliocene, and provided appropriate parameter ranges of hydraulic conductivity, compressibility, erosion rates and boundary conditions are selected. However, it is questionable how far long-lasting denudation can produce subnormal pressure remnants, which are still significant today with respect to the superimposed effects of more recent glacier events.

The results of different types of simulations converge and tend to show that for reasonable erosion rates in the order of 0.4 mm/a, a significant portion of the underpressuring dissipates during the erosion process itself. It is consequently postulated that the contribution of pre-Pleistocene erosion to current abnormal pressure is negligible. As a consequence, more recent potential candidates of geologic forcing, covering different duration, were looked for:

1. Differential erosion and glaciations from Pliocene to today.
2. Two last glaciations occurring during the Pleistocene.

7.3 Requirements on the geologic system

The transient nature of processes and parameters contributing to the generation of disequilibrium pressure is implicit in the definition of geologic forcing (Subsect. 7.2.1). Moreover, natural rocks seldom deform following a linear-elastic path as assumed in poroelasticity, but exhibit nonlinear stress-strain relationships, depending on various factors as the rock state (overburden pressure, differential stress, temperature, rock-fluid interactions, petrographic composition, etc.) and on the deformation path. If, for instance, strains are not fully recoverable, the linear-elastic approximation and the assumption that the material will deform following Hooke's law[1] could result in misinterpretation of pore pressure.

Scrutiny of various contributions in the field of hydraulic-mechanical coupled literature reveals a series of potential problems and limitations, which can be categorised as follows:

1. the deformation behaviour of the natural rock under investigation, i.e. the potential for inelastic deformation
2. the link between the parameters necessary in governing equations and the available data, which is itself connected to the level of site investigation

---

[1] Hooke's law assumes linear, instantaneous and reversible relations between the components of stress and the components of strain (TIMOSHENKO & GOODIER, 1970; MEANS, 1976). Instantaneous means that no time lag exists between the stress change and the strain change expressed by: $\sigma = E\varepsilon$

3. the representativity of key parameters derived from in situ or laboratory experiments (i.e. problems of sampling density and upscaling from local parameters to regional parameters),
4. the time-dependency of key parameters
5. the role of boundary conditions.

Problem (1) listed above will be treated in the frame of the description of the effective stress principle (Sect. 7.4), whereas problems (2) - (4), relating to key parameters, and problem (5), related to the definition of appropriate boundary conditions, are discussed hereafter, as "requirements on the geologic system", i.e. as conditions necessary for the operation of the poroelasticity theory.

7.3.1 Requiremants on the rock framework

Key parameters are defined as those parameters which play a governing role in the constitutive equations described in Section 7.4. The first objective is to compare parameter values and parameter ranges estimated for Wellenberg with similar values and ranges cited in the literature in order to gain confidence in the parameter ranges. The second objective is to comment on the potential time-dependency of parameters and on the consequences of using time-invariant parameters, as done in most model scenarios.

Diffusivity

The *diffusivity ratio* or simply *diffusivity* D is defined as the ratio of hydraulic conductivity K_{eff}, representative of the volume of interest, to specific storage S_s as follows:

$$D = \frac{K_{eff}}{S_s} \quad [m^2/s]$$

Rocks with small diffusivity ratios can experience significant pore pressure reduction when unloaded by even moderate rates of erosion. NEUZIL & POLLOCK (1983) use diffusivity ratios of the order of $10^{-10} < D < 10^{-7}$ m^2/s in their analysis. DOMENICO & SCHWARTZ (1990) mention that, in order to maintain overpressures over significant geologic time, the required diffusivity must lay within the range $10^{-8} < D < 10^{-7}$ m^2/s, whereas CORBET & BETHKE (1992) consider a broader bandwidth, i.e. $10^{-10} < D < 10^{-8}$ m^2/s.

NEUZIL (1986) proposes a compilation of diffusivity ratios estimated for various aquitard rocks as represented in Fig. 7.3-1. This sketch has been complemented with the estimated range of diffusivity of the marl-shale aquitard. Wellenberg's values lay within estimated ranges of other occurrences. For Wellenberg, S_s-values between 10^{-6} m^{-1} < S_s <10^{-5} m^{-1} seem reasonable. If not, rock permeability values must be reduced at least by one order of magnitude with respect to those applied in the K-model[2] (NAGRA, 1997). Scoping calculations by means of the analytical solutions by TERZAGHI & FRÖHLICH (1936) and OLSON (1977), show that underpressures can develop easily starting from K_{eff} values of the order of K = 10^{-12} m/s. K-values in this range are consistent with the K-model (NAGRA, 1997; MARSCHALL et al., 1997) used in model scenario Q2 an Q3 (Sect. 9.4).

---

2 the K-model is a stochastically generated K-distribution

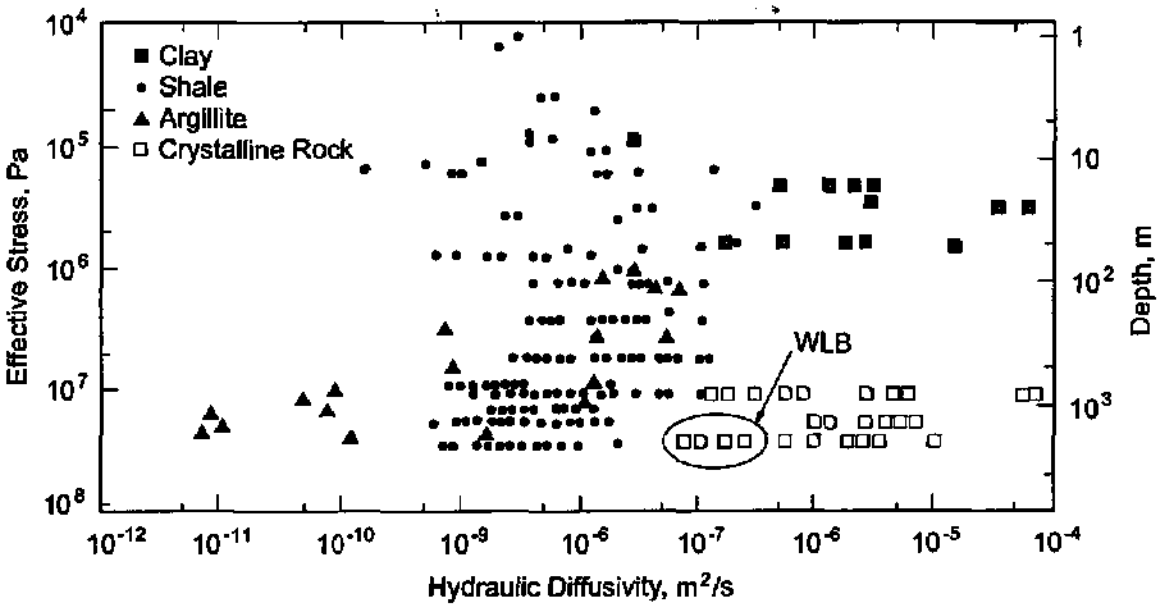

Fig. 7.3-1: Compilation of diffusivity ranges in different aquitard rocks including Wellenberg (after NEUZIL, 1986)

It is often assumed that diffusivity values derived from hydraulic transient tests are 2 to 3 orders of magnitude higher at large scale than at the scale of laboratory experiments. How far this scale effect can be accounted for at Wellenberg is unknown.

Hydraulic conductivity and specific storage

Estimation of hydraulic conductivity K is one of the most challenging aspects of hydrogeology. Especially for jointed and fractured rocks, as represented by the marl-shale aquitard, the "upgrade" and conversion from transmissivity measurements in boreholes to hydraulic conductivity values representative of hectometric REV's[3] is to a large degree a matter of conceptualisation (NAGRA, 1997) as well as the modelled K-distribution of the aquitard (MARSCHALL et al., 1997).

Nagra's observations and conceptualisation at Wellenberg are consistent with NEUZIL & POLLOCK (1983) who state that fractures and permeable zones, especially if they form connected pathways for groundwater flow, are driving the effective permeability of the rock. Therefore, it is the fracture network and not the block permeability which is the key issue. Consequently, connectivity cannot exceed a certain level, otherwise K_{eff} is no more compatible with generation and maintenance of abnormal pressures. NEUZIL (1993) estimates the "local" hydraulic conductivity of the Pierre shale to be between 10^{-14} and 10^{-13} m/s, which corresponds to the estimated K-range for the very-low permeability sections of the marl-shale aquitard at Wellenberg (NAGRA, 1997).

In their calculations, BREDEHOEFT & HANSHAW (1968) show that for thick sedimentary sequences, K of the order of 10^{-14} m/s, combined with S_s of 10^{-7} m^{-1} ($D = 10^{-7}$ m^2/s), can maintain abnormal pressures over geologic times. Additionally, they point out that specific storage for most rocks can vary up to two orders of magnitude, which is much less than the uncertainty ranges associated with hydraulic conductivity. BREDEHOEFT & HANSHAW (1968) consider that K can vary by as much as seven orders of magnitude. Although this range is

[3] REV: representative elementary volume

probably exaggerated, it remains incontestable that *uncertainties associated with K are many times larger than those associated with* S_s. However, since most geological media deform viscoelastically over long periods of time, there is a potential for S_s to be substantially larger for long time spans, than inferred from comparatively short-term laboratory or in situ tests.

Most mathematical expressions relating pore pressures to stress and/or strains, assume invariant parameters. This is illustrated for example by the formulations in NEUZIL & POLLOCK (1983)[4], where the key parameters K and S_s are considered as constants, although these authors assume a strong decrease in K with increasing total applied stress and also - although less pronounced - a decrease in S_s under compaction.

BREDEHOEFT & HANSHAW (1968) state that "the creation and maintenance of anomalous fluid pressure depends largely upon K and S_s of clay layers in the system", which implies that the lowest permeability layer in an aquitard controls both the generation and decay of disequilibrium pressure. As will be seen in Chapters 8 to 10, current model calculations tend to confirm this statement.

Specific storage depends on the bulk rock compressibility α, the compressibility of the pore fluid β, and is often derived from elastic constants, i.e. the shear modulus G, and more frequently from the Young's modulus E. At Wellenberg, static and dynamic Young's moduli were determined by means of laboratory experiments and in situ borehole tests (NAGRA, 1997). E varies strongly on the orientation of the sample with respect to foliation, but no depth-dependency could be identified. Hence, considering equation (15) below (Subsect. 7.4.1) with due caution, and recalling the proportionality between α and E, S_s is therefore almost constant, i.e. invariant from depth. From the above it follows that the D is almost exclusively driven by the K-distribution. Therefore, S_s is considered as a constant in all models, while variable K-distributions are applied for models in Chapter 9.

In the marl-shale aquitard, the zone with increased K is limited to the upper rim, a couple of hundred meters at most. At greater depth, the K-variability is restricted to one standard-deviation around an average value oscillating between 10^{-14} and 10^{-13} m/s. Therefore, neglecting progressive denudation and decompaction may result in a local overestimation of the permeability of the shallow aquifer of about 1 - 2 orders of magnitude.

Porosity and compressibility

Representative measurements of porosity of the marl-shale aquitard are difficult to achieve, because porosity is extremely small, of the order of 1 - 1.5 %, and therefore in the same range as measurement error. Furthermore, it is impossible to use porosity as indirect estimate of hydraulic conductivity (using standard Athy's or Archie's type-of-laws). There are, fortunately, two properties of porosity that make this parameter less critical:

1. Porosity of an overconsolidated rock remains almost constant even when exposed to further loading-unloading cycles. The small porosity of the aquitard is to a large extent a function of the former maximum overburden stress (KAELIN et al., 1992), and has therefore probably not varied significantly since then. Strain path analysis as shown by LAMBE & WITTMAN (1979) support this statement.
2. small bulk porosity decreases the significance of the corresponding compressibility term.

---

4 based on DOMENICO & PALCIAUSKAS (1979)

7.3.2 Requirements on boundary conditions and applied forces

7.3.2.1 Erosion and uplift rates

Erosion is commonly considered as the most likely process, which is consistent with the observation that even moderate erosion rates suffice to produce disequilibrium pressures in tight rocks. NEUZIL & POLLOCK (1983) report standard erosion rates of the order of 0.01 - 0.3 mm/a. These values seem low in comparison to the Alps, where from the end of the Neoalpine phase, erosion rates in the order of 0.4 - 1.0 mm/a seem reasonable (CLARK & JAEGER, 1969). Such rates are compatible with simultaneous deposition rates in the foreland molasse basins of 0.1 - 0.6 mm/a (KAELIN et al., 1992). Actually, Cenozoic was not only an active era in orogenic regions, but in large sedimentary basins also, tectonic activity coincides with this period, exhibiting erosion rates amounting up to 7 mm/a.

NEUZIL & POLLOCK (1983) note that the smaller the size of the investigated region, the higher the rate of denudation. This is particularly true in mountainous regions like Wellenberg.

7.3.2.2 Stress states

The stress state in the underground of the Wellenberg region is relatively well known (NAGRA, 1997) and shows, beneath an upper domain dominated by regional and local topographic effects (LIU & ZOBACK, 1992), a remarkable correspondence with overall stress measurements made in the Alps and their surrounding (MÜLLER et al., 1992). This is a clear case of differential stress[5] of tectonic origin, referred to also as "tectonic stress" (ENGELDER, 1993), with magnitudes following the scheme $S_H > S_V > S_h$.

At Wellenberg, near-surface stress due to the strong topographic relief[6] is replaced progressively at greater depth by typical tectonic stress[7]. The vertical stress component is considered to arise from the overburden load only, i.e. $S_v = \rho gz$. In flat terrains and for vertical boreholes, it can be assumed with some confidence, that the principal vertical stress corresponding to the weight of overburden is represented by the long axis of the borehole. Although at Wellenberg the situation is more complex, the same assumption is made (NAGRA, 1997).

Tectonic stress was accounted for in the coupled mechanical - hydraulic models (Chap. 10) by assuming plane strain conditions, which means that the horizontal strain occurs in the one horizontal direction, but not in the other, normal to the first one. This is a valid assumption for many orogenic events where shortening takes place along an extended front.

NEUZIL (1986) states that rates of tectonic stress change as high as 1 - 10 MPa/a are not unusual, and, that if associated with denudation and erosion, expansion (or compaction) can occur in the lateral direction also. In other words, the stress ellipsoid will accommodate changes in overburden stress by reduction (or increase) in lateral stress. Model calculations in Section 10.4 were designed to test this statement.

---

5 the differential stress is the difference between the overburden stress or vertical stress S_v, and the horizontal stress components S_H and S_h.

6 topographic effects are best represented by the orientation of the horizontal principal stresses, which rotate below a level of 500 b.g. from the topographically influenced zone to the zone influenced by the regional tectonic stress state

7 tectonic stress is the quantity of stress added to or subtracted from a horizontal component of stress to cause the state of stress to deviate from a reference state (ERLANGER, 1993).

7.4 Poroelasticity and the effective stress principle

7.4.1 Water-saturated rocks

7.4.1.1 Consolidation and unconsolidation

Provided the rock can be considered as a water-saturated, hydraulically conductive, equivalent porous medium (EPM), which deforms linear-elastically, any change in the external stress σ (normal stress due to overburden) will affect the stress state inside the rock body as follows:

$$(1)\quad \sigma = \sigma' + p$$

with:
- σ external total stress [Pa]
- σ' effective stress [Pa]
- p pore pressure [Pa]

The stress inside the rock is composed of the inter-granular stress or effective stress σ' and the pore pressure. Equation (1) means that the part of the total stress not borne by the porous skeleton as effective stress is borne by the fluid as pressure. The relative contribution of both will vary through time.

The theory of consolidation is based on a series of simplifying assumptions, which are in the original version (TERZAGHI & FRÖHLICH, 1936; TERZAGHI, 1943):

- voids (i.e. pores) are completely water-saturated
- both water and solids are perfectly incompressible
- Darcy's law is strictly valid
- hydraulic conductivity is constant
- the time lag of the consolidation process is entirely due to the low K of the soil.

The vertical deformation, ΔL, of a rock sample initially of length, L can be expressed in terms of vertical strain ε_z. The following relationship relates the deformation of the sample to the Young's modulus E:

$$(2)\quad \frac{\Delta L}{L} = \varepsilon_z = \frac{\sigma_z}{E}$$

The next equation defines the Poisson ratio, which is the ratio of the horizontal to the vertical strain experienced by the sample:

$$(3)\quad \nu = -\frac{\varepsilon_x}{\varepsilon_z}$$

The bulk modulus K^*[8] is the inverse of the (vertical) bulk rock compressibility α, and is defined as:

$$(4)\quad K^* = \frac{\sigma_{mean}}{\varepsilon_{vol.}} \text{ which relates to E by: } (5)\quad K^* = \frac{E}{3(1-2\nu)} \text{ , while } (6)\quad \alpha = \frac{1}{K^*}$$

---

[8] the superscript (*) is used to avoid confusion with the hydraulic conductivity K

and for the last Biot's constants $G = \frac{E}{2(1+\nu)}$; $\zeta = \frac{K}{H}$

where G and H are elastic constants, K' is the bulk modulus, α the bulk rock compressibility, which represents a strain in response to a change in effective stress σ', and which can be converted to a change in pore volume. ζ is a measure of the volume of water injected or squeezed out for a given volume change of material (under drained conditions).

For a fhree-dimensional medium, it is assumed that one of the principal stresses is oriented in the vertical direction, therefore:

$$(7) \quad \sigma = \sigma_v = p_b \cdot g \cdot z$$

where ρ_b is the density of the water-saturated rock (assumed constant) and σ_v is the pressure exerted by the total weight of overburden (i.e. solids + water), which corresponds to the geostatic pressure (DOMENICO & SCHWARTZ, 1990).

If the porous skeleton is a linear elastic solid, a change in porosity can be related to the change in total stress, as described by DOMENICO & PALCIAUSKAS (1979) in form of a mass balance equation for the fluid in a small control volume of saturated porous medium:

$$(8) \quad \frac{1}{\phi(1-\phi)}\frac{\partial\phi}{\partial t} + \frac{1}{\rho}\frac{\partial\rho}{\partial t} + \frac{1}{\rho\phi}\cdot\nabla(\rho\bar{q}) = 0$$

The first two terms in equation (8) describe the change in storage due to a change of the pore volume and the density. The last term quantifies the net flux across the boundaries. This equation relates the accumulation of mass in the control volume to the net flow of mass across the boundaries and is valid if the system is isothermal.

The change in storage due to change in fluid density ρ is controlled by equation (9) below:

$$(9) \quad \frac{1}{\rho}\frac{\partial\rho}{\partial t} = \alpha\frac{\partial p}{\partial t}$$

Following the effective stress principle (1), for a linear elastic solid medium, the change in porosity ϕ caused by a change in effective stress σ' is:

$$(10) \quad \frac{1}{(1-\phi)}\cdot\frac{-\partial\phi}{\partial t} = -\alpha\frac{\partial\sigma'}{\partial t} = -\alpha\left(\frac{\partial\sigma}{\partial t} - \frac{\partial p}{\partial t}\right)$$

where α stays for bulk rock compressibility.

Equation (8) becomes after appropriate substitution with expressions (9) and (10):

$$(11) \quad -\nabla\rho q = \phi\rho\left(\beta + \frac{\alpha}{\phi}\right)\frac{\partial p}{\partial t} - \rho\alpha\frac{\partial\sigma}{\partial t}$$

where β stays for the compressibility of water.

This mass balance equation stems from BREDEHOEFT & COOLEY (1983). The last term, $\alpha(\partial\sigma/\partial t)$, occupies the position of a source term. They rewrote equation (11), which derives from the effective stress law formulated by JACOB (1940), by combining with Darcy's equation (12) and obtained equation (13), written here in terms of hydraulic head h:

$$(12) \quad q = -K\nabla h$$

$$(13)\quad -K\nabla^2 h + \alpha\frac{\partial\sigma}{\partial t} = \rho g(\alpha + \phi\beta)\frac{\partial h}{\partial t}$$

where h: hydraulic head [m] defined as (14) $h = \frac{p}{\rho_f \cdot g} + z$

with z representing elevation below a referential datum, usually ground surface.

This expression applies to both drained and undrained conditions and assumes essentially vertical deformation of the rock skeleton, constant K and ρ. One can easily note that this equation is essentially of the same form than expression (16) below, after having defined the specific storage as:

$$(15)\quad S_s = \rho_f g \cdot (\alpha + \phi\beta)$$

S_s is "the volume of water a unit volume of aquifer releases from storage because of expansion of the water and compression of the grains under a unit decline in average head within the unit volume" (HANTUSH, 1964). Equation (15) is normalised with respect to the bulk rock volume and takes both the compressibility of the bulk rock and the compressibility of the water phase into account. The underlying assumption is that grain compressibility cannot be separated from the rock framework compressibility, and that changes in the density of the fluid can be neglected (NARASHIMAN & KANEHIRO, 1980).

Several forms of the above expression can be written. The following mass balance differential equation[9] (16) is best suited for this study. In this case, the modification of the external stress directly affects the source term Q_s.

$$(16)\quad \frac{\partial}{\partial x}\left(-K_x\frac{\partial h}{\partial x}\right) + \frac{\partial}{\partial y}\left(-K_y\frac{\partial h}{\partial y}\right) + \alpha\frac{\partial\sigma}{\partial t} = S_s\frac{\partial h}{\partial t}$$

or in a more general form:

$$\nabla\left[-K\nabla h\right] + Q_s = S_s\frac{\partial h}{\partial t}$$

with K_i being the hydraulic conductivity in i direction [m/s]

Equation (16) has often been used for one-dimensional vertical deformation. Note that if the change in vertical stress with time is negligible, $\partial\sigma_v/\partial t \rightarrow 0$, the well-known groundwater flow equation of JACOB (1940) is obtained. The term "$\partial\sigma/\partial t$" affects flow through changes in porosity.

This equation has been extensively applied in the Quaternary models (Chap. 9). The advantage is that geologic forcing i.e. the stress rate is constant (SENGER et al., 1987), provided the erosion rate or rate of removal is kept constant over a defined period of time, i.e. $\partial\sigma/\partial t$ = ct. SENGER et al. (1987) verified equation (16), implemented in a FE scheme, with OLSON's (1977) analytical solution and obtained an almost perfect agreement between both solutions. The technical implementation is described in Subsection 7.5.1.

NEUZIL & POLLOCK (1983) applied for the 1D space a slightly modified form of the above equation, expressed in term of excess fluid pressure u, and assuming also that the vertical component of the vertical bulk rock compressibility α_v is much larger than the

---

9 DOMENICO & PALCIAUSKAS (1979), BREDEHOEFT & COOLEY (1983); this formulation is expressed for 2D space and is easily extrapolable to 3D space

compressibility of water β, i.e. $\alpha_v >> \beta$. A related analytical formulation derived by GIBSON (1958) was used by BREOEHOEFT & HANSHAW (1968) to demonstrate that abnormally high pressures are indeed possible. NEUZIL & POLLOCK (1983) used this equation for unloading under isothermal conditions and NEUZIL (1985) proposed more general forms of this equation for cases where $\alpha \neq 0$.

7.4.1.2 Discussion and conclusions for water-saturated rocks

The poroelasticity theory describes the coupling between pore fluid pressure and solid strain. The first complete description was provided by BIOT (1941) for linear-elastic materials. His constitutive equations relate the strain tensor linearly to both stress tensor and pore pressure. Time-dependent fluid flow is incorporated by combining the continuity requirements with Darcy's law, as shown in the above equations. Further improvements and extensions, particularly to non-linear elasticity were formulated by BIOT himself (BIOT & WILLIS, 1957) and other authors. However, most of these expressions require an understanding of the long term deformation behaviour of materials, which go far beyond our current state of understanding.

In aquitards, the pressure disturbance occurs because the change in total stress is rapid as compared to the rate of dissipation of pore pressures. In the case of rebound, pore water will gradually fill the increasing pore volume caused by expansion of the porous skeleton. This phenomenon happens even in "tight" and (over)consolidated rocks.

NEUZIL (1993) notes that for relatively deformable media, such as the Pierre shale, erosion will provoke rock expansion in response to the stored strain energy. The Pierre shale is supposed to deform like a Kelvin substance in response to changes in the vertical effective stress, which means that an initial instantaneous deformation of the material is subsequently replaced by plastic creep ("viscous" deformation in NEUZIL's terminology). In the Pierre Shale, "viscous deformation remains nearly "caught up" with natural effective stress changes and is additive with and indistinguishable from the instantaneous component", which implies that irreversible strains must be taken into account at any stage of the rebound process (NEUZIL, 1993). What applies to the "soft" Pierre Shale, does probably not apply to the overconsolidated rock at Wellenberg. Although long-term plastic deformation is likely, most of the small strains due to changes in overburden stress are expected to follow approximately a linear-elastic deformation path. Inelastic strain tends to amplify the response of unloading on pore pressures.

However, the potential role of inelastic deformation has been explored also, by using the elasto-plastic Cam-clay model, since there is no appropriate material model available for the marl-shale aquitard.

7.4.2 Dissipation process in low-permeability media

In a very-low permeability and compressible rock mass, every modification of the external stress state will result in a re-equilibration process of pore pressure and effective stress. Pore pressures will recover to equilibrium pressure (hydrostatic pressure) on the boundaries of the UPZ-formation only once the driving force has ceased its activity. Overpressures and underpressures can therefore be a consequence of such stress changes and originate under strong rates of overburden change together with particularly low hydraulic diffusivity.

The dissipation process of underpressures can be compared with an aquifer standing in equilibrium with its exfiltration zone and reacting to a sudden change in the exfiltration area. DE MARSILY (1988) describes the adaptation duration $t_{50\%}$ of the hydraulic head at an observation point with distance L to the exfiltration area by an analytical formulation, which, in a simplified form, can be written as follows (17):

$$(17)\quad t_{50\%} = \frac{L^2}{D}$$

This equation shows clearly the negative correlation between D and the duration of the excess pore pressure dissipation. It also shows that the dissipation duration is proportional to the square of the distance from the source of perturbation. Using the same approach, TERZAGHI (1943) explained why the abnormal hydraulic pressures are largest at the centre of aquitards and why the corresponding duration of pressure re-equilibration to the conditions in the adjoining aquifers is the longest. For the Pierre shale, NEUZIL (1993) assumes that natural transient flow conditions exist for 2 to 4 Ma, with flow directed towards the centre of the pressure anomaly.

7.4.3 Rebound under two-phase flow conditions

Limited amount of free gas may exist locally in the pore space of the marl-shale aquitard. Free gas has basically two opposite effects on pore pressures: On the one hand, due to its high compressibility, it will lower the absolute magnitude of pore pressure disequilibrium when the applied load is changed, and, on the other hand, free gas will, owing to capillary forces, preferentially reside in larger pores, and therefore reduce the permeability of the water-phase, thus prolong the time necessary to dissipate disequilibrium pressures. Studies performed to investigate the potential impact of free gas are summarised in Section 8.5.

Departing from the basic effective stress law (equation (1), FINSTERLE (1992) derives a series of equations for the case of unloading applied to an aquitard comprising initially both water and free gas in the pore space. The effective stress law states that:

$$(1)\quad \sigma = \sigma' + p$$

while at any time the following condition must be fulfilled:

$$(2)\quad \Delta\sigma = \Delta\sigma' + \Delta p$$

The change of fluid pressure Δp may be expressed as a function of the applied total stress release $\Delta\sigma$:

$$(3)\quad \Delta p = B \cdot \Delta\sigma$$

where B is a coefficient depending on the gas S_g and water S_w saturation, hydraulic diffusivity D, and rate of stress change. The saturation is defined as the ratio of the considered phase (liquid of free gas) to the pore volume. Assuming incompressible solid grains, unloading will reduce the effective stress and since the bulk rock is a compressible material, the pore volume will support the entire change in volume of the rock. This is best expressed by equation (4) for fully saturated conditions:

$$(4)\quad \phi V_0 \cdot \Delta p \beta = V_0 \cdot \alpha\left(\Delta\sigma - \Delta p\right)$$

Combining equations (3) and (4) yields:

$$(5)\quad \frac{\Delta\sigma}{\Delta p} = B = 1 + \frac{\phi\beta}{\alpha}$$

For relatively deformable porous media, the compressibility of the bulk rock is much larger than that of water, i.e. $\alpha >> \phi\beta$, and therefore $B \approx 1$. This implies that when unloading begins, the fully saturated system will convert all the change in overburden stress to an equivalent change in pore pressure. With elapsing time, in aquitards, the dissipation process of the "initial pressure removal" will lag behind for longer periods and will only be compensated by net inflow of water into the pores. Two processes are acting

simultaneously: the fluid pressure difference will be progressively reduced, while more and more of the change in total stress will have to be borne by the effective stress (Δp decreases while $\Delta\sigma'$ increases). The final effect is a (small) increase in rock volume.

When a free gas phase occupies part of the pore space, the compressibility of the fluid β has to be replaced by a term β^* taking into account both the compressibility of water β_w and that of gas β_g, since gas will dramatically increase the total fluid compressibility as a function of increased gas saturation S_g. The total wetting and non-wetting fluid compressibility will therefore be related to saturation and total compressibility in the following way:

$$(6)\quad \beta^* \approx S_g\beta_g + S_w\beta_w$$

For deformation constrained to the vertical direction, the relationship between the change in porosity and change in effective stress is:

$$(7)\quad \Delta\phi = \frac{\Delta l}{l} = \frac{\Delta V_\phi}{V} = \alpha\Delta\sigma'$$

l [m] represents the thickness of the expanding layer and Δl the corresponding expansion of the rock skeleton. This relationship is based on linear-elastic deformation. The effects of gas, assuming a perfect gas and that the total volume change is taken up by the bulk rock (and not by water), the progressive decrease of pore pressure is:

$$(8)\quad \Delta p = (p - p_0) = -p_0 \frac{\Delta\phi}{\Delta\phi + \phi_0 S_{g_0}}$$

Furthermore, this equation neglects degassing of dissolved air and assumes isothermal rather than adiabatic conditions. Equation is a recursive formula because the effective stress leading to the change in porosity is itself a function of the change in pore pressure due to the basic assumptions (1) and (2).

After insertion of (2) and (7) in (8) and rearranging the terms, the following quadratic equation results:

$$(9)\quad -\frac{1}{p_0}\Delta p^2 + \left\{1 + \frac{\Delta\sigma}{p_0} + \frac{\phi_0 S_{g_0}}{p_0\alpha}\right\}\Delta p - \Delta\sigma = 0$$

This equation relates the initial pressure change to any value of instantaneous change in total stress. From this point in time onwards, unloading is described by coupling mechanical deformation to flow of gas and water (two-phase flow). A further simplification by FINSTERLE (1992) is to assume that at any time the change in effective stress equals the change in total stress ($\Delta\sigma' = \Delta\sigma$), so that the porosity change is no more time-dependent and therefore changes instantaneously from ϕ_0 to $\phi_0 + \Delta\phi$ (with $\Delta\phi = \alpha\Delta\sigma$). FINSTERLE estimates the error due to this simplification to be less than 10%.

7.4.4 Potential temperature effects

Assuming that over the last 15 million years, the geothermal gradient remained nearly constant (25 - 30° C/km), that the highest temperature at culmination of the Neoalpine metamorphic phase was of the order of 210 - 230° C, and that the eroded rock layer amounts about 6'000 m, the temperature decrease which the marl-shale aquitard experienced at depth represents a maximum of 180° C. This implies significant cooling, but when distributed linearly over a very long time span, cooling becomes insignificant for the

Quaternary era, which is the time range we want to model. Therefore, isothermal conditions are postulated in all simulations. Since thermal effects are often mentioned as a key process, neglecting them deserves further argumentation:

1. Isothermal conditions are considered appropriate because most of the cooling occurred before the Quaternary, and because additional cooling of aquifers during glaciations is deemed negligible at large depth. When considering longer time spans involving orogenic erosion, cooling might have played a significant role long ago. But even in this case, thermally induced disequilibrium pressures must have decayed long ago.
2. Convection as another thermal effect can be neglected as well as buoyancy effects since characteristically for aquitards, fluxes are very small and are not able to disturb conductive heat flow from the lower crust (BETHKE, 1985; BURGER et al., 1984).
3. Cooling manifests itself essentially because water contracts more than the sediment framework that contains it. However, citing DELANAY (1982), NEUZIL (1986) points out that this process will result in a noticeable decrease of pore pressures only if the total porosity is > 1 % (which is much higher than at Wellenberg) as shown by the last term in following equation:

$$\nabla\left[-K\nabla h\right] = S_s \frac{\partial h}{\partial t} - (\alpha - \alpha_s)\frac{\partial \sigma_t}{\partial t} - \alpha_{T_f} \cdot \phi \frac{\partial T}{\partial t}$$

   where α_{T_f} is the thermal expansivity of pore water.

4. NEUZIL (1986) considers that neglecting thermal effects for depths less than 2'500 m is valid, because at shallow depth, the matrix strain (purely mechanical deformation of the rock skeleton) is the dominant pore pressure producing mechanism. At larger depth the marked decrease of the bulk rock compressibility with depth changes the situation, but this is for a depth range far deeper than the one studied at Wellenberg.
5. Cooling and unloading are additive for production of underpressures and are difficult to distinguish form each other. Calculations applied to Alberta (Canada) show that groundwater cooling plays a minor role in decreasing fluid pressure when compared to erosional unloading (CORBET & BETHKE, 1992)

Temperature effects are often addressed in the literature for rapid subsidence of sediments. Since unloading is the inverse process of loading, thermal effects have perhaps too readily been advocated for rebound also (BREDEHOEFT & HANSHAW, 1968).

7.4.6 Potential effects of inelastic material behaviour

The question whether linear-elastic material models and related coefficients adequately describe the actual deformation behaviour of tight rocks is posed by various authors (e.g. PALCIAUSKAS & DOMENICO, 1989; DOMENICO & PALCIAUSkas, 1979; NEUZIL, 1985 & 1988) NEUZIL (1985), for instance, remarks that "because laboratory tests are conducted on scales of length and time and under conditions quite different than those in situ, the parameters derived from laboratory tests may not adequately reflect in situ behaviour." Two reasons explain this statement:

1. *Time-dependency:* Most coefficients are measured by means of short-term measurements. The time gap between few hours or days in the laboratory and millions of years in nature is striking.
2. *Scale effects:* Most coefficients are derived from laboratory tests using small rock

samples or from borehole dilatometer tests. Here also the scale gap between few centimetres to metres and hectometre or kilometre large rock bodies is striking.

7.4.6 Potential effects of density and/or salinity contrasts

SENGER (1993) shows that in case of highly saline aquitards, like Wellenberg, fluid density tends to increase with increasing depth. When strong contrasts of density occur, thermohaline convection caused by fluid instability might occur (HERBERT et al., 1988). In this case, flow is not driven only by the head gradient arising from topographic relief, but also by buoyancy forces resulting from contrasting fluid densities. This effect is very unlikely in very low-permeability environments (because of very small Raleigh number) like Wellenberg.

7.4.7 Conclusions

Four main conclusions may be reached with respect to generation of underpressures:

1. Based on theoretical considerations and on the probable cooling history of the aquitard, it can be affirmed with due caution, that temperature effects do not contribute significantly.
2. Density effects do probably not play a major role. The aquitard is probably very homogeneous with respect to salinity because of ionic diffusion.
3. The upscaling of key parameters, K and S_s, has been discussed extensively in the literature. It follows that K may be overpredicted or underpredicted (by 2 - 3 orders of magnitude), S_s underpredicted (by 1 - 2 orders of magnitude), and therefore D overpredicted when estimations base on measurement scale exclusively. These postulated effects have been considered in parameter variations.
4. Inelastic behaviour is related to time-dependency and to the non-recoverability of strain. Since the marl-shale aquitard is overconsolidated, it is justified to consider elastic deformation as an adequate approximation of the real (and unknown) long-term deformation behaviour. No generally valid mathematical expressions exist for characterising inelastic behaviour. Empirical material models are set up for each type of rock and an appropriate material model still does not exist for the marl-shale aquitard. It is, further, questionable that such a material model will really be applicable.

7.5 Mathematical treatment of physical processes in the applied computer codes

7.5.1 Basic information

Based on the above statements and hypotheses as well as on previous and related studies summarised in Chapter 8, three main abstraction schemes have been set up and tested by means of numerical models. They can be summarised as follows:

1. the *Quaternery evolution abstraction scheme* comprising alternating glaciations and temperate periods with differential erosion (Chap. 9)
2. the *orogenic erosion or long-term denudation abstraction scheme* (Sects. 10.3 and 10.4)
3. the *differential erosion abstraction scheme*, combining erosion and loading-unloading cycles due to varying glacier loads (Sect. 10.5).

Two main types of hydro-mechanical coupling have been applied, which are:

a. the expanded source-term approach

b. the fully hydraulic-mechanic coupled approach

Two different numerical codes, both based on the method of the finite elements (FE), have been used to solve the model scenarios addressed above. They are:

I. CASA (KUHLMANN, 1992)

II. ABAQUS (HIBBIT et al., 1995)

The source-term procedure has been implemented into CASA for modelling the Quaternary evolution scenarios. ABAQUS has been applied for simulating the long-lasting denudation and differential erosion scenarios. Tab. 7.5-1 shows the links between abstraction schemes and numerical codes.

Tab. 7.5-1: Links between abstraction schemes and computer codes

	Quaternary evolution	Denudation (orogenic erosion)	Differential erosion
CASA	X		
ABAQUS		X	X

7.5.2 CASA with source-term approximation

CASA is a powerful FE computer code for 1D to 3D space, which combines all standard features of deterministic groundwater flow modelling and parameter estimation features, i.e. inverse modelling capabilities. It provides an automated estimation of hydrological model parameters for saturated conditions from measurements and from prior information on the parameters. Elements of different dimension can be combined, which further enables CASA to calculate hybrid, i.e. channel and fracture-matrix type of systems. Among the large amount of code capabilities, the subset listed below was of particular use:

I. Transient groundwater flow simulations in 2D and 3D space, i.e. diffusion of previously generated disequilibrium pressure

II. Transient groundwater flow simulations in 2D and 3D space, taking the unloading of the rock skeleton into account (expanded definition of the point-source)

III. Inverse modelling for parameter estimation

IV. Kriging for interpolation of K-distributions produced in a regular grid onto irregular FE meshes (NAGRA, 1997)

V. Versatile, ready-to-use input and output commands and formats, the latter being used for graphical representation using TECPLOT (AMTEC Eng., 1996).

The source-term approximation enables one to simulate quasi-coupled hydro-mechanical processes, i.e. loading - unloading of the rock skeleton. The equation of groundwater flow including elastic deformation used in this approach, has been proposed by DOMENICO & PALCIAUSKAS (1979) and by BREDEHOEFT & COOLEY (1983), as presented in Subsection 7.4.1, and repeated here for convenience.

$$(1)\quad \frac{\partial}{\partial x}\left(-K_x\frac{\partial h}{\partial x}\right)+\frac{\partial}{\partial y}\left(-K_y\frac{\partial h}{\partial y}\right)+\alpha\frac{\partial \sigma}{\partial t}=S_s\frac{\partial h}{\partial t}$$

As explained in Paragraph 7.4.1.1, NARASHIMAN & KANEHIRO (1980) indicated that the last term on the left hand side, $\alpha\partial\sigma/\partial t$, represents the additional part of the source-sink term due to the deformation of the rock skeleton. Therefore, if the rock compressibility, α, and the stress change over time, $\partial\sigma/\partial t$, are known, elastic deformation can be simulated with the general groundwater flow equation. The quantity of the stress term, $\alpha\partial\sigma/\partial t$, is multiplied by the volume represented by each edge-node of the involved FE, which corresponds numerically to assigning discharge rates to individual nodal points, representing flow conditions for fixed pore volumes.

Any change in the load on top of the prescribed topographic surface of the model, i.e. any loading or unloading increment, induces a new calculation of the sink or source term. This calculation implies that the change in overburden $\Delta h_{e(x)}$ will be calculated for each node (x) as the difference between the added/removed level of load (horizontal ice load or topographic surface) and the model surface. In other terms, the decompaction will be given by a function relating the change in head at any nodal point in the FE network, i.e. $\Delta h_{e(x)}$, which will be used for calculation of the source term q_s.

The source term is calculated as follows:

$$(2)\quad q_s=\frac{\alpha\cdot\Delta h_e\cdot\rho_s\cdot g}{\Delta t}$$

where α: rock compressibility [1/Pa], approximated as: (3) $\alpha=\frac{S_s}{\rho_f\cdot g}$ [Pa^{-1}]

ρ_s: density of the loading material (i.e. 1 for ice, 2.6 for rock mass) [t/m^3]

ρ_f: density of water

Δt: duration of the loading/unloading phase [a]

g: gravitational acceleration

The underlying assumptions ruling this approach are that:

1. deformation is small compared to the total thickness of the layer, that is, the FE mesh is not deformed
2. hydraulic properties do not change during elastic deformation.

The stress change can be related to the change in the volume of rock (or in the volume of a FE) through:

$$(4)\quad \frac{\Delta V}{V}=\alpha\Delta\sigma$$

Assuming that the rock grains are incompressible (i.e. do not change volume due to change in external stress), the volume change is represented by the change in pore volume. This approximation is justified since RIVERA in VINARD & MCCORD (1991) estimated that the magnitude of rebound due to glacier retreat is less than 3 m for a representative thickness of the aquitard of 700 m.

The approach is not limited to glacier rebound, but may also take erosion and landslide movements into account. In the latter case, time-varying head boundaries are assigned along the upper boundary of the model domain, in addition to the source-term, representing the stress release associated with overburden removal. Note that the source-term approximation represents a virtual fluid source/sink, and does not simulate changes in

porosity, but the equivalent change in water volume within the rock body.

KUHLMANN (memorandum TK CONSULT, Nov. 1994) compared the source-term approximation in two steps. In the first step he compared the source-term with a 1D analytical solution, and in the second step, the comparison was performed based on ABAQUS calculations in 2D (memorandum TK CONSULT, Sept. 1995). The source-term approach was also compared with the analytical solutions by TERZAGHI & FRÖHLICH (1936) and OLSON (1977). For instantaneous unloading, the problem was defined as a 1D homogeneous column of porous aquitard rock, instantaneously unloaded by an excess pressure Δp_0 equivalent to a water column of 755 m (removal of ice). Hydraulic parameters were taken from RIVERA & SENGER (1993), which are summarised in Tab. 8.3-1.

Three alternative FE-meshes were used to discretise the vertical column, as represented in Fig. 7.5-1: 1D line elements, 2D quadrilateral elements, and 3D brick elements.

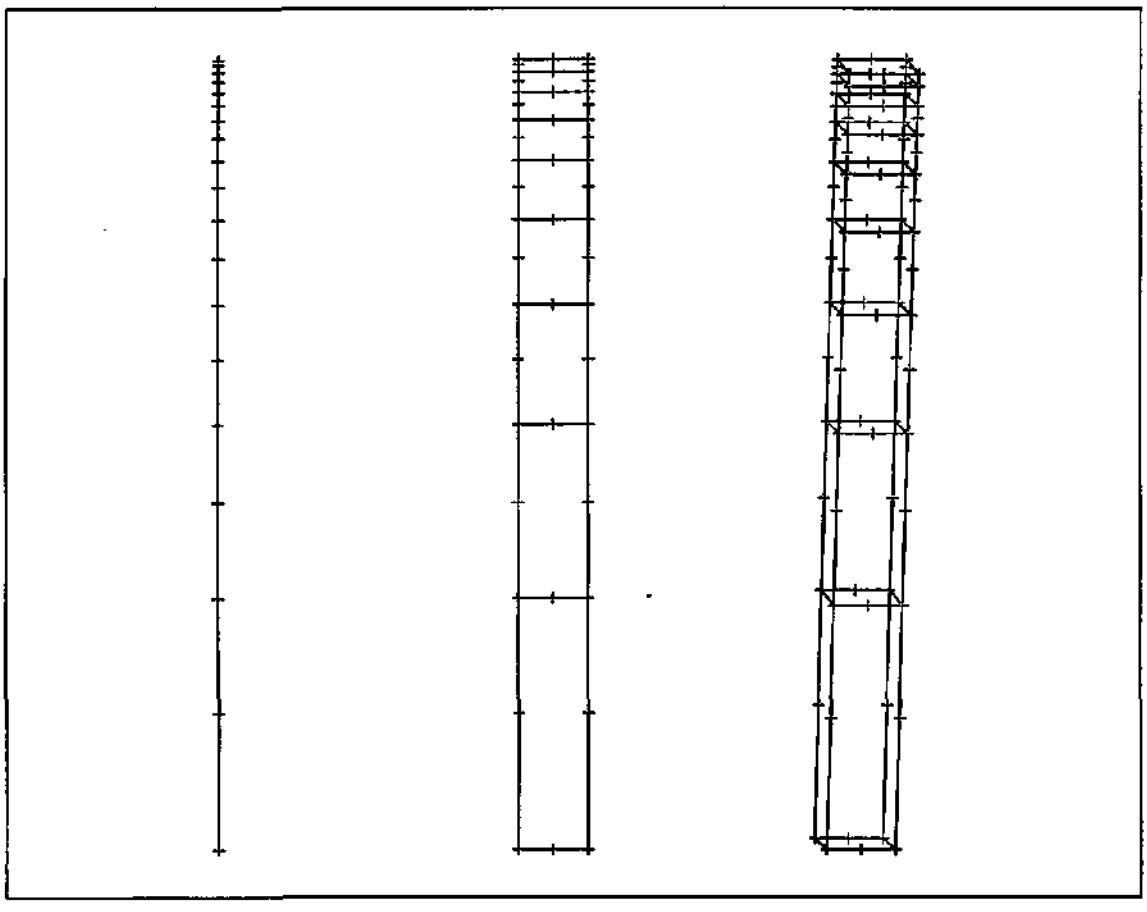

Fig. 7.5-1: Finite Element meshes used for the vertical column unloading calculations (left: 1D-mesh, centre: 2D-mesh, right: 3D-mesh)

The effect of the instantaneous unloading is represented in Figs. 7.5-2 and 7.5-3. Fig. 7.5-2 illustrates the time evolution of the underpressures at various depths within the column. Fig. 7.5-3 presents the evolution of the vertical pressure distribution at various times. As expected, at the beginning of the transient process, the excess load is entirely borne by the pore water (Δp_0), and is gradually dissipated. Actually, this case simply shows that the flow dissipation equation matches the analytical solution perfectly (as already verified by SENGER, 1983).

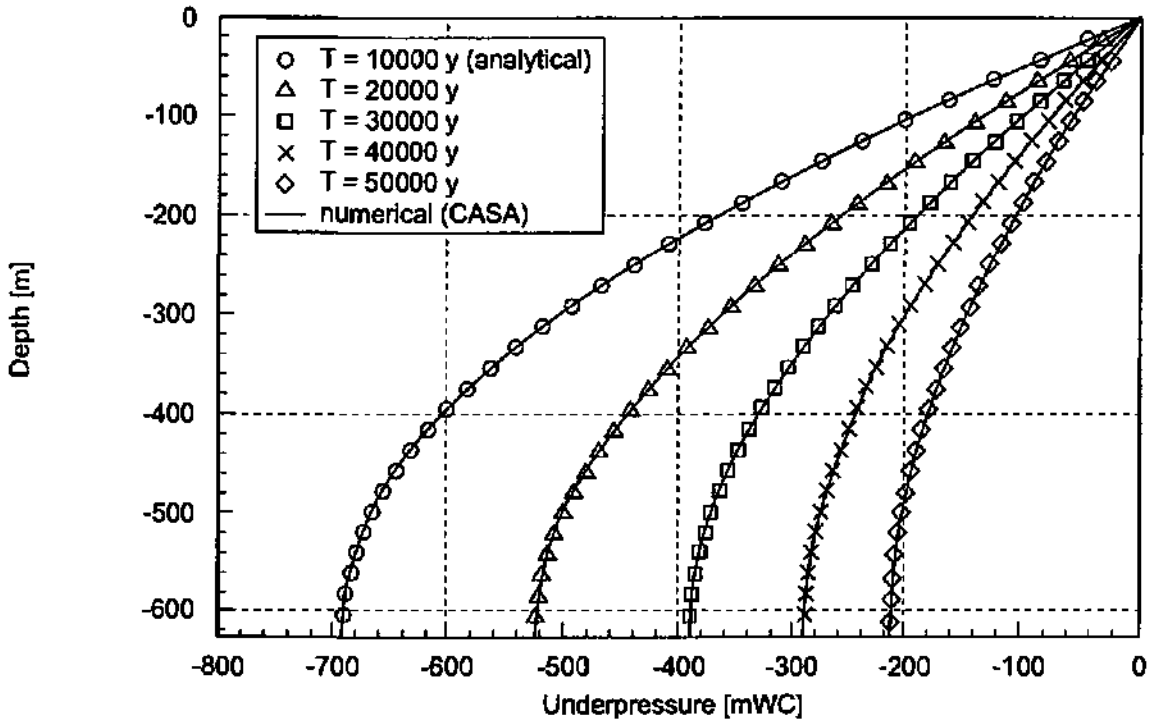

Fig. 7.5-2: Instantaneous unloading - Evolution of underpressures at various depth levels in e column

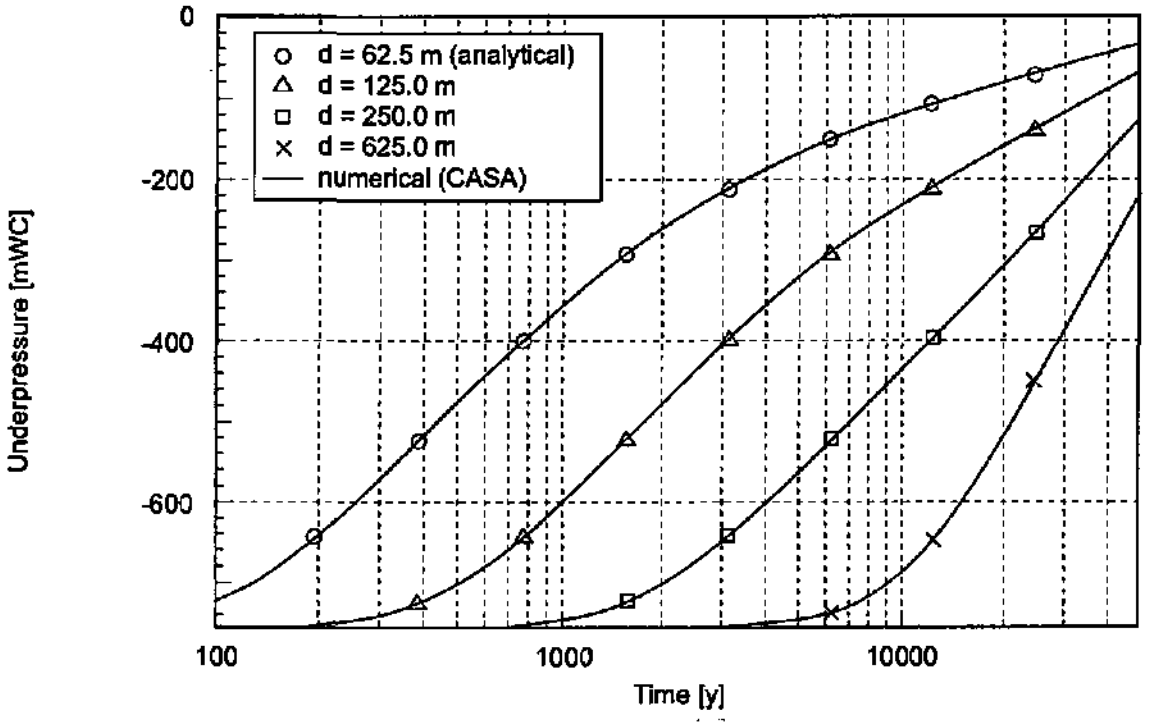

Fig. 7.5-3: Instantaneous unloading - Vertical underpressure distribution at various times

Using the same initial load as before, but applying a constant rate pressure reduction over 16'000 e, the pressure development is this time simulated by applying the source-term approximation (equation (1) above). This simplifies itself in the case of ice load to:

$$q_s = \alpha \cdot \frac{\partial \sigma}{\partial t} = 6.6 \cdot 10^{-11} \cdot \frac{-755 \cdot pg}{16'000} = -3.11437 \cdot 10^{-8} [a^{-1}] = -9.8756 \cdot 10^{-16} [s^{-1}]$$

Fig. 7.5-4 shows the results of the transient computation at various depth levels inside the column. Underpressures increase during unloading ($q = q_s$) and dissipate subsequently ($q = 0$). Again, a perfect agreement exists between CASA-simulation results and OLSON's (1977) analytical solution, regardless of the type of FE.

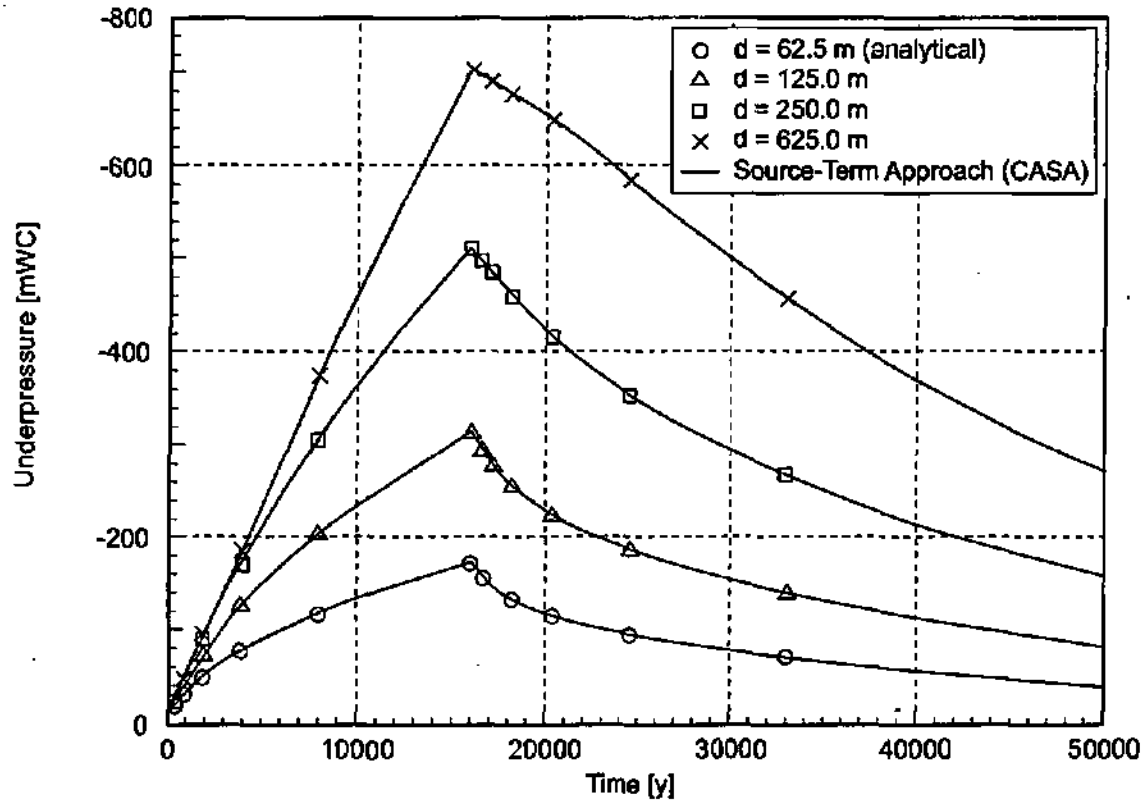

Fig. 7.5-4: Time-dependent unloading - Evolution of underpressures at various depth levels in a column

The source term approximation was compared with the single glacier event model scenario (see Subsect. 8.4.4). For the comparison, the model parameters B (Tab. 8.4-2) were used. The ice level is constant over the model surface at 1'800 m a.s.l. During melting away of the glaciers, an unloading function, $\Delta h_{(x)}$, is determined, which enters into the required source-term in the following way:

$$q_s = \alpha \cdot \frac{\partial h(x) \cdot \gamma_w}{\partial t}$$

where: $\alpha = \frac{\nu}{E} = 8 \cdot 10^{-11}$ [Pa^{-1}] compressibility

$\gamma_w = 10^4$ [Pa/m^3] specific weight of ice

$\Delta t = 0.05$ a duration of unloading

The specific storage necessary for the calculation of the source-term is approximated by following equation, applicable for the case of ice:

$$S_s = \alpha \gamma_w$$

Fig. 7.5-5 represents the applied 2D FE mesh, and, in colour, the distribution of the source term. The model study was performed by means of five separate runs (Tab. 7.5-2).

Tab. 7.5-2: Description of the performed runs for comparison between source-term approximation and hydraulic-mechanical coupling

Run	Description
1	Simulation of the unloading process by applying the source-term approximation. No-flow boundaries on all sides (i.e. non-draining conditions on surface). Initial conditions are hydrostatic, i.e. h = 0.
2	Simulation of the dissipation of disequilibrium pressures produced by run 1 over the time range of 40'000 a. Top drainage is applied, i.e. atmospheric pressure at surface (corresponding to "drainage conditions 1" in Subsect. 8.4.4).
3	Simulation of the distribution of underpressures after instantaneous unloading by means of a steady-state simulation, by which the unloaded pressure is imposed on surface.
4	Dissipation of the distribution of underpressures produced by run 3 over the time range of 40'000 a.
5	Variation of case 1: the ice load is removed over a time span of 10'000 a (instead of 0.5 a), by changing the source-term in accordance to the calculated unloading of run 3. Drainage occurs on top and bottom boundaries (atmospheric pressure, corresponds to "drainage conditions 2 in Subsect. 8.4.4).

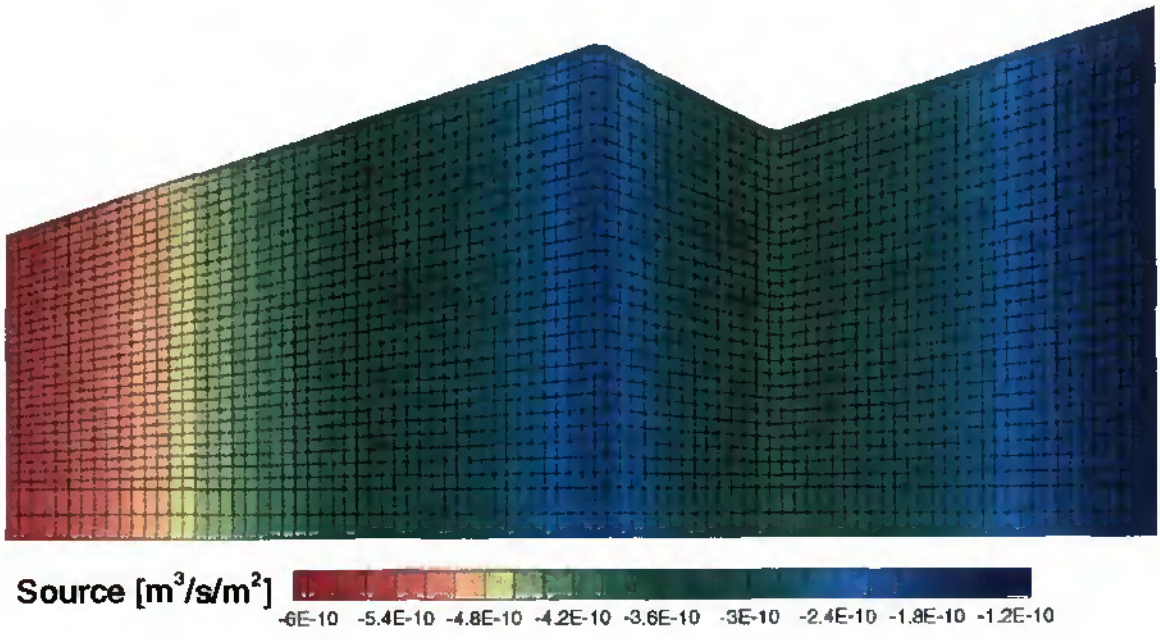

Fig. 7.5-5: FE Mesh for comparison and distribution of the source-term

Results and discussion

Because runs 1 and 2 could not fully reproduce the sequence of events simulated by ARISTORENAS & EINSTEIN (1993), three additional simulation cases were needed.

The computed underpressures of runs 1 and 2 are represented in Figs. 7.5-6a to 7.5-6d, after 5 a, (early part of the dissipation process) and after 9'638, 21'638 and 40'000 a respectively. Comparison with the results provided by ARISTORENAS & EINSTEIN (1993), (Figs 7.5-9a and 7.5-9b) reveals that, especially at the beginning of the model scenario, large differences between the two sets of simulated underpressures show up. For the source-term approximation, hydraulic underpressures develop in the horizontal direction only, due to the prescribed no-flow boundaries. In the ABAQUS-model, however, two-dimensional effects of the unloading are taken into account. At the end of the modelling sequence, however, the difference reduces to $< \pm 100$ m.

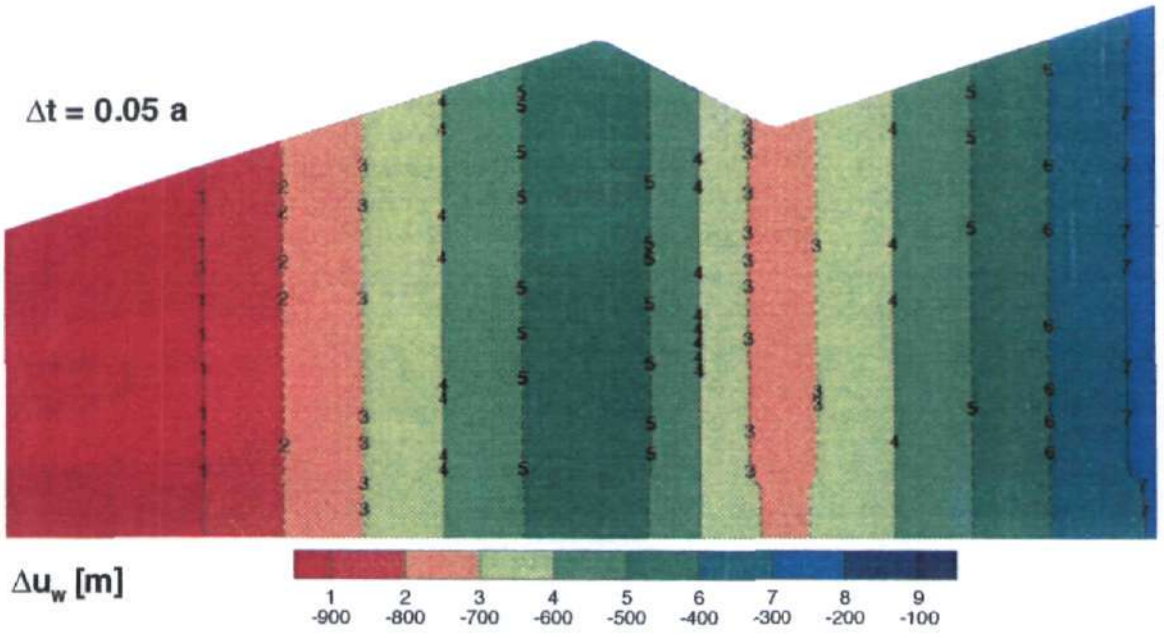

Fig. 7.5-6a: Run 1 - Underpressure distribution after 0.05 a

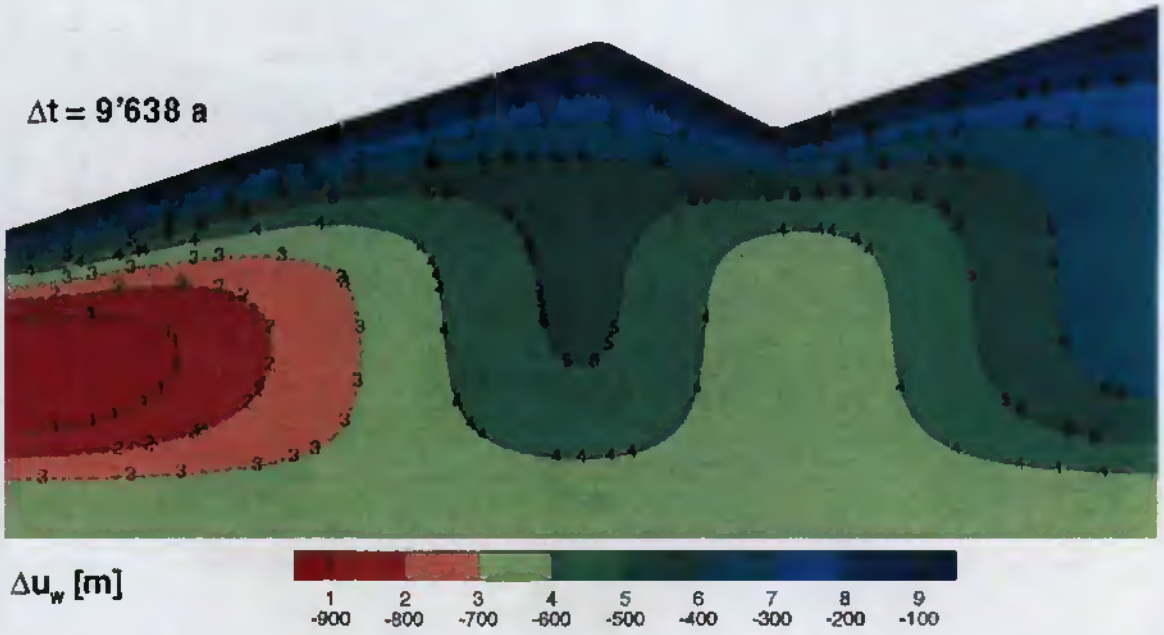

Fig. 7.5-6b: Run 2 - Underpressure distribution after 9'638 a

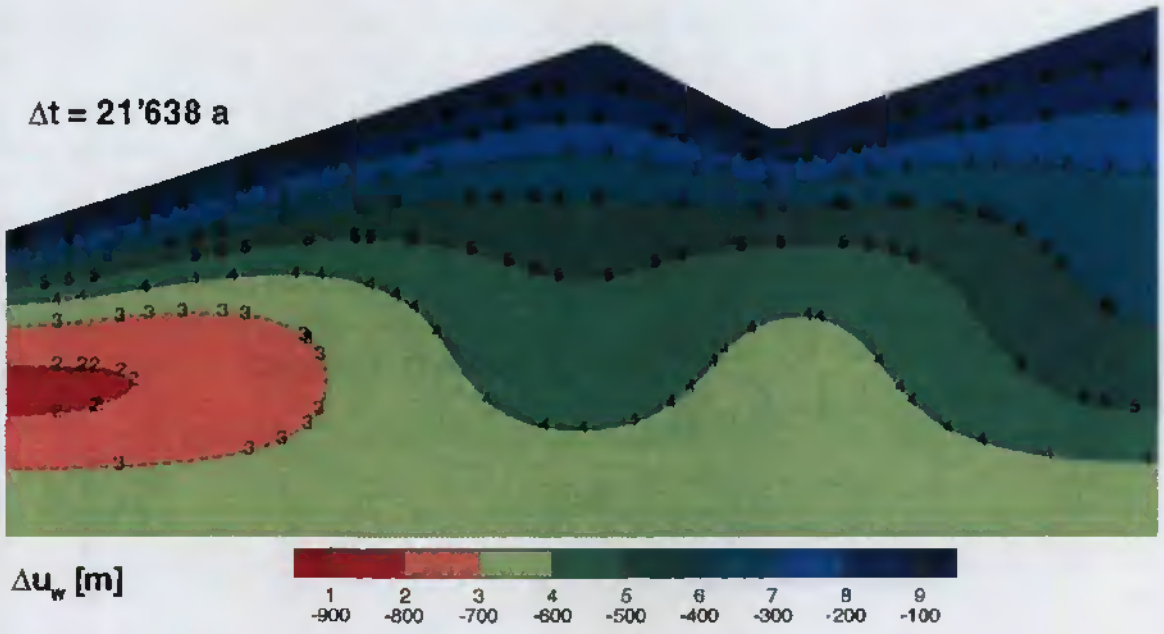

Fig. 7.5-6c: Run 2 - Underpressure distribution after 21'638 a

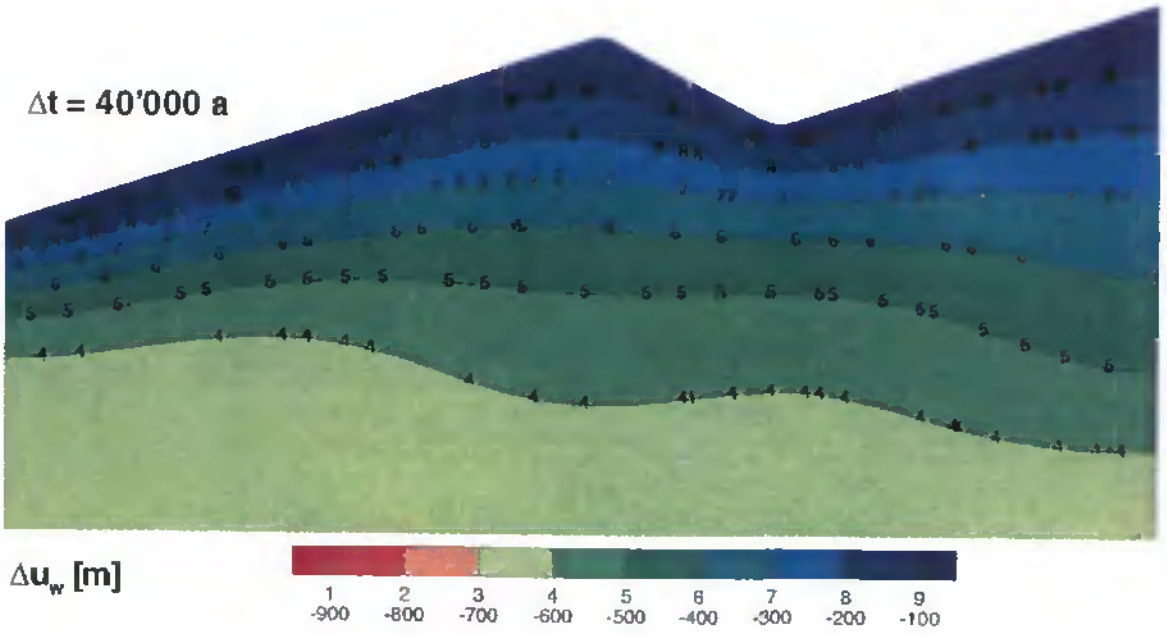

Fig. 7.5-6d: Run 2 - Underpressure distribution after 40'000 a

Two reasons exist for the small differences between simulations:

1. The depth-invariant source-term leaves the stress distribution unaffected during the period of decompaction. In ABAQUS, however, the stress field changes during the unloading period, as it is to be expected.
2. Differences in the geometry of the model domain used here and the "original" (but slightly erroneous) model domain of ARISTORENAS & EINSTEIN (1993) slightly affects the pore pressure distribution. This is the reason why runs 3 to 5 were performed using a modified FE mesh, closer to the one used by ARISTORENAS & EINSTEIN (1993).

Based on the results, the source-term is considered applicable for short periods of loading or unloading with respect to the posterior pressure re-equilibration period.

Fig. 7.5-7a represents the calculated underpressure distribution resulting from the steady-state run 3, where the unloading pressure is imposed on the surface of the model. Comparison with Fig. 7.5-9a shows a striking similarity, except from minor differences at the upper left corner of the model. Figs. 7.5-7a to 7.5-7d show the underpressure distribution for the modified source-term approach. The final underpressuring (Fig. 7.5-7d) is, with the source-term approximation, about 100 m below the computed values shown in Fig. 7.5-9b. The difference stems from the above mentioned different initial conditions.

For run 5 it was supposed that the 2D rebound distribution due to instantaneous glacier retreat can be predicted by a steady-state simulation (run 3). Since the total decompaction is known for each element of the model (average over each element), the source term approximation can simulate the pressure evolution also for linear reduction of overburden (similar to OLSON's 1977 approach). Fig. 7.5-8 shows the resulting underpressure distribution after rebound over a time span of 10'000 a, considering top + bottom drainage.

In conclusion, it can be affirmed that, on the contrary to the 1D problem, the application of the source-term approach to 2D and 3D problems is restricted to well defined situations. In the case of rapid unloading, the source-term approximation is applicable as it is. However, in the case of long duration unloading, a modified source-term approach is necessary, in which a 2D unloading function is implemented as explained above.

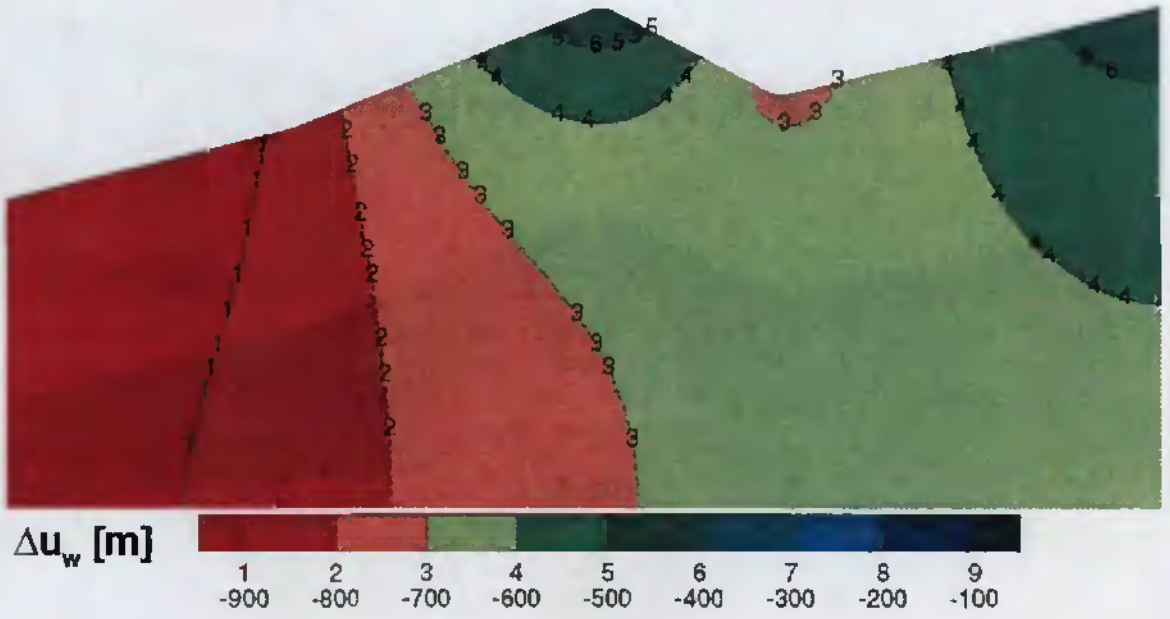

Fig. 7.5-7a: Run 3 - Underpressure distribution after instantaneous unloading

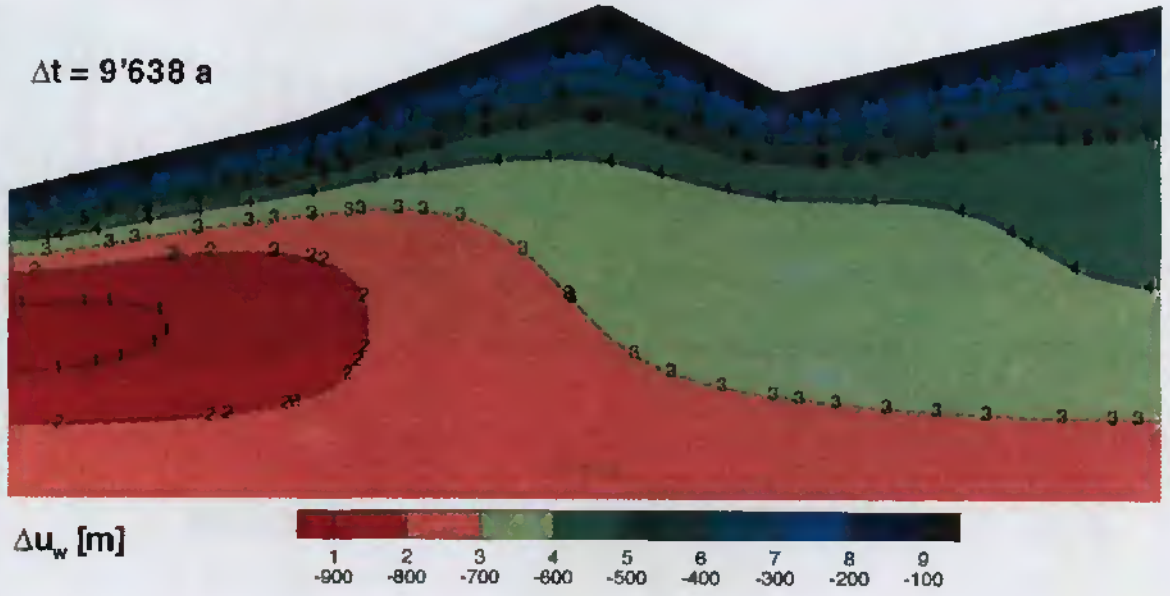

Fig. 7.5-7b: Run 4 - Underpressure distribution after 9'638 a

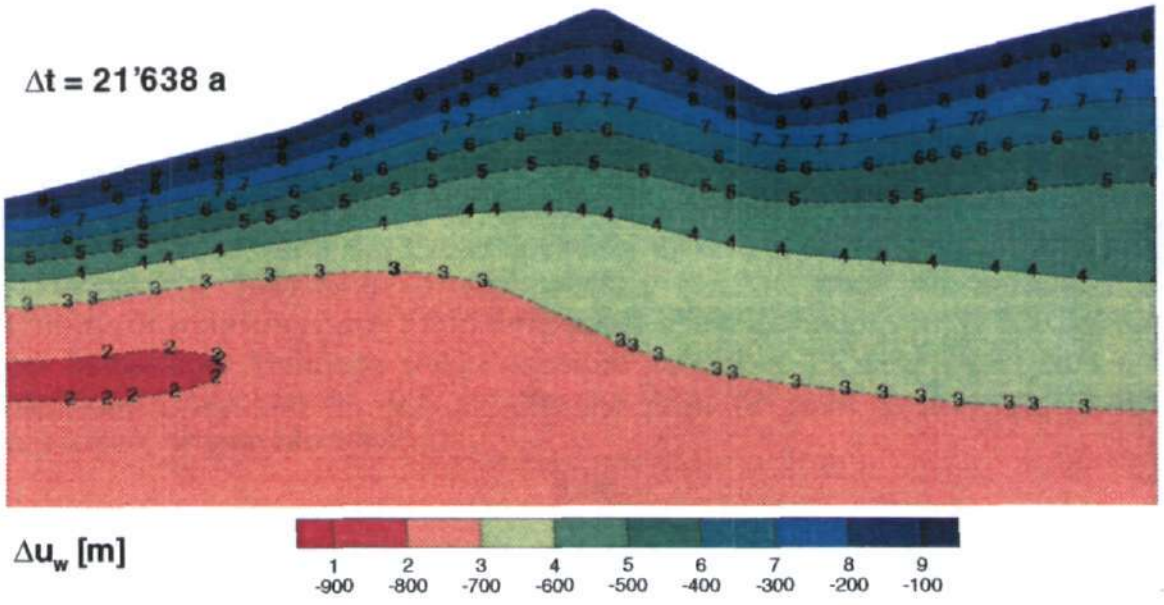

Fig. 7.5-7c: Run 4 - Underpressure distribution after 21'638 a

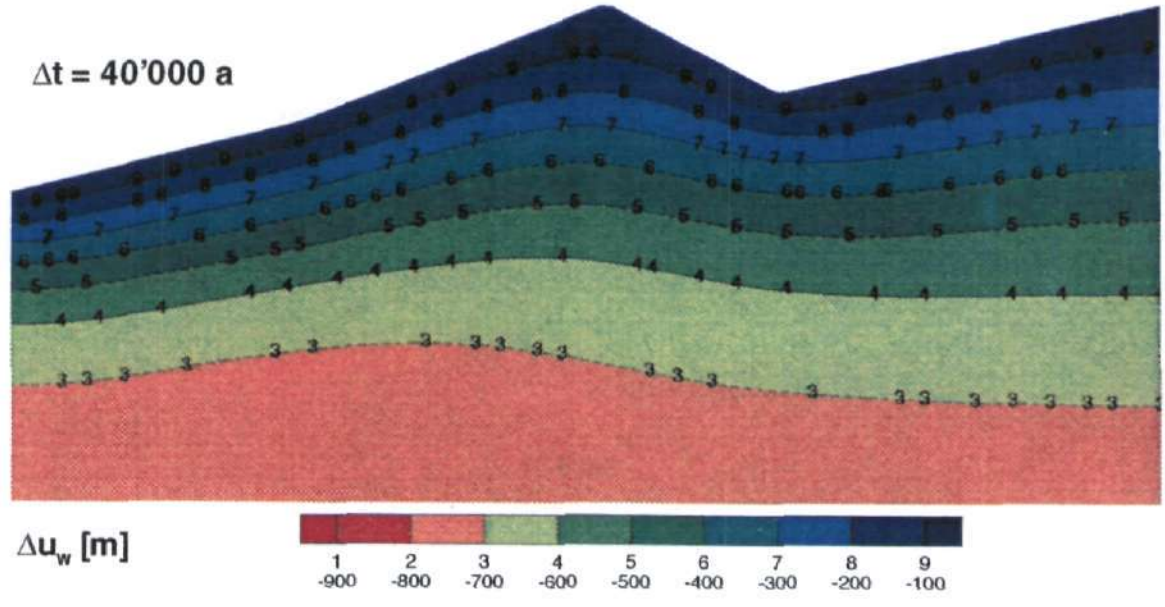

Fig. 7.5-7d: Underpressure distribution after 40'000 a

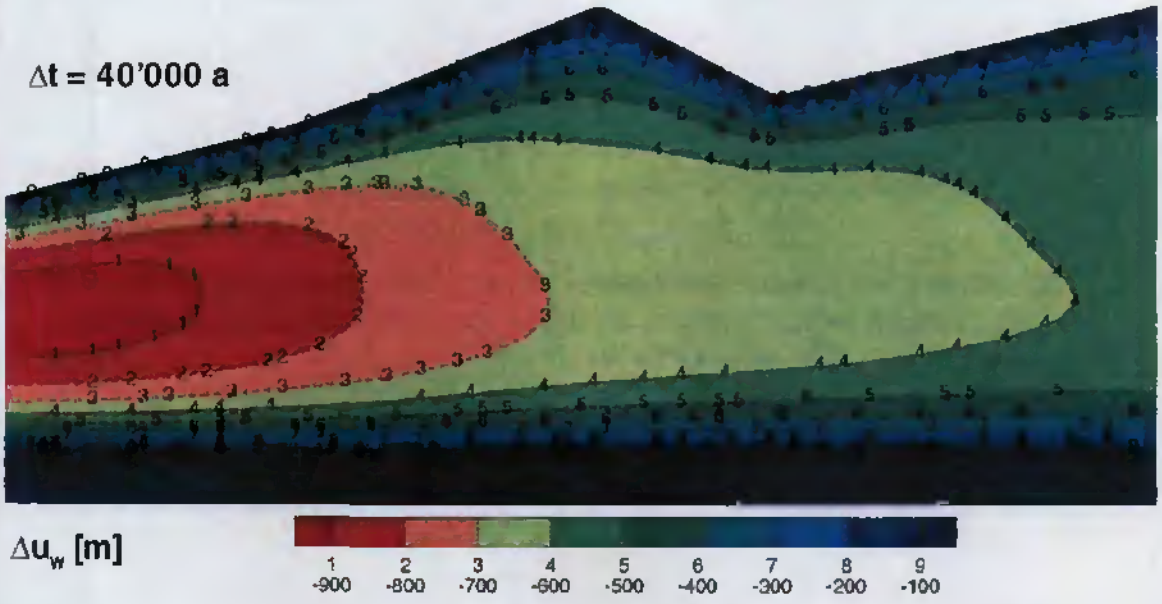

Fig. 7.5-8: Run 5 - Underpressure distribution after linear unloading over 10'000 a, assuming top + bottom drainage

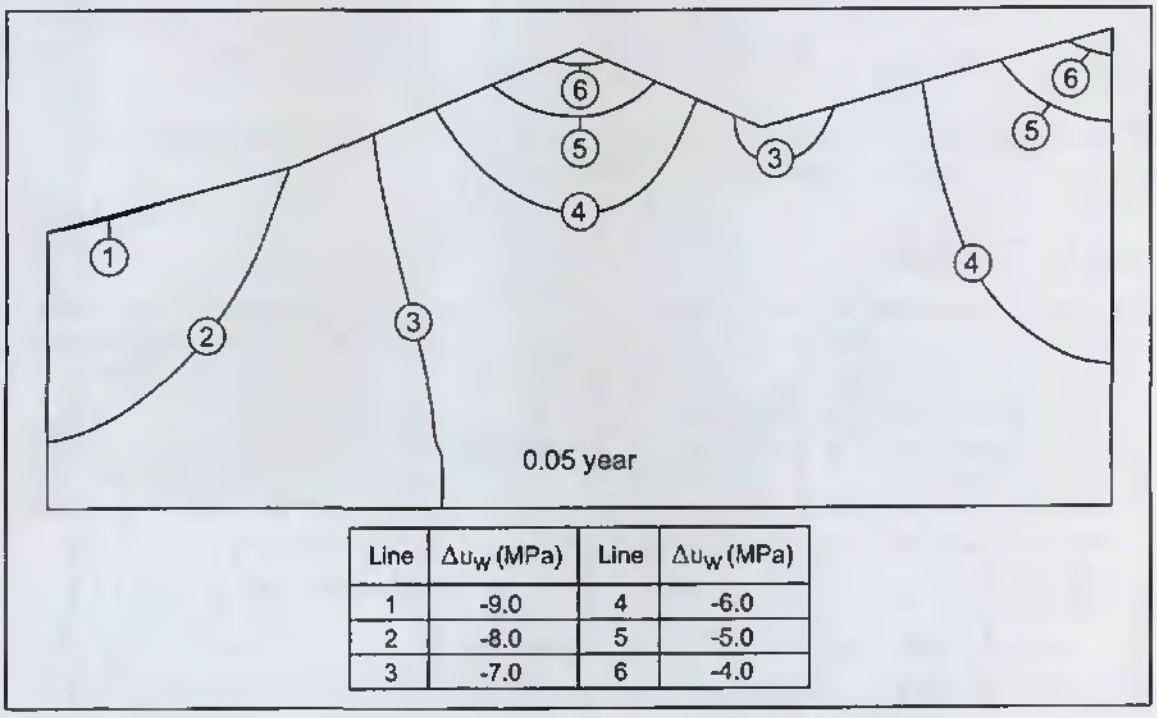

Line	Δu_W (MPa)	Line	Δu_W (MPa)
1	-9.0	4	-6.0
2	-8.0	5	-5.0
3	-7.0	6	-4.0

Fig. 7.5-9a: Single glacier unloading (Subsect. 8.4.4) - Underpressure distribution after 0.05 a (material B, drainage conditions 1)

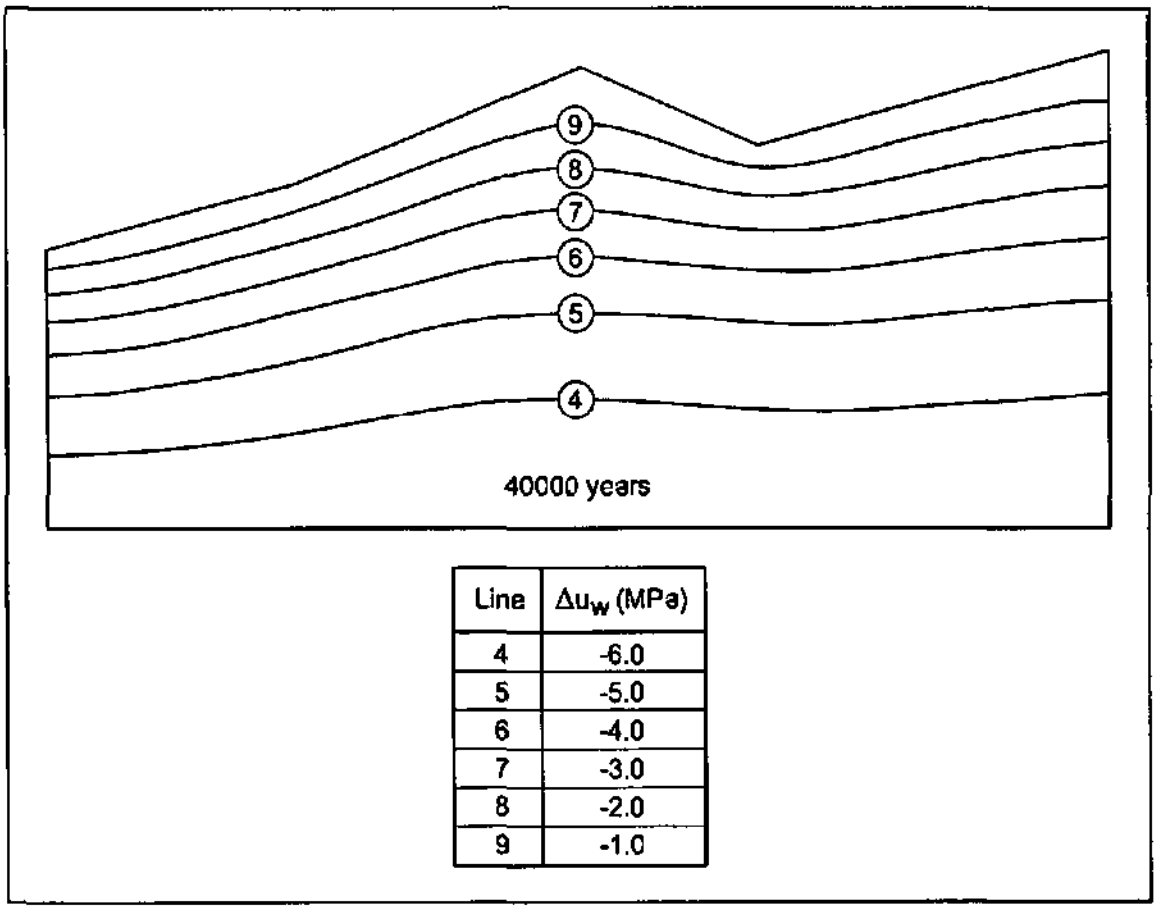

Line	Δu_w (MPa)
4	-6.0
5	-5.0
6	-4.0
7	-3.0
8	-2.0
9	-1.0

Fig. 7.5-9b: Single glacier unloading (Subsect. 8.4.4) - Underpressure distribution after 40'000 a (material B, drainage conditions 1)

7.5.3 ABAQUS

A coupled mechanical-hydraulic approach implies that the geomechanical processes are fully taken into account by mathematical expressions relating the material properties of the rock to the stress state and the corresponding pore pressures. Since pore pressures, in cases where external forces are acting on the hydrodynamic system, i.e. when "consolidation" (in the geomechanical terminology this term refers to any loading or unloading, i.e. also to "unconsolidation") occurs, the strains in the system directly influence pore pressures. Mathematical expressions linking groundwater flow, external stress and material properties together are describing coupled mechanical-hydraulic phenomena.

Applying a coupled mechanical-hydraulic approach allows one to:

- simulate various realistic unburdening scenarios
- verify the results of analytical scoping calculations
- consider time-dependent loading and unloading cycles with one forward run
- evaluate the effects of elastic material inherent properties (parameter variations on the Young's modulus, Poisson ratio, etc.), and to
- test alternative material models, especially those elaborated for clay-rich formations, which include non-recoverable strain and dilation of the rock skeleton in response to a change in octahedral stress.

ABAQUS is best suited to cope with the above objectives. The main advantages of this code are that it supports a large number of elements and material models, including non-linear processes associated with plastic material, creep and large deformation phenomena, and that it is routinely used in research institutes as for example MIT and ETHZ, and in large civil engineering companies, as for example OBAYASHI in Japan. The most current applications are in the field of construction and rock mechanics. The code is therefore well optimised and debugged to a fairly high level. However, as any other commercial code, ABAQUS requires a license and the source code is not available. Moreover, for the type of problems that were simulated with ABAQUS, rather large system capacity was required, so that the simulations were performed on a mainframe computer at MIT.

ABAQUS is based on the effective stress principle introduced in Section 7.4. For simulation, water-saturated conditions were assumed initially. Water is considered as a relatively compressible liquid, which when driven by a pressure head gradient, is free to move through the solid medium, as defined by the continuity equation. Additionally, the equilibrium equation for porous media and constitutive assumptions which incorporate the effective stress principle are necessary. ABAQUS uses Newton's method to solve the governing equations in the implicit time integration. The equilibrium condition governing the virtual work applied on the rock volume is approximated as a finite set of equations by introducing interpolation functions. For the description of the constitutive equations of the porous medium, the liquid, solid constituents and strains are approximated in the following way:

$$\text{Liquid: } \frac{\rho_w}{\rho_w^0} \approx 1 + \frac{p}{K_w^*} - \varepsilon_w^{th}$$

where ρ_w is the density of the liquid and p^0 is the density of the reference configuration, p is pore pressure, K_w^* is the liquid's bulk modulus, and ε^{th} is the volumetric expansion of the liquid caused by temperature change. Note that since in our case strictly isothermal conditions apply, the last term $\varepsilon_w = 0$.

The solid matter in the porous medium is assumed to obey the following relationship:

$$\frac{\rho_g}{p_g^o} \approx 1 + \frac{1}{K_g^*}\left(s \cdot p + \frac{\bar{\bar{P}}}{1-\phi-\phi_t}\right) - \varepsilon_g^{th}$$

where K_g^* is the bulk modulus of the solid matter (grains), s is the water saturation (= 1 in our case), and ε_g^{th} is the volumetric thermal strain. The change in grain density is assumed to be negligible. The porous medium as a whole will exhibit a softer bulk behaviour than is indicated by K_g^*, and will also show a different thermal expansion.

The effective strain is composed of the volumetric strain $-p / K_g^* + \varepsilon_g^{th}$ caused by pore pressure acting on the solid matter in the porous medium and by thermal expansion of that solid matter, which is zero in our study since isothermal conditions are applied. In addition, entrapment of liquid in the medium may cause additional volume change ratio as well as the volumetric swelling of the solid skeleton in partially saturated flow conditions. Both these contributions are also ignored in our study. Therefore, the remaining part of the strain in the medium is the strain which is assumed to modify the effective stress in the medium. That is, the following assumption is made:

$$\sigma' = \sigma' \text{ (history of } \varepsilon', \mathbf{T}, \text{ state variable, etc.)}$$

This assumption enables one to derive an expression relating the rate of change of the effective stress in terms of the rate of change of the cinematic and pore pressure variables. The continuity requirement is written for the water phase (trapped liquid and gaseous phase being ignored in our approach). The FE mesh is bound to the solid. Liquid flows through the mesh and requires therefore a continuity equation equating the rate of increase in liquid mass stored at a point to rate of mass of liquid flowing into the point within the time increment. The continuity equation is satisfied approximately in the FE model by using excess pressure as the nodal variable, interpolated over the elements. Technically, the time integration is done by using the backward Euler approximation. This is required for the Newton iterations used to solve the non-linear, coupled equilibrium and continuity equations.

The constitutive equation for flow is Darcy's law. By introducing the flow constitutive law, the mass continuity equation can be derived. The total volumetric strain in the liquid and grains is obtained by combining equations above for each medium. In our case, as stated earlier, only saturated conditions are considered, which implies that $p > 0$ ($u_w > 0$ in rock mechanics terminology). Since drastic unburdening produces desaturation in the pore space, i.e. negative values ($p = u_w < 0$), this will stand for capillary effects in the medium. The corresponding saturation conditions are limited by functional relationships that describe phase transitions (BEAR, 1972 "scanning" curves), which are approximated by straight lines in ABAQUS. As a consequence, since saturation is a state variable, it may have to change if the saturated pore pressure moves outside the range for which its value is admissible.

To solve the two coupled governing sets of equations of pore fluid diffusion-deformation (one set for equilibrium requirement, one for flow continuity), there are two solutions. The one is the so called "staggered" approach in which the first set of equations is solved first, and then use the results to solve the second set of equations, which - in turn - will feed the first set if any change is perceptible. The other approach, and this is the one used in our case, is to solve the coupled systems directly. This procedure ensures rapid convergence even in severely non-linear cases. More information about this procedure can be found in the ABAQUS handbook.

7.5.4 Material models

7.5.4.1 Use

The model scenarios consider two types of alternative materials as being representative of the marl-shale aquitard: the linear-elastic material model, which is used as base case, and the Cam-clay model. Both material models are considered as bounding cases for the "real" and unknown deformation behaviour of the aquitard materials. This approach has been chosen, because of the lack of appropriate material model for the marl-shale aquitard. The recently developed material model by HETTKAMP & RUMMEL (1996) came too late and does not fulfil the requirements.

7.5.4.2 The elastic material model

Following the definition given by JAEGER & COOK (1979), the properties of a material can be best identified when observing the stress-strain curve for a cylindrical rock sample under uniaxial compression. A linear elastic material is characterised by a perfectly linear relationship between applied stress and resulting strain. This dependency is provided for

both stress increase and stress reduction. Failure occurs at a critical stress level and provokes irreversible deformation (brittle).

Most natural rocks do not beheve in a linear-elastic way, but exhibit non-lineer pattems. Therefore, a more general definition of elastic materials, comprising non-linear functional relationship between applied stress and strain is required, which implies hysteresis between loading and unloading cycles, as shown in Fig. 7.5-10. The corresponding definition is: *a material is called elastic, if after loading and subsequent unloading to zero* stress, the strain returns to 0, but possibly by a different path. The hysteresis between loading and unloading cycles originates because more work is necessary to deform the sample while loading than while unloading. However, for this study we restrict ourselves to the simple linear-elastic formulation.

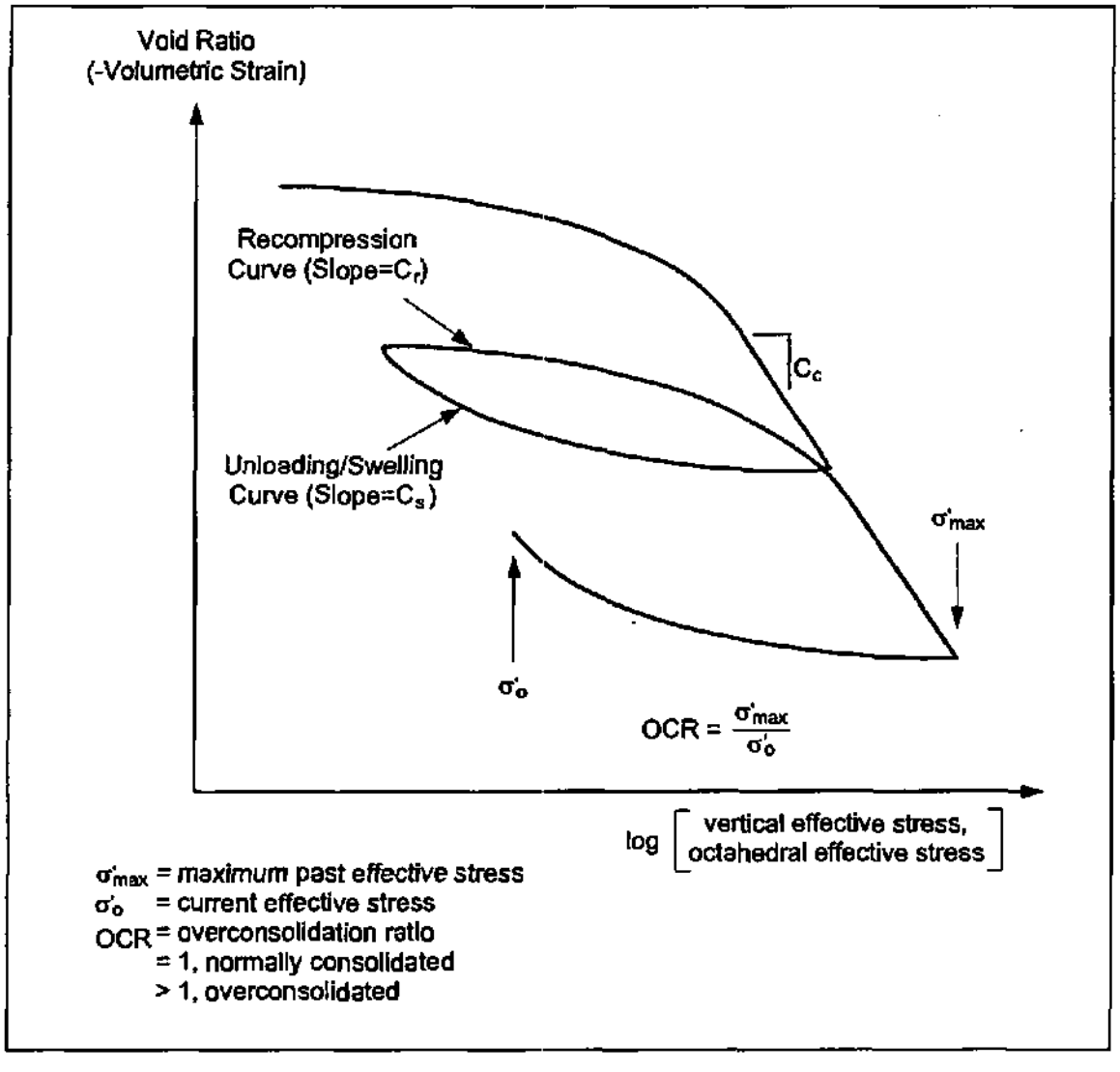

Fig. 7.5-10: Stress-strain paths for loading-unloading cycles for an elastic material (after EINSTEIN, 1993)

Fig. 7.5-10 shows the different paths followed by a rock sample during unloading and recompression. This deformation behaviour occurs provided the failure criterion is not reached. Experimental work shows that for small stress increments and for stress levels

below yield, most consolidated geological materials behave in a nearly elastic way (BERNABE & FRYER, 1995). The aquitard rock clearly exhibits both ductile and brittle deformation patterns (NAGRA, 1997; MAZUREK, 1997). Ductile deformation under high load and stress was progressively replaced by brittle deformation while the rock was uplifted and cooled down.

7.5.4.3 The Cam-clay material model

The Cam-clay is an elastic-plastic material. ABAQUS treats this type of material by defining an elastic component (conventional poroelastic material) and adding specifications for the plastic behaviour, more specifically for hardening or softening. The Cam-clay model is based on a large variety of shale occurrences and has been applied for various simulations reported in this thesis.

The Opalinus shale is a dilatant material, which means that volumetric (plastic) strain is larger than zero when loaded. The main mechanism for that is micro-cracking (cataclastic flow). Additionally, the Opalinus shale creeps. Creep tests show that both shear- and volumetric creep occur and that they are both linearly related to the logarithm of time. Creep increases with shear stress, i.e. the closer to failure, the larger the creep strains.

8 OVERVIEW OF EARLIER UNDERPRESSURE STUDIES

8.1 Objectives

This Chapter describes in more detail the approach applied to study the hydraulic underpressure phenomena outlined in Section 6.1 and the corresponding modelling studies, following both a historical and thematic guide line. Are presented: the conceptual models, their implementation in terms of analytical and numerical models, and the relevant outcome of the studies that were performed to better understand the pressure anomaly at Wellenberg. These studies paved the way for the more sophisticated abstraction schemes described in Chapters 9 and 10.

8.2 Historical approach

Almost immediately after the first indication of abnormally low hydraulic pressures in the first deep investigation borehole SB4, a project was launched in order to identify possible causes for the pressure anomaly and to test them by means of modelling studies (Chap. 6). A series of different categories of issues were identified as shown in the first row of Fig. 6.1-1. Among them, the first avenue of investigation was the reliability of the extrapolated packer test head data since, at that time, no direct (long-term) measurements were available to confirm or infirm the suspected phenomenon. The main concern was to exclude any kind of measurement or interpretation error. Two sub-categories were identified that could affect data quality or integrity: namely equipment failure or malfunction and erroneous conceptual models while interpreting the test responses. Borehole effects potentially leading to erroneous pressure measurements were analysed first because of borehole effects. While drilling a borehole, the radistribution of stress along the drillhole might deform the well in such a way that subnormal pressures are derived by packer tests. Analysis by means of the numerical code ABAQUS showed that this effect is marginal (ARISTORENAS & EINSTEIN, 1993). Moreover, as hydraulic testing and desk studies went on together, both investigation lines came more or less simultaneously to the same conclusion, which is that the subnormal pressures are real indeed, i.e. are not artefacts due to drilling or testing. The long-term pressure measurements provided the unmistakable demonstration of the reality of the phenomenon and therefore definitely concluded the debate.

8.3 Preliminary models

As a consequence of the confirmation of the physical significance of underpressures, all effort was redirected towards the true physical system response. As for the previous investigation phase, work took place iteratively, always with focus on the currently most plausible hypothesis. At this time, solely SB4 data was available. Minimum head values were estimated in the range 340 - 380 m a.s.l. This head range is not compatible anymore with exfiltration into the nearby Engelberger Aa valley (540 m. a.s.l.), nor with exfiltration into the Secklisbach valley (720 m a.s.l.), but a regional-scale discharge into the alluvial sediments of Lake Lucerne (340 m a.s.l) was still possible, although not very likely.

Therefore, a schematic 2D model was set up, led by the assumption that steady-state flow can generate subhydrostatic pressures in the observed range. The results showed that, although drainage towards the lake is theoretically able to produce a pressure decline as observed in SB4, the pressure increase to artesian at the bottom of the well could be reproduced only by implementing an ad hoc and very unlikely transmissive fracture connecting infiltration areas at the Eggeligrat with deep regions of the borehole. This

doubtful scenario contributed in convincing colleagues and experts of the existence of disequilibrium pressure at Wellenberg.

Boreholes SB1 and SB3, drilled some months after SB4, fully traversed the marl-shale aquitard and confirmed the pressure depression already observed in SB4. They even exhibited minimum head values down to values in the range of the current sea level, proving the transience of the hydrodynamic system.

8.3.1 Analytical models

The analytical models based on analytical solutions by TERZAGHI (1943) for instantaneous (un)loading and OLSON (1977) for constant rate loading and unloading. Analytical solutions are by nature restricted to 1D space and simple evolution scenarios. The most straightforward mechanism that comes to mind to any geologist familiar with alpine geology is glacier rebound, i.e. the unloading of the ground while the glaciers are melting away at the end of an ice age. Instantaneous glacier retreat 20'000 a ago was simulated based on TERZAGHI (1943), and slowly retreating glacier (constant-rate unloading) was modelled by means of the OLSON (1977) model (Fig. 8.3-1).

The relevant parameters K and S_s were derived from available hydraulic and mechanical data available at the time of analysis. They are presented in Tab. 8.3-1. The results, presented in Fig. 8.3-2 (calculations by LOW in VINARD & MCCORD, 1991 and by RIVERA in RIVERA & SENGER, 1993) show that simple analytical models are able to reproduce the observations. Although schematic, these models provide both quantitatively (match of observed head data) and qualitatively (shape of head profile) fairly convincing pressure profiles. The robustness of the preferred hypothesis was thus confirmed, encouraging to continue in this avenue of investigation.

Tab. 8.3-1: Key-parameters used in the 1D analytical solutions by Terzaghi and Olson

Parameters	K [m/s]	Specific storage S_s [m^{-1}]	Hydr. Diffusivity D [m/s^2]	Layer half-thickness L [m]	Time t [a]
Terzaghi model	$3.5 \cdot 10^{-14}$ $4 \cdot 10^{-14}$	$4.3 \cdot 10^{-7}$ $4.3 \cdot 10^{-7}$	$8.13 \cdot 10^{-8}$ $8.3 \cdot 10^{-8}$	**275** 300	20'000 20'000
Olson	$\mathbf{1 \cdot 10^{-13}}$* $1 \cdot 10^{-12}$	$\mathbf{6.6 \cdot 10^{-7}}$	$\mathbf{1.5 \cdot 10^{-7}}$ $1.5 \cdot 10^{-6}$	**825**	6'000 to 38'000

* data in bold refer to base-case values

The results suggest that D must be $\leq 1 \cdot 10^{-7}$ m^2/s. This value lies within a realistic bandwidth of K and S_s values.

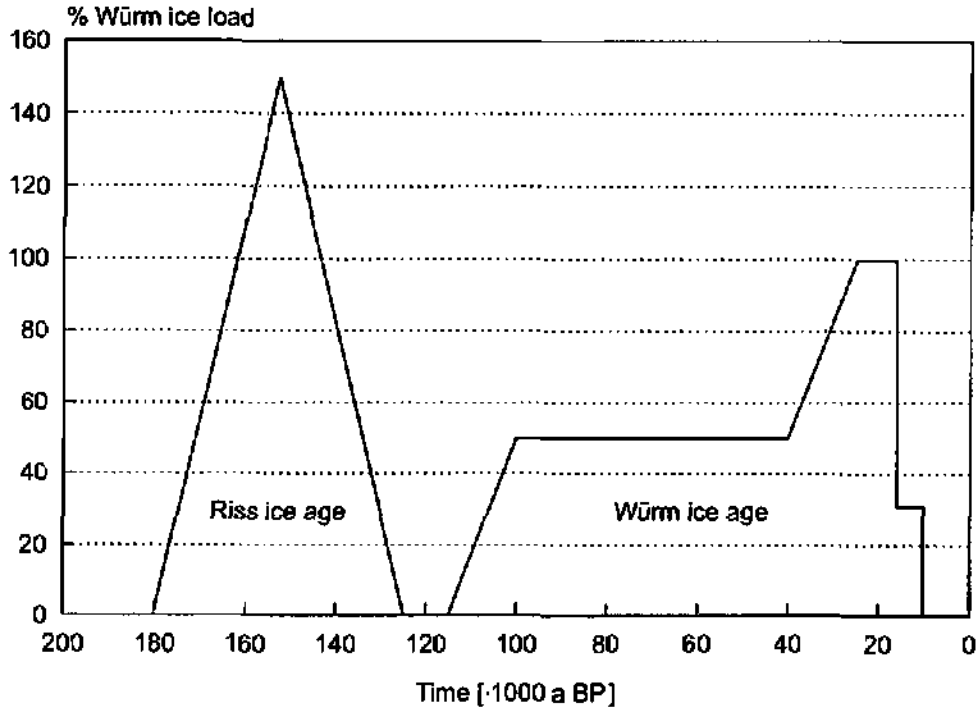

Fig. 8.3-1: Riss and Würm ice loading/unloading cycles used in OLSON's scenario

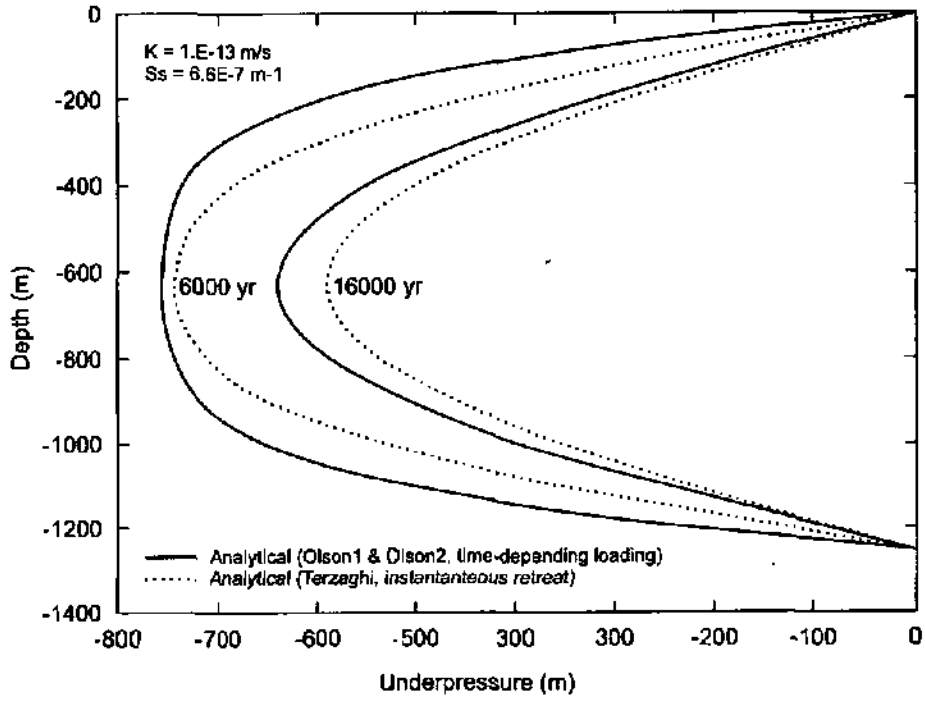

Fig. 8.3-2: 1D unloading - Comparison between TERZAGHI's and OLSON's analytical solutions (parameters in Tab. 8.3-1)

8.3.2 *Preliminary numerical model assuming an underpressure zone*

RIVERA & SENGER (1993) set up a model focussing primarily on potential effects of a UPZ in

and around the marl-shale aquitard aquitard. To do so, the model domain corresponds to the Pilot Model[1] domain (NAGRA, 1993a; MISHRA et al., 1993b), which is a schematisation of the hydrogeological units in and around the marl-shale aquitard (for definition of the according hydraulic units, see VINARD & LAVANCHY, 1994). The purpose of this study was to evaluate the time ranges for equilibration, and not the investigation of mechanisms leading to the observed head situation. It was assumed that the initial transient groundwater flow regime resulted from glacier retreat. The same approach was used in a more sophisticated way by VOBORNY et al., 1997 and also departs from an initial situation comprising an extensive UPZ.

The model simulations, albeit limited by misinterpretations of the geometry and boundaries of the UPZ, concluded with some basic statements that are generally valid and which can be summarised as follows:

1. A hydraulic underpressure zone strongly influences orientation and magnitude of hydraulic gradients. Hydraulic gradients are oriented from the lowest head value to normal head values in the periphery of the UPZ, thus indicate pressure dissipation by inwards flow. It is only after full dissipation of the UPZ that magnitude and orientation of hydraulic gradients in the aquitard will be typical for topography-driven groundwater flow.
2. As for the preliminary analytical calculations, the sensitivity of pore pressures to the diffusivity D is clearly demonstrated. D in the range of $1 \cdot 10^{-7}$ m^2/s is able to maintain underpressures over significant periods of time, in agreement with analytical results (Subsect. 8.3.2).
3. The study also shows that an interconnected fracture network traversing the aquitard strongly reduces the duration of the UPZ. This observation shows that large-scale, transmissive fractures are incompatible with an UPZ and therefore, that underpressures may serve as an exploration tool for investigating suitable aquitards for waste repository (Chap. 12).

8.4 Coupled geomechanical-hydraulic stress-release model study

8.4.1 Introduction

Analytical solutions are restricted to extremely simple problems in 1D space. For more realistic processes and geological settings, numeric treatment is necessary. ABAQUS was chosen on grounds of different criteria, which are presented, together with a brief code description, in Subsection 7.5.3.

8.4.2 Use

The model study was designed by myself and performed in close co-operation with Prof. Einstein and Dr. Aristorenas from the department of civil engineering of the Massachussetts Institute of Technology (MIT). The setup and interpretation work involved all three task members, while reporting was chiefly worked out at MIT (ARISTORENAS & EINSTEIN, 1993). Important results of this study are summarised in VINARD et al. (1993).

The major part of the modelling work was devoted to glacier rebound scenarios. A first phase studied the case of a single ice age, while a second phase analysed, for the first time in history, a succession of two glacier events. The rationale for designing glacier

---

[1] the Pilot Model is a schematic hydrodynamic model applied in the early nineties by NAGRA to test a variety of hypotheses

rebound scenarios can be summarised as follows:

- Glacier unloading was already investigated by means of analytical solutions (Subsect. 8.3.2), and represents therefore a valuable comparison basis.
- Two different cases can be studied independently: The sole of glaciers can either be considered as impermeable, in which case permafrost is assumed ("cold glacier" ⇒ non-draining conditions) or as permeable, in which case melting water from the glacier and groundwater can move freely ("temperate glacier" ⇒ draining conditions).
- Ice ages comprise all types of loading and unloading events, i.e. rapid and slow loading and unloading can be investigated separately.
- Glacier unloading represents the latest possible unloading process, and is therefore conservative in terms of dissipation duration.
- Glaciations are fairly well reported in the Quaternary era and provide a much more reliable database as any other type of geologic forcing.

8.4.3 Description of the different model scenarios

Tab. 8.4-1 summarises the topic of the two investigation phases devoted to glacier rebound and to tectonic thrusting IN ARISTORENAS & EINSTEIN (1993).

Tab. 8.4-1: Model scenarios evaluated by means of coupled mechanical-hydraulic models

Ph.	Title	Hypotheses	Cases
2	Effect of glacier melting on pore pressures	Simple unloading due to glacier melting. Ice build up and melting is almost instantaneous (0.5 a). Total duration of post-glacial phase: 40'000 a	1. top drainage only 2. top and bottom drainage
3	Effect of multiple glaciation on pore pressures	Two glaciation loading/unloading cycles as represented in Fig. 8.3-1	
4	Effect of tectonic thrusting on pore pressures	Lateral constant rate thrusting	

Phases 2 - 4 studies base on the same 2D model domain, which corresponds approximately to section Q - Q' (oriented southwest - northeast and traversing the reference boreholes SB1 and SB3). The units present in the profile are the aquitard ("marl" in Fig. 8.4-1), a highly permeable basal layer representing the Parautochthonous ("basis layer") and a pervasive ice sheet covering completely the marl.

In phases 2 and 3, the aquitard-material is elastic-isotropic. Three classes of material-stiffness were tested, defined by Young's modulus selected based on laboratory measurements. These values are reported in Tab. 8.4-2 (E is Young's modulus, ν is Poisson ratio, K is hydraulic conductivity and γ is buoyant unit weight.

The simulations are performed assuming plane strain conditions. The ground surface and the bottom permeable layer provide drainage if so specified. No drainage occurs during glacier retreat (usually 0.5 a). This corresponds to assuming a continuous permafrost layer at the sole of the glacier (undrained conditions), which allows drainage as soon as the ice load is removed (drained conditions).

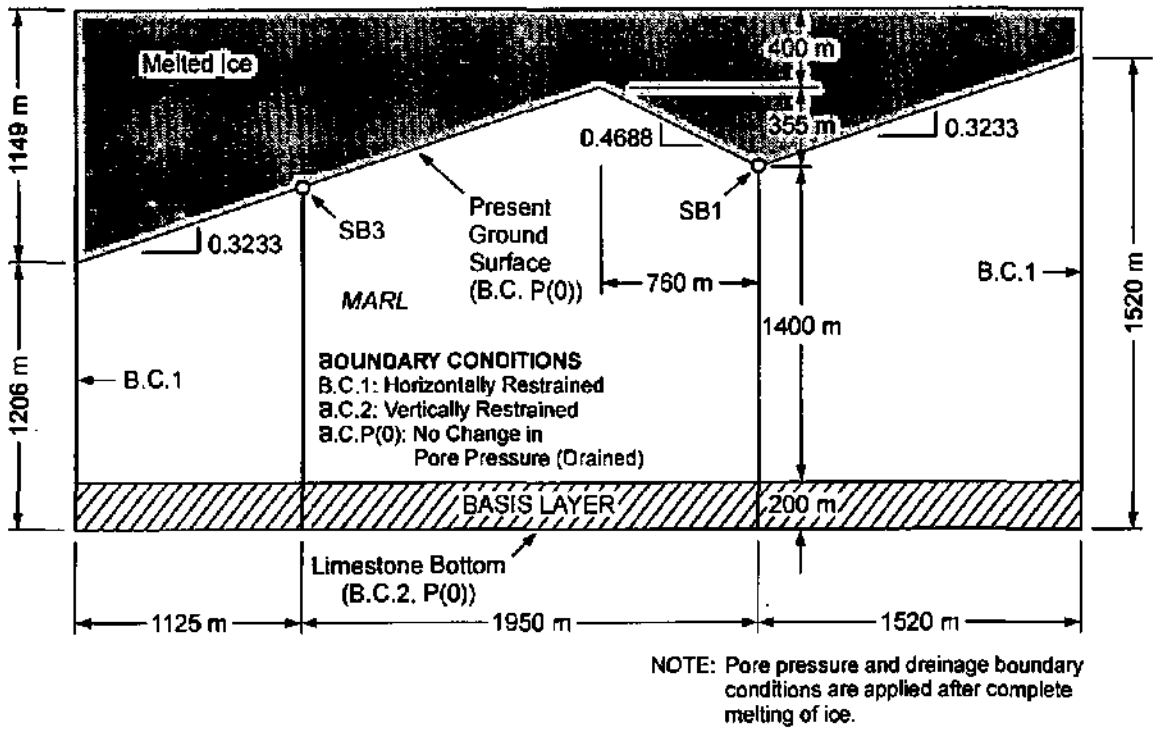

Fig. 8.4-1: Schematic cross-section used in glacier rebound study

Tab. 8.4-2: Properties of the materials used in phase 2 and 3 calculations

Material	Parameters			
A	E: 1 GPa	ν: 0.3	$\gamma = 0.015$ MPa/m	$K = 1 \cdot 10^{-13}$ m/s
B	E: 15 GPa	ν: 0.3	$\gamma = 0.015$ MPa/m	$K = 1 \cdot 10^{-13}$ m/s
C	E: 30 GPa	ν: 0.3	$\gamma = 0.015$ MPa/m	$K = 1 \cdot 10^{-13}$ m/s
Bottom layer	E: 15 GPa	ν: 0.3	$\gamma = 0.013$ MPa/m	$K = 1 \cdot 10^{-8}$ m/s

8.4.4 Singla glacier event model scenario

Initial conditions are set at the end of a former glaciation, i.e. at a time when possible overpressures due to the ice load have already decayed. Two cases each with three parameter variations corresponding to materials A, B and C were computed.

In case 1, only the ground surface is a drainage boundary, while the bottom layer remains impermeable. In case 2 both ground surface and bottom layer are open boundaries, i.e. dissipate excess pore pressure. These two cases represent extreme scenarios encompassing any real situation.

As expected, the stiffness of the aquitard material determines, together with K, the rate and duration of disequilibrium pressures. Material A produces the strongest head deficit (- 900 m) and the longest duration of underpressures. After 40'000 a, only minor dissipation of negative excess pressure has occurred since the rate of dissipation is proportional to the stiffness of the material. While different material properties impact little on the absolute magnitude of abnormal pressure, large differences arise in the duration of dissipation.

Assuming top and bottom dreinage simultaneously, produces a head pattern in conformity with the observed one as illustrated in Fig. 8.4-2. The best correspondence with actual measurements is for material B, which Young's modulus actually represents the average of measured laboratory data. Fig. 8.4-2 shows the distribution of excess pore pressures (Δu_w) and the corresponding change in head ($\Delta h = \Delta u_w/\Delta_w$) with depth along SB1 and SB3, respectively. Both observed and simulated data exhibit the strongest underpressures near the middle of the aquitard. Zero or positive excess pore pressures occur at the ground surface and in the underlying unit.

The largest difference between simulated and observed data occurs in borehole SB3, whera the upper 500 m of tha aquitard did not reveal underpressures, whereas underpressures are predicted by the simulations. This difference is due to a relatively large decompaction zone in SB3 as revealed by its transmissivity profile (NAGRA, 1997). Tha model, however, considers the aquitard as an isotropic medium with continuous properties. Negative excess pore pressures could dissipate in the zone around SB3 due to the localised occurrence of higher permeability. This observation is important because it reveals how underpressures can be indicative of K-heterogeneity at hectometre scale.

In conclusion of phase 2 model scenarios, ARISTORENAS & EINSTEIN (1993) state that "although glacier retreat alone may not entirely explain the occurrence of underpressures, it may be a significant component of a more complex combinations of mechanisms, including multiple glaciation and/or tectonic thrusting". That is why two additional model phases were performad which specifically address these aspects.

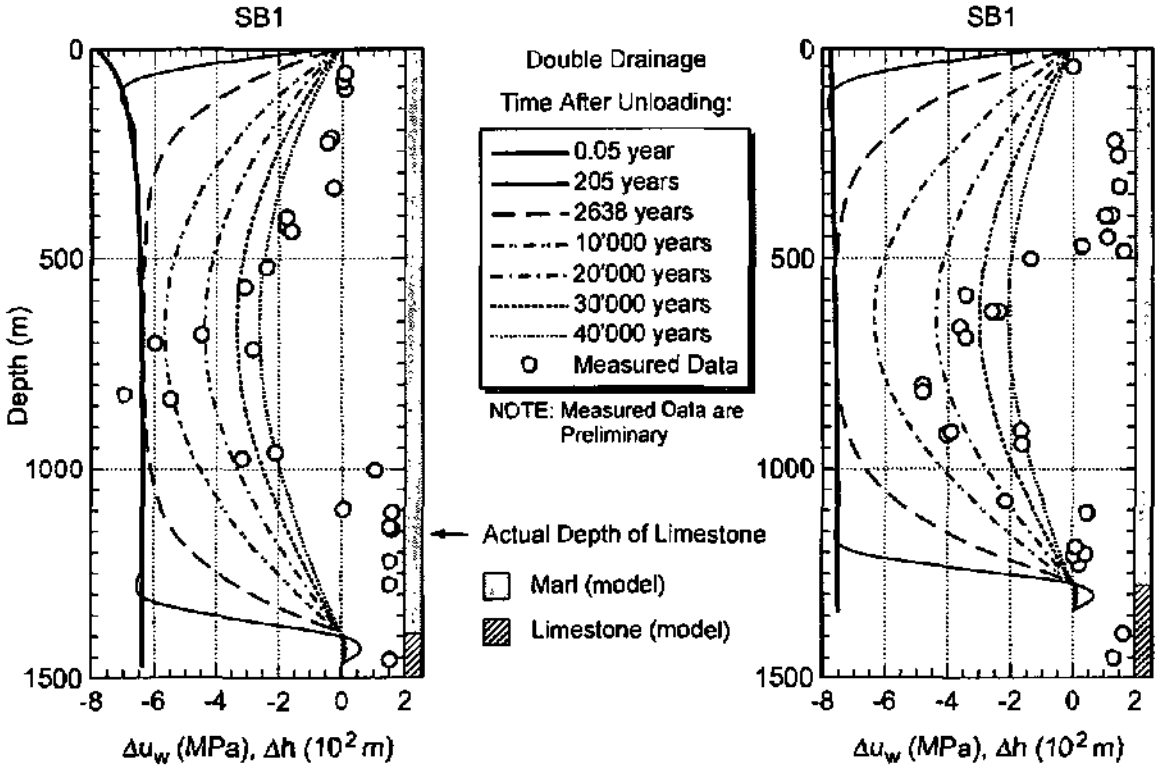

Fig. 8.4-2: Comparison between observed and computed excess pore pressures in boreholes SB1 and SB3 (after VINARD et al., 1993)

8.4.5 Multiple glaciations model scenario

Two successive ice ages have been assumed, which duration, build up and dating are no longer in conformity with recent findings of the Quaternary geology. This scenario, however, still produces important results, which helped refining the next model generation (Chap. 9). Here also, influence of top and bottom drainage is analysed (material B) As expected, assuming permafrost results in the generation of overpressures during the ice load reaching up to Δu_w = 14 MPa. The pressures are almost uniformly distributed over ice ages, because the fluid flow within the domain redistributes pore pressures. In the case where excess pore pressures can dissipate during the ice ages themselves, the absolute magnitude of overpressuring is lower and the distribution of pore pressures is not uniform with overpressures concentrating at places where the marl-shale aquitard thickness is most. This is due to the greater distance from drainage boundaries.

Another interesting outcome is that the duration of an ice age is at least as critical as the applied load. Without drainage, i.e. dissipation of overpressures during ice ages, underpressures could not be explained by the glacial hypothesis. Equally important is the finding that the pore pressures generated during a previous ice age do not significantly affect the pore pressures generated during the next glacier event. The main reason for this behaviour is not so much bound to the respective duration of glaciations and interglacials, but to the use of an elastic-isotropic material. This type of material results in zero residual volumetric strain (i.e. is not afflicted by a hysteresis in deformation). Since volumetric strains are, by definition, responsible for disequilibrium pressure, if the net balance between loading and unloading equals zero, the system cannot "remember" former deformation stages, i.e. formar underpressures, unless the glacial cycle is of a higher frequency than the hydraulic system response, which is obviously not the case.

Assuming plastic deformation with a significant dilatant component, irrecoverable plastic volumetric strain will result, even assuming equal duration loading and unloading cycles. These strains will produce remnant (residual) negative excess pore pressures. In this case a genuine "memory effect" may develop.

8.4.6 Schematic tectonic thrusting

Tectonic thrusting is a very complicated phenomenon, especially in case of polyphase deformation. Crustal movements are in essence three-dimensional and are described by kinematic or rheologic models. This type of modelling is by itself a distinct area of research. Most kinematic models are built at the scale of entire mountain chains (The Himalayas, Andes, Alpes) and encompass the lower crust, i.e. depths down to 30 km or even down to Moho. At this scale, modern rheologic models provide rather satisfactory evolution schemes (e.g. BEAUMONT et al., 1994; CLOETHING et al., 1995). However, at the scale of some few kilometres, no useful models do exist. Moreover, the constitutive material laws applied in tectonic modelling are very primitive and do not take groundwater flow into account or else only in terms of high pore pressure boundaries at the interface between adjacent thrusting or sliding units.

For the preliminary attempt by ARISTORENAS & EINSTEIN (1993), the simplifying assumption was made that tectonic thrusting produces a finite uniform horizontal displacement. This means that as for the Casagrande experiment, the material is constrained in a box and is compressed laterally by a continuous and uniform strain increment Δ applied to the one of the lateral boundaries. The 2D, plane strain FE analysis of tectonic thrusting was performed using the same idealised section of the Wellenberg area as for the glacier model scenarios (simplified cross-section Q - Q'). The horizontal displacement Δ was prescribed in such a way, that the horizontal effective stress σ'_h resulting from thrusting is approximately twice σ'_v, the vertical effective stress component. This represents, in two dimensions, the actual situation supposed to exist at Wellenberg.

In terms of volumetric behaviour, two key mechanisms can occur under such conditions:

1. contraction (or positive excess pore pressure generation) due to the increase in the octahedral (mean) effective stress
2. dilation (or negative excess pore pressure generation) due to extension shearing normal to the thrusting movement.

Since no appropriate material model is available, the model was run with the Cam-clay model briefly introduced in Subsection 7.5.4.

The numerical simulation produced only positive excess pore pressures. This implies that the contraction due to an increase in the octahedral effective stress dominates the dilation due to extensional shearing. However, the reader - as the authors state - should not be "... lured to believing that tectonic thrusting can never produce underpressures in the ground...". Actually, two factors may play a governing role which were not acknowledged in the study:

a. since no displacement normal to the plane of the vertical section was allowed, a substantial increase in the horizontal stress normal to the plane results, which produces a substantial increase in the octahedral effective stress. This, in turn, enhances strongly positive excess pore pressures. In reality, some movement of material normal to the plane would occur. If so, the horizontal stress normal to the plane, i.e. the effective octahedral stress would not increase as much as under the assumed plane strain conditions and thus, only small positive excess pore pressures would result. Therefore the negative excess pore pressures produced by extensional shearing might be sufficiently large to result in net underpressures.
b. the shale model and its material properties used here might well not accurately represent the behaviour of the marls and shales at Wellenberg. The bulk stiffness of the Cam-clay is probably much smaller than the one of the marl-shale aquitard. Although a stiffer material will contract less (i.e. will produce lower positive excess pore pressures), due to an increase in octahedral stress, it still may be dilatant and may therefore possibly produce negative excess pore pressures.

Whatever promising it might be theoretically to investigate this field, the following reasons led the course of further studies:

I. too little is known about both the processes and evolution of material parameters during the deformation of the marl-shale aquitard to properly design "reliable" model scenarios
II. noticeable underpressures do probably not result primarily from anisotropic dilatant deformation normal to the thrusting movement.
III. it is very unlikely that tectonic events that markedly influenced rock behaviour in a time range between 25 millions and 11 millions years and that are, to some extent, still active today, contribute decisively to generation and especially maintenance of abnormally low pore pressure.

8.5 Two-phase flow models

8.5.1 Scope

A lot of effort was spent to derive model scenarios describing steady-state and transient gas flow through the marl-shale aquitard. The objectives were two-fold: on the one hand,

and keeping the Oberbauenstock underpressure phenomenon in mind, the idea was to investigate the potential for free gas to produce - under natural conditions - hydraulic subnormal pressures in the observed range, and, on the other hand, to evaluate the robustness of the rebound theory in presence of minor amounts of free gas in the aquitard. Later on, an additional objective arose once the results of the first two studies were available with focus on the porous matrix. The hypothesis revolved around the potential for dissolved gas in the pore water to come out of solution and affect pore pressure development.

8.5.2 One-dimensional stationary and transient gas-flow models

8.5.2.1 Introduction, scope

Gas, especially methane, has been observed both at Wellenberg and Oberbauenstock, at surface and in boreholes. Soil gas surveys (gas extraction immediately below ground surface) and gas discharges into boreholes were to some extent interpreted as indications of free gas in the aquitard. Therefore, the study summarised hereafter was designed to investigate the potential for free gas to produce subnormal pore pressures (FINSTERLE et al., 1992). The calculations were performed on a 1D column, applying the multiphase simulator TOUGH2 (PRUESS, 1991).

The objectives of this scoping study were:

I. to assess possible two-phase flow mechanisms able to reproduce the anomalous head profiles in boreholes

II. to provide an order-of-magnitude estimate of the corresponding gas flow rates, pressure and saturation profiles

III. to determine the time scale of the pressure transience

IV. to discuss model requirements and parameter sensitivities.

The conceptual idea is that the gas bearing Valanginian marl[2] (Palfris formation) is being depleted either continuously or discontinuously by buoyancy effects. Since in this tight formation water will refill the pores left by methane with some delay, a transient UPZ of varying position and extension will result, which acts like a sink for groundwater.

8.5.2.2 Model setup

The model space is a 1D vertical column extending from ground surface to a depth of 1'100 m b.g. The overlying unit consists of a 300 m thick layer of Quaternary deposits, followed by a 700 m thick marl section underlain by permeable Tertiary sediments (subhelvetic Flysch) at the bottom of the model. Model calculations base on Van Genuchten functional relationships (capillary pressure - liquid saturation, capillary pressure - relative permeability) as well as on corresponding parameters (S_{gr} residual gas saturation, S_{lr} residual liquid saturation, and $1/\alpha$), (LUCKNER et al., 1989).

Three model cases were analysed: Cases A and B differ only in the hydraulic properties of the aquitard, whereas in case C, the marl has been subdivided in three units of decreasing permeability with depth.

---

[2] the Tertiary shales were not considered at that time, but bear similarly properties

8.5.2.3 Results and conclusions

Fig. 8.5-1 presents the steady state pressure and saturation profiles for case B (permeability of the marl: $k = 1 \cdot 10^{-18}$ m^2 $\Rightarrow$ $K \approx 1 \cdot 10^{-11}$ m/s). Gas is generated in the basal layer at a total mass flow rate of about 2.5 g/a/m^2. The resulting pressure and saturation distributions (Fig. 8.5-1) show that gas is flowing continuously upwards through the marl which is acting as a pressure seal. The gas saturation in the marl reaches up to 18 %. The most important result is "that gas pressures in the marl exceed the single-phase liquid profile exactly by the value of the capillary pressure" (FINSTERLE et al., 1992). Thus, not underpressures but overpressures result from steady-state gas flow, disproving at the same time the steady state gas flow model (Model B) set up for the Oberbauenstock site (NAGRA, 1988). Moreover, this result has implications of paramount importance since it indicates that whatever physical mechanism is considered for the generation of subnormal pressure, *the head anomaly at Wellanberg can only result from a transient process or a combination of transient processes.*

On the contrary of steady state gas flow, transient gas flow, as illustrated by Fig. 8.5-2, is able to generate subnormal pressures of the order of the observed ones. By assuming a gas reservoir, either within the aquitard or in the underlying formation, which - for any reason - ceases production or considerably reduces it, transient depletion of gas inside the marl occurs. Water is literally sucked away from the aquitard by buoyancy from both underneath and above (1D model) and will only progressively occupy vacant pore space. Fig. 8.5-2 shows that both gas saturation and pressure vary through time. Even after 5'000 a, significant underpressuring persists.

Case C resembles the previous case with the difference that the marl is subdivided in three sub-units with decreasing permeability from top to bottom (upper marl section: $k = 5 \cdot 10^{-16}$ m^2, middle marl section: $k = 1 \cdot 10^{-17}$ m^2, lower marl section: $k = 2 \cdot 10^{-19}$ m^2; in comparison, Quaternary: $k = 1 \cdot 10^{-14}$ m^2, basal layer: $k = 1 \cdot 10^{-14}$ m^2). As a consequence, the initially overpressured lower marl section becomes progressively underpressured. The subnormal pressures are constrained within the tightest section of the aquitard. The impact of K-heterogeneities on the development and maintenance of disequilibrium pressures is, hence, demonstrated once more.

These results prove that the two-phase flow hypothesis can be substantiated. However, this conceptual model bears two striking weaknesses:

1. According to the simulations, very low pressures are synonymous of significant amount of free gas (up to 18 %). This high amount of free gas is not conform with observations nor with geochemical equilibration calculations (NAGRA, 1997).

2. Transient gas flow simulations predict a dissipation of most of the disequilibrium pressures within few thousands of years. Therefore, the gas source at depth must have been depleted more or less completely also few thousands of years ago in order to allow a free gas "bubble" inside the aquitard to migrate upwards. No appropriate geological event could be identified within the last millenniums which could explain recent gas production or migration. Gas production occurred much earlier, during the Neoalpine deformation phase. The interruption of gas generation is contemporaneous with surrection and unburdening of the marl-shale aquitard, more than 15 Ma BP, when these sediments were removed from the oil/gas production window (NAGRA, 1997).

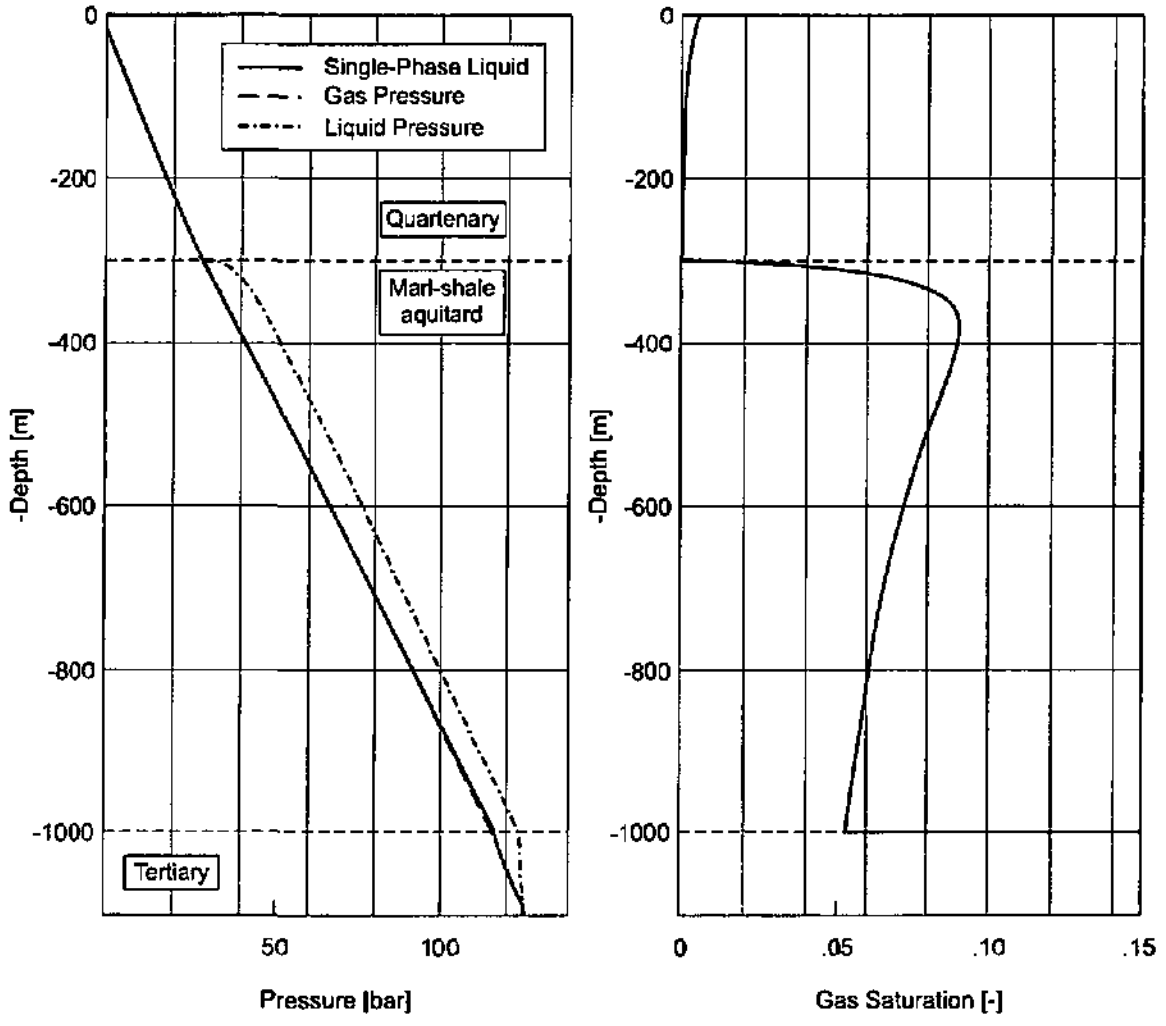

Fig. 8.5-1: Hydraulic pressure (left) and saturation (right) profiles for steady-stete gas flow

8.5.3 One-dimensional mechanical rebound model under two-phase flow conditions

8.5.3.1 Conceptualisation

Acknowledging the results of the preceding study (FINSTERLE et al., 1992), the next investigation steps were designed to test the compatibility of the mechanical rebound model with realistic amounts of free gas in the aquitard.

The basic physical conceptualisation and simplifying assumptions are summarised in Subsection 7.4.3. As a rule, free gas - owing to its high compressibility - will "absorb" as a function of its saturation, a relatively large portion of the change in pore volume provoked by unloading. Hence, free gas will reduce the magnitude of pore pressure changes. Free gas will preferentially occupy larger pores (capillarity) and hence constrict water to smaller pores, which in turn reduces the permeability to water and therefore prolongs the duration of disequilibrium pressure.

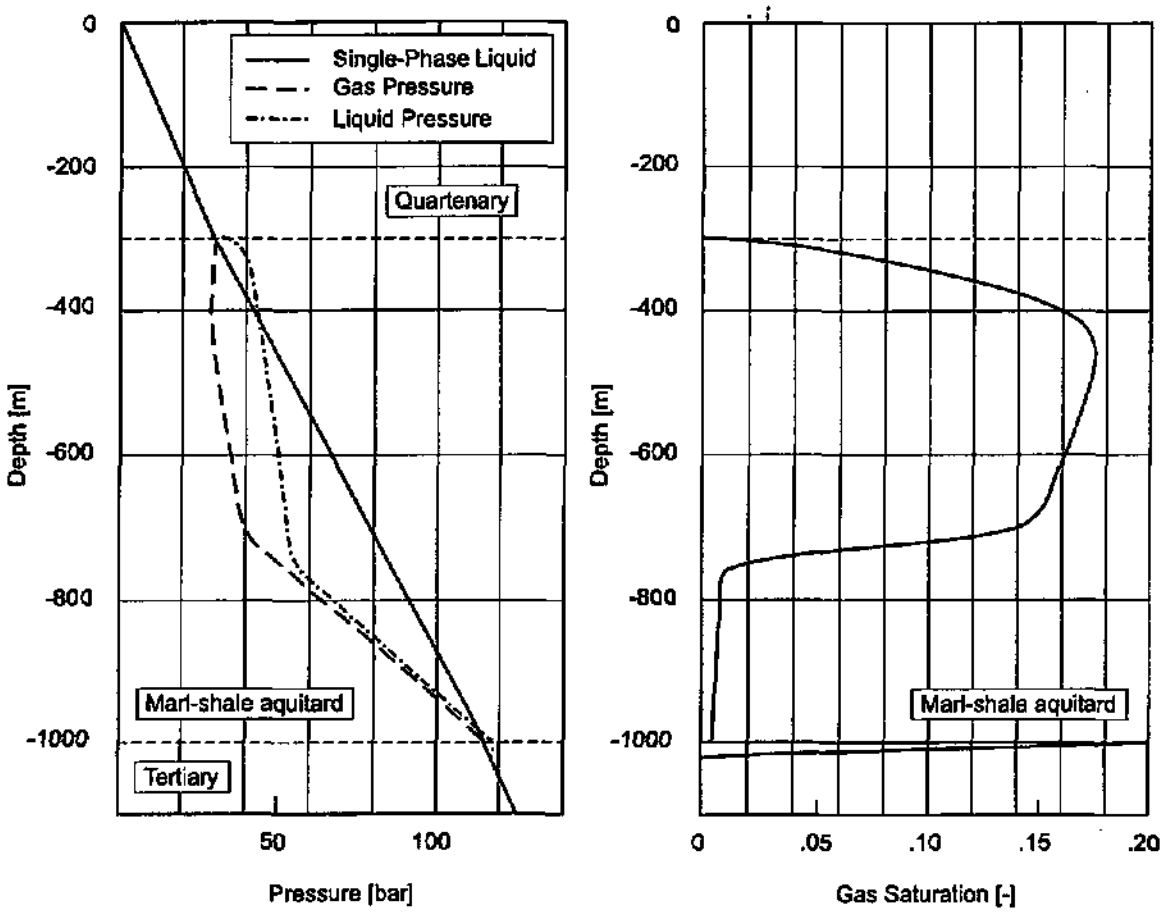

Fig. 8.5-2: Hydraulic pressure and saturation profiles for transient gas flow

8.5.3.2 Model setup

In a first step, FINSTERLE (1992) applied the same 1D approach as for the previous gas flow study and used the following conceptual model.

The rebound due to glacier retreat happens instantaneously on the fully consolidated linear-elastic aquitard rock, which contains initially both water and gas as continuous phases. The stress release $\Delta\sigma$ provokes an instantaneous increase in porosity ($\Delta\phi$) and in gas saturation (from S_{g0} to S_g). The initial excess pressure is based on the assumption that the change in porosity $\Delta\phi$ results from a change in the total stress (instead of the change in the effective stress, leading to an error of less than 10 %). The initial pressure decline is governed by the ideal gas law and that rock properties are homogeneous and constant with time. The pressure recovery is calculated using the two-phase numerical simulator TOUGH (PRUESS, 1987), using the extension of Darcy's law for two-phase flow conditions.

The model study revolves around a base case (Fig. 8.5-3), a thorough parameter sensitivity study by means of Monte Carlo simulations, and a more complex model case taking gravity, geothermal gradient, degassing and the impact of pore fluid pressure on the initial pressure decay into account. The setup of the model considers a 800 m layer thickness, which is instantaneously unburdened by glacier melting, resulting in a stress reduction ($\Delta\sigma$)

of 15 MPa (1'500 m of ice), 20'000 a BP. Tab. 8.5-1 summarises the relevant parameters.

Tab. 8.5-1: Mechanical rebound under two-phase flow conditions: model parameters

		Base case	Range	Remarks
Permeability k	[m^2]	$3.25 \cdot 10^{-21}$	10^{-21} - 10^{-20}	constant
Rock compressibility α	[1/Pa]	$2.66 \cdot 10^{-10}$	10^{-11} - 10^{-9}	constant
Initial porosity	[-]	0.01	0.01 - 0.05	prior to unloading
Gas saturation in aquitard	[-]	0.1	0.01 - 0.99	prior to unloading
Gas saturation in drainage boundaries	[-]	0.2	0.01 - 0.99	constant
Initial pressure	[MPa]	5	—	prior to unloading

After a first verification of TOUGH with the analytical solution by TERZAGHI & FRÖHLICH (1943), the calculation of the base case produces an increased porosity of 0.014, a gas saturation of about 0.36 and a pressure decay of 4 MPa. Starting with an initial negative excess pressure head of -400 m, the dissipation process acts by water and gas inflows from the top and bottom drainage layers, producing a moving gas-water front towards the centre of the aquitard. The diffusivity change across these gas-water fronts leads to the pronounced kinks, especially at the beginning of the dissipation phase (curve t: 5'000 a in Fig. 8.5-3). About 75 % of the additional pore space due to rebound is filled with gas, the remaining volume being occupied by water.

Comparison between single-phase and two-phase cases shows clearly that although the initial magnitude of subnormal pressure is considerably lower if free gas is initially present (only 400 m reduction in head versus 1'500 m in the fully water-saturated case), the lower diffusivity ratio causes the pressure equilibration process to recover much slower. Therefore, under the assumed model conditions, the underpressures resulting after 20'000 a would be similar in both cases.

The more complex model accounting for gravity, degassing and thermal effects yields following conclusions: For mobile gas and water, gravity leads to buoyancy effects provoking phase segregation, the geothermal gradient induces density effects. In addition, the thermophysical properties of gas and water are depth-dependent. By lowering the initial static pressure, dissolved air in the pore water will degas, when neglecting this effect, one will overestimate the initial pressure deficit borne by the water, and finally relating pore pressure changes to the change in total stress instead of effective stress also leads to an overestimation of the initial excess pressure. Taking the above effects into account impacts on the shape of the pressure and saturation profile. However, the main features of the stress-release model are conserved. The main difference is that the initial excess pressure is no more symmetric, but increases with depth because of the higher pressure and thus lower compressibility of the gas phase.

8.5.3.3 Results and conclusions

In summary, the stress-release model remains valid even if a certain amount of free gas exists inside the aquitard. Minor amounts of free gas do not notably modify unloading properties, i.e. do not affect noticeably the magnitude of pressure decrease, but small amounts of free gas are able to reduce the permeability to water in such a way that the diffusion of the pressure perturbation is delayed.

8.5.4 Mechanical rebound models under dual porosity two-phase flow conditions

8.5.4.1 Rationale

This new abstraction scheme is based on the same evolution scenario and boundary conditions than the one described above (Subsect. 8.5.3), but considers the rock as a dual porosity system (detailed information is to be read in SENGER, 1997.

In a dual porosity system, it is expected that any change in overburden stress acting on an aquitard comprising initially both gas-filled macropores and water-filled micropores, will affect pores differently initially and with ellapsing time, pressures tend to equilibrate between micropores and macropores. Pore pressure change will depend on the gas saturation in the macropores and initial pore pressure. The main goal was to check if a dual porosity system reacts differently than an EPM-model.

The concept is that the matrix[3] - in this case we consider only the Palfris formation - contains micropores filled with water and macropores filled with gas (either methane or trapped air). The origin of this conceptual model resides in a misinterpretation of the signification of centimetric geodes, unevenly distributed in calcite veins of the Palfris formation (Subsect. 3.2.2.2). Total porosity values for the matrix as presented in NAGRA (1997) were subject to a strong debate: < 2 % for NAGRA, between 2.3 - 4.1 % for some experts, but all agreed that most of the pores are micropores and that the ratio between the open macroporosity and the total matrix porosity is about 5 to 10 %, whereby geodes represent only 0.3 % of the open matrix macroporosity. Therefore, geodes *cannot* play a significant role on pore pressures. Consequently, this model is based on purely imaginary macropores.

In the base case, a high initial gas saturation of 11 % in the macropores is assumed. An instantaneous unloading of 5 MPa (500 m) is imposed. The reequilibration decreases rapidly the initial pressure difference between macropores and micropores, reaching an evenly distributed equilibrated pore pressure of about -3.76 MPa, which corresponds to a transmission of 76 % of the initially applied stress release. Gas moves from the macropores to the adjacent micropores. As parameter variations show, the increase in gas permeability affects the time necessary for the pressures in macropores and micropores to equilibrate, but not the magnitude of underpressuring. Similarly, increasing the rock compressibility delays pressure reequilibration. The rock compressibility affects the magnitude of the initial pressure decrease in the gas-filled macropores associated with the stress reduction through an increase in porosity. Two parameters influence decisively the magnitude of underpressure: initial porosity and initial gas saturation. Other potential effects as gravitation, thermal phenomena, and degassing of dissolved gas represent less than 15 % as shown in Subsection 8.8.3.

---

[3] the matrix in this definition encompasses the rock volume not affected (or only marginally) by brittle deformation. In other words, discrete features - especially water-conducting features - are not considered as part of the matrix

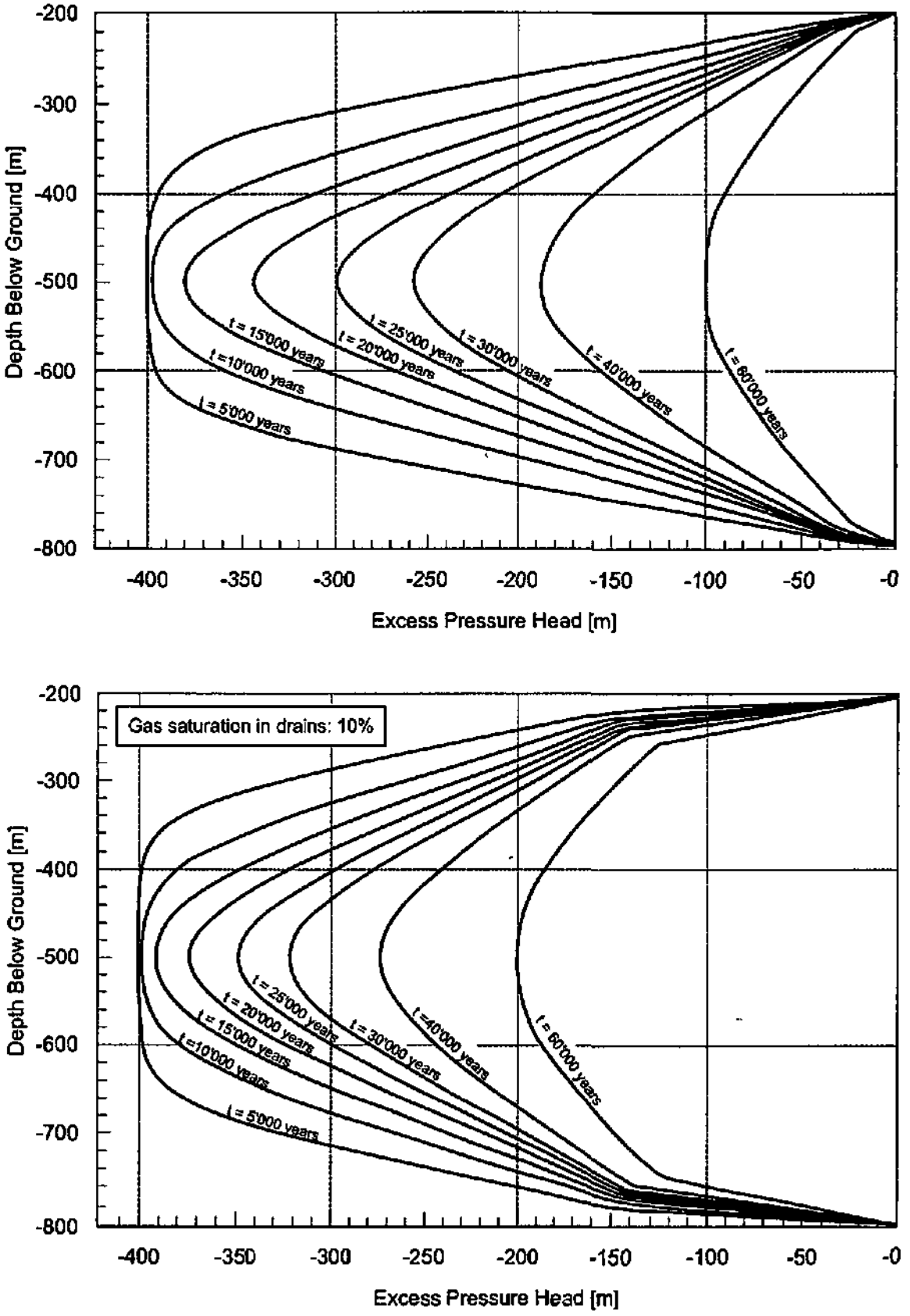

Fig. 8.5-3: Pressure head profiles stemming from single-phase (above) and two-phase (below) simulations using base case parameters in Tab. 8.5-1

8.5.4.2 Full-scale model

This model considers a vertical stack of blocks of the type of those used in the small-scale model. The total thickness is 300 m, and represents approximately the vertical half-thickness of the marl-shale aquitard. Because of symmetry, only top-drainage is allowed.

The initial underpressure is -5 MPa. The pressure response is delayed in the two-phase flow system with respect to the single-phase. The initial gas saturation in the macropores is 8 %. Pressure differences between macropores and micropores are compensated within 40 a. The maximum excess pressure is about -3.1 MPa after 60'000 a with respect to -5 MPa in the saturated model. However, the pressure equilibration is comparatively slackened, since 81 % of the initial pressure disturbance is obtained today in the two-phase flow case against only 70 % in the saturated case.

8.5.4.3 Summary and conclusions

This study, although unrealistic in terms of pore distribution and initial gas saturation, provides, however, interesting results:

- High initial free gas saturations result in underpressure magnitudes and dissipation durations which are incompatible with hydrotest data. Thus this simulation helps to constrain the amount of free gas which is actually possible in the marl-shale aquitard
- The pressure equilibration process between macropores and micropores is not an issue, since the duration necessary for pressure equilibration between pores is many orders of magnitude shorter than the one necessary to dissipate underpressures, and, the energy consumed to reach equilibrium does not noticeably affect the overall pore pressure evolution. This rapid equilibration process is mainly a factor of the small length scales involved
- As compared to the EPM model presented in Subsection 8.5.3, the magnitude of initial underpressures is slightly higher in the dual porosity model
- The magnitude of underpressure is inversely proportional to the amount of free gas and to porosity
- The decay of underpressure is delayed in the dual porosity model compared to both the EPM two-phase flow model and the single-phase model. Therefore, the duration necessary to dissipate abnormal pore pressures is rather underestimated by using an EPM approximation
- Some few percent of free gas in the pore space do not significantly affect the generation of underpressures in the low-permeability aquitard. On the contrary, model calculations tend to show that free gas rather contributes to increase the amount of time necessary for the system to re-equilibrate, due to reduction of permeability to water. Neglecting small gas saturations in model calculations is supported by these results (slight underprediction of the dissipation duration of abnormal pressure), unless absolute negative pore pressures are predicted.

8.6 Alternative conceptual models based on non-hydraulic flow phenomena

Two types of non-hydraulic flow phenomena are distinguished by NEUZIL (1986). The first category shows no direct proportionality between gradient and flux and can be summarised under the generic term of "non-Darcian behaviour". The second set comprises processes that produce flow as a response to gradients others than hydraulic (osmotic gradients, coupled flow). Coupled flow is, according to NEUZIL (1988), fluid flow which is not driven

only by hydraulic head gradients, but also, through coupling, by gradients of chemical and electrical potential and of temperature.

Interestingly, inspection of NEUZIL's contributions in the field of abnormal pressure show that his interpretation of the importance of coupled flow in low permeability environments evolves: while in 1986 he expressed the opinion that non-hydraulic flow might be underestimated because of the analogy in processes often made with high-permeability environments, in 1994 he considers that non-Darcian flow models are in most cases insignificant.

Fig. 3.1-1 shows that a large variety of alternative conceptual models have been addressed. Most of them have already been reviewed in VINARD & MCCORD (1991). Those briefly discussed here represent processes for which the discussion on their potential contribution to underpressure is not concluded yet. These are by order of importance:

- osmosis or its inverse effect i.e. ultrafiltration
- swelling of clay particles in clay-rich formations

8.6.1 Osmosis and ultrafiltration

An osmotic membrane (i.e. in our case geological formation) is a semi-permeable barrier that allows transport of the solvent (water) but not of the solutes (ions). As a consequence, water flows from regions of high water activity to those of low activity, i.e. from the lower concentration of solute to the higher concentration of solute. A rock will act as membrane only when adjacent formations exist with different ionic concentration. This is the case at Wellenberg (Chaps. 6 and 7; NAGRA, 1997) with the low activity groundwater systems on top of the aquitard and below it (Ca-CO_3 to Na-HCO_3).

The magnitude of differential hydraulic pressure in groundwater systems caused by osmosis "depend primarily upon concentration differences across the membrane, the type of ions, the type of clay, and the pore size." (MARINE & FRITZ, 1981). Since natural systems are non-ideal membranes, essentially because geological formations are often thick, inhomogeneous and of composite nature, rather small increments of excess pore pressures are to be expected, in the order of about 90 meters (SOLER & PEARSON, 1997).

If osmosis was a likely process at Wellenberg, the highly saline pore water (i.e. Na-Cl) in the tight marl-shale formation would be rather overpressured than underpressured, since the membrane would provoke flow from low-salinity regions to high salinity regions. In the own words of SOLER & PEARSON (1997) this yields: "Any effect of osmosis on underpressure at Wellenberg would be in the opposite sense to the observed underpressure." This argument is supported by MARINE & FRITZ (1981) who state that osmosis would rather lead to slightly overpressured salty clay-rich formations than the contrary, "since the activity of water in the two solutions is unequal, water from the less saline solution passes through the membrane to the high-concentration side in order to increase that solution's aqueous activity by increasing the hydrostatic pressure of that side." NEUZIL (1995) comes to the same conclusion when he says that "... osmotically-driven flow cannot be ruled out when abnormal high fluid pressures coincide with regions of comparatively high salinity or abnormal low fluid pressures coincide with regions of comparatively low salinity. Obviously, this is exactly the opposite case than the one prevailing in the marl-shale tight rock at Wellenberg and, therefore, osmotically-driven flow appears most unlikely. The only case in which osmosis could have played a role is during drilling and especially during hydraulic testing operation due to the salinity contrast between drilling fluid and formation water.

Despite the relatively narrow database, it is quite clear that the aquitard contains a highly saline Na-Cl brine. According to MAZUREK et al. (1994), the last significant rock-water interaction episode occurred during the Neoalpine metamorphic phase, some twenty million

years ago. Since no Cl-bearing minerals are available in the marl, the Cl^- was probably transported by diffusion in this time window (PEARSON, 1996). Thus, the rock-water chemistry has been equilibrated long ago and therefore cannot play the role of a membrane.

8.6.2 Swelling of clay-rich rocks

Swelling is a rather complex physico-chemical mechanism which is still not fully understood. Essentially, swelling is supposed to occur as a function of the repulsive pressure acting between clay platelets due to Van der Waals and electric forces. LOW in VINARD & MCCORD (1991) estimated for the Opalinus Clay a one-dimensional swelling pressure in the range of 0.7 - 2.2 MPa based on analyses by MADSEN & MÜLLER-VONMOOS (1985). This range is probably strongly overpredicted for Wellenberg marls and shales.

HORSEMAN (1997) has recently advanced an elaborate physico-chemical model which goes beyond the mechanisms described earlier by HORSEMAN et al. (1990 and 1996). He postulates interfacial phenomena as contributing to the observed underpressuring. Interfacial phenomena regroup mineral surface hydration and so-called "thin-film-effects". The driving force is the "disjoining pressure" between narrowly-spaced plates or particles, essentially clay minerals. HORSEMAN (1997) states that "in order for the formation to reach thermodynamic equilibrium with its surroundings (i.e. same chemical potential inside and outside), the pressure of the water in the thin films must rise to compensate for the effect of these surface interactions". This pressure increment is known as "disjoining pressure". The disjoining pressure can be regarded as a sub-component of the total stress acting on the rock." As described, these phenomena are present during compaction of mudrock. HORSEMAN (1997) assumes that "this argument can be reversed to demonstrate that a reduction in the stress acting on a compact sedimentary rock with very narrow interparticular spaces can lower the chemical potential of the water present in the surface films. Thus the erosional destressing of a rock formation can lead to a non-equilibrium thermodynamic state." In other words, disjoining pressure acting at microscopical scale may be able to contribute to the generation of subnormal pressure and would act parallely to mechanical rebound. Unfortunately, no quantitative data is advanced by this author, so that it is impossible to give a quantitative estimate of the potential contribution of this process. Furthermore, as no chemical gradient seems to exist inside the aquitard rock, it seems unlikely that this process had a significant impact on the subnormal pressures that we observe today.

The results remain inconclusive at present. The problem should not be addressed in terms of fundamental research, but in terms of defining the potential magnitude of excess pore pressure generation and their kinetics, i.e. reasonable duration of these processes.

9 QUATERNARY EVOLUTION CONCEPTUAL MODEL

9.1 Context

Climate and more especially climatic fluctuations are responsible for most of the geomorphological changes on Earth. In the investigated region, climatic changes provoked recurrent glaciations and associated retrogressive erosion, characteristic of most alpine valleys. Although climatic fluctuations existed long before the Quaternary, it is during this latter era that climate changes produced the strongest repercussions on the currently observed hydrodynamic conditions and this for two reasons:

1. Climate changes during the Quaternary are recent by definition. They will consequently impact more strongly on the hydraulic pressure distribution than any other former event, which will have decayed either completely or to a large extent.
2. Climate changes seem to become more frequent and stronger in the Quaternary with respect to former geological ages.

According to the Milankovitch theory, the climatic oscillations of the Quaternary are based on changes in the high-latitude summer insolation of the Northern hemisphere, which themselves result from fluctuations of the Earth axis with respect to the perihelial position. Recent research on climatic oscillations (PAUL & BERGER, 1997) suggest that climatic transitions which lead to ice mass fluctuations of first near 41'000 a period and then 100'000 a period can be induced by a slow and steady decrease of the atmospheric carbon dioxide level. Additionally, it seems that the climatically generated ice masses have themselves a feed-back effect on the frequency of glaciations.

In the Alps, glaciers invaded narrow valleys, scraped them down to the bedrock and progressively widened and deepened them. Landslides, rockslides and rockfalls occurred due to the instability provoked by rapid melting of ice masses. Strangely enough, in the literature on natural transient flow conditions, glacier effects are not considered as a major mechanism for the generation of underpressures. Most authors advocate for erosion. Three main reasons may explain the difference in conceptualisation between Wellenberg and other occurrences of subnormal pressures (Chap. 5):

1. Wellenberg is located in a moutaineous region, whereas most other occurrences of subnormal pressure are located in large sedimentary basins, as for instance, the plains of Canada and USA (Alberta Red Earth Region, Denver basin, etc.). In some regions, like the Texas panhandle, glaciers did not develop and cannot, therefore, be accounted for the observed underpressure. In regions where glaciers existed, they formed extended ice caps and even continental ice sheets. Under such conditions, extensive basal drainage is extremely unlikely due to large-scale permafrost and therefore overpressures in the ground resulting from the ice load could probably not dissipate during the glaciation itself. This situation is referred to as "cold glaciers", for which hydrogeologists correctly consider that the net effect between loading and unloading is close to zero.
2. The smooth topography characterising most of the large sedimentary basins does not allow strong glacier induced erosion.
3. The timing and duration of the last glaciations is far shorter than the durations assumed by many authors for the dissipation of disequilibrium pressures (e.g. CORBET & BETHKE, 1992).

Without conjecturing on the conceptual models elaborated for other occurrences of

underpressures in the northern hemisphere, it is likely that, in light of the observations made at Wellenberg and although field conditions are sometimes very different, the potential role of glacier rebound should be reconsidered elsewhere also. This recommendation is based on two arguments:

a. Recent contributions show that eskers (glacier sole tunnels) might have played the role of basal drainage system for glacier melting water and, possibly also, for groundwater (BOULTON & CURLE, 1997).

b. The durations of disequilibrium pressure cited in the literature may be exaggerated. Confronted with abnormal pressure, some authors may be inclined to assume too readily geologic time scales and might therefore underestimate potential effects of (comparatively recent) ice ages.

9.2 Scope

As seen in the above Section, climatic forcing provokes two distinct changes on the land surface:

1. irreversible changes, i.e. erosion due to glaciers and subsequent slope instability (landslides, rockslides, rockfalls and compaction)
2. reversible changes: i.e. ice mass build up and melting.

The combination of both irreversible and reversible changes is considered to be the actual geologic forcing at Wellenberg, which is why its contributions have been studied in greater detail. From this hypothesis, a set of subordinate objectives derive, which are:

- to test the potential for memory effects[4], i.e. the role of a penultimate glaciation on pore pressures with respect to the last glaciation
- to estimate the influence of various ice loads in time and in space
- to compare with realistic estimates of properties from measurements
- to evaluate the effects of time increments of glaciations, interglacials, and transition periods (rapid or slow build up and melting periods)
- to distinguish between the effects of glacier loading-unloading and the effects of associated glacier erosion (landslides, accentuation of topographic relief)
- to determine diffusivity distributions able to produce hydraulic underpressures in the range of the observed magnitude and consistent with borehole data.

9.3 Geological basis and modelling approach

9.3.1 Procedure and geological basis

A lot of work was necessary to translate the most likely past climatic and geomorphological evolution scenarios at scale of Switzerland or of the Alps to site-scale scenarios, and therof to construct comprehensive evolutionary cross-sections or 3D topographic surfaces at different time steps. This work was further complicated, but also considerably furthered, by

[4] "memory effects" in this context is limited to the determination of initial conditions for a given model scenario, without considering the mechanical hysteresis between loading and unloading cycle (Chap. 7)

recent findings on the dating of glacier events (SCHLÜCHTER, 1995; SCHLÜCHTER & RÖTHLISBERGER, 1995; SCHLÜCHTER & MÜLLER-DICK, 1996), which led to a new definition of ice ages. This new information became public amidst the elaboration of the first abstraction scheme (Q1), and provoked a thorough reassignment of the geomorphological events in the investigated area, which was applied to the succeeding abstraction schemes (Q2 and Q3).

Based on a list of questions relevant for the reconstruction of the Quaternary evolution (VIHARD in KLEMENZ, 1995) and on the literature on the Quaternary of the Helvetic domain, KLEMENZ proposed a plausible geomorphological evolution scheme at site scale. His contributions (KLEMENZ, 1995; KLEMENZ, 1996) served as basis for the three abstraction schemes presented hereafter (Tab. 9.3-1).

Tab. 9.3-1: Duration and definition of the glaciations relevant to the abstraction schemes Q1, Q2 and Q3

Time scale[1] [a BP]	Definition (NAGRA, 1997)	Former definition	Abstraction scheme		
14'800 - 28'000	Last glaciation II	Würm s.l.	Q1	Q2	Q3
28'000 - 60'000	Interstadial of Gossau	Würm s.l.	Q1	Q2	Q3
60'000 - 115'000	Last glaciation I	Würm s.l.	Q1	Q2	Q3
115'000 - 140'000?	Interglacial period (Eem)	Interglacial period	Q1	---	Q3
185'000 - 140'000?	Penultimate glaciation	Riss s.l.	Q1	---	Q3
700'000 - 190'000?	Differential erosion	---			Q3

[1] The periods refer to the conditions in the foothills of the Alps

9.3.2 Definition of abstraction schemes

Three abstraction schemes were defined. The first abstraction scheme (Q1 or "Quaternary evolution of the site during the two last prominent ice ages", duration: approx. 200'000 years) was simulated with a 2D model (along geologic profile Q - Q'). The corresponding model scenario was based on the old definition of ice ages as well as on the old definition of hydrogeological units (VINARD & LAVANCHY, 1994).

Abstraction schemes Q2 and Q3 use the new chronology of glaciations (SCHLÜCHTER & MÜLLER-DICK, 1996), including the detailed sequence of events during glaciations and interglacials. Both model scenarios consider the volume of the 3D-hydrodynamic regional model of the Wellenberg site described in Section 9.5. The FE mesh reproduces the detailed morphology of the geological units as produced by the 3D geological model of the Wellenberg site[5] (TACHER, 1994). While abstraction scheme Q2 concentrates on the two distinct glacial periods of the last (Würm) ice age (duration: approx. 115'000 years), abstraction scheme Q3 encompasses scenario Q2 and comprises additionally the differential erosion occurring in the last 700'000 years. In all these models glaciations earlier than 190'000 a BP were ignored because of their likely negligible role.

[5] the 3D geological model of the Wellenberg site is a numerical model representing interfaces between geologic units and the volumes of the geological units. This model has been build with the code EarthVision (DYNAMICS GRAPHICS Inc.)

9.3.3 Input parameters

9.3.3.1 Objectives

A lot of effort was necessary to identify key-parameters and ranges. For this, parameter estimation was performed in two steps: an early phase, during which important parameters and appropriate ranges were defined and a second phase, which applied likely K-distributions and storage coefficients, based on measurements and up-scaling techniques presented in NAGRA (1997).

The first parameter sensitivity study is documented here in some detail since it increased significantly the understanding of the relative importance of parameters and their interaction in 3D space. This study was performed to achieve the following goals:

1. to analyse the temporal behaviour of the 3D evolution of hydraulic pressures in the ground and more particularly the role of different K layers (hydrogeological units)
2. to identify the most relevant parameters for the generation and maintenance of underpressures and their actual role
3. to determine, by comparison between measurements and simulated underpressure values, the best parameter ranges for forward simulations.

This procedure is quite similar to the one applied by BOUR & LERCHE (1993).

9.3.3.2 Procedure

The basic assumption is an instantaneous glacier retreat applied on the 3D model domain of the regional model Wellenberg (NAGRA, 1997). Initial time is 40'000 a BP, the ice level is set to 2'355 m a.s.l. per analogy with ARISTORENAS & EINSTEIN (1992). Actually, neither the amount of ice, nor the chronology are correct. Moreover, the rebound function as computed produces absolute negative pore pressures, which would necessitate a two-phase flow approach. Both these aspects were intentionally disregarded, the objective being solely the parameter sensitivity and a preliminary parameter estimate.

The numerical simulations were performed in three steps:

1. Rough calculation of the rebound distribution on top of the topographic surface assuming homogeneous rock properties (aeral distribution of the unloading function)
2. Determination of initial conditions for the transient forward simulation of the pressure anomaly dissipation by using a superimposition of the rebound distribution with steady-state initial conditions
3. Simulation of the transient pressure evolution over a time span of 40'000 a.

In a first step, the input parameters K and S_s were optimised by means of inverse modelling (KUHLMANN, 1995). In a second step, the optimised parameters were employed in a test run.

9.3.3.3 Initial conditions

The rebound distribution was calculated by means of a steady-state run, assuming that the load removed can be calculated from the difference in elevation between each surface element and the corresponding top of the vertical ice column (Subsect. 7.5.2). Figs. 9.3-1a and 9.3-1b represent the obtained rebound distribution in the profiles Q - Q' and D - D'. As expected, the strongest rebound of about $\Delta h \approx -1'800$ m is located at the western boundary

of the model, i.e. the Engelberger Aa valley, which exhibits the lowest elevations, and consequently the strongest glacier unloading.

The initial conditions for the dissipation of the abnormal pressures are obtained by superimposing the rebound distribution and the steady-state head field conditioned by the boundary condition on the surface. The resulting head distribution is represented in Figs. 9.3-2a and 9.3-2b. Unrealistically low head values of h ≈ -1'300 m in the Engelberger Aa valley and h ≈ -400 m below the Eggeligrat are computed.

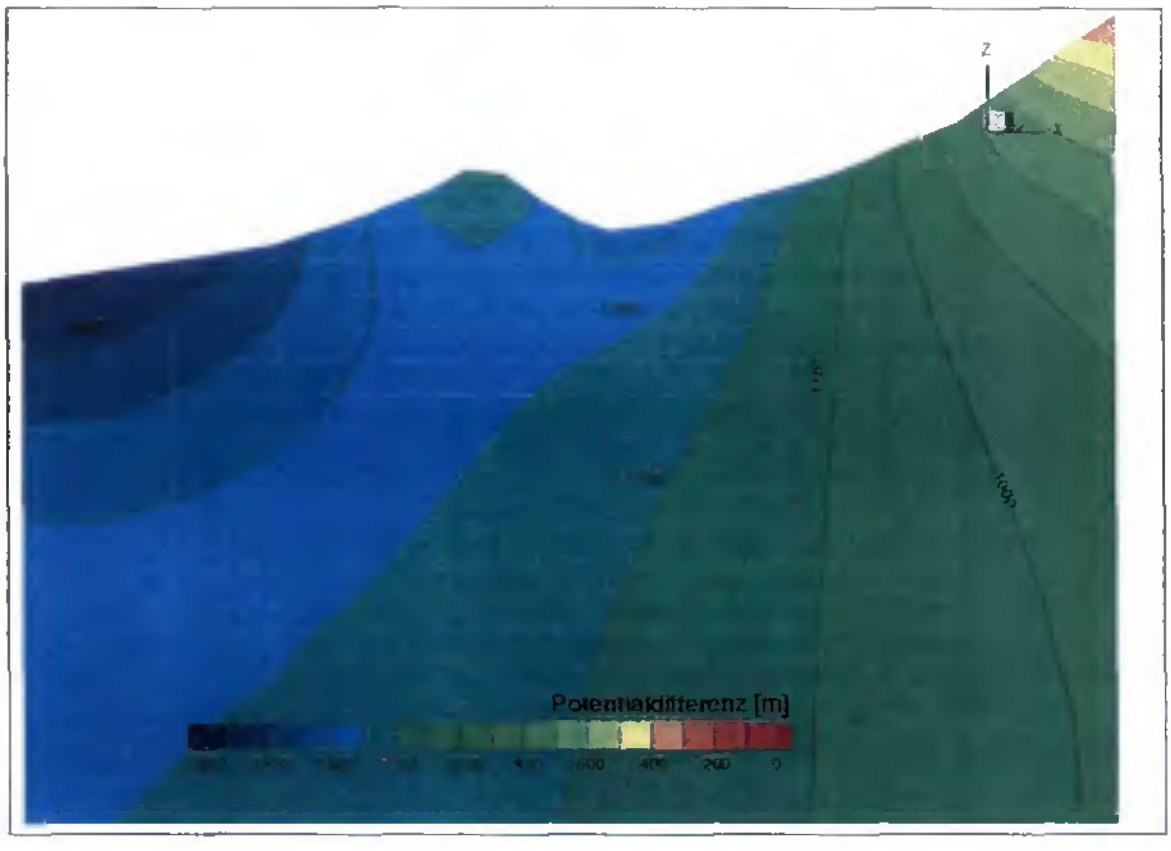

Fig. 9.3-1a: Distribution of unloading in cross-section Q - Q'

9.3.3.4 Sensitivity analysis and parameter estimation

Tab. 9.3-2 presents the base case parameters and the estimated parameters for all hydrogeological units (in the old definition). Sensitivity coefficients were derived for each parameter after 40'000 a of pressure decay at boreholes SB1, SB3 and SB4. Positive coefficients indicate that the corresponding parameter value will tend to increase abnormal pressure, negative coefficients point out to the contrary. Fig. 9.3-3 represents the different sensitivity coefficients along the axis of the representative boreholes. As expected, the K-value of the low and very-low permeability aquitard units (C and D) play the governing role with a minor contribution of the storage coefficient for unit D. K and S_s values of all other units are comparatively insignificant, which confirms the governing role of the tightest part of an aquitard for the maintenance of abnormal pressure.

The next step was to perform an automatic calibration of the most sensitive parameters in order to achieve a simulated head distribution after 40'000 a, which corresponds more or

less to the observed head profiles. This was done by applying the inverse routines of CASA (KUHLMANN, 1995). 40'000 a is more than three times longer than what is suggest by modern data, i.e. 12'000 a from the end of the last glaciation. As a consequence, estimated diffusivity values are far below what is necessary for a realistic postglacial period (Tab. 9.3-2).

As indicated by "!!!", the uncertainty range around unimportant parameters is sometimes quite large. This shows clearly that for the estimation of the head conditions inside the marl-shale aquitard, S_s and especially K-values of the surrounding, highly permeable, limestone units are meaningless. Only the position of the water table is of importance (Sect. 9.5).

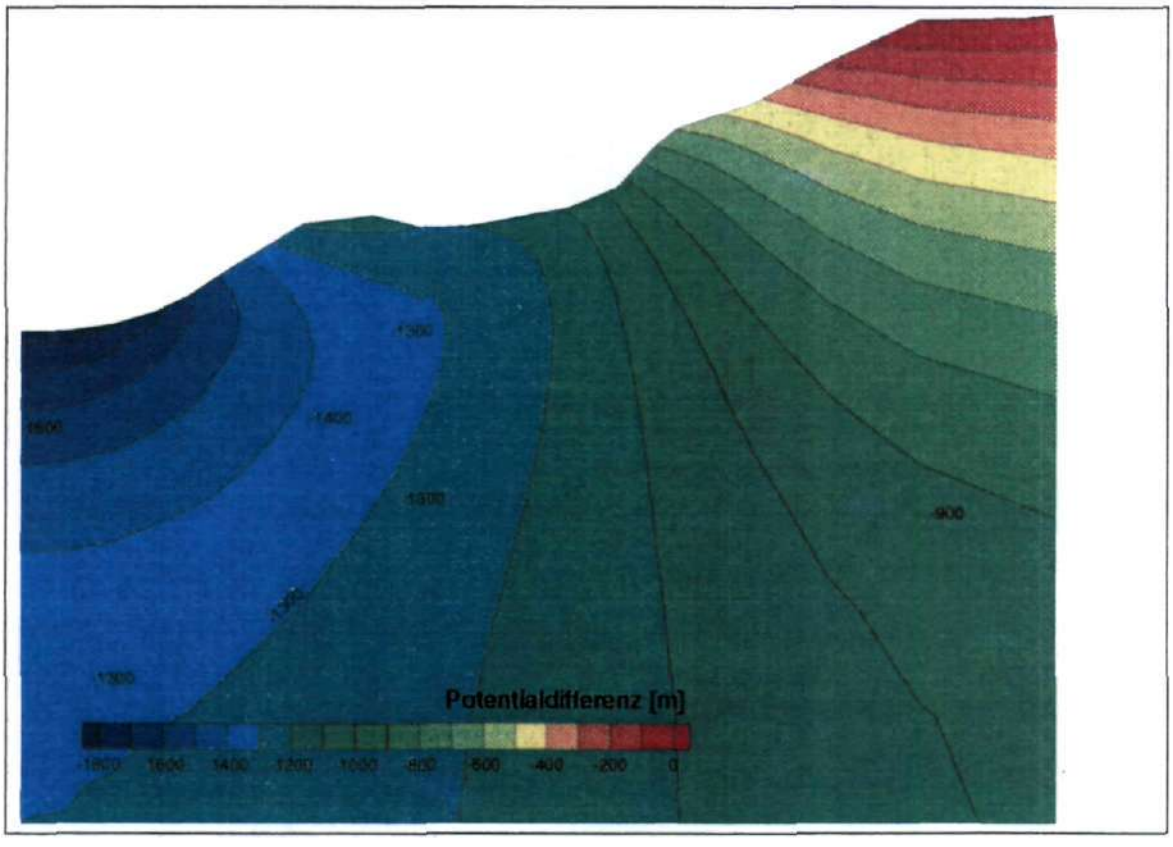

Fig. 9.3-1b: Distribution of unloading in cross-section D - D'

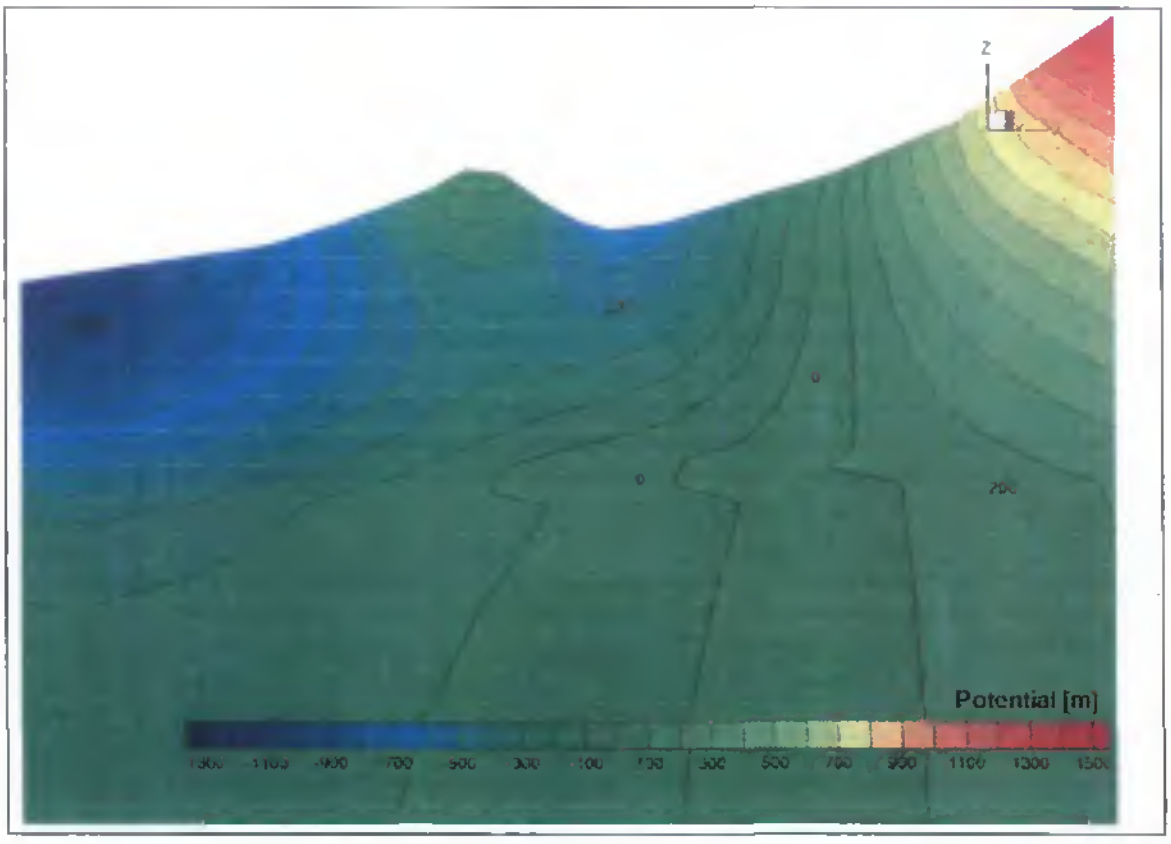

Fig. 9.3-2a: Initial head conditions in cross-section Q - Q'

Tab. 9.3-2: Base case and estimated K and S_s parameters for Quaternary abstraction schemes

Hydrogeological unit	K [m/s] and S_s [m/s^2] classes	Base case	Best estimate
Landslide of Altzellen	K S_s	$1 \cdot 10^{-8}$ $1 \cdot 10^{-6}$	$1.08 \cdot 10^{-6} \pm 4.99 \cdot 10^{-1}$ ---
Aquitard (hydrogeol. unit B)	K S_s	$1 \cdot 10^{-9}$ $1 \cdot 10^{-6}$	$9.35 \cdot 10^{-10} \pm 4.99 \cdot 10^{-1}$ ---
Aquitard (hydrogeol. unit C)	K S_s	$1 \cdot 10^{-11}$ $1 \cdot 10^{-6}$	$3.95 \cdot 10^{-13} \pm 1.77 \cdot 10^{-1}$ $3.87 \cdot 10^{-6} \pm 2.85 \cdot 10^{-1}$
Aquitard (hydrogeol. unit D)	K S_s	$1 \cdot 10^{-12}$ $1 \cdot 10^{-6}$	$2.82 \cdot 10^{-13} \pm 6.52 \cdot 10^{-2}$ $3.51 \cdot 10^{-6} \pm 7.41 \cdot 10^{-2}$
Limestones Drusberg nappe	K S_s	$1 \cdot 10^{-6}$ $1 \cdot 10^{-6}$	$9.97 \cdot 10^{-9} \pm 1 \cdot 10^{0}$!!! ---
Limestones Axen-nappe	K S_s	$1 \cdot 10^{-6}$ $1 \cdot 10^{-6}$	$1.13 \cdot 10^{-7} \pm 9.67 \cdot 10^{-1}$!!! ---
Equivalent Wissberg Schuppe	K S_s	$1 \cdot 10^{-6}$ $1 \cdot 10^{-6}$	$8.03 \cdot 10^{-6} \pm 9.67 \cdot 10^{-1}$!!! ---
Parautochthonous	K S_s	$1 \cdot 10^{-8}$ $1 \cdot 10^{-6}$	---

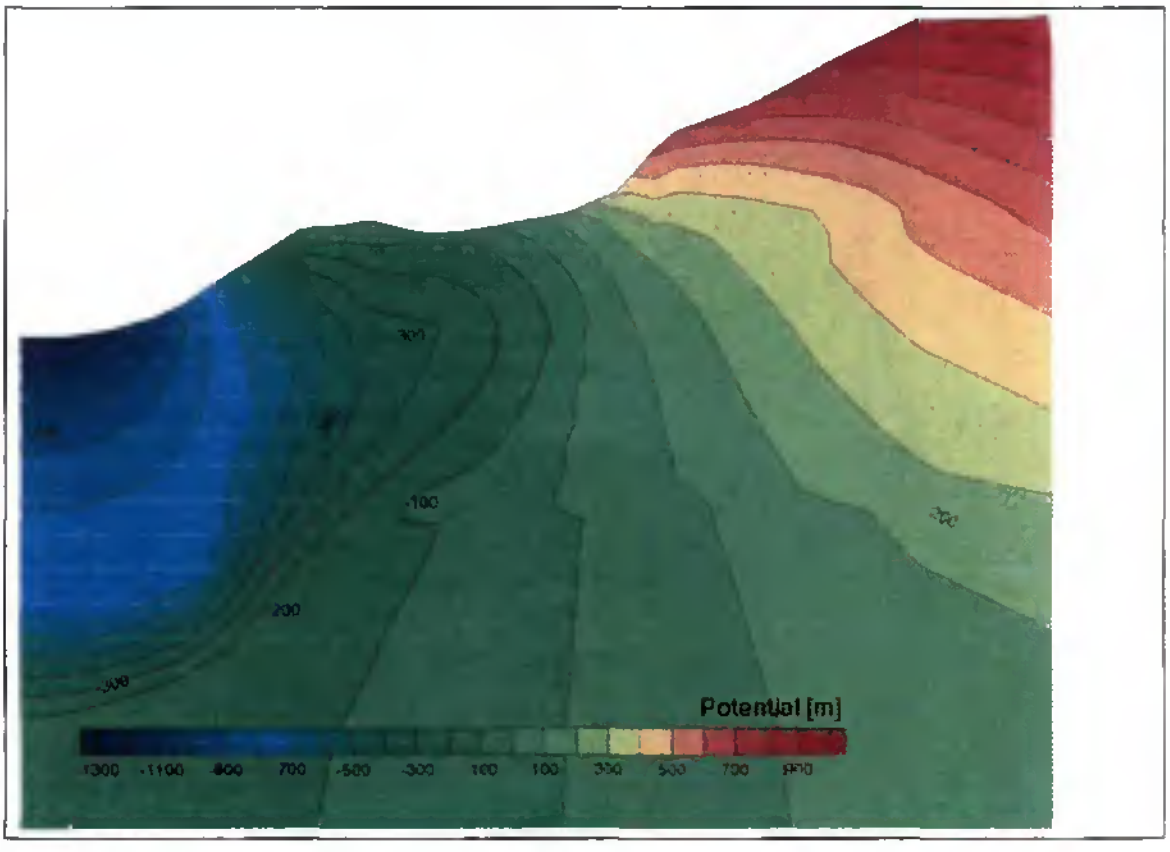

Fig. 9.3-2b: Initial head conditions in cross-section D - D'

9.3.3.5 Dissipation of the pressure anomaly

The dissipation of the initial pressure anomaly was calculated twice, the first time by using the base-case dataset, and a second time by applying the estimated parameters listed in Tab. 9.3-2. The base case dataset corresponds to the best guess estimates for the parameters K and S_s of all hydrogeological units represented in the model domain (NAGRA, 1993), while the second dataset is the outcome of the sensitivity analysis presented in Paragraph 9.3.3.4. Using the estimated parameters produces for today an extended UPZ located in the long axis of the marl-shale aquitard (Fig. 9.3-4).

The evolution of the head profiles in the representative boreholes SB1 and SB3 over the time span of 40'000 a is illustrated in Figs. 9.3-5 and 9.3-6. In both figures, results based on base case parameters are shown on top and the ones based on the estimated parameters are at the bottom. The results are unrealistic to some extent (desorption), but are nevertheless interesting since they show that:

1. underpressures are compensated within few years in the high-permeability units
2. in the low to very-low permeability aquitard (units C and D) the duration of dissipation takes from 10'000 a to 20'000 a when using estimated parameters, but is completed to a large extent within 5'000 a if base case parameters are applied (see for comparison Tab. 9.3-2).

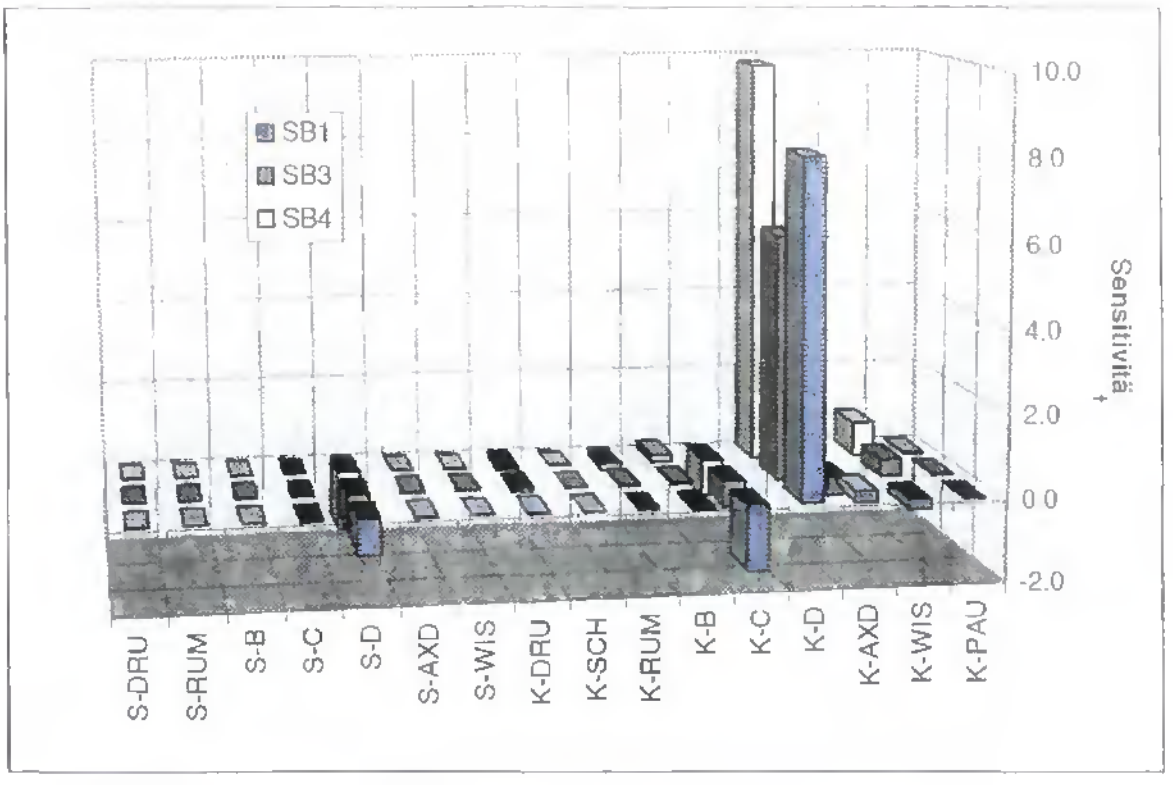

Fig. 9.3-3: Sensitivity of the observed head distribution in the boreholes on parameter variation

S: specific storage; K: hydraulic conductivity; DRU: limestone formations of the Drusberg nappe; B, C, D: hydraulic units of the marl-shale aquitard; AXD: limestone formations of the Axen nappe; WIS: Wissberg slab; PAU: Parautochthonous

9.3.3.6 Summary and conclusions

Interestingly, the preliminary parameter estimation results in K and S_s values very close to those applied in recent model scenarios (Q2 and Q3, Secs. 9.6 and 9.7): estimated K-values range from $3.95 \cdot 10^{-13}$ m/s to $2.82 \cdot 10^{-13}$ m/s for the very-low permeability zones of the marl-shale aquitard, and from $3.87 \cdot 10^{-6}$ m^{-1} to $3.51 \cdot 10^{-6}$ m^{-1} for S_s. These values tend to demonstrate the robustness of the parameters required to maintain underpressures over significant time. Moreover, as mentioned before, the parameter estimation demonstrates that K and S_s-values of the very-low permeable marl-shale aquitard are decisive for the generation and "survival" of sub-normal head conditions, whereas K- and S_s-values of the adjacent units (primarily the limestone formations of the Axen-nappe and Drusberg-nappe) are not important. Hence, the importance of the adjacent rock units is almost entirely a matter of prescribed saturation (water level). This parameter estimation was repeated based on more realistic scenarios and using the K-model (Sect. 9.5); the outcome is summarised in Tab. 9.3-3.

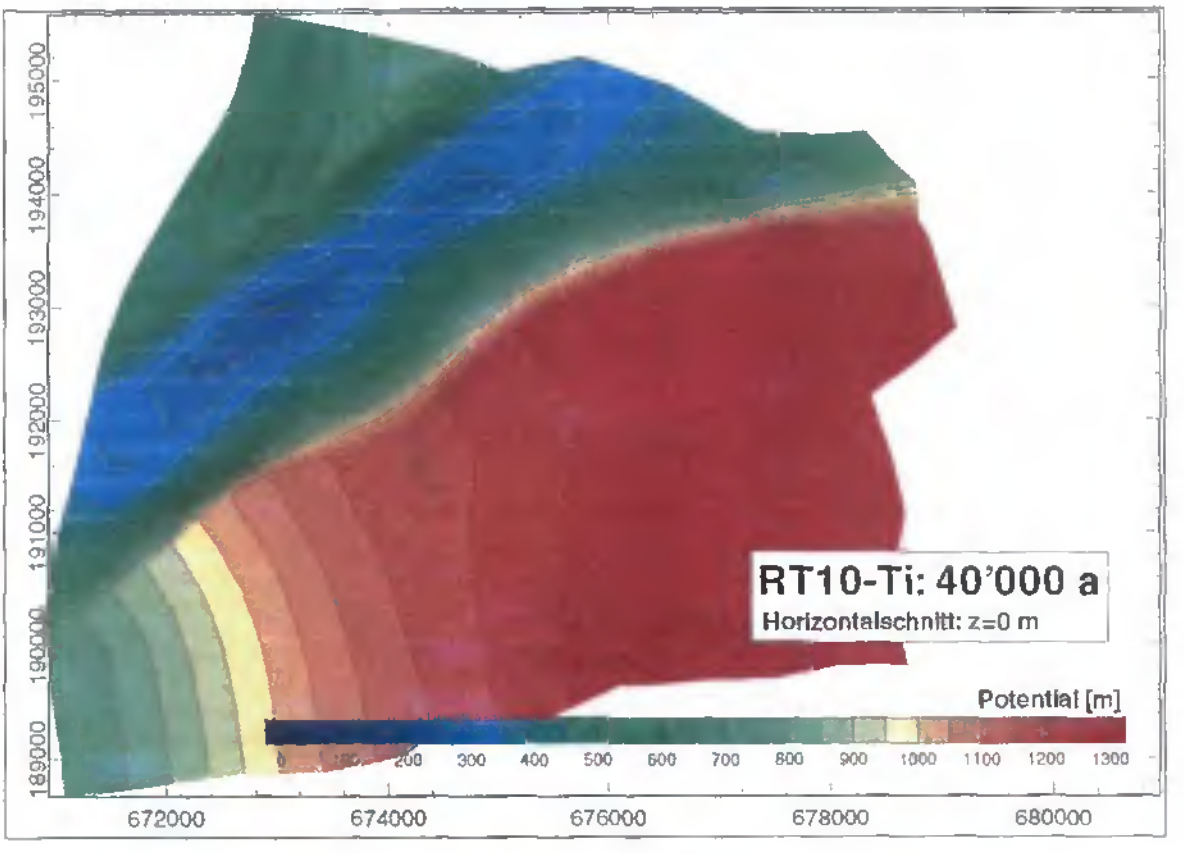

Fig. 9.3-4: Head distribution after 40'000 a of pressure decay on the horizontal section at sea level (0 *m* a.s.l.) of the regional model domain (NAGRA, 1997)

Tab. 9.3-3: Input parameters for model scenarios Q1, Q2 and Q3

Hydrogeological unit	Base case K [m/s]	Base case S_S [m^{-1}]
Quaternary	$1 \cdot 10^{-4}$	$1 \cdot 10^{-6}$
Landslide mass of Altzellen	$1 \cdot 10^{-8}$	$1 \cdot 10^{-6}$
Marl-shale aquitard	from K-model	$1 \cdot 10^{-6}$ *
Limestones of the Axen-nappe	$1 \cdot 10^{-6}$	$1 \cdot 10^{-6}$
Limestones of the Drusberg nappe	$2 \cdot 10^{-6}$	$1 \cdot 10^{-6}$
Equivalent of the Wissberg slab	$1 \cdot 10^{-6}$	$1 \cdot 10^{-6}$
Parautochthonous	$1 \cdot 10^{-8}$	$1 \cdot 10^{-6}$

* is varied within the range: $4 \cdot 10^{-6} \leq S_s \leq 1 \cdot 10^{-5}$

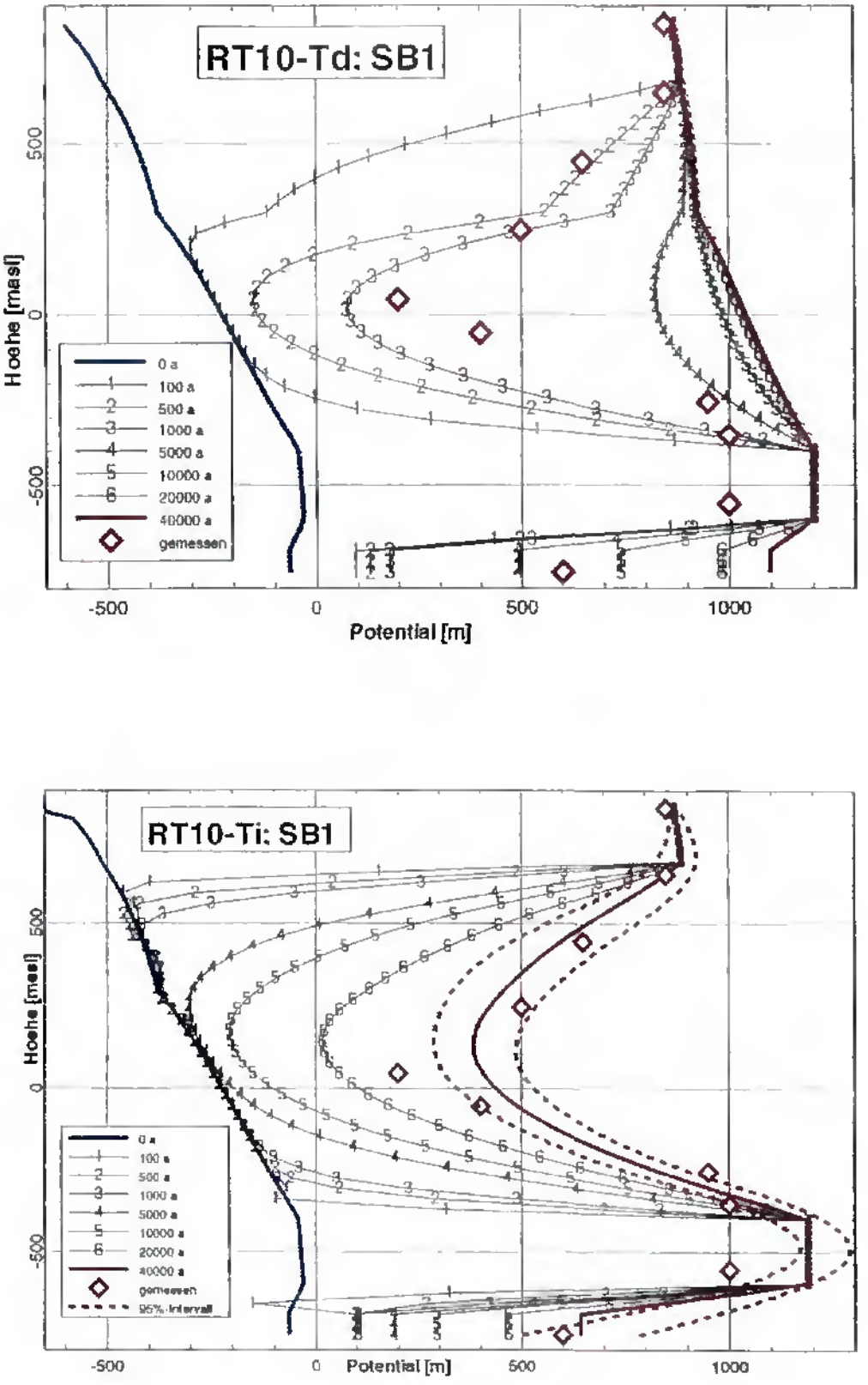

Fig. 9.3-5: Head evolution in SB1 with base case parameters (above) and estimated parameters (below)

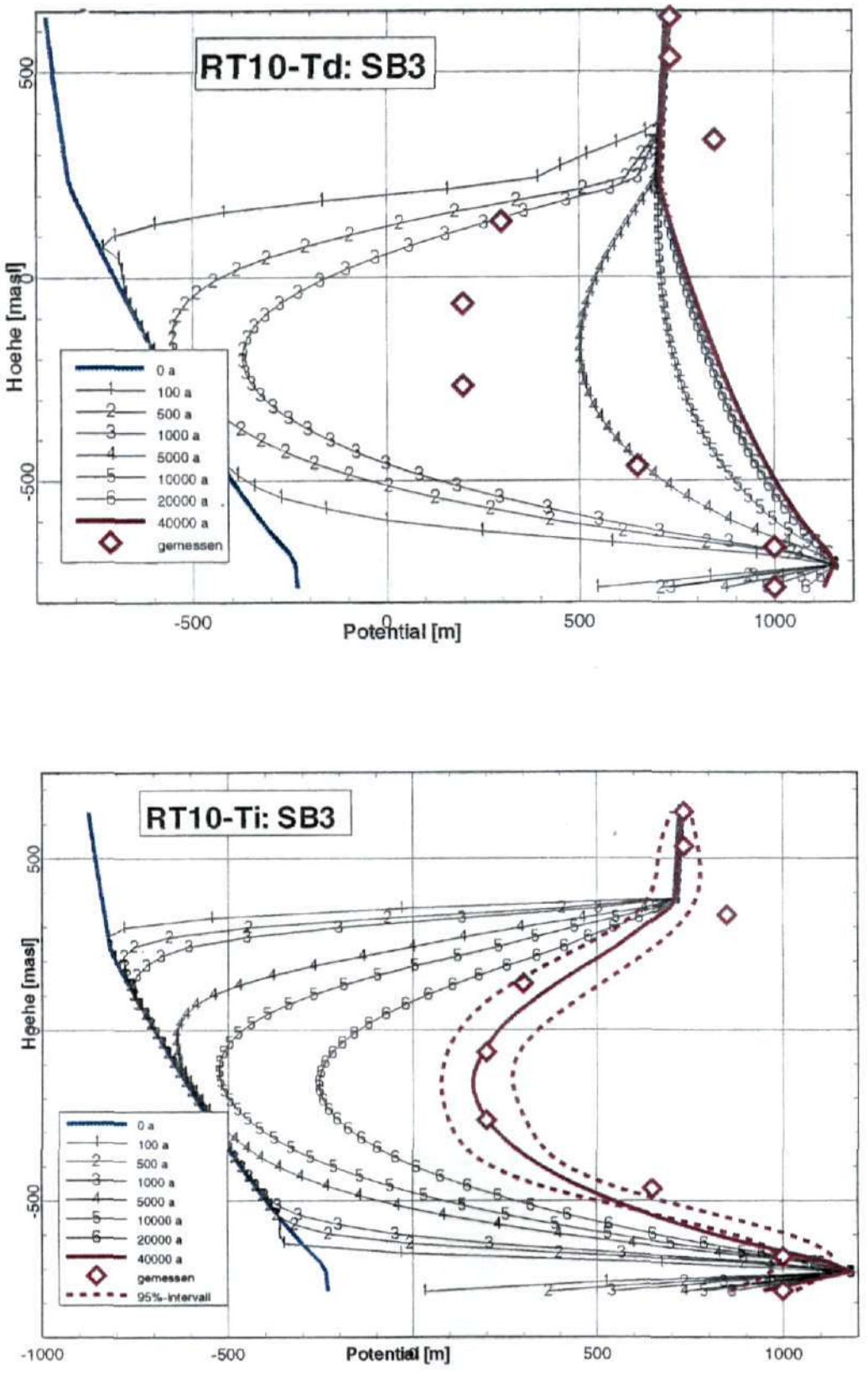

Fig. 9.3-6: Head evolution in SB3 with base case parameters (above) and estimated parameters (below)

9.4 Abstraction scheme Q1

9.4.1 Model specifications

Within the simulated time span (approx. 200'000 a), a relatively complex sequence of events takes place, which consists of two ice ages separated by an interglacial period (Tab. 9.4 -1) accompanied by landslides and settlements as well as extensive erosion of the ground surface. Special emphasis was given on the estimate of the relative contributions to underpressuring of glaciations on the one side and erosion (especially landslides) on the other. The interstadial period documented in the alpine foreland during the last ice age ("Würm") was neglected in this schematic model and rather slow build up and melting of glaciers are postulated, which is not quite consistent with modern interpretation.

Tab. 9.4-1: Geological evolution since penultimate glaciation

Stage	Time [a BP]	State	Duration [a]	Process
0	195'000	Interglacial period		
1	190'000		5'000	Build up of glaciers
2	145'000	Penultimate glaciation[1]	45'000	Ice load rest
3	130'000		15'000	Glacier removal
4	129'900	Landslide of Altzellen	100	Beginning of the interglacial period
5	70'000	Interglacial period	59'900	Denudation
6	65'000	Last glaciation I[2]	5'000	1st build up of glaciers
7	40'000	Last glaciation I	25'000	Ice load rest
8	30'000	Last glaciation II	10'000	2nd (additional) build up of glaciers
9	20'000	Last glaciation II	10'000	Ice load rest
10	10'000	Last glaciation II	10'000	Glacier removal
11	0	Interglacial period	10'000	Denudation

[1] "Riss" in the old terminology

[2] "Würm" in the old terminology

9.4.2 Results of model scenario Q1

The evolution of the head distribution at various time steps is represented in Figs. 9.4-2a to 9.4-2d. Head isolines are plotted in cross-section Q - Q' together with the corresponding head profiles in the reference boreholes SB1 and SB3. Fig. 9.4-2a represents the initial conditions at 195'000 a BP. Figs. 9.4-2b and 9.4-2c represent the head distributions after the penultimate glaciation (130'000 a BP) and the last glaciation (10'000 a BP) respectively. The head patterns along SB1 are, for instance, identical after both ice ages. For SB3, where the ice load was comparatively higher during the penultimate glaciation than during the last one, the head reaches its absolute minimum at the end of the penultimate glaciation.

Further consideration of Figs. 9.4-2a to 9.4-2d shows that the shape of the UPZ (as observed along isopotential line h = 500 m a.s.l.) below the Eggeligrat-saddle and the Engelberg Aa valley includes a vertical narrowing (constriction). This peculiarity is due to the 2D design of the model and not too much emphasis should be laid on it (see model scenario Q2 for comparison).

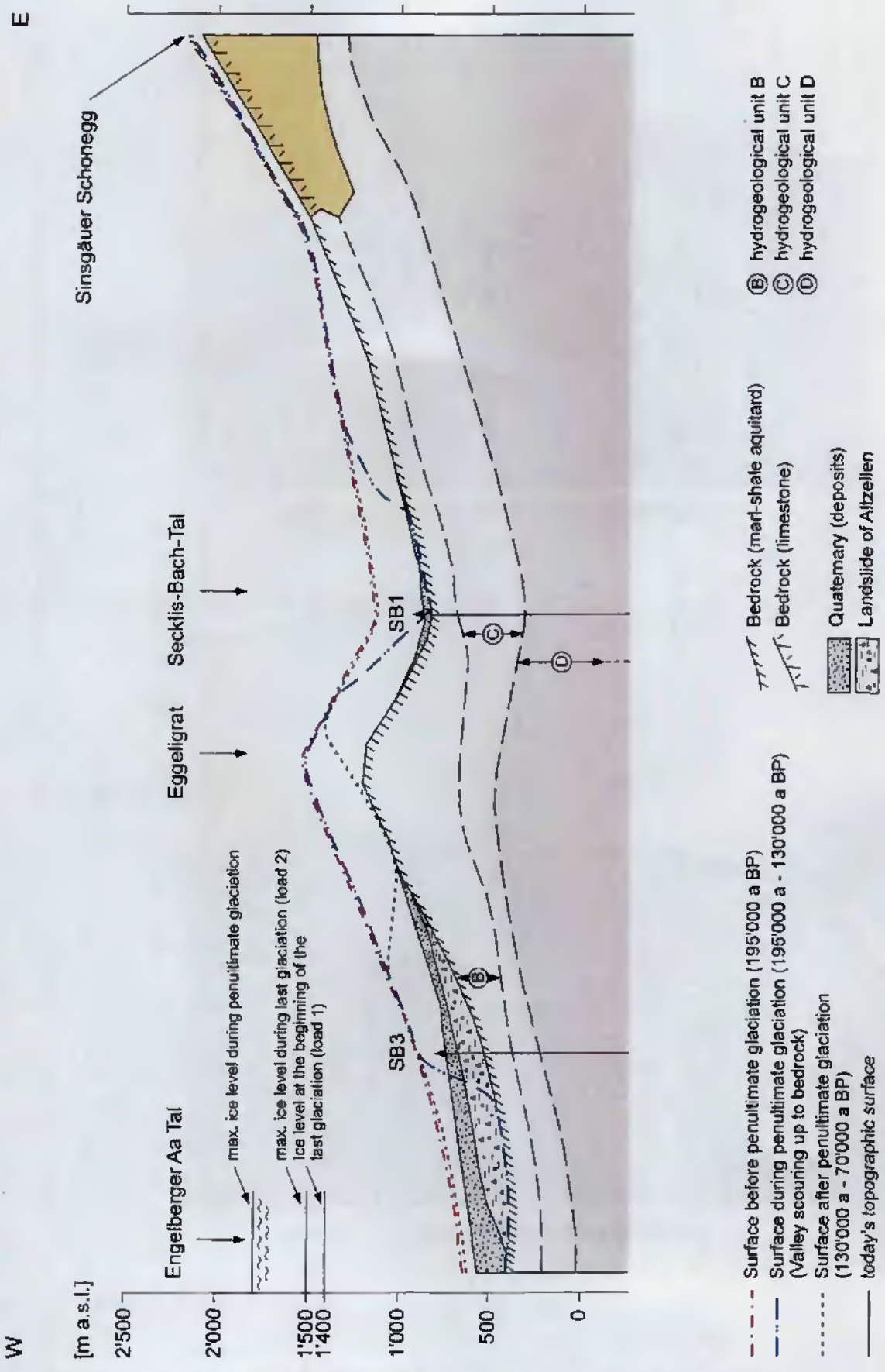

Fig. 9.4-1: Evolution of topography in abstraction scheme Q1 (cross-section Q-Q')

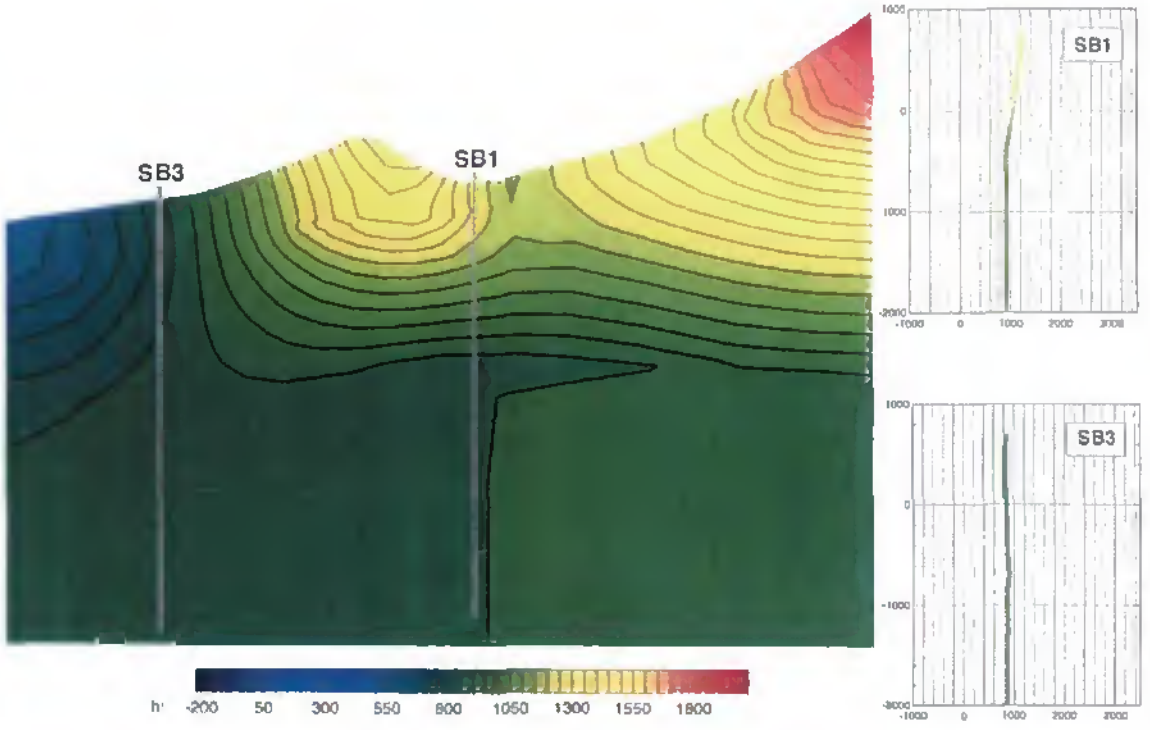

Fig. 9.4-2a: Model scenario Q1 - Head distribution at the beginning of the simulation, before the penultimate glaciation (195'000 a BP)

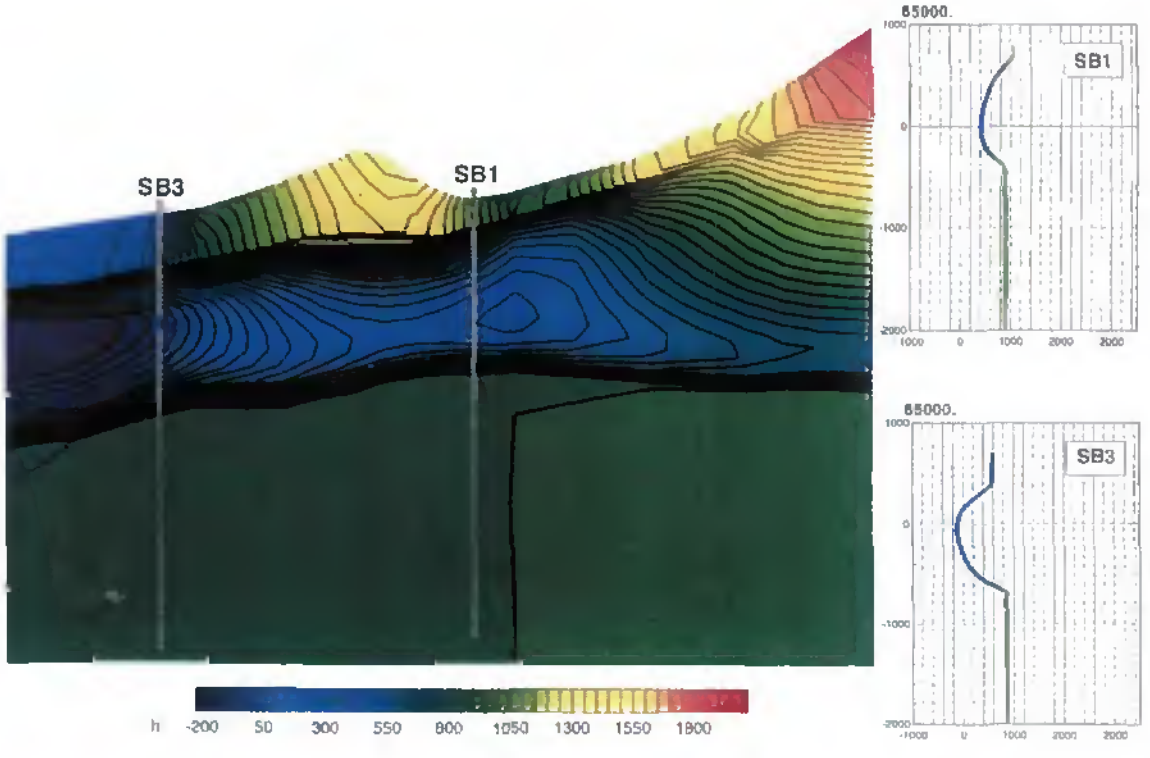

Fig. 9.4-2b: Model scenario Q1 - Simulated head distribution directly after the end of the penultimate glaciation (135'000 a BP)

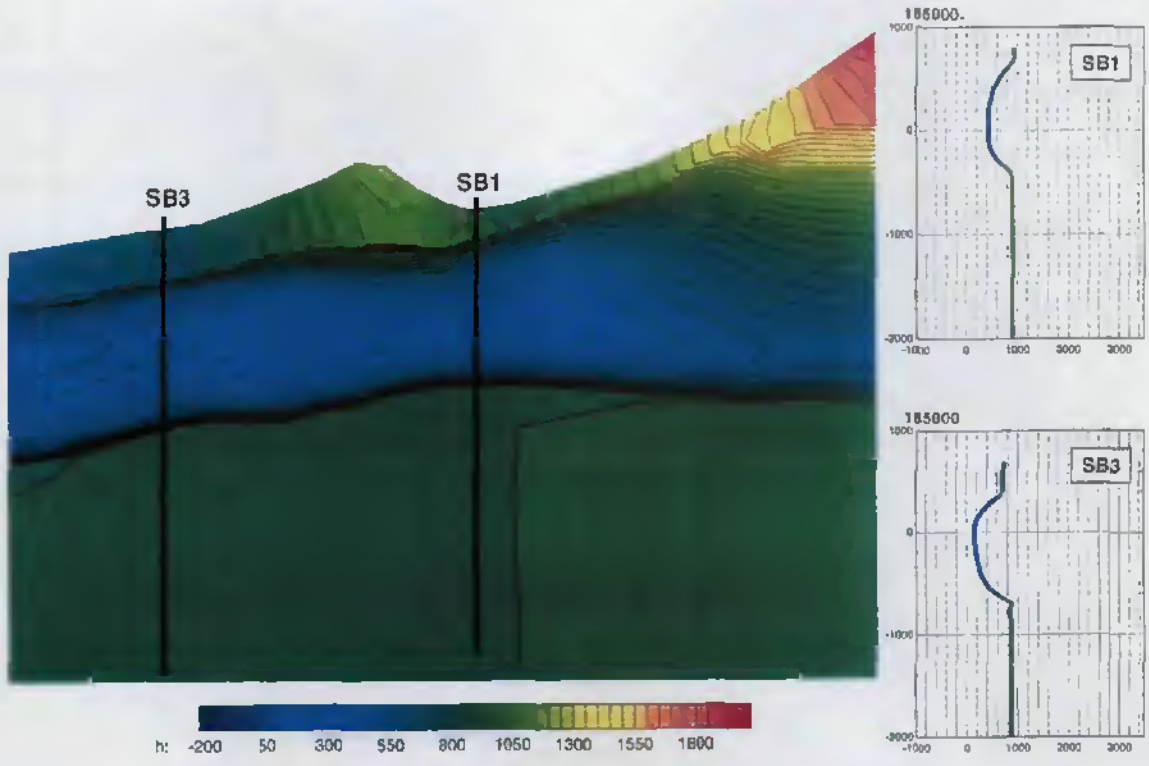

Fig. 9.4-2c: Model scenario Q1 - Simulated head distribution immediately after the end of the last glaciation II (10'000 a BP)

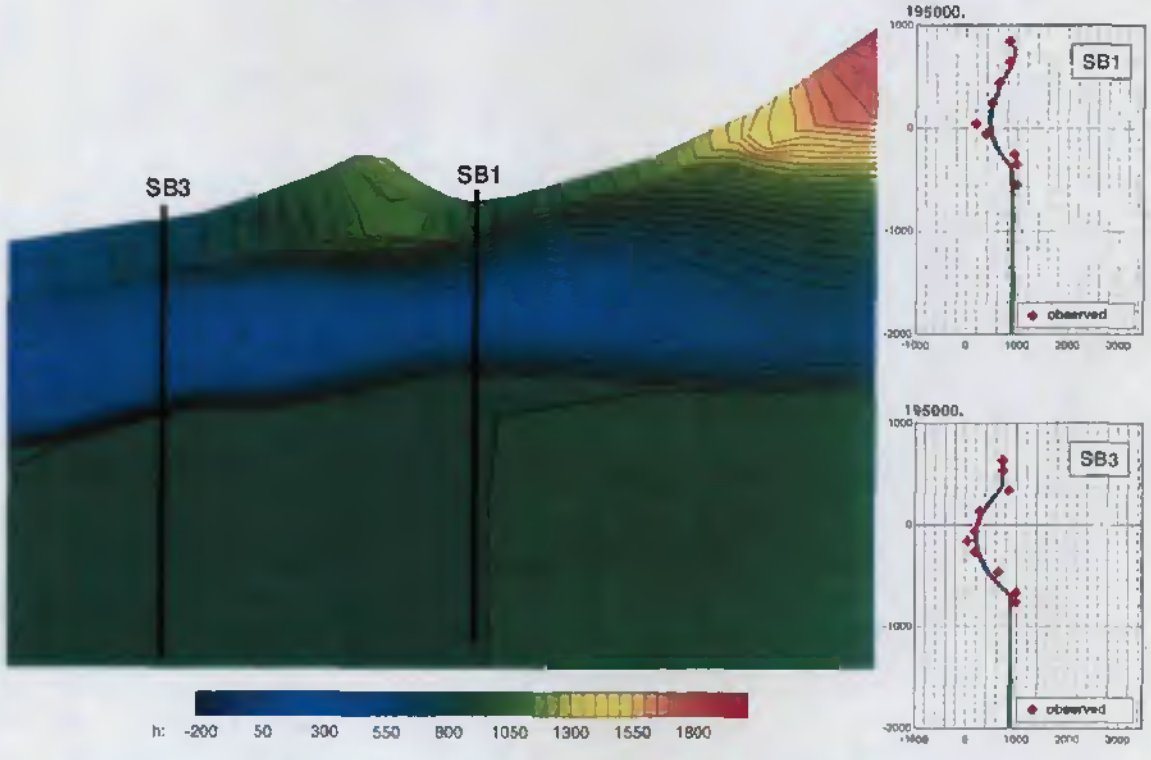

Fig. 9.4-2d: Model scenario Q1 - Simulated head distribution for today (i.e. 10'000 a after the end of the last glaciation II)

Fig. 9.4-3 shows the evolution of the head values at three reference points in the aquitard. These reference points correspond to locations of the head minima observed today in SB1 and SB3 as well as the piercing point of the upright projection of the tip of the Eggeligrat saddle through the Engelberg Aa valley level (540 m a.s.l.). The dashed lines show the levels of the three reference points. The represented head curves result from the evolution of the ice load and the erosion with changing boundary conditions.

Fig. 9.4-3 makes it further clear that the change in overburden pressure strongly influences the head in the deeper sections of SB3. The heads at valley level, however, are only marginally affected. The reason for this different behaviour is that the valley level between SB1 and SB3 lies under present conditions in a higher permeability zone (decompaction zone) of the marl-shale rock. The different levels of the drilling starting points SB1 and SB3 (difference in altitude: approx. 200 m) also explains the head difference at the end of the simulation period. This difference temporarily enlarged itself during the last glaciation. Although the head in SB1 did not react directly to the landslide, the shift of the Eggeligrat-saddle to the east due to the landslide caused a delayed reaction in SB1 by raising the head minima (Fig. 9.4-1).

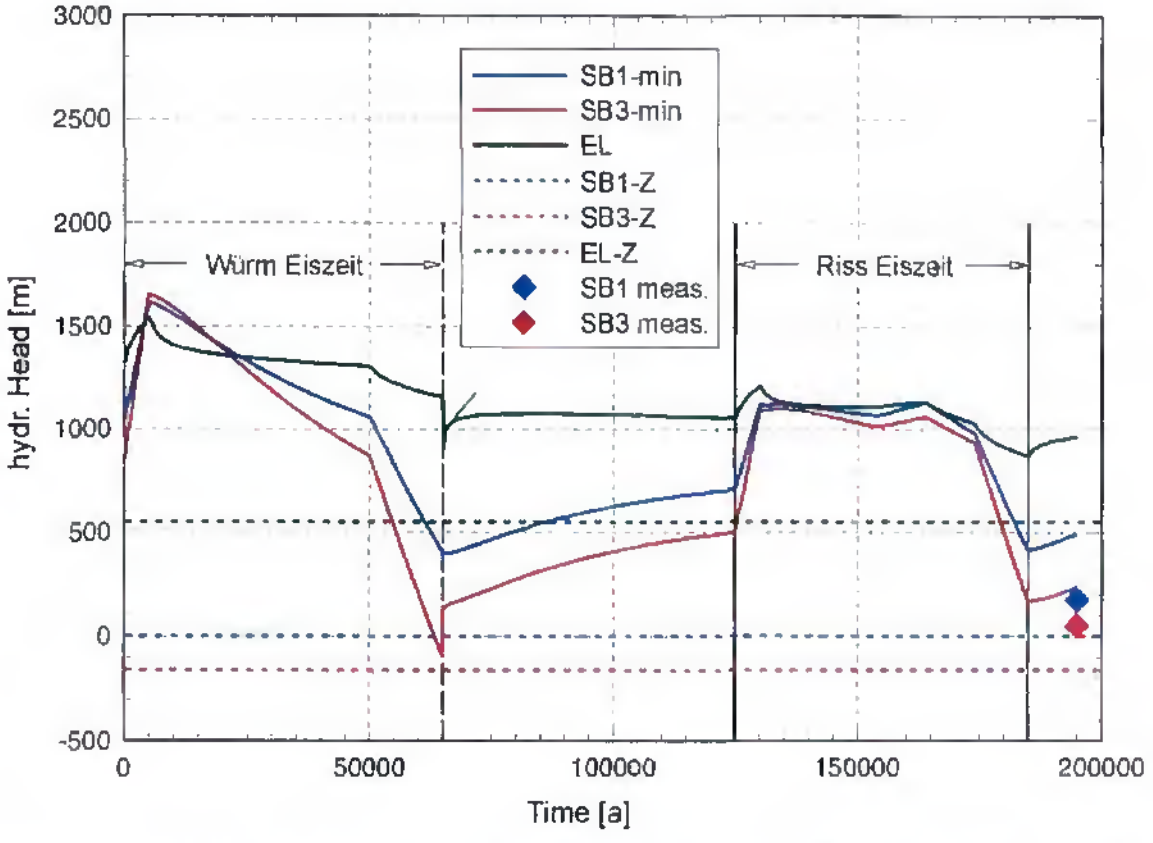

Fig. 9.4-3: Model scenario Q1 - Simulated head evolution on different reference points (head minima in SB1 and SB3 as well as at valley level, 540 m a.s.l.)

SB1-min, SB3-min: evolution of the minimum head in the boreholes ; EL :evolution of the head at altitude 540 m a.s.l. below the Eggeligrat saddle; SB1-Z, SB3-Z: point in the borehole where the minimum head was measured; EL-Z: altitude level of the point at level 540 m a.s.l. exactly below the Eggeligrat saddle; SB1 meas., SB3 meas.: current measured minimum head values.

In order to estimate the individual contribution of topography, erosion and glacier unloading, three independent simulations were conducted. The first run was limited to changes of the topographic surface. The second run ignored the glacier loading-unloading cycles, i.e. applied the source term only during erosional phases, while the third simulation applied the source-term only during glacier build up and retreat, keeping the boundary conditions constant. The results of this deconvolution are illustrated by Figs. 9.4-4 to 9.4-6 hereafter.

Fig. 9.4-4 represents the head change produced exclusively by the changed boundary conditions applied to the topography, while Fig. 9.4-5 shows the effect of erosion alone. As can be noticed from this latter graph, the influence on the head conditions in the aquitard is fairly limited, since even the strong and rapid landslide of Altzellen produces only small and short-term effects (it actually even contributes to increase the pore pressures at SB3 due to the accumulation of rock mass). However, comparison between Fig. 9.4-3 and Fig. 9.4-6 shows clearly that glacier rebound contributes most to the generation of the UPZ, indeed 79 % at SB3 (600 m depth a.h.[6]). The change in boundary conditions contributes only to 8 % and erosion only to 13 % of the total underpressuring at this representative point.

The excess pore pressures in the ground generated by the ice load dissipates gradually during the presence of the glaciers, thanks to basal drainage. This effect was especially marked during the penultimate glaciation, because of the long stay of the glaciers. At the end of the last glaciation, some overpressuring survived because the ice mantle increased by about 100 m in the second part of the glaciation. The Eem interglacial period, lasting for about 60'000 a, was not sufficiently long to remove completely the pressure anomaly generated by the former glaciation. This explains why, in spite of its lower ice level, the last glaciation caused underpressures almost in the same range as the preceding event. Succeeding ice ages, separated by relatively short interglacial periods, appear to be able to maintain underpressures over significant periods of time.

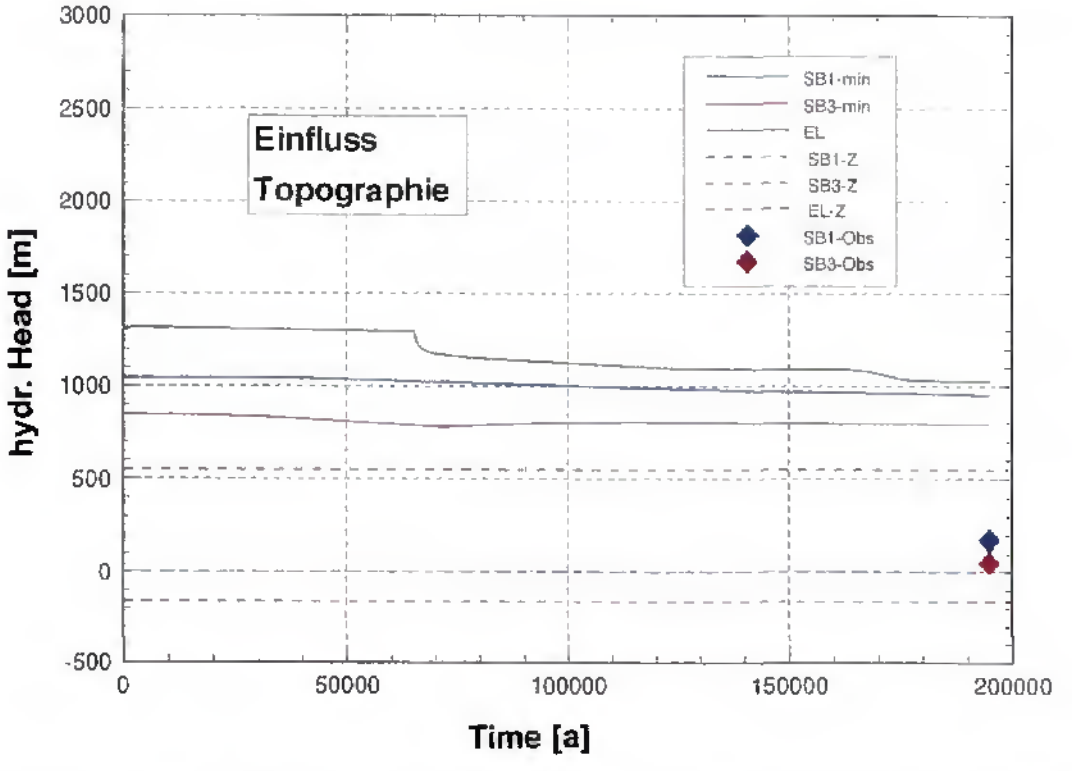

Fig. 9.4-4: Model scenario Q1 - Simulated head evolution due only to changes in boundary conditions on topographic surface (legend in Fig. 9.4-3)

6 a.h.: along hole

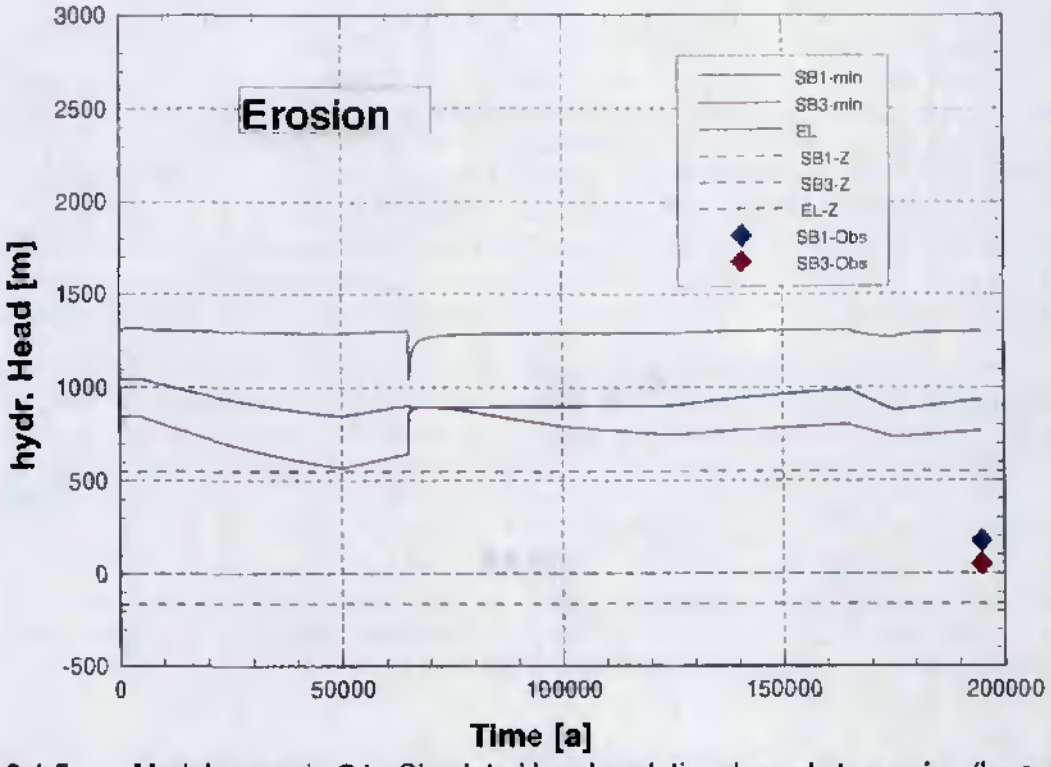

Fig. 9.4-5: Model scenario Q1 - Simulated head evolution due only to erosion (legend in Fig. 9.4-3)

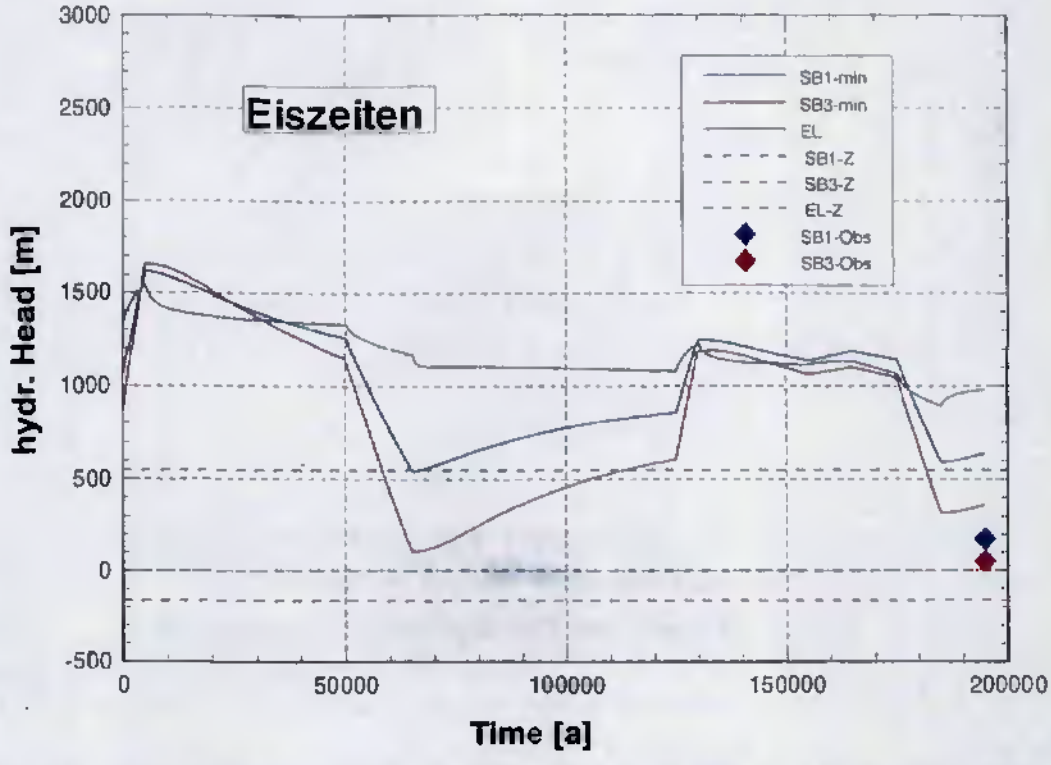

Fig. 9.4-6: Model scenario Q1 - Simulated head evolution due only to glaciations (legend in Fig. 9.4-3)

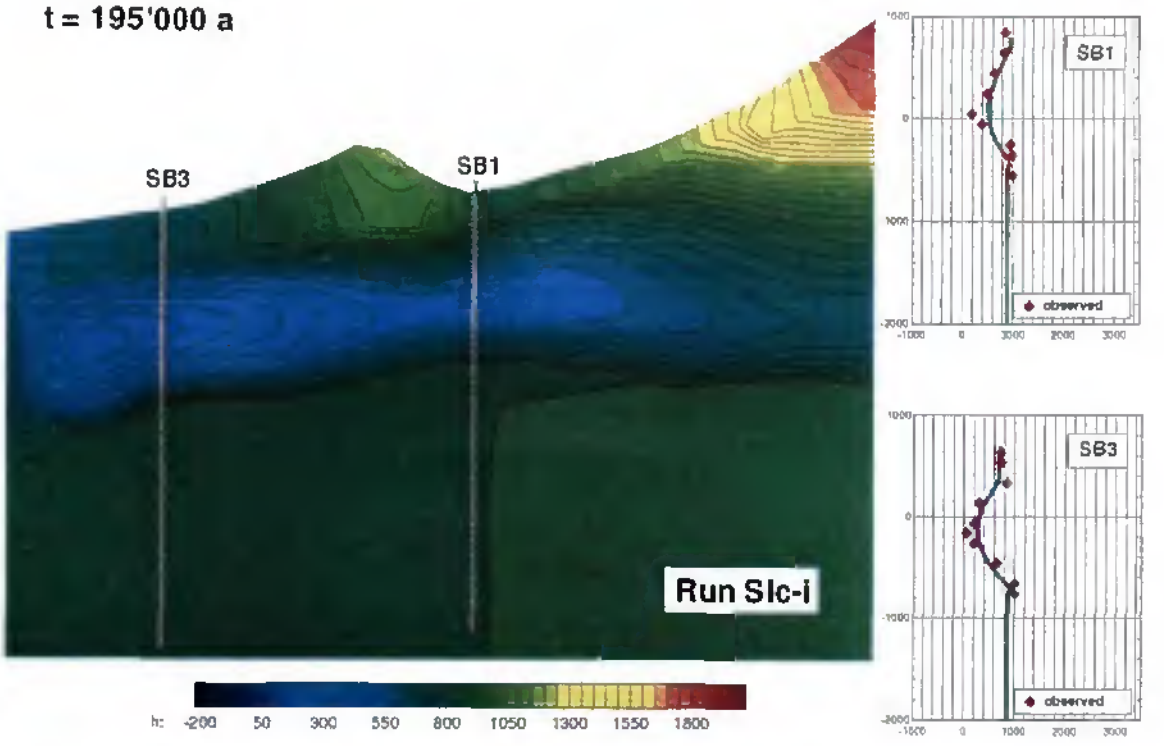

Fig. 9.4-7: Model scenario Q1 with western drainage boundary - Simulated head distribution for today (after 195'000 a)

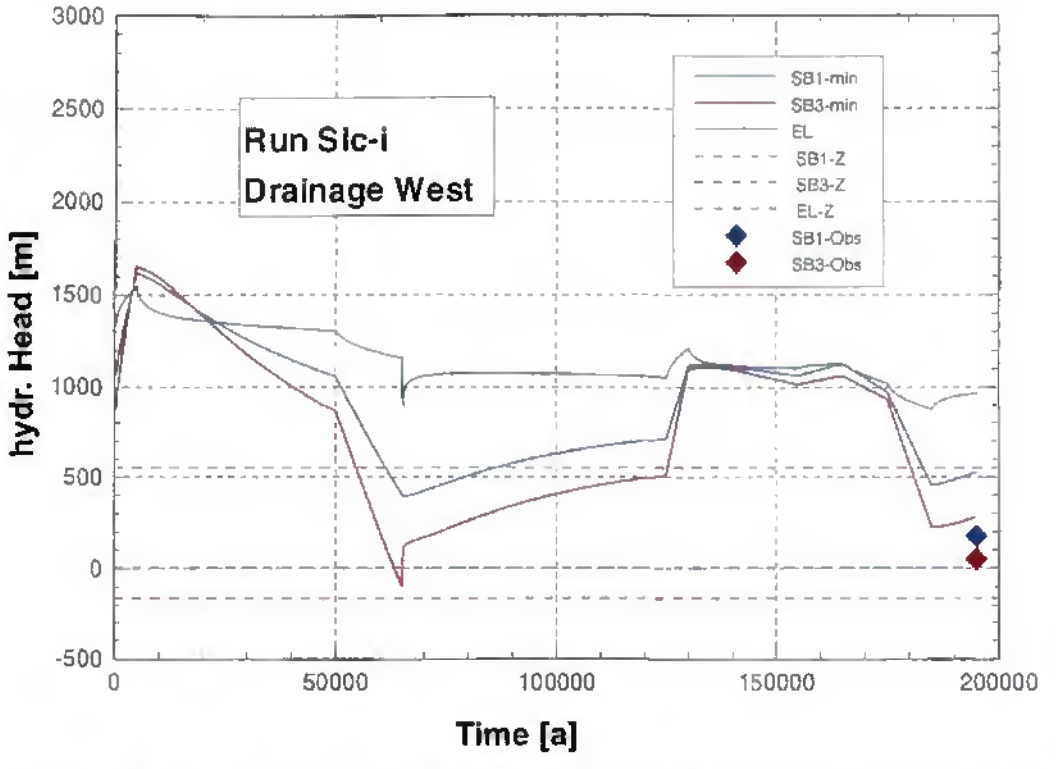

Fig. 9.4-8: Model scenario Q1 with western drainage boundary - Simulated head evolution

Model scenerio Q1 with drainege in the Engelberger Aa velley

This model scenario assumes that the western model boundary, i.e. the Engelberger Aa valley, corresponds to a zone of subvertical large-scale water-conducting features, draining groundwater into the valley floor. After 195'000 a (today) the shape of the UPZ as illustrated in Fig. 9.4-7 results. Fluxes below the valley floor would be nearly horizontal and oriented west to east from the valley towards the interior of the aquitard. With respect to the head conditions at SB1 and SB3 respectively, this simulation is nearly identical with the base case model (Fig. 9.4-7 and Fig. 9.4-8).

9.5 Regional model setup for abstraction schemes Q2 and Q3

9.5.1 Introduction

Starting with the first site-model built in 1986 (HÜRLIMANN et al., 1990) before the exploration of the Wellenberg site, over the schematic "Pilotmodell" in 1993 (NAGRA, 1993a), to the currently used regional model ("Regionalmodell"; NAGRA, 1997), geometry, discretisation and level of information evolved considerably. The regional model, in particular, was modified several times from 1994 to 1997, ultimately in order to take the K-model into account (NAGRA, 1997).

The FE-mesh of the regional model used in abstraction schemes Q2 and Q3 best reproduces the geological model of the Wellenberg site (TACHER, 1994). The K-distribution resulting from kriging is interpolated onto the irregular 3D FE-mesh (VOBORNY et al., 1997; KUHLMANN, 1997).

This Section presents the necessary information on the regional model setup, which are by order:

1. The extension, geometry and level of discretisation of the model as well as the rationale for defining model boundaries
2. The K-distribution in the marl-shale aquitard (K-model)
3. The boundary conditions.

9.5.2 Model geometry

Fig. 2.1-2 presents a perspective view of the modelled region observed from southwest; it provides insight into the rugged topography and the complex geological conditions. Minor geological formations were lumped together, resulting in the following hydrogeological units, surrounding the marl-shale aquitard:

- Quaternary deposits
- landslide of Altzellen
- nondifferentiated limestones of the Axen-nappe
- nondifferenciated limestones of the Drusberg-nappe (Kieselkalk and Valenginienkalk)
- Equivalent of the Wissberg slab (Scholle)
- Parautochthonous

The infrahelvetic Mélange formation exhibits relatively low K-values and was therefore

considered as part of the aquitard in this model[7]. A large portion of the model is occupied by the limestone formations of the Helvetic nappes (Axen- and Drusberg-nappes) in order to follow (likely) natural topographic groundwater divides (Engelberger Aa valley or mountain crests, e.g. Walenstöcke). Different types of boundary conditions can be assigned to the limestone units. The same idea applies to the lower boundary of the model, which was placed inside the Parautochthonous formation. It is believed that within the Parautochthonous, flow is predominantly horizontal and that therefore cross-formational flow between marl-shale aquitard and Parautochthonous is limited.

The surface of the model is given by the topography, which is derived from the digital topographic model of Switzerland (grid resolution: 100 m). The source-term was calculated by deriving a function relating the current topography to former topographic levels for erosion and to former ice levels for glaciations. However, the mesh was kept constant in all simulations based on the assumption that topography has not significantly changed in the last 20'000 a. This assumption holds for most places, but not for the valley floors, where large changes occurred induced by glaciations.

The geometry of the represented hydrogeological units follow quite exactly the 3D geological model of the Wellenberg site generated by interpolation between and extrapolation from the geological profiles illustrated in NAGRA (1997). The code EARHVISION (DYNAMICS GRAPHICS INC.) was applied by TACHER et al. (1994). More on the method can be read in TACHER & MAYORAZ (1993). The FE-mesh of the regional model was constructed iteratively by applying a novel method. The geometry of the boundaries between pairs of hydrogeological units were extracted from the Earthvision model and used to adapt to the pre-constructed generic FE-mesh. For more information, the interested reader is referred to SCHRÖDER et al. (1994).

9.6.3 K-distribution in the marl-shale aquitard

MARSCHALL et al. (1997) provide an overview of the methodology and application of the K-model. Details are to be found in JAQUET et al. (1997).

For the present study (model scenarios Q2 and Q3), the K-distribution generated by the Kriging method was used exclusively. K-distributions produced by conditional simulations were not used, although they are much more realistic and in agreement with observations and conceptualisation, which is not the case of the (smooth) kriged distribution. Five reasons dictated this choice:

1. The model scenarios describing erosion and glaciations are fraught with a higher level of uncertainty than the one associated with the K-variability.
2. The currently estimated K-variability is based on a sparse dataset (few boreholes). It is evident that the K-variability depends on the level of information on hydraulic properties of the rock, i.e. might evolve, perhaps considerably, as a function of additional data. Therefore, the "validity" of the proposed K-variability is questionable and can only be assessed a posteriori, i.e. after completion of further investigations.
3. The influence of the K-variability on the dissipation of abnormal pressure has already been explored (NAGRA, 1997). The UPZ represented in Fig. 1.4-2 was used as initial condition. The decay of 90 % of the initial underpressures varies between 20'000 a and 43'000 a by considering 12 conditional simulations (base case K and S_s-values).
4. The use of K-realisations might mask the manifestations of the overall mechanisms that

[7] In NAGRA (1997), however, this formation covering the Parautochthonous was considered separately to avoid definition problems

are tested by means of the abstraction schemes.

5. The use of K-realisations is computationally intensive and was not possible within the restricted budget allocated for the study of abnormal pressures.

The represented K-distribution was ported onto the irregular FE mesh of the regional model by using a kriged interpolation. The head difference with respect to simulations using the regular hectometric grid of cubes is h < 20 m (i.e. negligible) as shown by comparison between models. The kriging method provides a best-estimate of a parameter at any point in the system, associated with a measure of the uncertainty of the interpolation at this point, expressed as the estimation variance σ_k^2, or, as the standard deviation σ_k. The parameter sensitivity presented in Section 9.7 takes advantage of this bandwith of uncertainty: the K-value of each hectometric bloc of the K-Model was reduced by a factor within the range of one standard-deviation of the average K-value.

9.5.4 Boundary conditions and input parameters

9.5.4.1 Scope and definitions

As shown by the parameter sensitivity study presented in Paragraph 9.3.3.4, the role of hydraulic parameters in the adjacent lithologies is subordinate, and therefore boundary conditions are almost entirely a matter of levels of saturation in the hydrogeological units adjacent to the marl-shale aquitard. In the following are presented, the saturation levels and the input parameters characterising the hydrogeological units surrounding the aquitard unit.

9.5.4.2 Groundwater levels in the hydrogeological units adjacent to the marl-shale aquitard

The boundary conditions imposed at the limits of the regional model domain are described by category. Tab. 9.5-1 provides an overview of available data and imposed boundary conditions in terms of hydraulic head (saturation) or no-flow.

Upper boundary

The Quaternary deposits as well as the landslide of Altzellen covering most of the Palfris-formation on the eastern flank of the Eggeligrat saddle are considered as saturated. Local and shallow occurrences of vadose zones are neglected. The marl-shale aquitard itself outcrops only at high elevation, on the Eggeligrat and on the Sinsgäuer Schonegg topographic saddles. Springs, some dozen metres below the Eggeligrat saddle are temporarily dry, suggesting that an unsaturated zone of < 100 m thickness is temporarily possible. However, the impact on hydraulic gradients at depth of locally unsaturated conditions is deemed negligible, and therefore the aquitard is also considered as a fully saturated body (h = z [8]).

Lateral boundaries

The marl-shale aquitard is laterally constrained by massive limestone formations which form the southern and eastern boundaries of the model domain. Therefore, the saturation conditions, or water-levels in these formations represent important boundary conditions. Limestone formations are well known for their complex groundwater flow patterns. Karst or fracture flow, depending on the lithology, produce heterogeneous saturation conditions,

---

[8] z stands for "topographic elevation"

both in space and in time (JAQUET & JEANNIN, 1994). Addressing this type of problems is well beyond the scope of this study, nevertheless, reasonable saturation conditions are necessary. Therefore, all units were approximated as EPM with continuous properties (K, S_s).

The northern boundary is represented by the limestone formations of the Drusberg nappe, which have been traversed by borehole SB2 and by several shallow piezometers. Additionally, information from spring surveys and the isolated topographic situation help to constrain possible water levels. It was assumed that the groundwater level is at the topographic level defined by the contact between the marl-shale aquitard and the limestones. The same simplification applies to the southern border of the aquitard, at the interface with the adjacent massive limestone units of the Axen-nappe. If the dataset was sparse for the limestones of the Drusberg-nappe, it is almost inexistant for the lithologies of the Axen-nappe. The situation is further complicated by the isoclinal fold structure implying lithologies of contrasted hydraulic properties, and by the high degree of fracturation. A large karstic spring a few metres above the level of the Engelberger Aa valley lies dry at some periods of the year, suggesting temporary "karstwater levels" slighly below valley level (exfiltration directly into alluvial sediments).

Recently, different scenarios have been elaborated for both tectonic units, among which one was selected for the calculations documented in NAGRA (1997). This scenario postulates extremely low groundwater levels in the limestone formations encapsulating the aquitard. This implies lower hydraulic gradients directed from the aquitard towards the limy boundaries and therefore lower fluxes directed towards the UPZ, i.e. longer durations for dissipation of subnormal hydraulic pressures. Using comparatively "high" saturation levels in the neighbouring units, as it is the case in this study, is less favourable for the maintenance of abnormal pressures, i.e. the modelled conditions are more conservative this way.

Boreholes SB1 and SB3 exhibit both artesian conditions in the Equivalent of the Wissberg Slab. In order to achieve artesian conditions in this thin hydrogeological unit, a connection to the southern boundary was established, where artesian conditions are imposed.

Tab. 9.5-1: Hydraulic head of the adjacent hydrogeological units (after NAGRA, 1997)

Hydrogeological unit	Database	Hydraulic head (m b.g. / m a.s.l.)	Head imposed in the model
Quaternary deposits	SB3, SB6, SB4a/v, springs, piezometers	hydrostatic to subhydrostatic (0 to -70 / 940 - 975)	hydrostatic
Landslide of Altzellen	SB3, SB6, SB4a/v	hydrostatic to subhydrostatic transition to aquitard: partly artesian (up to +80 / 1020)	hydrostatic
Mélange	SB1, SB3	artesian up to strongly subhydrostatic (+160 to -325 / 1006 - 520)	not imposed (considered as part of aquitard)
"Wissberg slab"	SB1, SB3	strongly artesian (+150 to +330 / 1006 - 1065)	head imposed at: 1'040 m a.s.l.
Parautochthonous	SB1	subartesian (single value: -140 / 706)	Bottom of the model: impermeable boundary
Limestones of the Drusberg-nappe	SB2, springs, piezometers	seldom subhydrostatic hydrostatic	partly unsaturated low groundwater levels
Limestones of the Axen-nappe	Springs, piezometers	seldom subhydrostatic hydrostatic	partly unsaturated low groundwater levels

9.5.4.3 Input parameters

Tab. 9.5-2 summarises the hydraulic conductivity estimates for the hydrogeological units adjacent to the marl-shale unit and provides a comparison with measured and estimated hydraulic data. Note that the hydraulic conductivity is simply obtained from the arithmetic mean of the average transmissivity for the total length of the tested borehole sections (LAVANCHY & MARSCHALL, 1997). For the limestone formations of the Axen-nappe, since no data is available, the K-value is based on an educated guess. The base case storage coefficient is for all hydrogeological units: $1 \cdot 10^{-6}$ m^{-1}. This value is increased up to $S_s = 4 \cdot 10^{-6}$ m^{-1} for parameter sensitivity study.

Tab. 9.5-2: K_{eff} of the adjacent hydrogeological units (after NAGRA, 1997)

Hydrogeological unit	Available data in boreholes	T_{tot} [m^2/s]	Tested intervals [m]	K[1] [m/s]	K-range[1] [m/s]	Applied K-values in scenarios O2 & O3 [m/s]
Quaternary deposits	SB3, SB6,	$7 \cdot 10^{-5}$	382	$2 \cdot 10^{-7}$	$0.4 - 4 \cdot 10^{-7}$	$1 \cdot 10^{-4}$
Landslide of Altzellen	SB4a/v					$1 \cdot 10^{-6}$
infrahelv. Mélange[2]	SB1, SB3	$1 \cdot 10^{-9}$	280	$4 \cdot 10^{-12}$	$0.9 - 9 \cdot 10^{-12}$	$4 \cdot 10^{-12}$
"Wissberg slab"	SB1, SB3	$4 \cdot 10^{-8}$	360	$1 \cdot 10^{-8}$	$0.7 - 3 \cdot 10^{-8}$	$1 \cdot 10^{-8}$
Parautochthonous	SB1	$5 \cdot 10^{-6}$	69	$7 \cdot 10^{-10}$	$0.3 - 3 \cdot 10^{-9}$	$1 \cdot 10^{-8}$
Limestones Drusberg-nappe	-	-	-	-	-	
Kieselkalk	SB2	$7 \cdot 10^{-4}$	430	$2 \cdot 10^{-6}$	$0.8 - 4 \cdot 10^{-6}$	$2 \cdot 10^{-6}$
"Valanginienkalk"	SB2	$1 \cdot 10^{-6}$	896	$1 \cdot 10^{-8}$	$0.1 - 6 \cdot 10^{-8}$	
Limestones Axen-nappe	-	-	-	-	-	$1 \cdot 10^{-6}$

[1] largest error determined from error bar of transmissivity values
[2] considered as part of the aquitard

9.6 Abstraction scheme Q2

9.6.1 Scope

Abstraction scheme Q1 was devoted to the influence of a sequence of events, such as ice ages and various types of erosion, without pretending to simulate realistic shapes of the UPZ nor to follow detailed paleoclimatic reconstructions. With the current model scenario, the particular influence of the last ice age (comprising two distinct glacier events) on the head distribution in the marl-shale aquitard is analysed in more detail using a 3D modelling approach and the mesh of the regional model 1995 (Sect. 9.5). Detailed paleoclimatic reconstruction was used to determine stages of various glacier apparatus and erosional events. Since it is known from the previous abstraction scheme (Q1) that the latest unloading will provoke the strongest underpressuring, special emphasis was put in characterising the terminal period of the last glaciation.

9.6.2 Model setup

Scenario Q2 is based on a compilation of Quaternary literature covering the main geomorphologic events at scale of the country, including the likely implications for Wellenberg. Fig. 9.6-1 provides a synoptic table with the noteworthy information. The corresponding sequence of events is summarised in Tab. 9.6-1 and extends over a duration of 116'000 a.

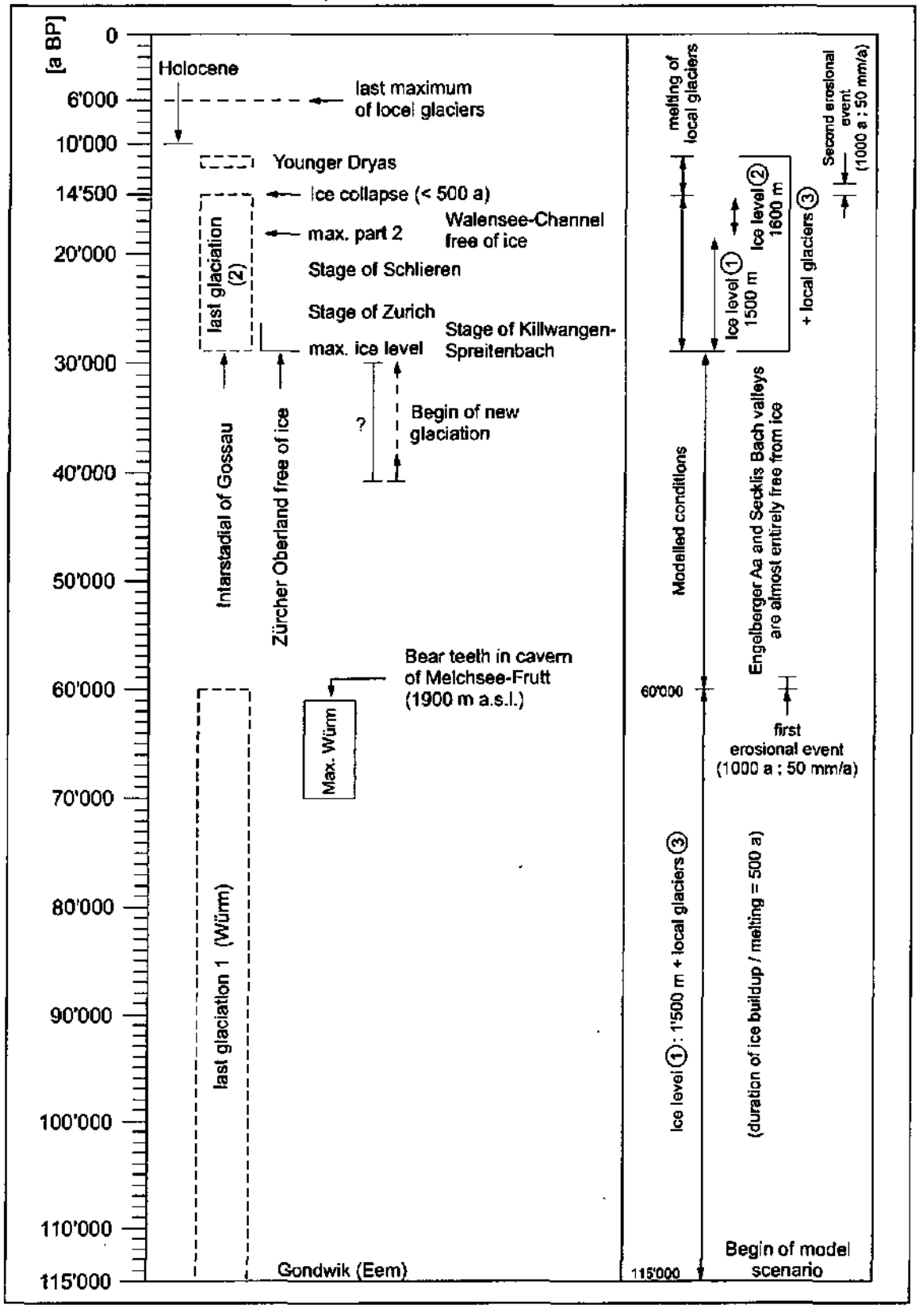

Fig. 9.6-1: Synoptic table of the principal geomorphological events in the last 116'000 a BP at scale of Switzerland and of the Wellenberg region (after SCHLÜCHTER & MÜLLER-DICK, 1996)

Tab. 9.6-1: Model scenario Q2 - Chronological sequence

Time [a BP]	State / event	Duration [a]	Process / load (Load / rebound)
116'000	---	---	Stationary hydraulic conditions
115'000	Build up of the last glaciation I	500	Ice cap 1 (1'500 m a.s.l.)➡ no erosion
60'000	Last glaciation I	55'500	Ice load
59'500	Decrease of the last glaciation I	500	Local glaciers (ice load 3)
60'500	Denudation	1'000	Erosion: 50 m withdrawal (50 mm/a)
28'500	Interstadial of Gossau	31'000	Erosion
28'000	Build up of tha last glaciation II	500	Ice cap ➡ no erosion
18'000	Last glaciation II	9'500	Ice cap 1 (1'500 m a.s.l.)
17'500	Last glaciation II	500	Increase of the ice load from 1 to 2
14'500	Last glaciation II	3'000	Ice cap 2 (1'600 m a.s.l.)
13'500	Denudation	1'000	Erosion: 50 m withdrawal (50 mm/a)
11'000	Complete glacier withdrawal	2'500	Local glaciers are melting, erosion
0	Postglacial period (Holocene)	11'000	---

The basic assumption is that the local Sinsgäu and Bannalp glaciers on the eastern part of the modelled region were still present during the interstadial of Gossau and also at the end of the last glaciation II. These local glaciers retreated slowly to higher altitude levels until they completely melted away about 11'000 a BP.

To implement the different ice loads which temporarily covered parts of the model domain, a series of cross-sections was sketched, which were interpolated by means of kriging. The corresponding 3D extension of the ice caps is illustrated in Figs. 9.6-2a to 9.6-2c. Fig. 9.6-2a shows the ice cover of the modelled region during glaciation I and the first part of glaciation II. Fig. 9.6-2b represents the maximum ice load during the climax of the "Würm" ice age (second part of glaciation II), while Fig. 9.6-2c represents the situation at the end of each glaciation, i.e. interglacial periods, when local glaciers survived sometime the retreat of the main glaciers. The K-distribution corresponds to the base case values.

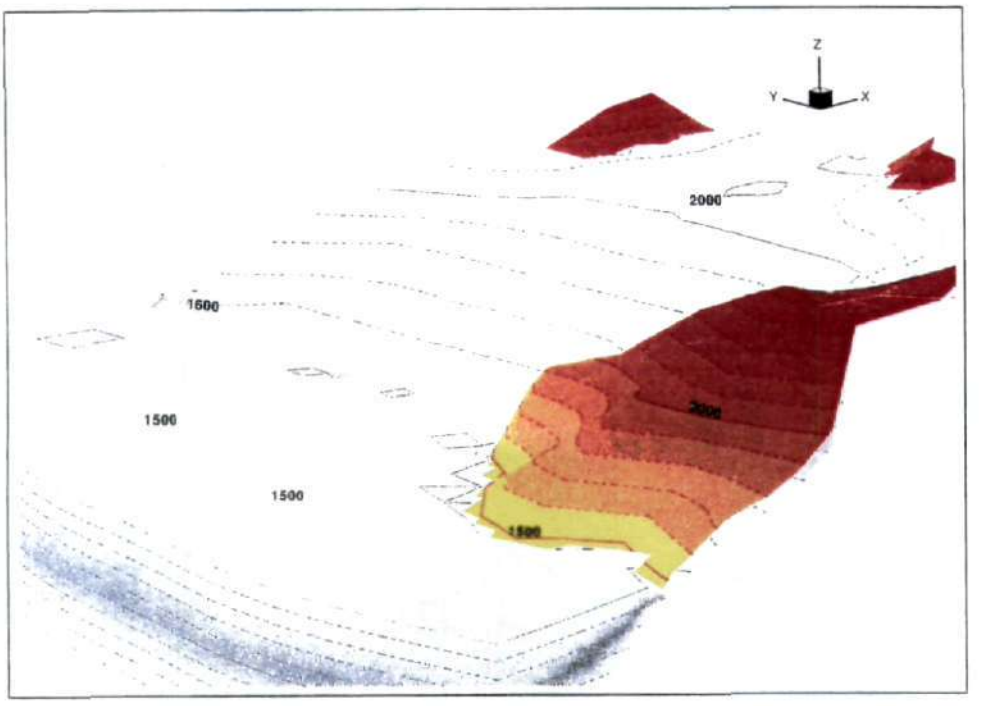

Fig. 9.6-2a: Model scenario Q2 - Ice level during glaciation I

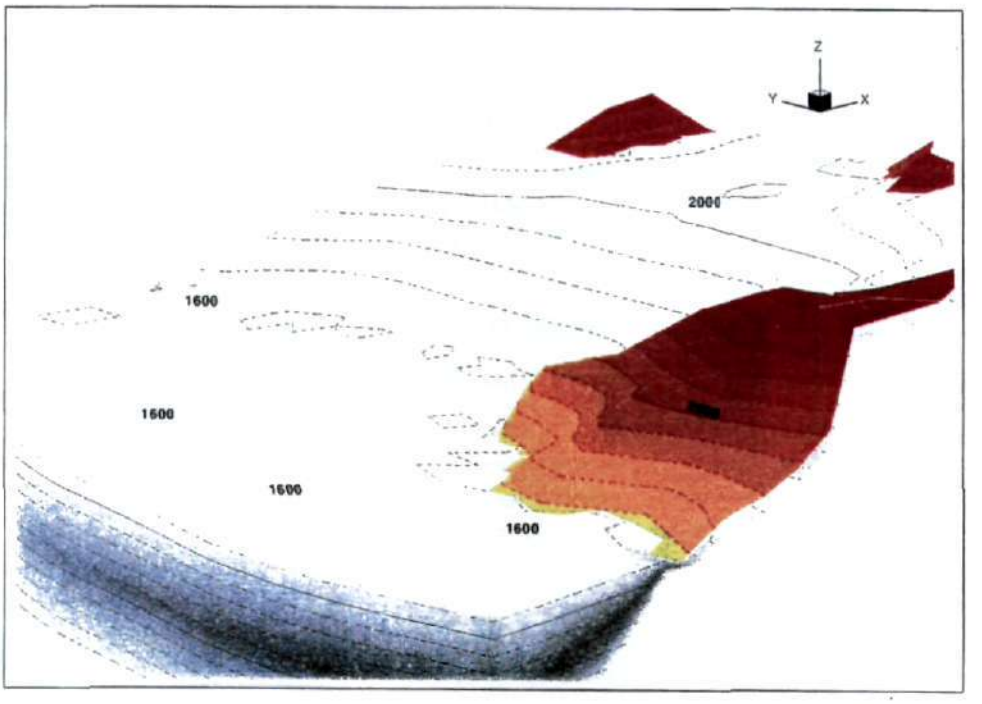

Fig. 9.6-2b: Model scenario Q2 - Ice level during second part of glaciation II

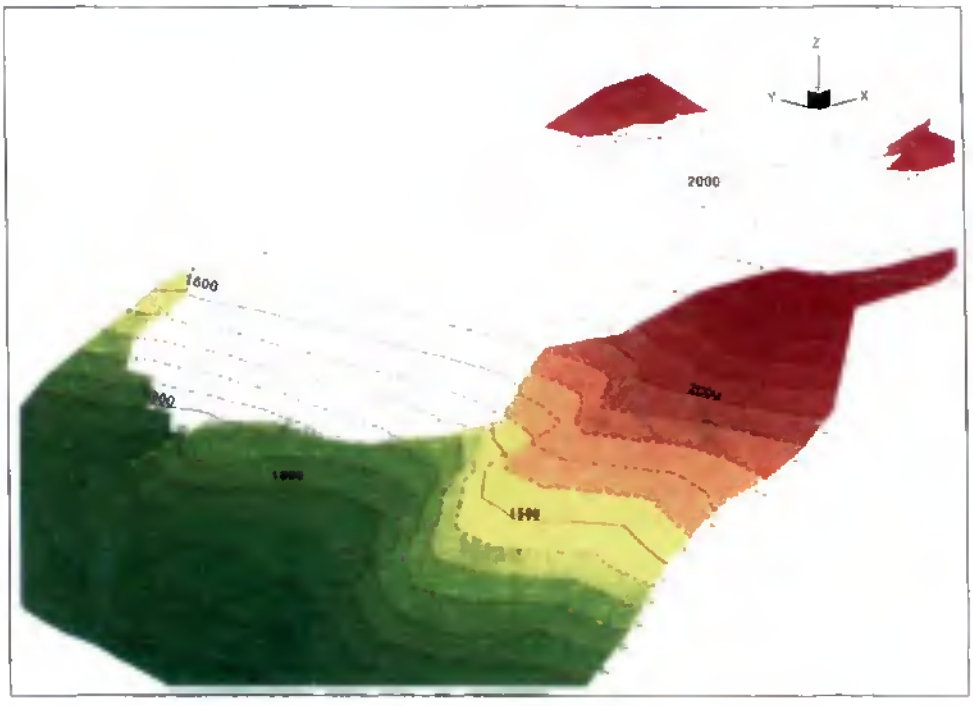

Fig. 9.6-2c: Model scenario Q2 - Local glaciers at the end of glaciations I and II

9.6.3 Results of abstraction scheme Q2

The evolution of the hydraulic heads for model scenario Q2 is represented in Fig. 9.6-3 (analogous to Fig. 9.4-3, model scenario Q1). Like for Q1, the deepest heads develop immediately after rebound due to glacier withdrawal. The absolute lowest head values do not only depend on the amount of rebound, but also on the duration of the melting process.

The head values resulting from model scenario Q2 match the bandwidth of the contemporary measured values in SB1 and SB3 quite well. Comparison between the current head distribution in Q2 (Figs. 9.6-4a and 9.6-4b) and Q1 (Fig. 9.4-2d) shows that:

1. The UPZ is developed more uniformly in the 3D model Q2 than in the 2D model Q1
2. The delayed glacial retreat in the Eastern part of the model domain is noticeable in the evolution of the underpressures
3. The volume and extent of the simulated UPZ is substantially larger than that of the prescribed UPZ (Fig. 1.4-2) documented in NAGRA (1997) although it is perfectly consistent with the base-case dataset (K-model, S_s).

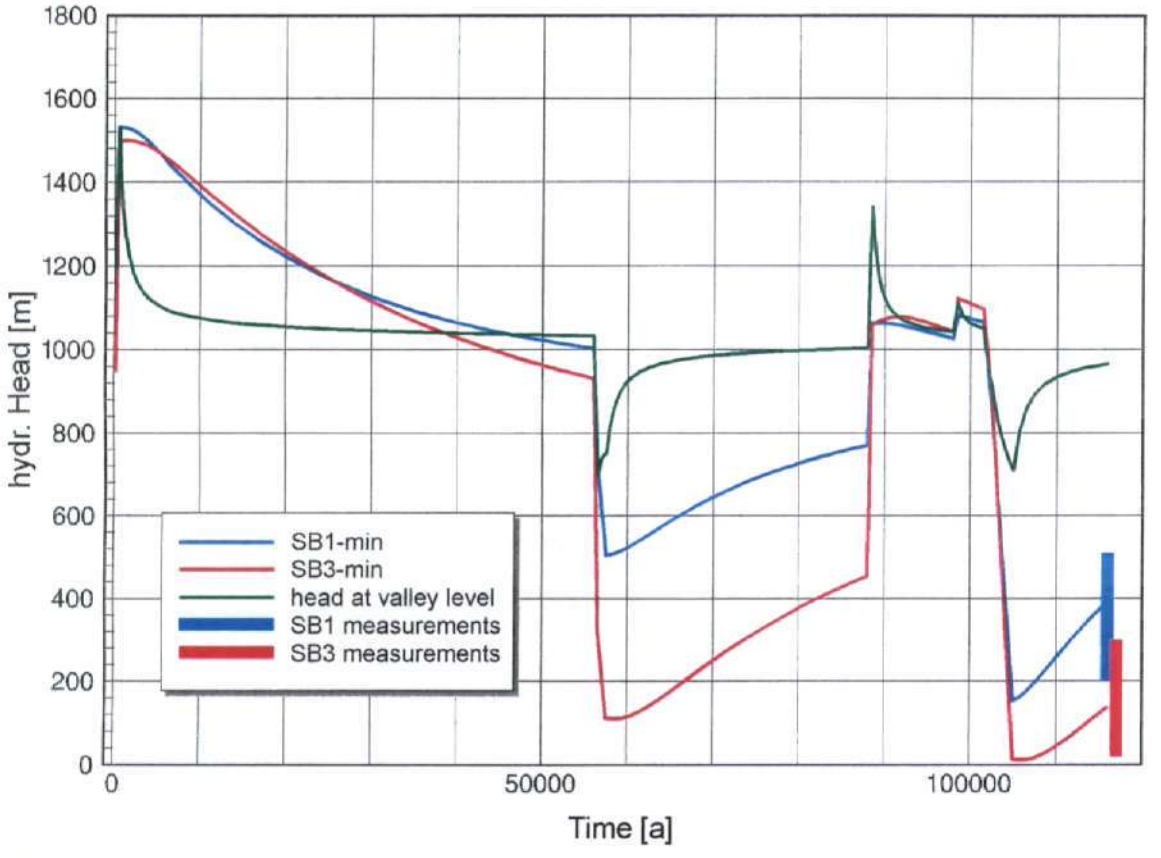

Fig. 9.6-3: Model scenario Q2 - Simulated head evolution during the last glaciation on different reference points

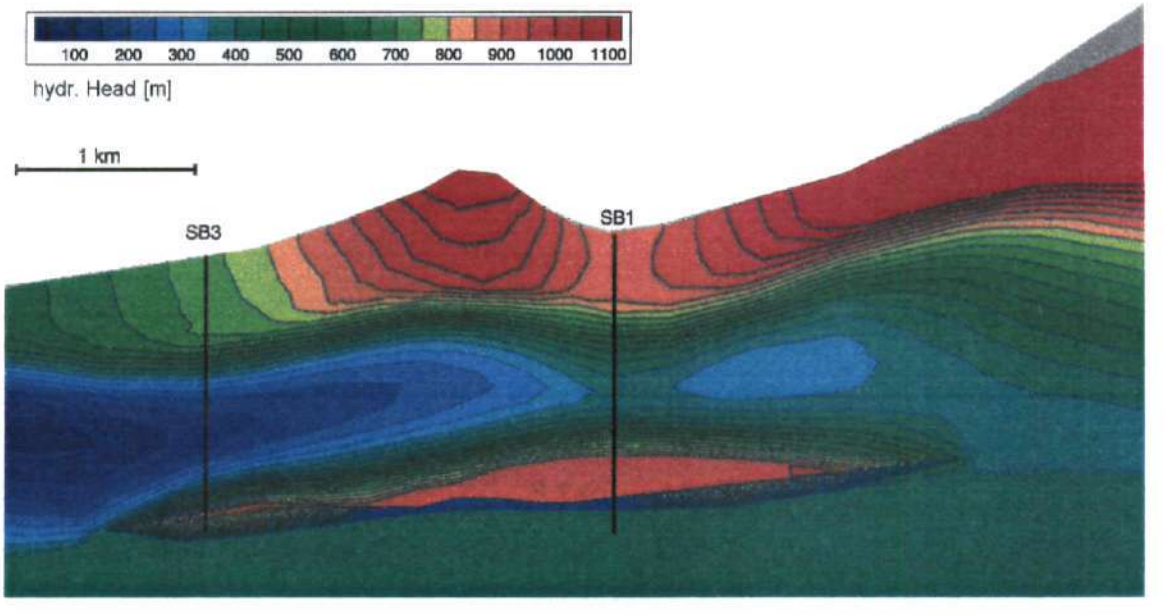

Fig. 9.6-4a: Model scenario Q2 - Simulated contemporary head distribution in cross-section Q-Q'

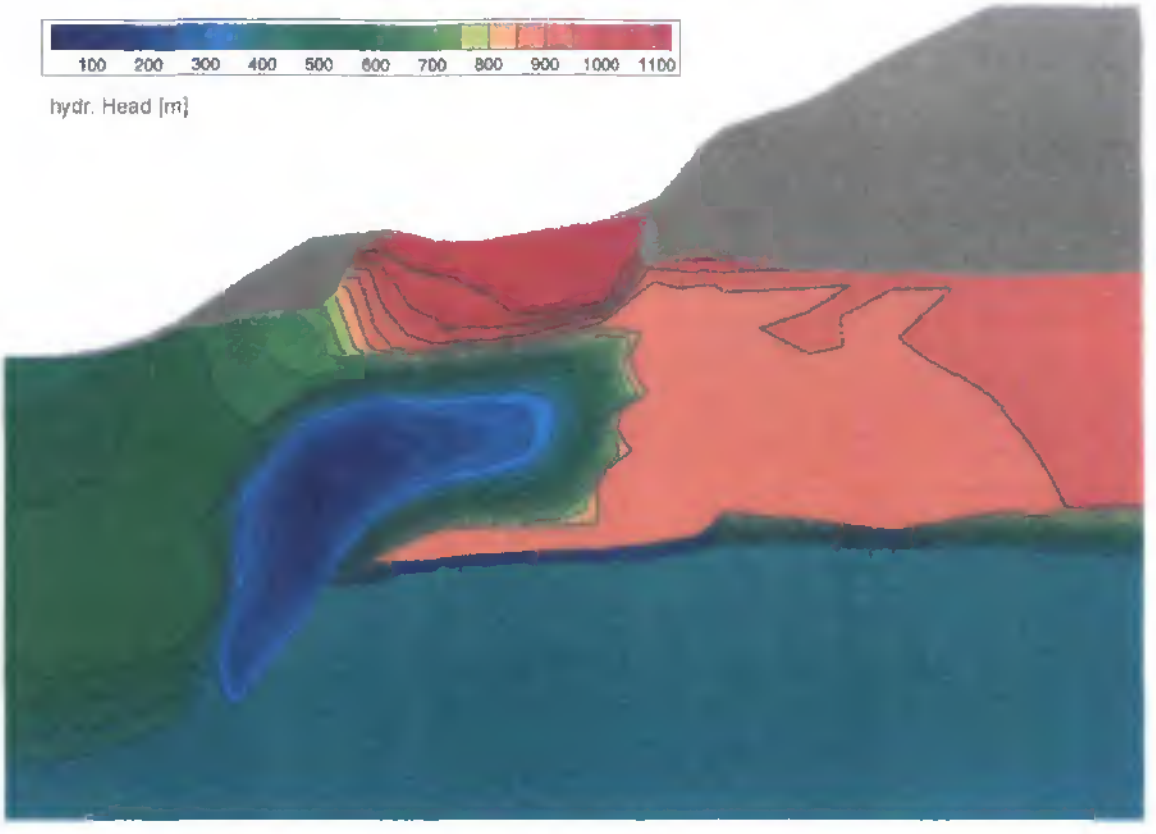

Fig. 9.6-4b: Model scenario Q2 - Simulated contemporary head distribution in cross-section D-D'

A variation of model scenario Q2 was performed by assuming a free surface, i.e. by assigning infiltration instead of fully saturated conditions h = z. The distribution of the water table generated by the model is dominated by very low water levels in the neighbouring limestone formations. Although the modelled free surface is not everywhere realistic, hydrodynamic simulations using the free surface as input confirmed that lower gradients between adjacent units result in a more extended and more resistant UPZ.

9.7 Abstraction scheme Q3

9.7.1 Scope

With abstraction scheme Q2, the influence of geomorphological events in the last 116'000 a was examined in detail. The results show that, by neglecting former events, the last ice age is able by itself to produce underpressures in the observed range. However, the orogenic erosion study performed parallely (Chap. 10) demonstrates that denudation and differential erosion also may produce underpressures in the observed order of magnitude, and this even without consideration of glacier unloading, provided very-low diffusivity values are used. Q3 was designed to value the contribution of differential erosion before the onset of the last "Würm" ice age (glaciations I and II in Sect. 9.6).

The problem actually reduces to assigning disequilibrium pressure at the start of model scenario Q2 and to performing a parameter sensitivity on K and S_s of the aquitard. With respect to the base case diffusivity distribution (K_{eff} taken from the K-model,

$S_s = 3 \cdot 10^{-6}$ m^{-1}), D was progressively reduced by reducing K_{eff} and/or increasing S_s). This way, the robustness of proposed parameters could be compared to the base case values.

9.7.2 Model setup

9.7.2.1 Definition of erosion stages

Departing from the situation 13.5 million years ago, three erosion surfaces were defined (Sect. 9.5), following the time chart presented in Tab. 9.7-1.

Tab. 9.7-1: Geomorphological evolution used for the construction of abstraction scheme Q3 (including Q2)

Time [a BP]	State / event	Scen.		Duration [a]	Process / load (Load / rebound)
13'500'000	Initial situation	Ch. 10		---	Surface evenly at level 7'000 m a.s.l.
6'000'000	Homogeneous denudation	Ch. 10		7'500'000	Surface evenly at level 4'000 m a.s.l
700'000	Onset of differential erosion	Ch. 10		5'300'000	Surface A (Fig. 9.7-1 & 9.7-2)
700'000	Differential erosion	-	Q3	---	Surface A (Fig. 9.7-1 & 9.7-2)
190'000	Differential erosion	-	Q3	510'000	Surface B (Fig. 9.7-1 & 9.7-2)
130'000	Glaciation	-	Q3	60'000	Surface B, ice cap ⇒ no erosion
115'000	Differential erosion	-	Q3	15'000	Surface C (Fig. 9.7-1 & 9.7-2)
115'000	Build up of last glaciation I	Q2	Q3	500	Surface C, ice cap ⇒ no erosion
60'000	Last glaciation I	Q2	Q3	55'500	Surface C, ice cap ⇒ no erosion
59'500	Decrease of last glaciation I	Q2	Q3	500	Local glaciers
60'500	Denudation	Q2	Q3	1'000	Differential erosion
28'500	Interstadial of Gossau	Q2	Q3	31'000	Differential erosion
28'000	Build up of the last glaciation II	Q2	Q3	500	Ice cap ⇒ no erosion
18'000	Last glaciation II	Q2	Q3	9'500	Ice cap ⇒ no erosion
17'500	Last glaciation II	Q2	Q3	500	Increase of ice load
14'500	Last glaciation II	Q2	Q3	3'000	Ice cap⇒ no erosion
13'500	Denudation	Q2	Q3	1'000	Differential erosion
11'000	Complete glacier withdrawal	Q2	Q3	2'500	Local glaciers are melting, erosion
0	Postglacial period (Holocene)	Q2	Q3	11'000	Today's topographic surface

The basis for the erosion surfaces is KLEMENZ (1996). Based on KLEMENZ' topographic evolution profiles, erosion stages were reconstructed using and extending the available set of ad hoc geological profiles (NAGRA, 1997). In the next step, kriging was applied to construct the three topographic surfaces presented in Fig. 9.7-1. On cross-section Q - Q', they fully coincide with the topographic profile used in model scenario Q3. The Engelberger Aa valley was several times scoured up to the bedrock during former glaciations, i.e. reaching below the today's topographic surface as illustrated in Fig. 9.7-1.

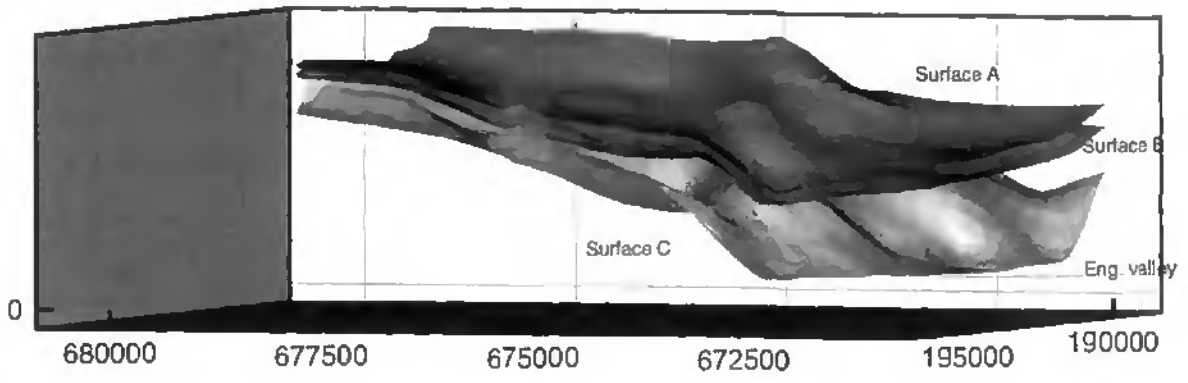

Fig. 9.7-1: Perspective view on the three erosion surfaces (seen from north-east)

9.7.2.2 Limitations

This study was fraught with several difficulties. The first problem was to translate general information on the geomorphological events of the Central Alps, providing only weak chronological information, into a sequence of events with quantitative data as necessitated by numerical models. For example, and based on borehole SB6 core analysis of the landslide mass (SCHLÜCHTER, 1995), the strongest movement was assigned to the penultimate ice age ("Riss"), taking the assumption that the last two glaciations played only a minor role on erosion.

Technically also, limitations associated with the source term approach necessitated an adaptation of the originally foreseen abstraction scheme. Thus, instead of modelling a time span covering the last six million years, the time range had to be reduced to the last 700'000 years, this because the huge decrease in overburden of the order of the current magnitude of the aquitard and more, would be impracticable for the source term approach and also because it would have required lowering of the model surface. Another more salient problem is the time-dependency of the K-field as discussed in Section 7.3. Ideally, the model should be computed in different steps, one per erosion stage. At each stage, a distinct model surface K-field would be used. Due to the lack of funding and of time, such computationally intensive work had to be redesigned. Therefore, the erosion history was approximated based on today's topography and today's (assumed) K-distribution. These assumptions may results in an underprediction of the absolute magnitude of the UPZ and of the duration of the dissipation process.

Finally, the glacier loading-unloading cycles of ice ages previous to 116'000 a BP were ignored. With respect to the long duration of the considered period (of the order of 600'000 a), the error associated with this simplification is considered negligible.

9.7.3 Results

The enhancement of erosion rates and additional consideration of glacier unloading in the last part of the modelled time span produce unreasonably low pore pressures reaching down to absolute negative pore pressures, which is out of reach of CASA's capabilities. In the following, Figs. 9.7-2 to 9.7-5 present the head distribution in cross-section Q- Q' at various time steps, using the base case parameters. Fig. 9.7-2 shows the head distribution 190'000 a BP, i.e. after 510'000 a of differential erosion (erosion surface B). Clearly, at this

stage, no underpressures exist. Fig. 9.7-3 shows the situation at 115'000 a BP, i.e. little after glacier unloading, at a time when erosion surface C is reached. As expected, the UPZ occupies most of the aquitard and results essentially from glacier retreat and not from erosion. Figs. 9.7-4 and 9.7-5 show the current simulated head distribution based on different values of diffusivity. While in Fig. 9.7-4, reasonable head levels are computed, the choice of very low-diffusivity ratios produces irrealistic negative pressures (Fig. 9.7-5).

Analysing the head evolution at different reference points in boreholes SB1, SB3 and SBx at level 540 m. a.s.l. over the entire time span of 700'000 a (Fig. 9.7-6) shows, beyond doubt, that differential erosion is not able to produce a significant decrease in pore pressures, at least not for the applied base case parameters and for this type of modelling (source-term approximation without changes in topographic surface). It is only with the retreat of the first considered ice age (130'000 a BP) that subnormal head values appear. *This result confirms that it is reasonable to consider only the time span covering the last 115'000 a BP, which is exactly the duration considered by model scenario Q2.*

A parameter sensitivity study was performed over the time range of 115'000 a. Initial head conditions correspond to generically produced UPZ some 20'000 and 30'000 a before the start of the model sequence. The dissipation stage achieved at 115'000 BP is used as initial conditions. The corresponding initial head values reported at SB1 and SB3 respectively are labelled "INI-1" and "INI-2" in Figs. 9.7-7a and 9.7-7b. Specific storage is varied from $S_s = 3 \cdot 10^{-6}$ m^{-1} to $S_s = 5 \cdot 10^{-6}$. The base case K-distribution corresponds to K-values prescribed by the K-model (labelled "$d_K = 0$" in the plots). The parameter variation on K is performed by taking advantage of the uncertainty range produced by the kriging method and corresponds to the average K-value estimate minus one standard deviation. A constant value "d_K" is added to individual average log K-values. For parameter sensitivity, two steps of K-reduction are computed: $d_k = -0.5$ and $d_k = -1$, corresponding, respectively, to a reduction of half an order of magnitude of log K and of one order of magnitude.

Comparison between Fig. 9.7-7a (SB1) and Fig. 9.7-7b (SB3) shows that the simulated head values for today chiefly depend on the appropriate choice of K and S_s and not so much on the careful definition of initial conditions. Moreover:

1. Simulating a duration of 700'000 years or of 115'000 years results in indistinguishable head patterns as of today (curves INI-1 and INI-2). The initial head difference 115'000 a BP of more than 130 m, already reduces to less than 15 m after 60'000 a and to less than a few metres today.
2. For an identical model sequence, the use of different D-values produce tremendous differences in the evolution of head conditions. As expected, very low diffusivity values result in prolonged pressure disequilibrium. However, the pore pressure change due to a sudden change in the applied overburden stress is less pronounced for very-low D-values with respect to higher D-values. This is because the dissipation process following an anterior event "buffers" to some extent the effects of the posterior event resulting in a so-called "memory effect".

Therefore, *especially the last glaciation is of importance for the magnitude of the current underpressures and for their future evolution.* The recent head evolution helps to constrain quite effectively possible diffusivity values (see also Chap. 12).

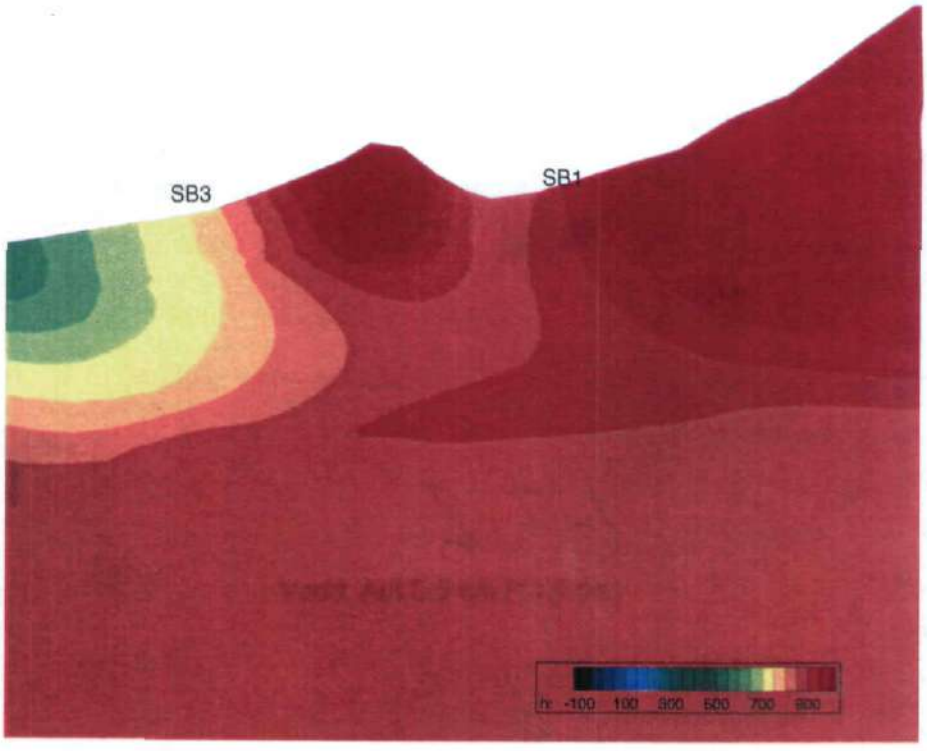

Fig. 9.7-2: Model scenario Q3 - Simulated head distribution in cross-section Q - Q' 190'000 a BP (base case parameters)

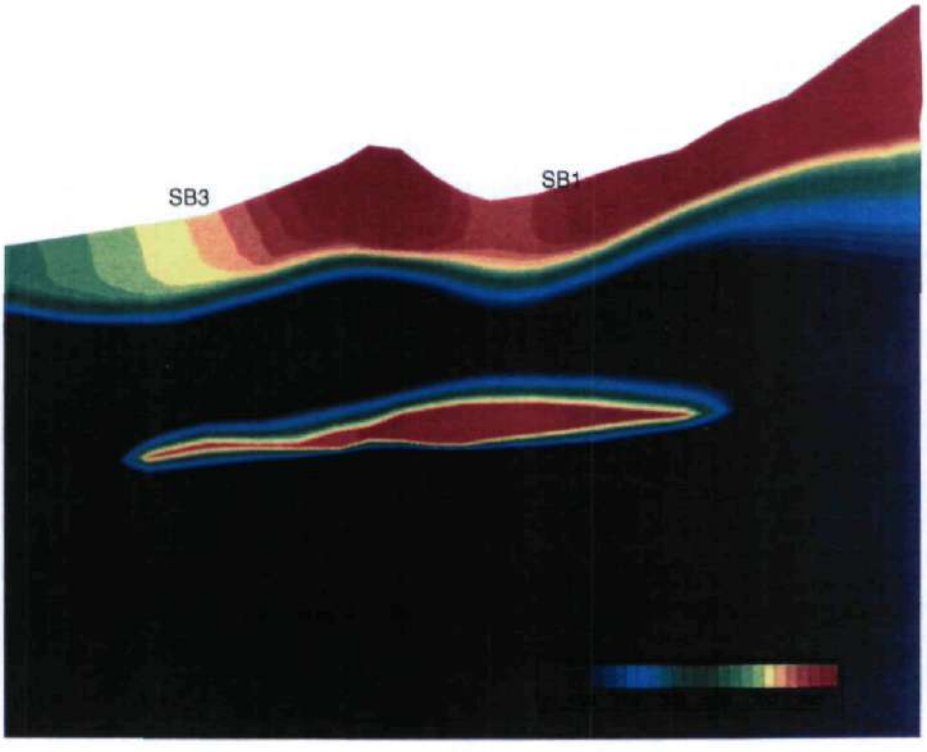

Fig. 9.7-3: Model scenario Q3 - Simulated head distribution in cross-section Q - Q' 115'000 a BP (base case parameters)

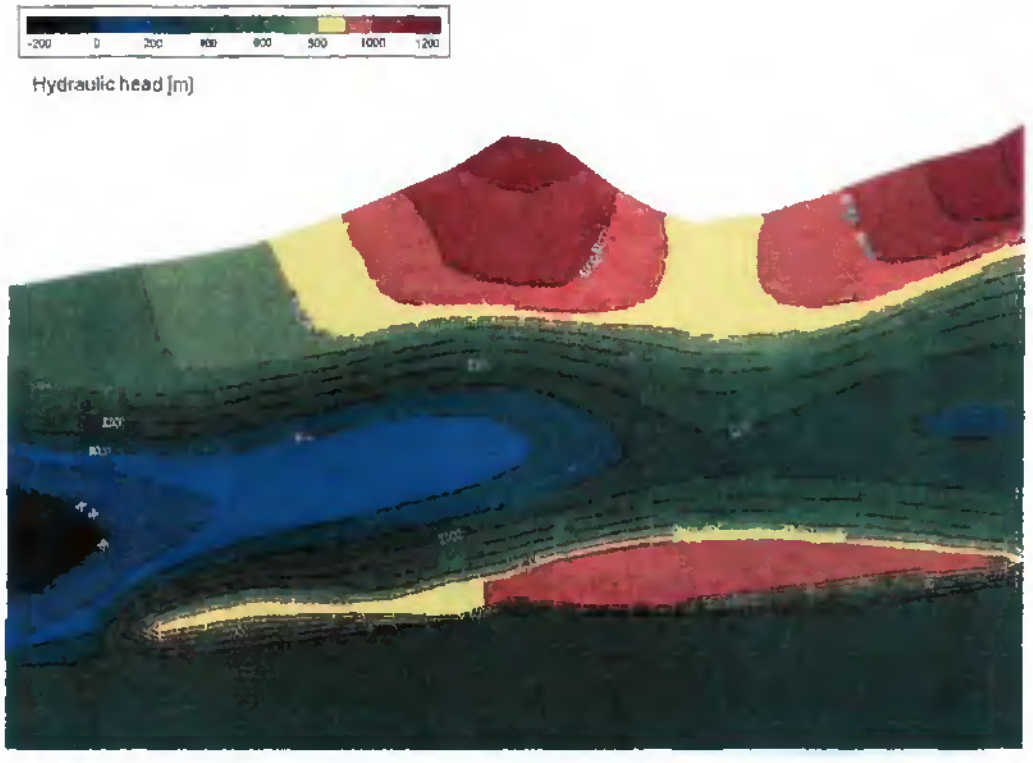

Fig. 9.7-4: Model scenario Q3 - Simulated contemporary head distribution in cross-section Q - Q' (base case parameters)

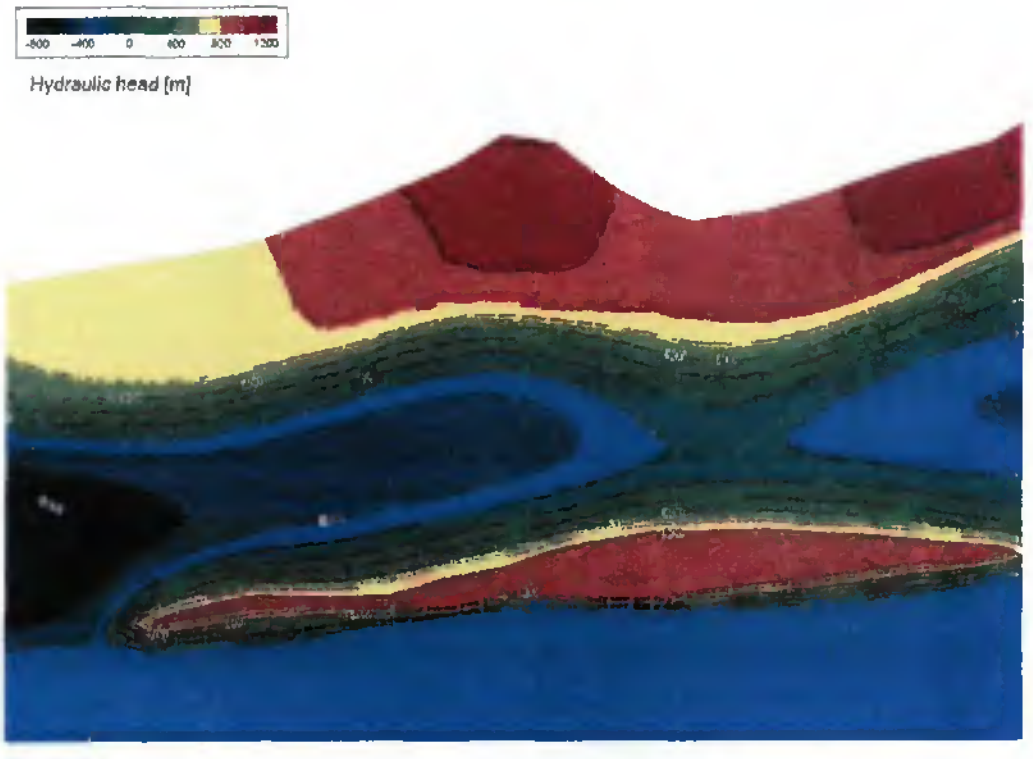

Fig. 9.7-5: Model scenario Q3 - Simulated contemporary head distribution in cross-section Q - Q' (very low diffusivity parameters)

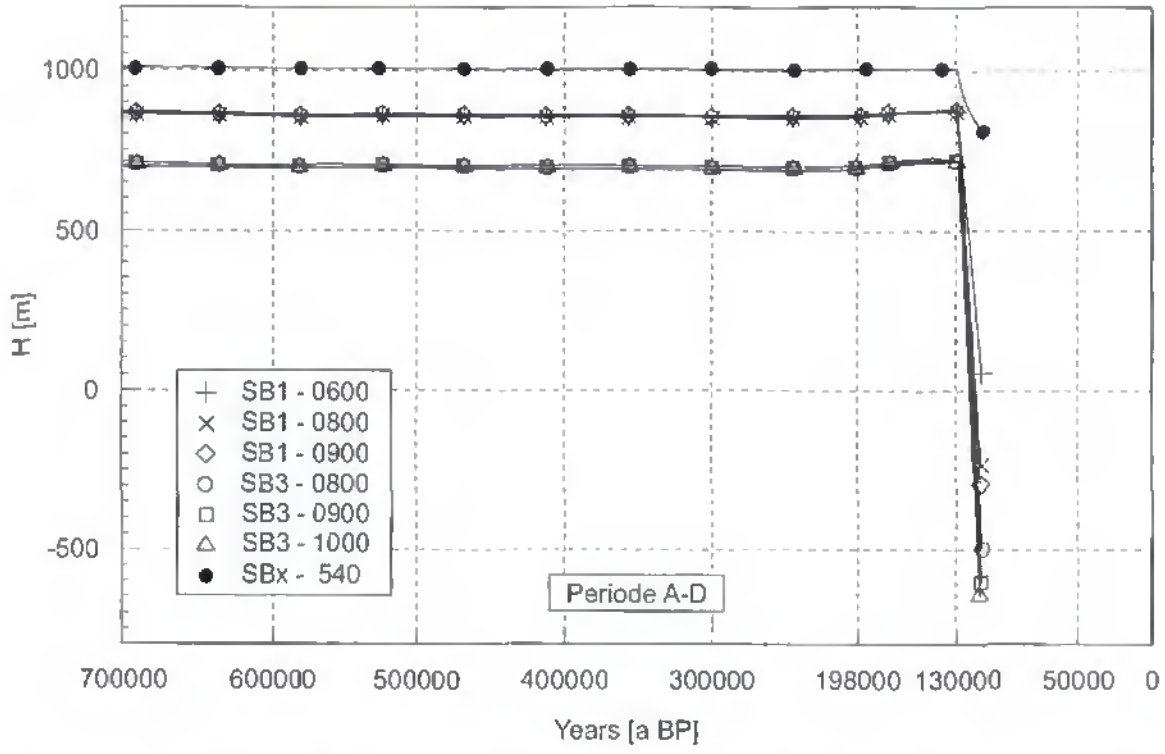

Fig. 9.7-6: Model scenario Q3 - Head evolution over the entire time span of 700'000 a observed at different reference points (base case parameters)

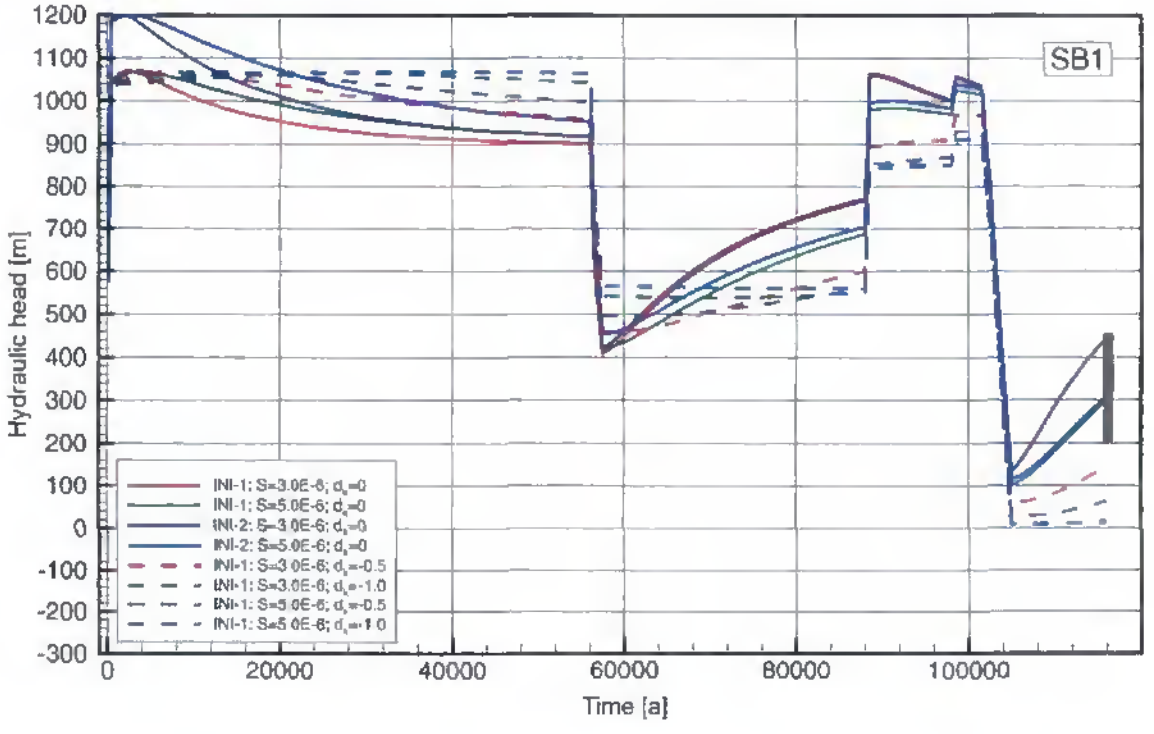

Fig. 9.7-7a: Model scenario Q3 - Parameter variation. Simulated head evolution over the last 115'000 a BP as observed on the reference point represented by the current head minima in SB1

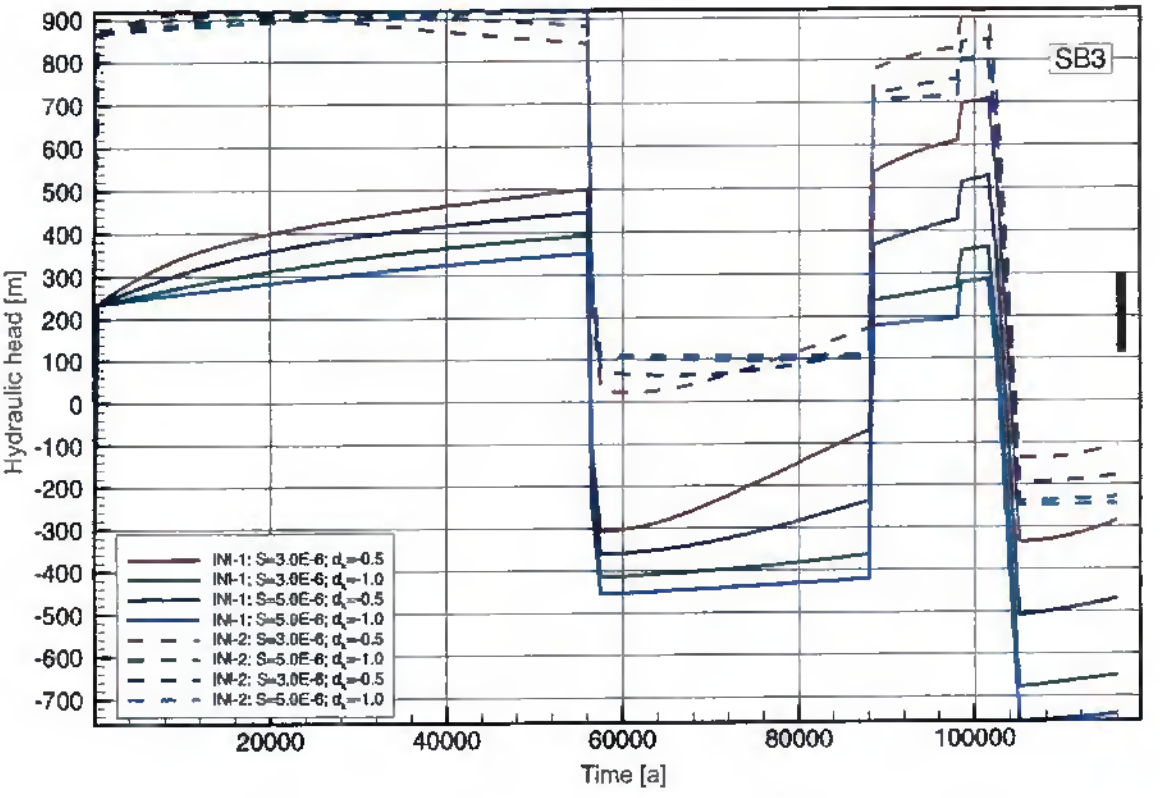

Fig. 9.7-7b: Model scenario Q3 - Parameter variation. Simulated head evolution over the last 115'000 a BP as observed on the reference point represented by the current head minima in SB3, Influence of parameter variation of K and S_s on the head evolution over the last 115'000 a. The grey vertical beam corresponds to the range of head measurements.

9.8 Summary of results and discussion

The glacial scenarios do not presuppose any complex processes according to the principle of the simplest explanation. Under "complex processes" is understood processes like changes in the tectonic extemal stress state, time and temperature dependence of key parameters, etc. The three computed abstraction schemes tend to support the hypothesis that any climate change provoking build up and melting of extensive glaciers is the actual key mechanism generating hydraulic underpressures. Under the assumption that the processes, model scenarios and values of diffusivity were well selected, it can be affirmed that the last glaciation - with or without a contribution from erosion - was able to cause by itself underpressures in the observed range.

With respect to forecasting the future evolution, the shortest possible geological period for the origin of hydraulic underpressures is thus defined. In other words, no other geologic forcing could be identified that is more recent than the last ice age. Therefore, careful extrapolation into the future should consider glaciations in the base line. Other, more sophisticated, evolution scenarios may be consistent with the glacier scenario in terms of results for today. This essentially because effects of other and especially older generation processes are in comparison with the last glacier forcing vanishingly small.

10 DENUDATION AND DIFFERENTIAL EROSION CONCEPTUAL MODELS

10.1 Introduction and definitions

"Denudation" refers to the extensive withdrawal of sediments acting more or less evenly on a relatively smooth ground surface, whereas "differential erosion" characterises a process by which topographic relief is progressively accentuated, i.e. pre-existing valleys are preferentially eroded in comparison to mountain ridges and hills.

This physical definition is overlain by a chronological definition. *Denudation* refers to all types of removal of sediments occurring concomitantly with the alpine orogenesis and the corresponding uplift of tectonic units. The time span ranges from early Paleocene to Pliocene. During this fairly long time range, erosion did not act uniformly on all outcropping terrains. However, paleorelief in this time range is of little importance because whatever it may have been, the Pleistocene, with its suite of ice ages, has considerably remodelled the landscape, obliterating most of the pre-existing relief. Consequently, only average paleo-altitude levels are used based on a constant denudation rate of 0.4 mm/a.

Differential erosion is the dedicated definition for the erosion provoked by the strong climate fluctuations of the Pleistocene (cyclically returning glaciations) and is chiefly the consequence of glacier progradations and retreats. The effects of differential erosion concentrated in an early phase on the Swiss plateau (development of large valleys) and later on progressed towards the alpine foothills. During the last 100'000 years even the internal domains of the Alps were exposed to erosion, resulting in the morphology we know today. How exactly the U-shaped valleys were created is still a matter of controversy among geomorphologists. Glacialists consider that the glaciers have enough kinetic energy to literally carve out (scour off) the valley floors, whereas tenants of the static school consider that glaciers did not affect strongly the underlying sediments and are responsible for the current topography only indirectly (slope instabilities enhanced by glacier melting). Whatsoever, glaciers considerably modified geomorphologic conditions, enhancing valley relief while hills and mountain crests were eroded at a much smoother pace.

10.2 Scope, geological background and modelling approach

10.2.1 Rationale

Linear-elastic rock deformation and isothermal conditions are considered appropriate approximations for Quaternary model scenarios (Sect. 7.4). However, when focusing on long-term erosion, the above approximations must be given some thought. In the latter case, a more realistic descriptions of long-term rock deformation behaviour coupled with groundwater flow is deemed necessary, which has been accounted for by using the coupled hydraulic-mechanical code ABAQUS (Subsect. 7.5.3).

The isothermal approximation also requires a critical review since material properties depend not only on the state of stress, but also on temperature. Heating affects both the pore fluid (expansion) and the rock framework (pore compression, solution and precipitation of minerals, microcracks), while cooling acts almost exclusively on pore pressure (fluid contraction). Theoretical considerations (Subsect. 7.4.4) support the statement that the effects of cooling are subordinate with respect to mechanical rebound. Therefore, isothermal conditions are considered as a valid approximation also for long-term modelling. Furthermore, cooling in the assumed magnitude and time range is not expected to result in decisive modifications of the rock properties (EINSTEIN, oral comm.). Cooling of relatively shallow aquifers during the presence of the glaciers, as shown by SPECK (1994 and 1995),

is the only effect that may have disturbed the geothermal gradient and at shallow depth only (300 m b.g.). It can therefore be neglected at greater depth.

10.2.2 Erosion rates

Even moderate erosion rates produce significant denudation in the order of several thousands of metres when geological time scales (millions of years) are considered. Moreover, for such long time spans, non-elastic deformation of the rock framework might become significant (NEUZIL, 1993). Furthermore, considering the geological and geomorphologic evolution of the Alps in the last 10 millions years, it appears clearly that not only large amounts of sediments were removed and transported up to the Swiss plateau, but that simultaneously tectonic shortening of the upper crust continued, as exemplified notably by the subalpine Molasse locally overthrusting Quaternary sediments (NAGRA, 1997). The average erosion rate of about 0.4 mm/a in the Helvetic domain is the base case value in the present simulations, although it is obvious that the denudation process is not pacing steadily, but comprises calm periods with minor erosion and periods of higher erosional activity, becoming more frequent in the relatively recent past (last million years).

10.2.3 Tectonic stress

As mentioned in Chapter 5, the particularity of Wellenberg resides in its tectonic position, and more specifically in the fact that the aquitard rock is still exposed to strong horizontal compressional stress. That underpressures could develop under such conditions is not trivial and requires dedicated investigation. Common sense would lead to expect abnormally high pore pressures in compressional fields, as noted for instance by DOMENICO & SCHWARTZ (1990) who consider that compressional stress associated with diffusivity ratios of about 10^{-9} m^2/s, and with very low strain rates in the order of $7 \cdot 10^{-16}$ s^{-1} suffice to produce overpressures. The following hypotheses provide explanations for this apparent paradox:

1. Tectonic compression prevails for more than 20 million years in the Central Alps and accompanied the rock transformations from lithification to more recent brittle deformation phases. The compressional stress is therefore almost a characteristic feature of the rock.
2. Excess pore water, except fluid inclusions (DIAMOND & MARSHALL, 1994), has been expelled long ago from the rock interstices by the combined effects of high overburden stress and tectonic compression. Consequently, overpressures that existed under such conditions have completely decayed long before underpressures were borne.
3. Horizontal compressional stress magnitude is either time invariant (for a given level of overburden) or, and this is more likely, decreased with time by virtue of the maintenance of octahedral stress (implying that horizontal stress will decrease as vertical stress decreases). Therefore, due to uplift and denudation, a given elementary volume of rock will experience a continuous decrease of the magnitude of octahedral stress.
4. Regional tectonic stress is described by the three components of the stress vector S_V, S_H and S_h. The relative magnitude is typically of the form $S_H > S_V > S_h$ in the Alps. It is thus likely, that in the direction of S_h, i.e. normal to the maximum compressive stress, expansion of the pore space occurs.

The first three hypotheses in combination represent the conceptual basis for this study. The fourth hypothesis was not tested in this study.

10.2.4 Scope and modelling approach

This Subsection presents the evaluation of the potential effects of denudation and erosion on the pore pressures in the marl-shale aquitard, under different boundary conditions, perameter values, horizontal stress distribution, and using an altemative material model. Because of the complexity of the processes and material laws, and also because long-term erosion scenarios are, compared to the more recent glaciations, afflicted with considerably more unknowns, the geological scenarios and the corresponding models are schematic and treated exclusively in 1D and 2D.

The identification of the key-processes and parameters are the prime goals. This is achieved by evaluating the relative contribution of denudation and differential erosion to the generation and maintenance of hydraulic underpressures. Therefore, the crucial question is not whether denudation and especially differential erosion may produce underpressures (this can be answered affirmatively), but it is to quantify the (potential) specific contribution of erosion to the generation of underpressures as compared to glacial rebound.

The investigation of erosion as an alternative to glacier rebound is reasonable on account of the following considerations:

a. Erosion is an irreversible mechanism that is not afflicted by reversals affecting the hydraulic pressure in the ground. For this reason, erosion is considered world-wide as the main driving force for underpressures, also in regions where glaciations did exist

b. On account of the difference in density between rock and ice, almost three times less rock as ice needs to be removed for the same reduction of overburden

c. Slopes are usually more unburdened after glacier melting (landslides, rockfalls) than valley floors, which best explains underpressures in the central part of the Wellenberg (underneath the Eggeligrat topographic saddle).

10.3 One-dimensional denudetion model

10.3.1 Scope

The geomechanical study was initiated by performing 1D scoping calculations in order to fulfil the following objectives:

1. Potential impact of long-lasting denudation on pore pressure at depth
2. Appropriate parameter ranges and combinations, essentially K and S_s as contributions to D, based on intrinsic rock properties (α, E; ν)
3. Role of top and bottom boundary conditions (1D-column). This encompasses the effect of a moving upper boundary as erosion proceeds and the influence on pore pressure of the lower boundary under both draining and non-draining conditions
4. Influence of different lateral stress magnitudes on pore pressures
5. Role of variable erosion rates with respect to constant rates
6. Preliminary estimate of the relevant time spans.

10.3.2 Model setup

The model domain is a 1D prismatic column with a fixed boundary at the bottom and lateral zero displacement boundaries. The vertical loading and drainage boundaries are varied while the horizontal stresses σ_h vary also but in a manner completely dependent on the

vertical stress through the choice of an appropriate Poisson ratio. As a consequence of the 1D setup, lateral (i.e. horizontal) strain is not permitted. This is referred to in the literature as "plane strain conditions" (flat deformation), as illustrated in Fig. 10.3-1a. Therefore σ_h is equal in all directions and is related to the Poisson ratio by the following equation:

$$(1)\ \sigma_h = \left(\frac{\nu}{1-\nu}\right) \cdot \sigma_v$$

This laterally constrained situation, without horizontal displacement, requires a Poisson ratio in the range $0.33 < \nu < 0.5$. This range is acceptable for most rocks since $\nu > 0.5$ characterises soft rocks (DOMENICO & SCHWARTZ, 1990).

Similarly, for plane stress conditions (no lateral stress) the following relationship prevails:

$$(2)\ \sigma_{h\ in\ plane\ of\ paper} = \nu * \sigma_v \ \text{ and } \ \sigma_{h\ in\ normal\ direction} = 0$$

whereby ν is constrained within the range: $0 < \nu < 0.5$.

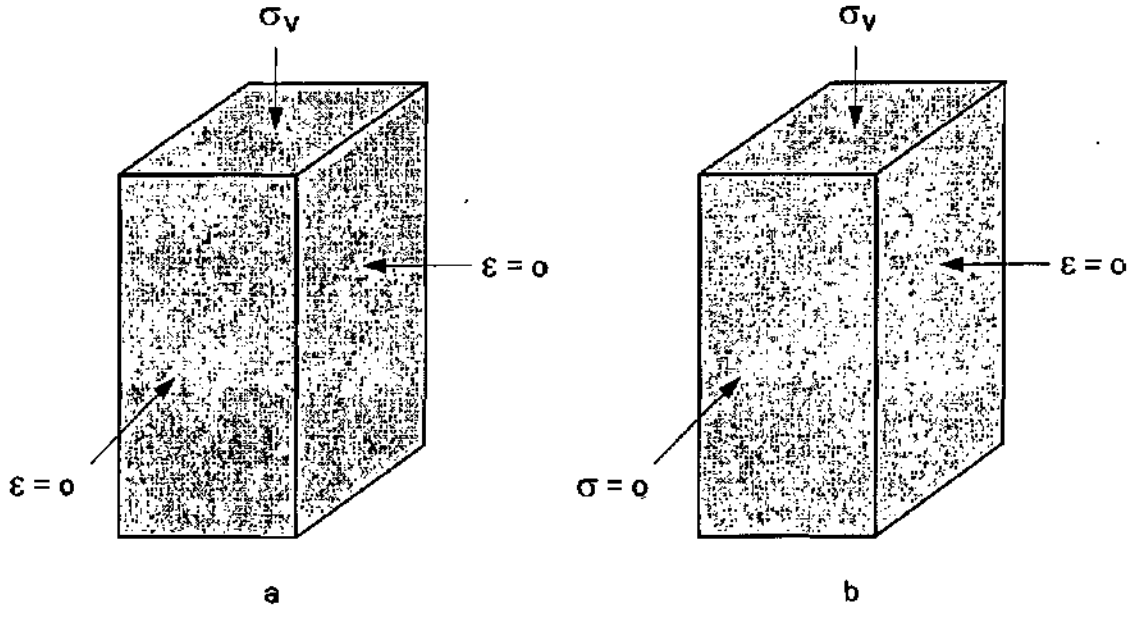

Fig. 10.3-1: Plane strain (a) and plane stress (b) conditions on a prism

Although horizontal stresses can be accounted for by means of the above equation, both vertical and horizontal stresses must equal 0 at the top boundary of the model domain. This situation is exemplified with the following sketch (Fig. 10.3-2) illustrating the stress distribution along a prismatic column undergoing step-by-step erosion.

This 0-stress condition near land surface is in most cases not very realistic, especially when tectonic stress plays a governing role (ZOBACK et al., 1989), and when the rock is overconsolidated like the marl-shale aquitard at Wellenberg. However, taking this limitation into account, 1D scoping calculation are best suited to test different sets of boundary conditions, various stress gradients with depth and different erosion rate scenarios. More sophisticated scenarios, based on the results of the 1D models, are treated in Section 10.4.

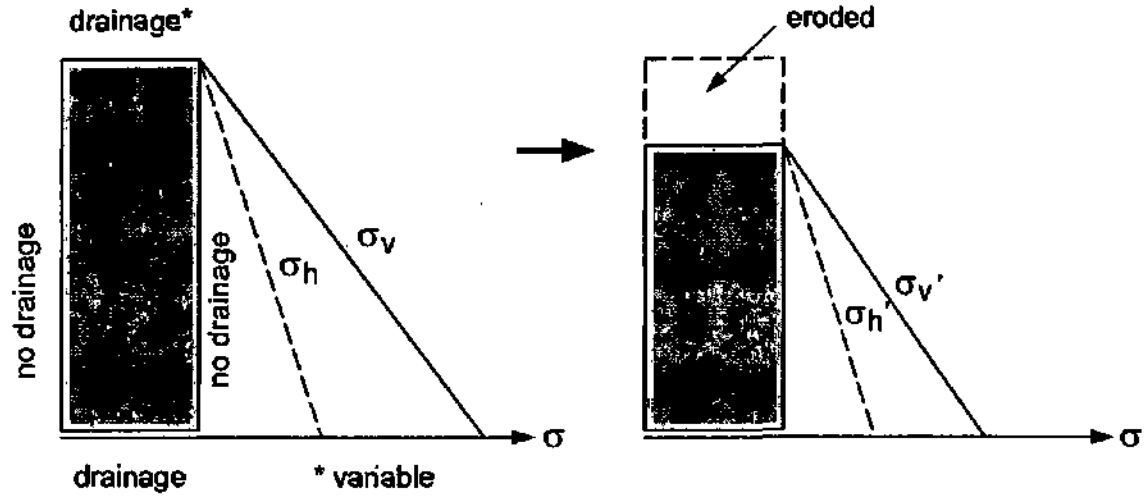

Fig. 10.3-2: Stress gradients along a one-dimensional prism of rock submitted to erosion

10.3.3 Abstraction scheme

Based on the current understanding of the geological evolution of the Central Alps, the following simplified abstraction scheme of the orogenic erosion, considered hereafter as a base case, is proposed: constant erosion rate of 0.4 mm/a over the lest 15 million years, resulting in the removal of 6'000 m of overburden from a column initially 7'000 m high. The constant erosion rate is approximated by 12 erosion steps of 500 m each, occuring every 1.25 million years.

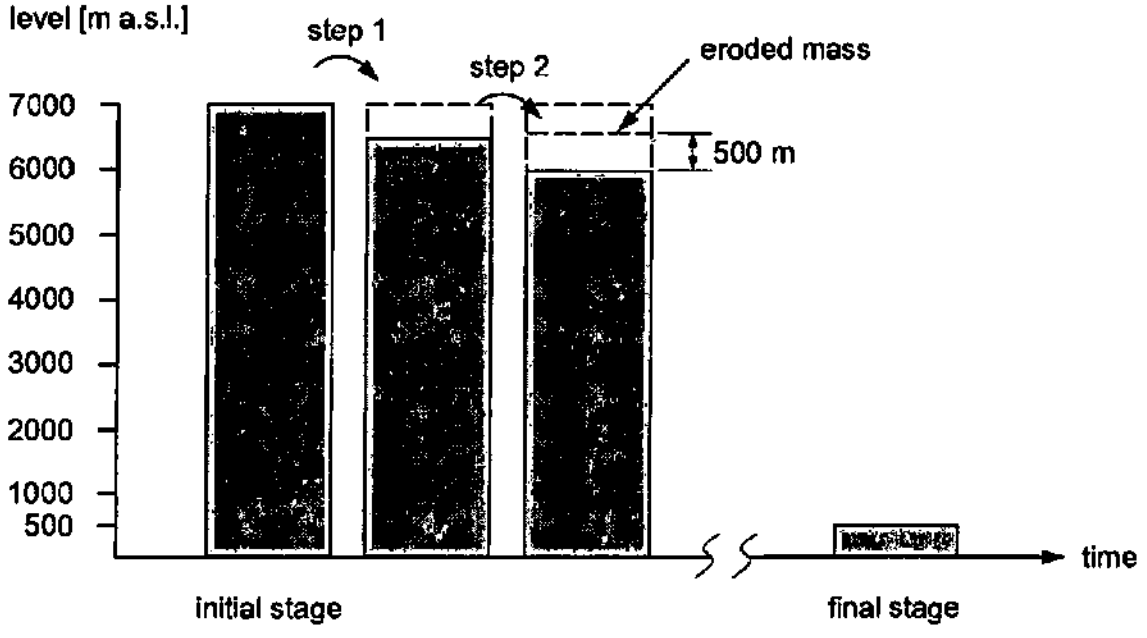

Fig. 10.3-3: Schematic orogenic evolution in the model domain under different boundary conditions

The vertical stress will depend on gravity only, while the mean horizontal stress $\sigma_h = (S_H + S_h)/2$ will be completely dependent on the vertical stress by assuming the above

mentioned plane strain conditions ($\varepsilon_H = \varepsilon_h = 0$). Accordingly, the Poisson ratio will be chosen in such a way that the relative stress rates from hydrofrac measurements can be reproduced satisfactorily. Hydrofrac measurements show that $S_H = 1.6 \cdot S_v$ and $S_h = 0.8 \cdot S_v$ in the upper 600 m of the present marl-shale aquitard and that this ratio changes at greater depth (NAGRA, 1997). This increase is disregarded here.

Two main cases are considered:

- Case 1 simulates the relation between vertical and minor horizontal stress, i.e. $\sigma_h = S_h$. From the stress distribution described above it follows that $S_h = 0.8\ S_v$, which results in a Poisson ratio $\nu = 0.44$ ($\nu = 0.8/1.8$)
- Case 2 investigates a situation in which the average horizontal stress is also considered. In this case $\sigma_h = (S_H + S_h)/2 = 1.2$, leading to an unrealistic Poisson ratio $\nu > 0.5$ (0.54). Consequently, the data has to be slightly adapted in order to allow for an acceptable Poisson ratio ($\nu = 0.49$), which leads to an almost hydrostatic case with: $\sigma_h = 0.96 \cdot \sigma_v$.

The 1D Scoping calculations ("model cases") comprise a variety of parameter variations, boundary conditions and erosion rates. Drainage is allowed through the upper boundary, whereas the lateral boundaries are impermeable. In most cases, the bottom boundary is set impermeable. The reason is that the depth of the bottom of the sediment column, especially at the early stages of orogenic erosion, is probably not suited for groundwater flow towards a discharge area. However, and in order to test the role of bottom drainage also, two model cases include either top and bottom drainage over the simulated duration, or - more realistically - bottom drainage only during the two last erosion steps. Fig. 10.3-3 illustrates the various boundary conditions, while the values attributed to the relevant parameters are listed in Tab. 10.3-1. These parameters fit into the measured ranges.

Tab. 10.3-1: Parameters used in the one-dimensional scoping calculations

Parameter		Base case	Variation range
E (Young's modulus)	[GPa]	15	1,5 - 150
K (hydraulic conductivity)	[m s^{-1}]	10^{-13}	10^{-12} - 10^{-14}
ρ (specific weight)	[MNm^{-3}]	0.0265	—
γ (buoyant unit weight)	[MNm^{-3}]	0.015	—
Erosion rate	[mm/a]	0.4	0.4 - 0.6

Note that the effect of decreasing K or decreasing E leads to the same result (see also Fig. 10.3.4), since:

$$c_v = \frac{K}{\gamma_w} \cdot \frac{E(1-\nu)}{(1+\nu)\cdot(1-2\nu)}$$

Tab. 10.3-2 summarises nomenclature and specifications of the different model cases performed as part of the 1D scoping calculations.

Tab. 10.3-2: 1D prismatic denudation model: Model cases (variations)

Title	Description	Parameter set	Ref.
Parameter variation K	top drainage only	K: $1{\cdot}10^{-12}$, $1{\cdot}10^{-13}$, $5\,10^{-14}$, $1{\cdot}10^{-14}$ m/s E: 15 GPa	Fig. 10.3-4
Parameter variation E	top drainage only	K: $1{\cdot}10^{-13}$ m/s E: 1.5, 15, 150 GPa	Fig. 10.3-4
Different boundary conditions	top only and top + bottom drainage	K: $1{\cdot}10^{-13}$ m/s E: 15 GPa	Fig. 10.3-5
Increasing erosion rates	top drainage only 0.4 mm/a from 0 to 5000 m 0.5 mm/a from 5000 to 5500 m 0.6 mm/a from 5500 to 6000 m	K: $1{\cdot}10^{-13}$ m/s E: 15 GPa	Fig. 10.3-6

10.3.4 Results and discussion

10.3.4.1 Parameter variation of K and E

To visualise the different model calculations, most plots represent two erosion steps: 500 m removal (end of first erosion step after 1.25 million years) and 6'000 m removal (end of ultimate erosion step after 15 million years), which corresponds to today's conditions.

Fig. 10.3-4 illustrates clearly the strong influence of D (through K and E). Under the prescribed conditions, and with all other parameters remaining unchanged, underpressures develop if K is of the order of $K = 1{\cdot}10^{-14}$ m/s (or if $K = 1{\cdot}10^{-13}$ m/s with a higher rock compressibility of the order of E = 1.5 GPa). This very-low K-value is between half a magnitude and one magnitude lower than the lowest values computed by the K-model (Sect. 9.5). Similarly, reducing E to 1.5 GPa is not very realistic. However, shifting slightly both K and E values to reduce the diffusivity ratio, allows generation of underpressures over that long time range and assuming a rather low erosion rate.

The physical meaning of the negative pore pressures that develop in Figs. 10.3-4b and 10.3-4d should not be misunderstood. These values are artefacts since, strictly speaking, ABAQUS cannot handle suction pressure properly. The code considers negative pore pressures as the result of a continuous air phase in equilibrium with atmospheric pressure, as it is commonly the case in the vadose zone. In the actual case - even though negative pore pressures are theoretically possible (NEUZIL & POLLOCK, 1983) - this cannot be deduced from these erroneous results.

10.3.4.2 Changing boundary conditions

The most significant change, as expected from analytical results using Terzaghi's equation, is the onset of drainage at both extremities of the sediment column. Under both, top and bottom drainage, underpressures still develop within the aquitard using the parameter combination $K = 1{\cdot}10^{-14}$ m/s and E = 15 GPa, but the absolute magnitude and the shape of the pressure profile vary considerably. The top and bottom drainage case produces a more realistic pressure distribution than the top drainage case. Moreover, only the last stages are relevant for the currently observed underpressures. Whatever large underpressures may have been in the remote past, most of it decayed long before today. This statement is

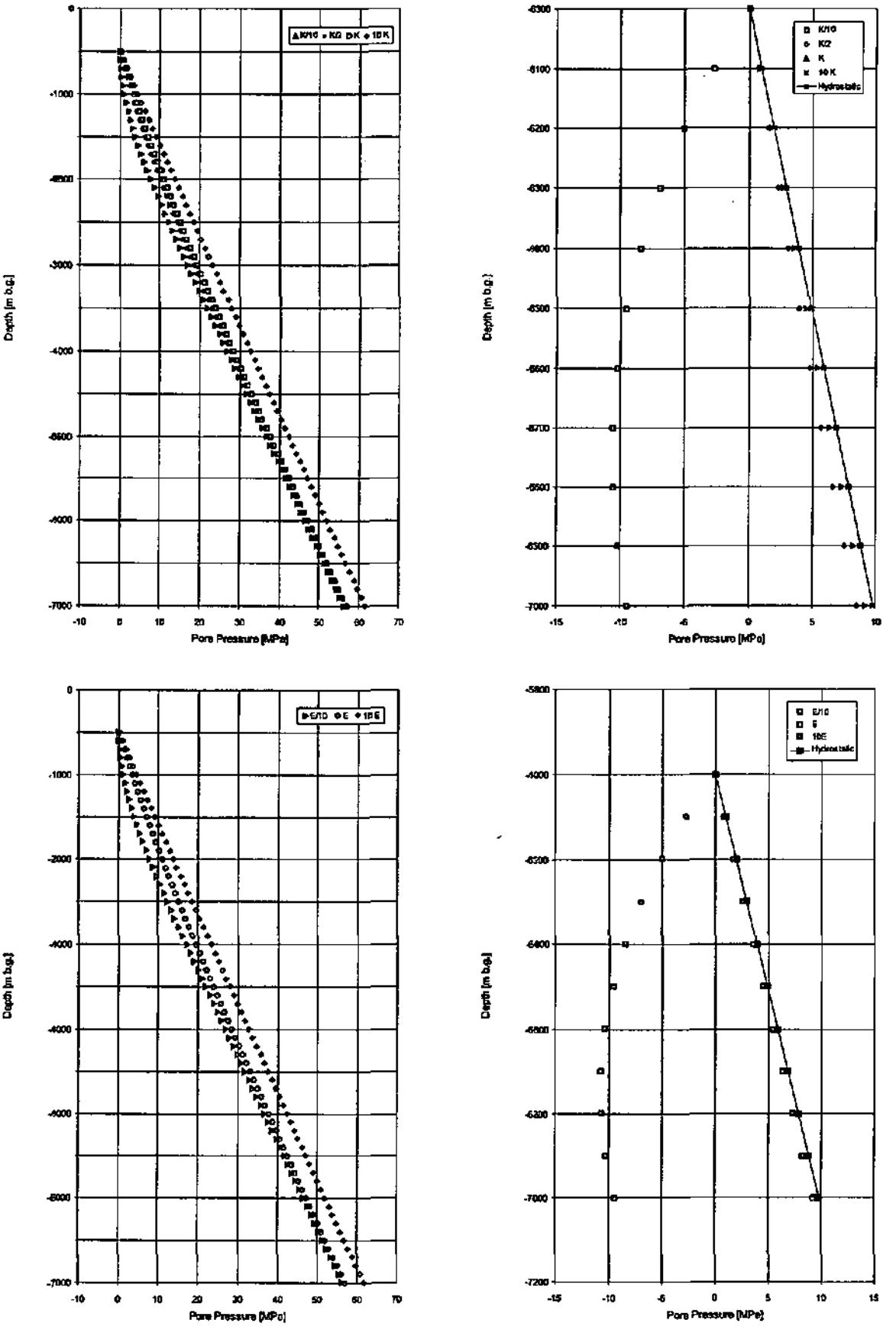

Fig. 10.3-4: Sensitivity on parameter variation of K (above) and E (below)

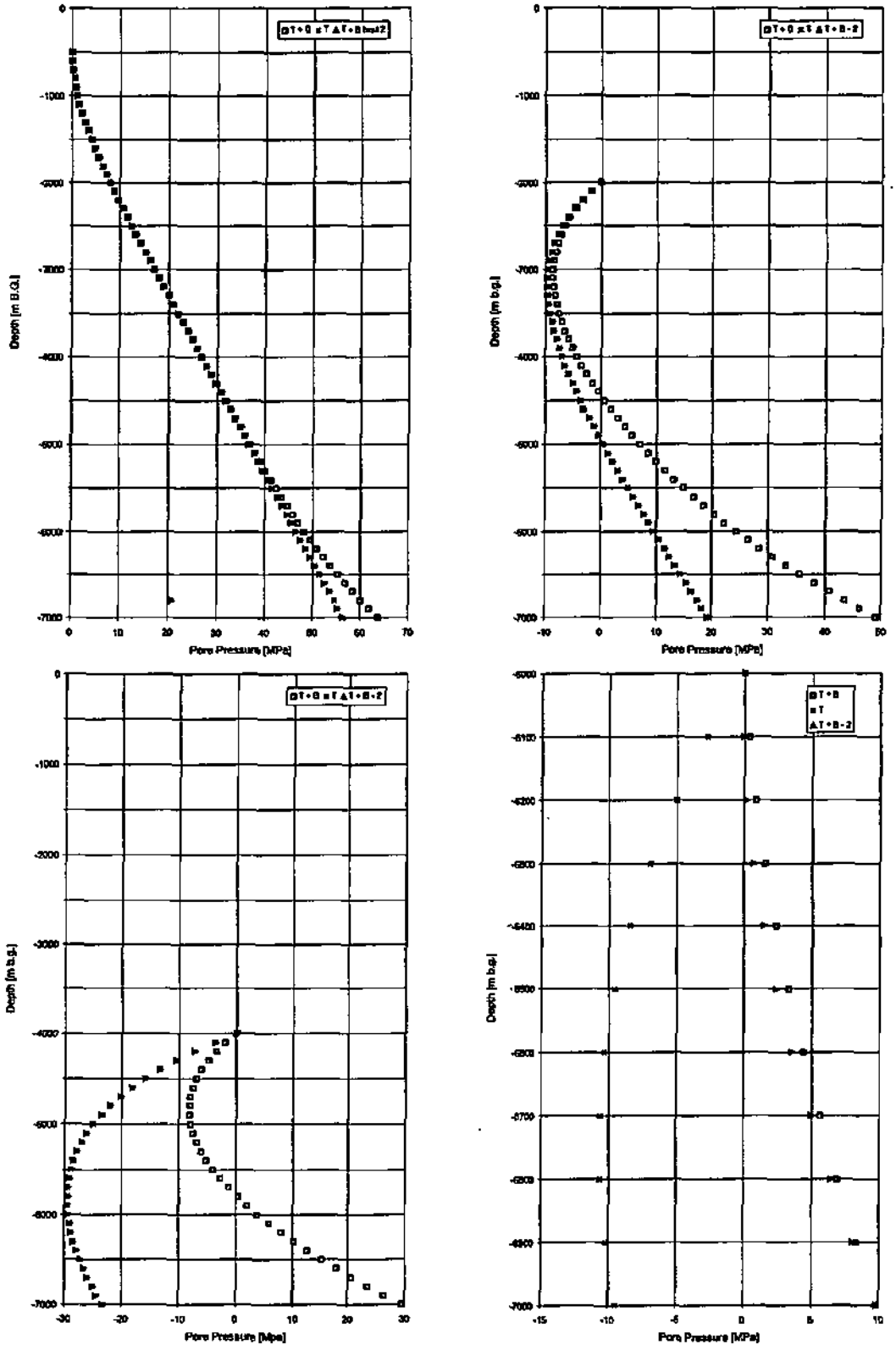

Fig. 10.3-5: Sensitivity on boundary conditions

On the bottom of the figure, the picture on the right hand-side depicts the situation after 10 Ma (4'000 m of erosion) and today. The lettera "T + B" refer to top and bottom drainage, "T" to top drainage and "T + B - 2" to top and bottom drainage over the last two erosion steps.

based on Fig. 10.3-5 where on top the pore pressures after 500 m erosion and after 2000 m erosion are shown respectively.

Comparison of two types of situation, a situation in which bottom drainage occurs over the entire erosion period and another one in which bottom drainage is possible during the two last erosion steps only, shows that the resulting pore pressures are absolutely indistinguishable.

10.3.4.3 Increasing erosion rates

Quaternary studies of the alpine region tend to demonstrate that erosion became gradually more active in favour of the ice ages having occurred in the last million years (SCHLÜCHTER & MÜLLER-DICK, 1996). As shown in Fig. 10.3-6, the increase in erosion rate (from 0.4 mm/a to 0.6 mm/a) does not significantly affect pore pressures. Although this model case was computed with the a K-value of $1 \cdot 10^{-13}$ m/s, the conclusion is readily extensible to lower diffusivity values (i.e. K = $1 \cdot 10^{-14}$ m/s). However, it must be emphasised that the parameter variation tested here is restricted to a narrow band, compared to the one of model scenario Q3 (Sect. 9.7) and of Section 10.5.

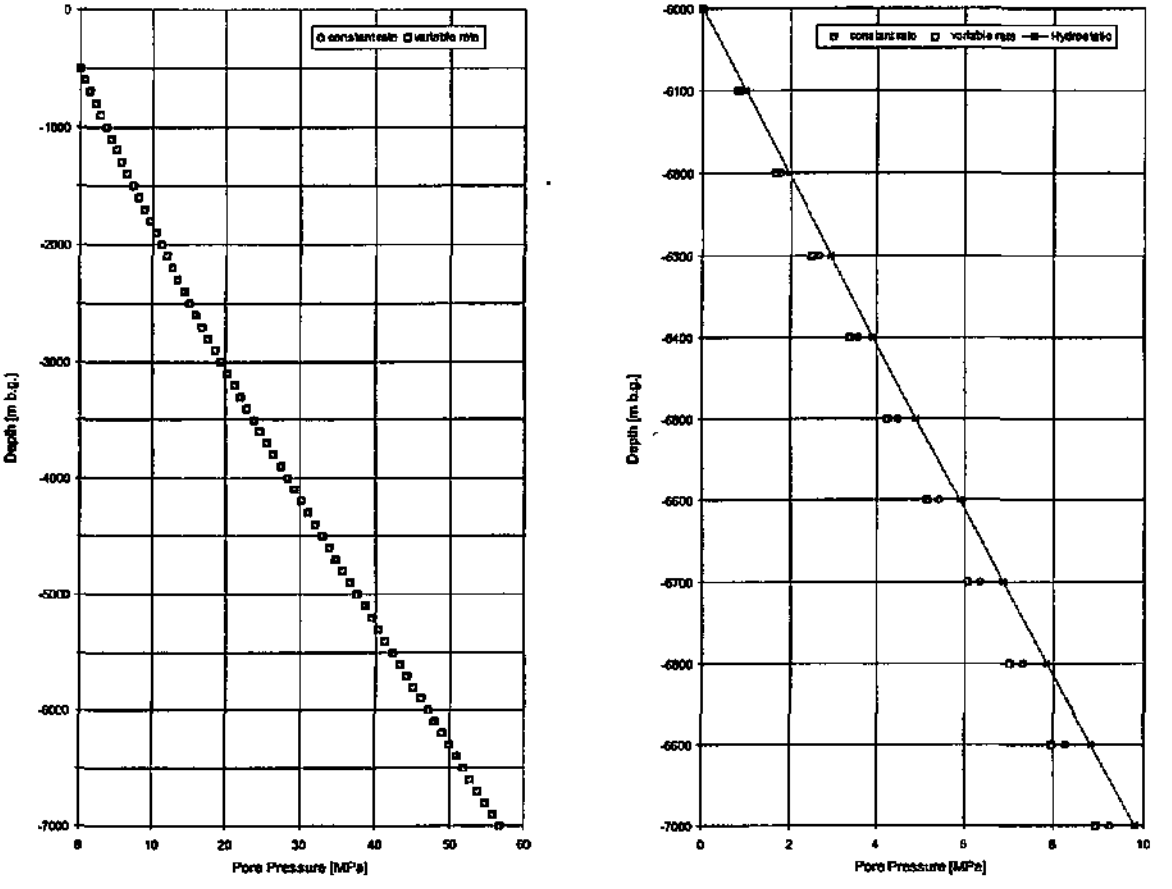

Fig. 10.3.-6: Sensitivity on increasing erosion rates

Main conclusions

1. Underpressures can result from denudation occuring over millions of years
2. The mechanisms initiating and maintaining disequilibrium pressures are very robust and

depend essentially on the parameters dictating the diffusivity of the aquitard

3. The time frame necessary to describe the phenomenon can be restricted to the last 2 to 3 million years at most. Whatever strong underpressures may have been in more ancient periods, most parts of the rock that exhibited strong abnormal pressure have been removed since then or have lost ideal rock properties. Today's pressure conditions are predominantly driven by the most recent forcing based on the rock characteristics and the boundary conditions of a comparatively recent past.

10.4 Two-dimensional denudation model

By virtue of adding a second dimension to the prism used for analysis in the 1D case, additional effects, especially different cases of lateral stress, can be investigated. While in the 1D case, horizontal stress was a function of the Poisson ratio, in the 2D prismatic model, horizontal strasses can virtually be set as desired. More specifically, horizontal stress need not to fulfil the criterion $\sigma_h = 0$ on ground surface.

10.4.1 Scope

The essential improvement with respect to the 1D approach resides in the possibility of testing variable horizontal stress conditions and alternative material models. The full set of questions that can be addressed by the schematic 2D model scenarios are summarised below:

- variable horizontal stress distributions with depth
- lateral drainage boundaries
- alternative (i.e. inelastic) material behaviour

For this model scenario, the way to simulate denudation is essentially the same than for the 1D analysis. 6'000 m rock will be eroded in 15 Ma, from an initially 7'000 m thick sediment pile by 500 m-erosion steps, lasting 1.25 Ma each.

10.4.2 Abstraction schemes

Conceptually, three distinct cases of applied horizontal stress are considered as schematised in Fig. 10.4-1. Cases 1 and 2 are conceptually unlikely, and are addressed merely in order to allow for comparison with the more likely case 3, as well as with the 1D model results. Changes in pore pressures, if all other conditions remain unchanged, are related to changes in octahedral stress. In 2D space, the variation in octahedral stress is of the form:

$$\Delta\sigma_{oct.} \sim \Delta\sigma_h + \Delta\sigma_v$$

which implies constant stress normal to the plane of paper. As a consequence, cases 1 and 2 do not experience any change in horizontal stress, and hence the computed pore pressure changes will be identical for both cases (pore pressures will only be related to change in overburden stress). Therefore, the simulation of case 1 was abandoned after the first modelling step. Although unrealistic, cases 1 and/or 2 provide a bounding case. The only "realistic" aspect of case 2 is that it is able to account for non-zero horizontal stress near the surface of the model domain.

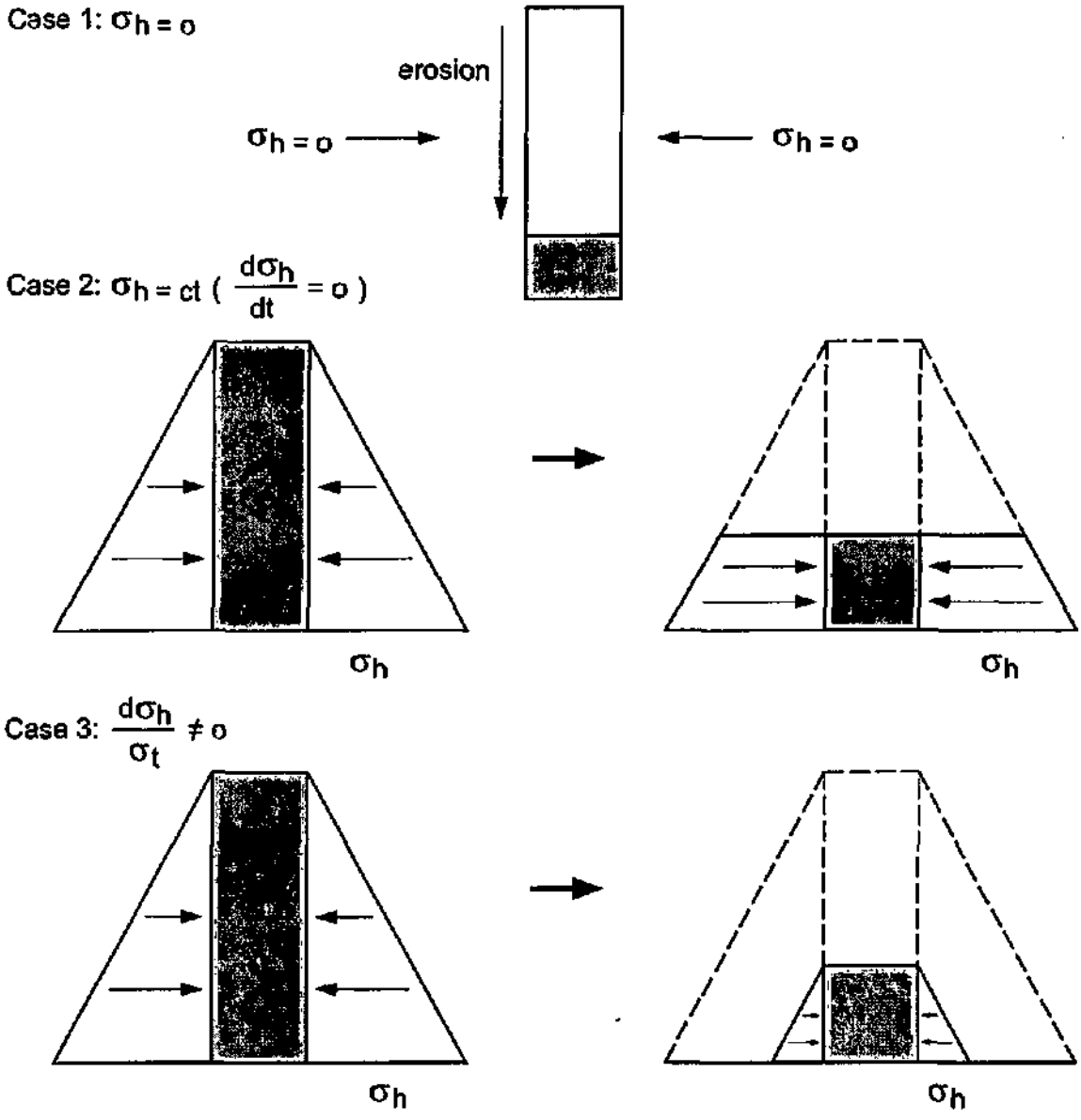

Fig. 10.4-1: Three different cases of applied horizontal stress

Case 3 simulates a situation in which a decrease in vertical stress is echoed by a proportional reduction in horizontal stress, and consequently in octahedral stresses and pore pressures. This case represents intuitively what is expected when sediment accumulations are uplifted and unburdened, otherwise - i.e. if horizontal stress would remain constant, as in Case 2 above, rock failure is likely to develop, leading to an increase in permeability, and therefore to a more rapid dissipation of abnormal pressure.

The actual modelling work was performed in three main steps as shown in Tab. 10.4-1 which summarises the different model cases simulated by means of the 2D prismatic denudation model. Tab. 10.4-1 also shows the relationship between the figures and model cases.

Tab. 10.4-1: Two-dimensional prismatic denudation model: model cases

Title	Parameter variation		
	Step 1	Step 2	Step 3
Case 1 ($\sigma_h = 0$)	Linear-elastic Fig. 10.4-2 - Fig. 10.4-5	—	—
Case 2 (σ_h = ct.)	Linear-elastic Fig. 10.4-2 - Fig. 10.4-5	Cam-Clay Fig. 10.4-6	K-sensitivity Fig. 10.4-5 & Fig. 10.4-7
Case 3 ($d\sigma_h / dt \neq 0$)	Linear-elastic Fig. 10.4-2 - Fig. 10.4-5	Cam-Clay Fig. 10.4-6	K-sensitivity

10.4.3 Results and discussion

10.4.3.1 Step 1 model scenarios

Fig. 10.4-2 (after last erosion step) illustrates the effects of different lateral stress conditions using the base case parameters ($K = 1 \cdot 10^{-13}$ m/s, E: 15 GPa) and using a reduced K-value of $K = 1 \cdot 10^{-14}$ m/s. The results confirm the theoretical considerations made in the previous Section, namely that cases 1 and 2 are indistinguishable with respect to their effects on pore pressures and that, as expected, these cases represent an extreme situation, since even the comparable 1D case produces slightly lower pore pressures. Furthermore, the simulations show the governing role of K and E with respect to any other model attribute (boundary condition, dependency of horizontal stress, etc.). The upper right picture of Fig. 10.4-2 represents an intermediate situation after removal of 4'000 m of overburden. Interestingly, at this stage, case 3 develops slightly less underpressuring than the comparable 1D model case. This situation is reversed at the end of the last erosion step. The reason for this behaviour is probably the proportionality of σ_h: for low overburden stress, the computed horizontal stress in the 2D case is larger than in the 1D counterpart.

Lateral stress reduction plays also a role in enhancing underpressure. Evidently, if pore space can expand both in vertical and horizontal direction, as a consequence of rebound, the magnitude of pore pressure decrease is enhanced. This statement, associated with the fact that zero-horizontal stress and constant horizontal stress produce identical pore pressures, i.e. change in horizontal stress and not absolute magnitude is important, contributes to explain why underpressures could develop at Wellenberg although strong lateral compression prevails (see also Fig. 10.4-4).

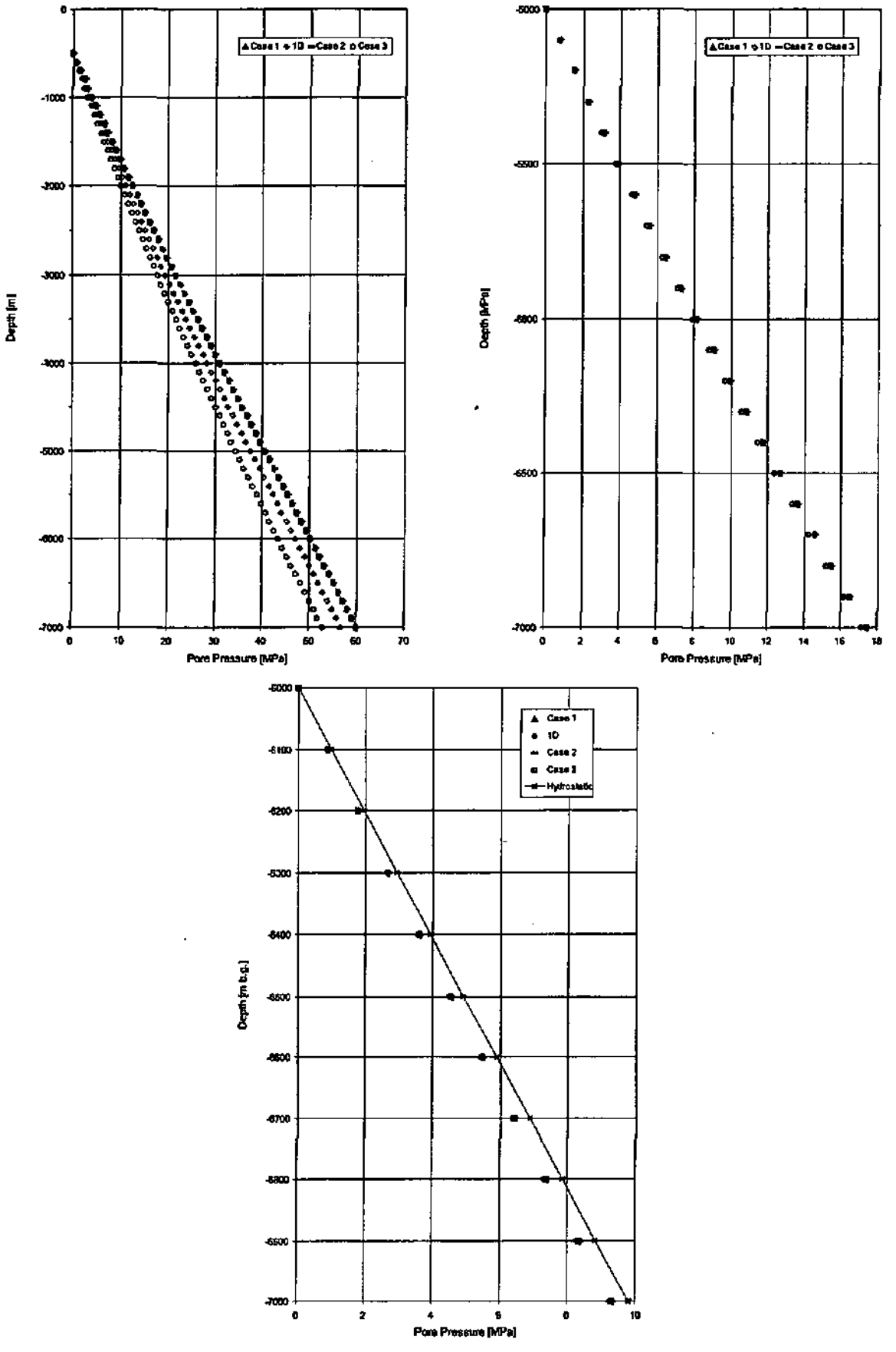

Fig. 10.4-2: Sensitivity on different lateral stress conditions

10.4.3.2 Step 2 model scenarios

The parameter variations performed in step 2 are based essentially on the same sequence as step 1, with further variations of K and E and assuming top and bottom drainage over the entire denudation period. As in the similar 1D case, reducing E by a factor of 10, i.e. softening the rock, leads to enhancing underpressures in the same way then reducing K by the same amount. This trend prevails for whatever lateral strass condition is imposed and is strongest for case 3. Fig. 10.4-3, left, presents the pore pressure profiles after the first erosion step (500 m removal) for all three cases. The right part of Fig. 10.4-3 shows the same three cases for today and provides comparison between pore pressure profiles for top drainage and for top and bottom drainage.

As for the 1D case, applying drainage at the bottom of the aquitard prism results in a dramatic reduction of the magnitude of underpressuring as compared to the top-drainage situation. The comparison between both drainage situations illustrates clearly the strong effect on pore pressures due solely to changing one boundary condition. However, the magnitude is still in the order of 2 to 3 MPa. An order of magnitude which is comparable to the current pressure deficit at Wellenberg. Additionally, the comparison shows once more that case 3 lateral strass condition will always result in the strongest pora prassure reduction as compared to cases 1 and/or 2.

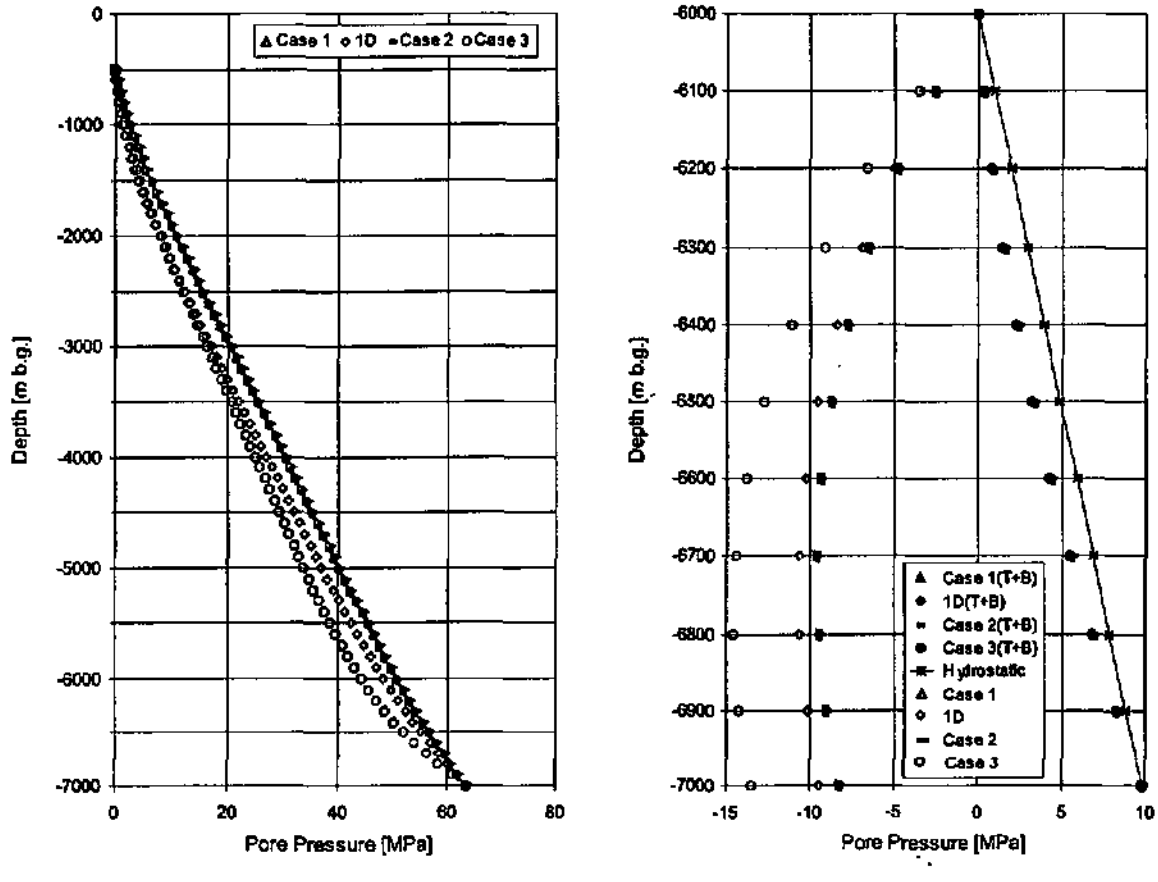

Fig. 10.4-3: Sensitivity on different drainage conditions

Fig. 10.4-4 compares the different lateral stress cases for the top drainage condition and for a very low K-value of $1 \cdot 10^{-14}$ m/s. The left hand-side picture presents the first two erosion steps (labelled "I" and "II" in the legend). The right hand-side picture illustrates the

simulated pore pressures for today and shows clearly that decreasing the lateral stress while removing overburden contributes to enhancing underpressures.

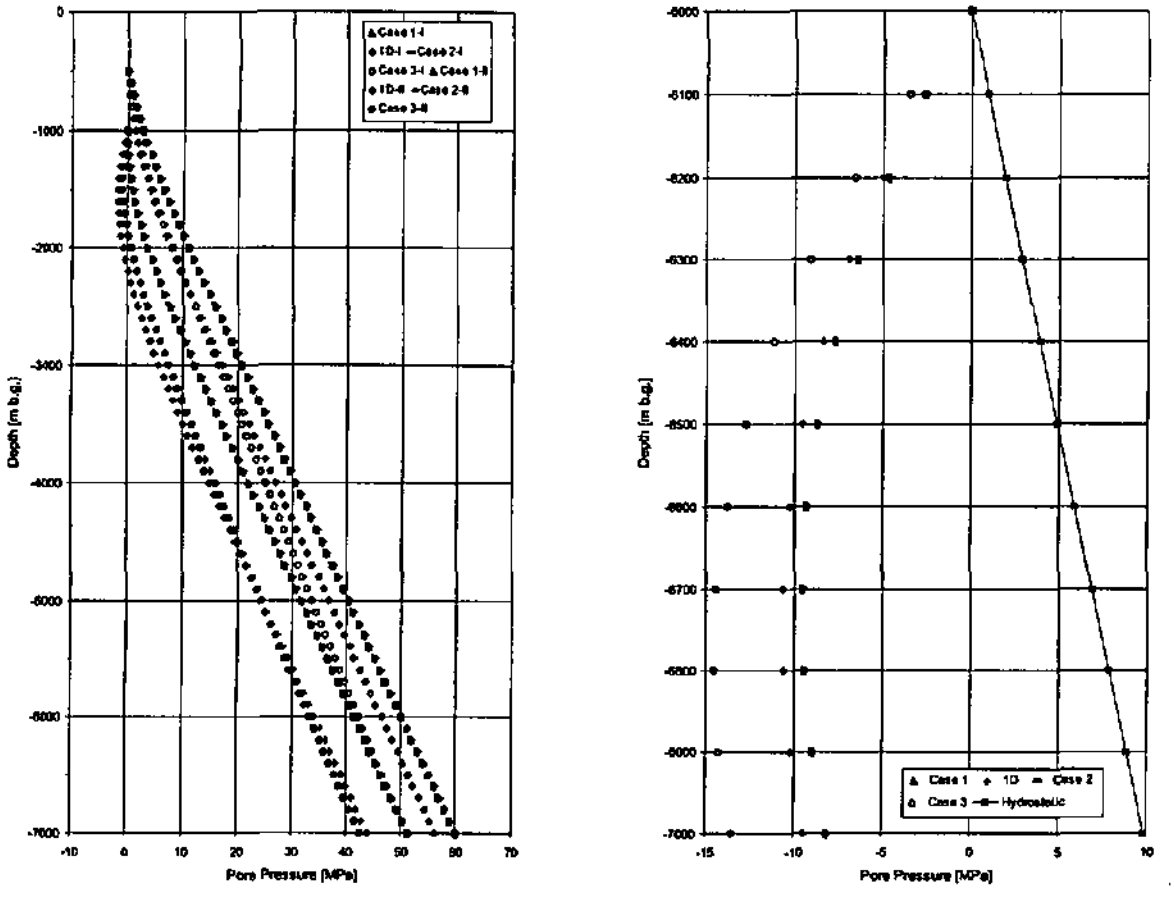

Fig. 10.4-4: Sensitivity on different lateral stress conditions for very-low hydraulic conductivity

In Fig. 10.4-5, the effects on pore pressures of changing K within an order of magnitude is presented. Although the magnitude of underpressures (in the range of absolute negative pore pressures) is stronger for case 3 (bottom) than for case 2 (top), both cases reveal the strong influence on K. Clearly, a K-value of $1 \cdot 10^{-14}$ m/s is a bounding value.

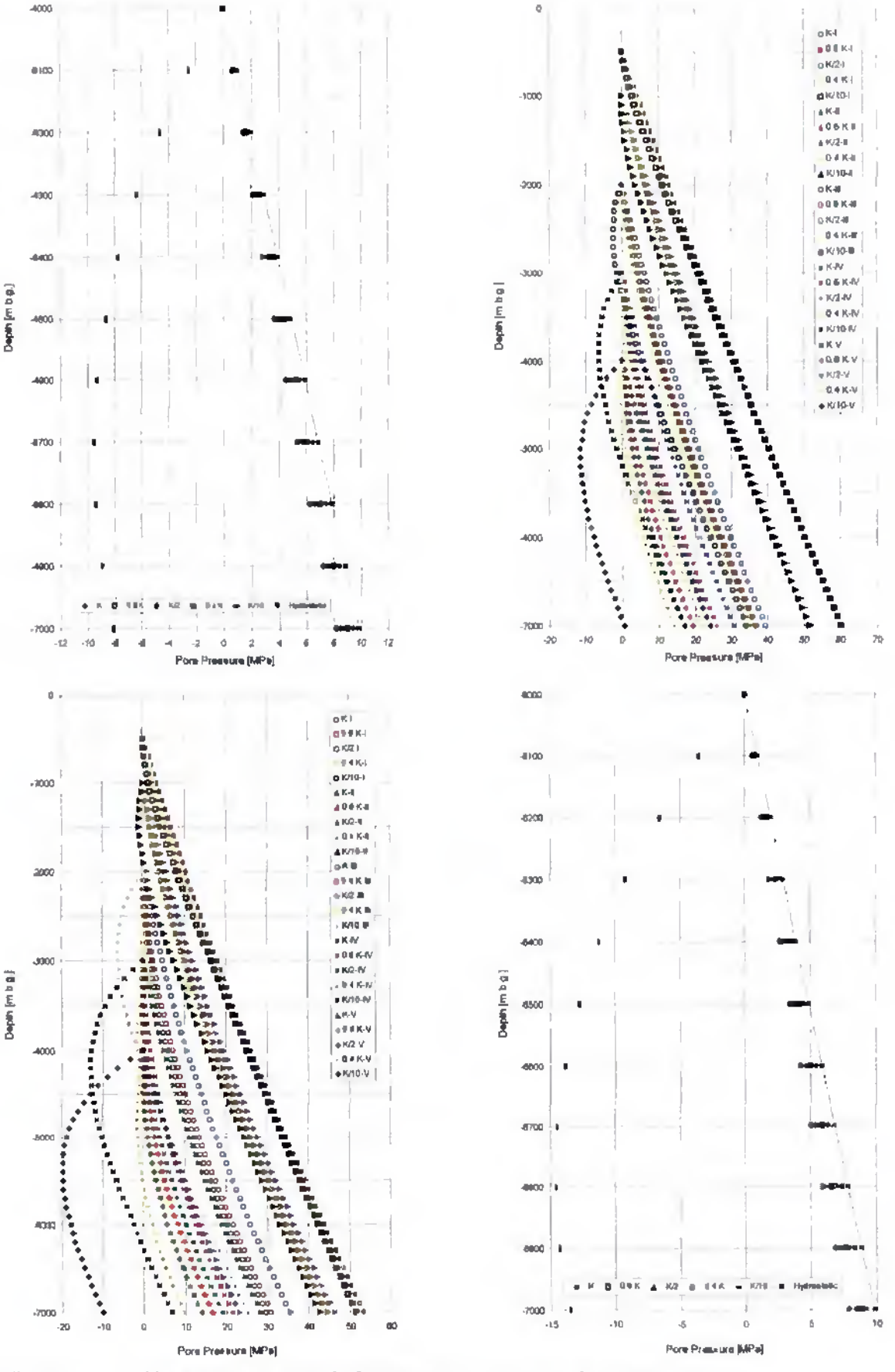

Fig. 10.4-5: K-sensitivity analysis for cases 2 and 3 (elastic material)

10.4.3.3 Step 3 model scenarios

In this step, the Cam-clay model, is used and compared to the linear-elastic material applied in previous calculations. The Cam-clay model is an elasto-plastic model for clay-type materials. This material is a bounding case for the marl-shale aquitard since it considers plasticity, and is useful since it provides an estimate of what effects on pore pressures long-term plastic deformation may have.

The material plastic compressibility C_c replaces E in the former simulations. In the first set of simulations, C_c = 0.00921 corresponds to the Opalinus shale (ARISTORENAS, 1992; aELLWALD, 1990). In a second step, the plastic compressibility was increased 20 times, i.e. C_c = 0.1842. This increase results in a strong decrease of the pore pressures and is comparable in effect to a reduction in E. The 2D model with a highly compressible material produces lower magnitudes of underpressures than the 1D counterpart and this even when compared to the 1D elastic case. This situation is illustrated by Fig. 10.4-6 which shows the pore pressure profiles for the two lateral stress cases and for the elastic and plastic 1D counterparts (with K = $1 \cdot 10^{-14}$ m/s).

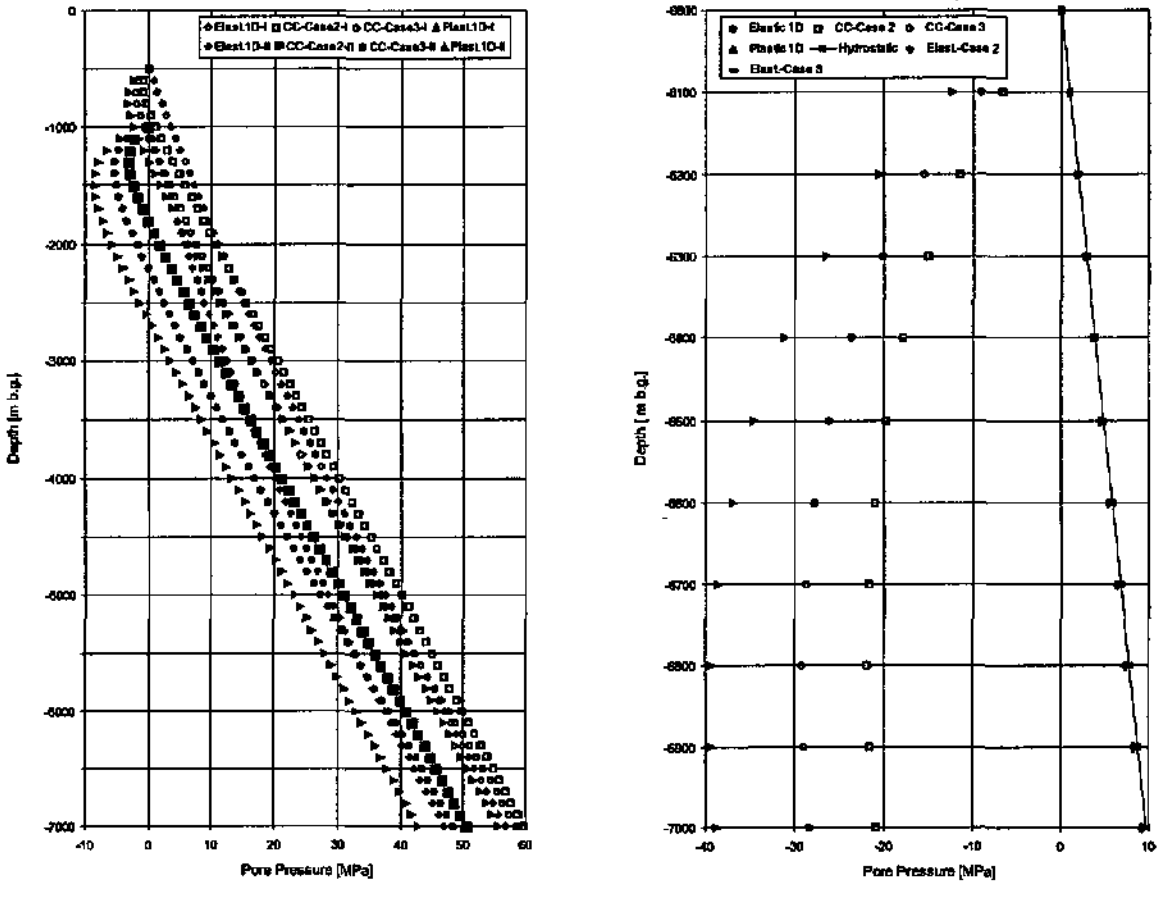

Fig. 10.4-6: Comparison between elastic and plastic materials in 1D and 2D

In the last step, K was reduced from the base case value, K = $1 \cdot 10^{-13}$ m/s, to K = $1 \cdot 10^{-14}$ while maintaining the plastic compressibility at the same value as in the previous case (C_c = 0.00921). As expected, the largest effect of this parameter variation can be attributed to the lower hydraulic conductivity, the enhancement of the underpressures provoked by the plastic behaviour (with respect to elastic) playing only a minor role (Fig. 10.4-7).

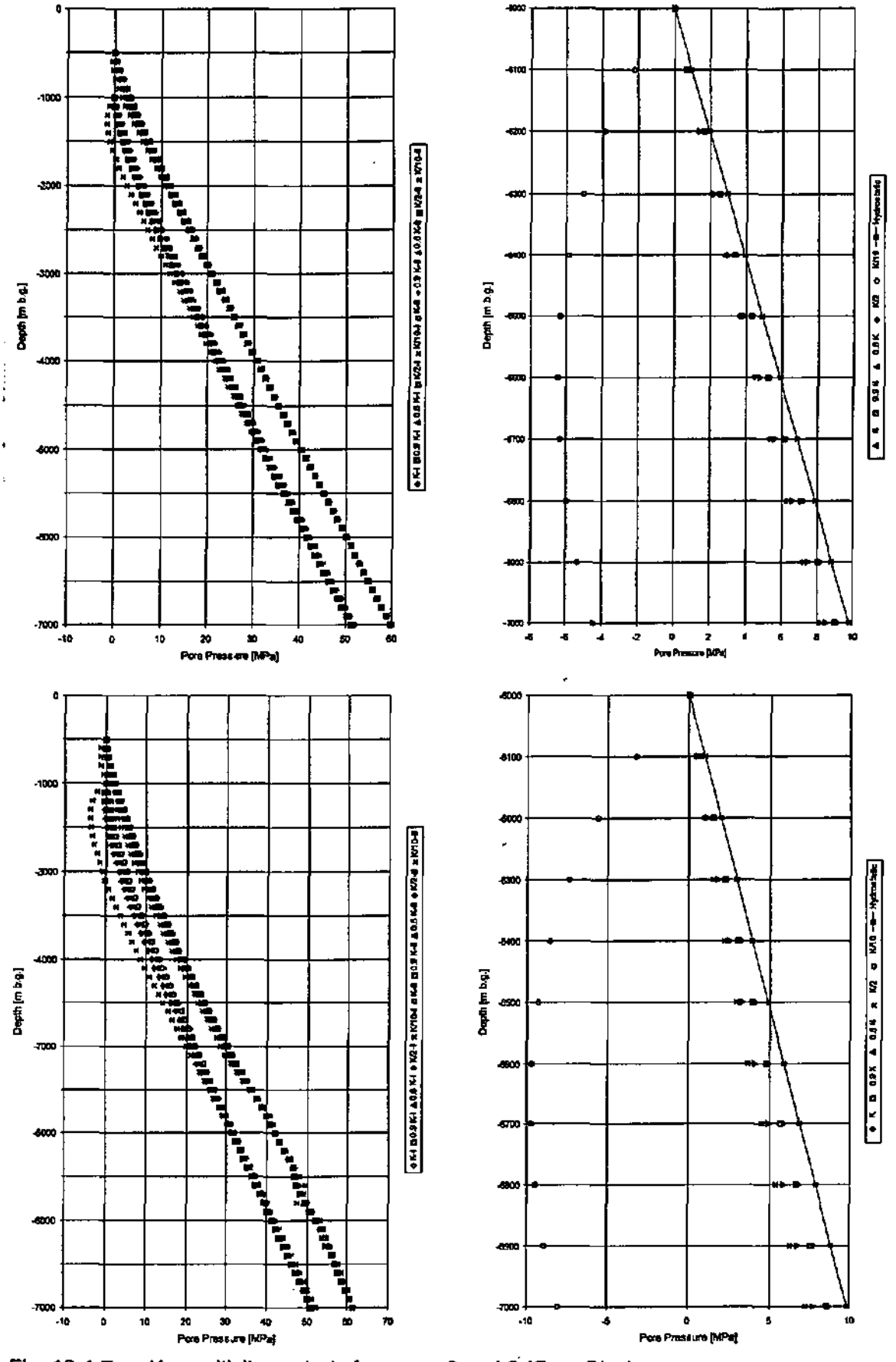

Fig. 10.4-7: K-sensitivity analysis for cases 2 and 3 (Cam Clay)

The goal for the K-sensitivity analysis shown in Figs. 10.4-5 and 10.4-7 is to define parameter combinations for which the computed pore pressures remain positive (i.e. do not extend into the range of absolute negative values). As mentioned before, suction pressures, as computed by ABAQUS, are unrealistic and have the disadvantage of biasing the pore pressure evolution over the different erosion steps. The simulations are performed under the assumption of an impervious lower model boundary, since bottom drainage hardly produces negative pore pressures.

Analysed were cases 2 and 3 using the elastic and Cam-clay models. The model scenario was simulated with the range $1 \cdot 10^{-13}$ m/s ≥ K ≥ 10^{-14} m/s. The results show that acceptable pore pressures slightly below and above absolute zero can be obtained with K-values in this range. Inspection of the model results leads to the following rule of thumb: The contribution of lateral unloading compensates to a certain degree "high" hydraulic conductivity (i.e. case 3 vs. case 2). This observation applies to both elastic and plastic materials, with emphasis on the latter one, where $0.9 \cdot 10^{-13}$ ≥ K ≥$1 \cdot 10^{-13}$ m/s are sufficiently low to produce significant underpressuring.

10.4.4 Summary and conclusions

Considering changes in horizontal stress during the erosion process is interesting and useful, not so much because lateral stress release contributes significantly to the generation of subnormal hydraulic pressure (in fact, the effect is limited), but essentially because it helps to gain further understanding of the mechanisms occurring during erosion. Conceptually, it is a point of utmost importance that *it is not the departing absolute horizontal stress, but the stress change that is significant.* Hence, a compressional stress-field - as long as it is not increasing - does not necessarily constitute an obstacle for the development of underpressures. On the contrary, by virtue of the octahedral stress principle, a diminution of compression in the marl-shale aquitard can be postulated as a function of erosional removal of overburden (case 3).

Tectonic compression is a hallmark of the Alps for more than 20 million years, and existed long before currently observed underpressures were generated. Tectonic stress magnitude and evolution can thus be considered - at worst - as a constant boundary condition for the time-scale associated with hydraulic pressure, and - at best - as a contribution to the generation and maintenance of subnormal pressures.

10.5 Differential erosion model scenarios

10.5.1 Introduction

This phase consists of more "realistic" 2D simulations of the orogenic erosion, especially with respect to differential erosion, i.e. accentuation of the relief between valley talwegs and valley flanks and ridges.

The previous modelling phases show clearly that early denudation - for whatever level of erosion rate - does not noticeably impact on the present-day pore pressure state, the time-constants being far too long. Therefore, emphasis is put on processes having most likely noticeable influence on today's pore pressures. Phase 3 abstraction scheme has been worked out after careful review of the specialised literature on both the processes (Sect. 7.4) and the typical geological evolution of the Central Alps. Note also that with respect to erosion steps, the abstraction scheme described below is fully compatible with the 3D Quaternary evolution abstraction scheme (Sects. 9.6 and 9.7).

10.5.2 Abstraction schema

10.5.2.1 General aspects

The geometry and contours of the model domain correspond schematically to the geological cross-section Q - Q'. Fig. 10.5-1 represents the current topographic relief and six topographic profiles corresponding each to a given erosion stage as specified in Tabs. 10.5-1 and 10.5-2. The time interval between two adjacent topographic profiles is in the order of some tenthousand years. The choice of the southwest - northeast orientation of the vertical 2D model section results from a compromise between the north - south orientation of the maximal horizontal stress and a section in which most of the extension of the aquitard is represented.

10.5.2.2 Evolution of the model geometry and boundaries

Fig. 10.5-1 depicts the evolution of the 2D model domain from the first to the last erosion step. Fig. 10.5-2 shows the corresponding FE mesh comprised of eight-noded quadratic elements. Note the progressive development of valleys and hillsides. The abstraction scheme comprises four different model scenarios, which were all derived from this basic evolution scheme and differ only in the treatment of glaciations and time-dependent boundary conditions.

The geological events, as well as the key parameters of the four model scenarios, are presented in Tab. 10.5-1. As initial condition, it is assumed that 13.5 million years previously, the marl-shale rock was overlain by approximately 6'500 m of overburden. During the first 7.5 million years, the upper 3'000 m were removed at a constant rate of 0.4 mm/a, resulting in an almost flat topography.

The conceptual model postulates that differential erosion became important only with the onset of the Quaternary ice ages, starting with the largest glaciation (in the new terminology after SCHLÜCHTER & MÜLLER-DICK, 1996) approx. 780'000 years ago (Tab. 10.5-1, Fig. 10.5-1). From then on, the erosion rates, principally driven by the progressive excavation of valleys, increased locally up to more than one or two orders of magnitude the 0.4 mm/a-denudation rate.

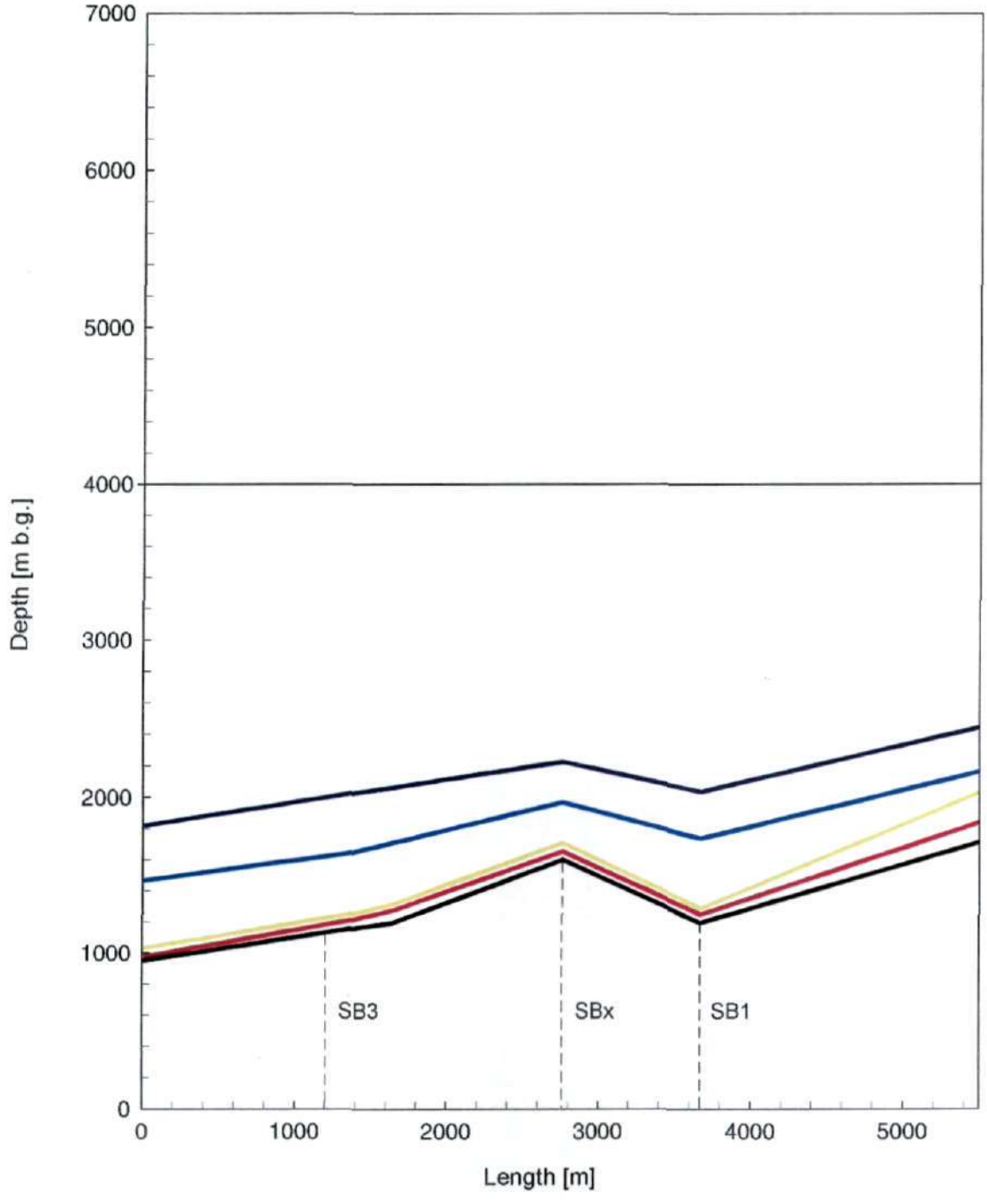

Fig. 10.5-1: Erosion stages in schematic cross-section Q - Q'

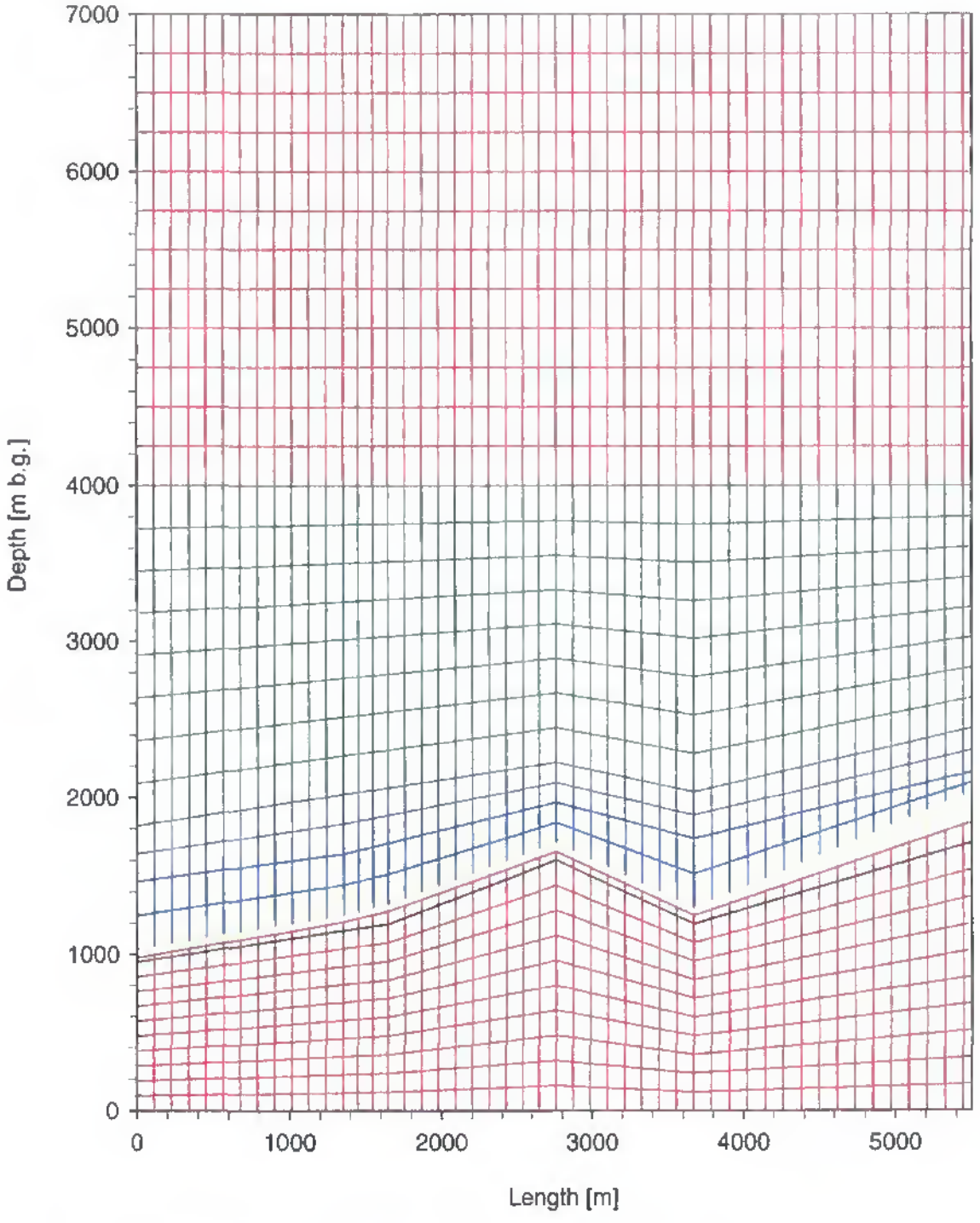

Fig. 10.5-2: Evolution of the Finite Element mesh through time

Tab. 10.5-1: Schematic process of the erosion scenario (common to all four model scenarios)

Time step [a BP]	Topo. in Fig. 10.5-1	Boundary conditions and processes	Duration [a]	Eros. stage	State / event
I 13'500'000	top	Topogr. level: 7'000 m			Initial condition in modelling phases 1 and 2
		Erosion rate: 0,4 mm/a	7'500'000		Alpine erosion (denudation)
II 6'000'000	black straight	Topogr. level: 4'000 m			Start of model scenarios
		Erosion rate: 0,4 mm/a	5'300'000	①	
III 700'000	violet	Onset of differential erosion			Excavation of valleys starts
			510'000	②	Differential erosion
V 190'000	blue	Ice load increase (build up)			Penultimate glaciation
		Ice level up to 1'800 m a.s.l	60'000	③	
V 130'000	blue	Collapse of the glaciers			
		no ice cap	15'000	④	Eem - interglacial period
VI 115'000	yellow	Ice load increase (build up)			
		Ice level up to 1'500 m a.s.l.	55'000	⑤	Last glaciation I
VII 60'000	yellow	Collapse of the glaciers			
		No glaciation	32'000	⑥	Interstadial of Gossau
VIII 28'000	red	Ice load increase (build up)			
		Ice level up to 1'800 m a.s.l.	14'000	⑦	Last glaciation II
IX 14'000	red	Collapse of the glaciers			
		No glaciation	14'000	⑧	Interglacial period
X present	black	No glaciation			Transition to Holocene

Tab. 10.5-2: Summary of similarities and differences between model scenarios A to D

Eros. stage	Time step [a BP]	Duration [a]	Process or events: Topography in Fig. 10.5-1	Model scenarios: A	B	C	D
	II 6'000'000		Initial condition (black straight)	x	x	x	x
①		5'300'000	constant rate erosion	x	x	x	x
	III 700'000		(violet)				
②		510'000	constant rate erosion	x	x	x	x
			open lateral and bottom bound.				x
	IV 190'000		(blue)				
			constant rate erosion	—			
③		60'000	erosion stop		x	x	x
			add glacier load at 1'800 m			x	x
			all boundaries open				x
	V 130'000		(blue)				
④		15'000	constant rate erosion	x	x	x	x
			all boundaries open				x
	VI 115'000		(yellow)				
		55'000	constant rate erosion	—			
⑤			erosion stop		x	x	x
			add glacier load at 1'500 m			x	x
			all boundaries open				x
	VII 60'000		(yellow)				
⑥		32'000	constant rate erosion	x	x	x	x
			all boundaries open				x
	VIII 28'000		(red)				
		14'000	constant rate erosion	—			
⑦			erosion stop		x	x	x
			add glecier load at 1'500 m			x	x
			all boundaries open				x
	IX 14'000		(red)				
⑧		14'000	constant rate erosion	x	x	x	x
			all boundaries open				x
	X present		(black)				

10.5.2.3 Parameter set and initial boundary conditions

Parameter set: All four model scenarios are based on an identical parameter set which is summarised in Tab. 10.5-3.

Tab. 10.5-3: Parameter set and initial conditions for model scenarios A to D

	Parameter / Condition		Value
Rock	Hydraulic conductivity	K	$1 \cdot 10^{-13}$ m/s
	Young's Modulus	E	15 GPa
	Poisson ratio	v	0.3
	Material		linear-elastic
Ice cap	Hydraulic conductivity	K	impermeable*
	Young's Modulus	E	10 GPa
	Poisson ratio	v	0.3
	Material		linear-elastic

Initial cond.	Erosion rate	0.4 mm/a
	Boundary conditions	lateral and bottom: no flow scenario D only: northern lateral boundary atmospheric pressure top: atmospheric pressure

* The interface between the bedrock and the sole of the glaciers is assumed to be permeable

10.5.2.4 Differences between model scenarios A to D

To check that the contribution of pre-Pleistocene erosion to the present-day pressure anomaly is negligible indeed, the same denudation scenario was run for two different start times: $13.5 \cdot 10^6$ years (middle Miocene) and $6 \cdot 10^6$ years (end Miocene). The simulation results converged to show identical computed present-day pore pressure distributions.

The four calculated model scenarios are differentiated in the following way:

- A continuous erosion of the model surface occurs in model scenario A as shown in Fig. 10.5-1. Glaciations were fully ignored, which implies that erosion acts continuously and that the ice loading-unloading cycles are not taken into account.
- Model scenario B also does not consider ice loads. However, the difference from scenario A consists in the discontinuous erosion. The removal of overburden is concentrated on interglacial periods, while during glaciations no erosional activity occurs (i.e. no modification of the topographic surface). This procedure leads to enhanced erosion rates over shorter time spans.
- Model scenario C is based on the same erosion scheme as scenario B. Additionally, from the beginning of the penultimate glaciation (190'000 a BP), ice loading-unloading cycles are fully taken care of. From the Quaternary evolution scenarios (Chap. 9) it is known that former glaciations are of no importance to the currently observed underpressures. Therefore, they were ignored in all scenarios.

- Model scenario D is virtually identical to scenario C, with only one remarkable difference acting in the last 700'000 a BP during which all boundaries were open to groundwater flow.

10.5.2.5 Modelling results

The results of model scenarios A to D are presented graphically by means of three types of graphs:

1. Diagrams representing pore pressures and principal stresses along boreholes SB1, SB3 and also along a virtual borehole located at the tip of the Eggeligrat (SBx in Fig. 10.5-1) at various time steps (see for definition Tabs. 10.5-1 and 10.5-2). For comparison, hydrostatic conditions are also represented for the last erosion stage.
2. Distribution of simulated pore pressures and hydraulic heads for today (time step X) in cross-section Q - Q'.

10.5.3 Model scenario A

10.5.3.1 Objectives and setup

The specificity of model scenario A resides in the continuously pacing erosion as illustrated by the erosion steps in Fig. 10.5-1. Scenario A comprises two different simulations, different only in the departure of the model scenario: While the first case starts 13.5 million a BP at a topographic level of 7'000 m a.s.l.[9] and simulates the evolution at a constant erosion rate of 0.4 mm/a up to reaching an altitude level of 4'000 m a.s.l. 6 million years ago, the second case starts at this latter moment in time. From then on, both cases follow exactly the same (continuous) erosion path up to reaching the present topographic surface as depicted in Fig. 10.5-1. The early denudation phase is simulated by using the same erosion rate as the one used in the base case of phases 1 and 2 model scenarios (Sects. 10.3 and 10.4, Tab. 10.5-3).

10.5.3.2 Results

Pore pressures at present time are essentially identical for both start times defined above. This demonstrates once more that considering extremely long time spans is superfluous. Nevertheless, in order to allow for comparison with the models run in phases 1 and 2, all phase 3 model scenarios, A to D, are calculated over the long time span of 13.5 million years.

Figs. 10.5-3 and 10.5-4 show that underpressures subsist up to the end of the last erosion step ⑧ at the location of boreholes SB1 and SB3. This is illustrated in terms of head by Fig. 10.5-5. Further, inspection of Fig. 10.5-3 and of the pore pressure distribution in SB3 reveals that simulated underpressures were stronger at the end of erosion step ④ than today, which demonstrates the competition between production of underpressures and dissipation.

---

[9] referred to the current sea level (i.e. 0 m a.s.l.)

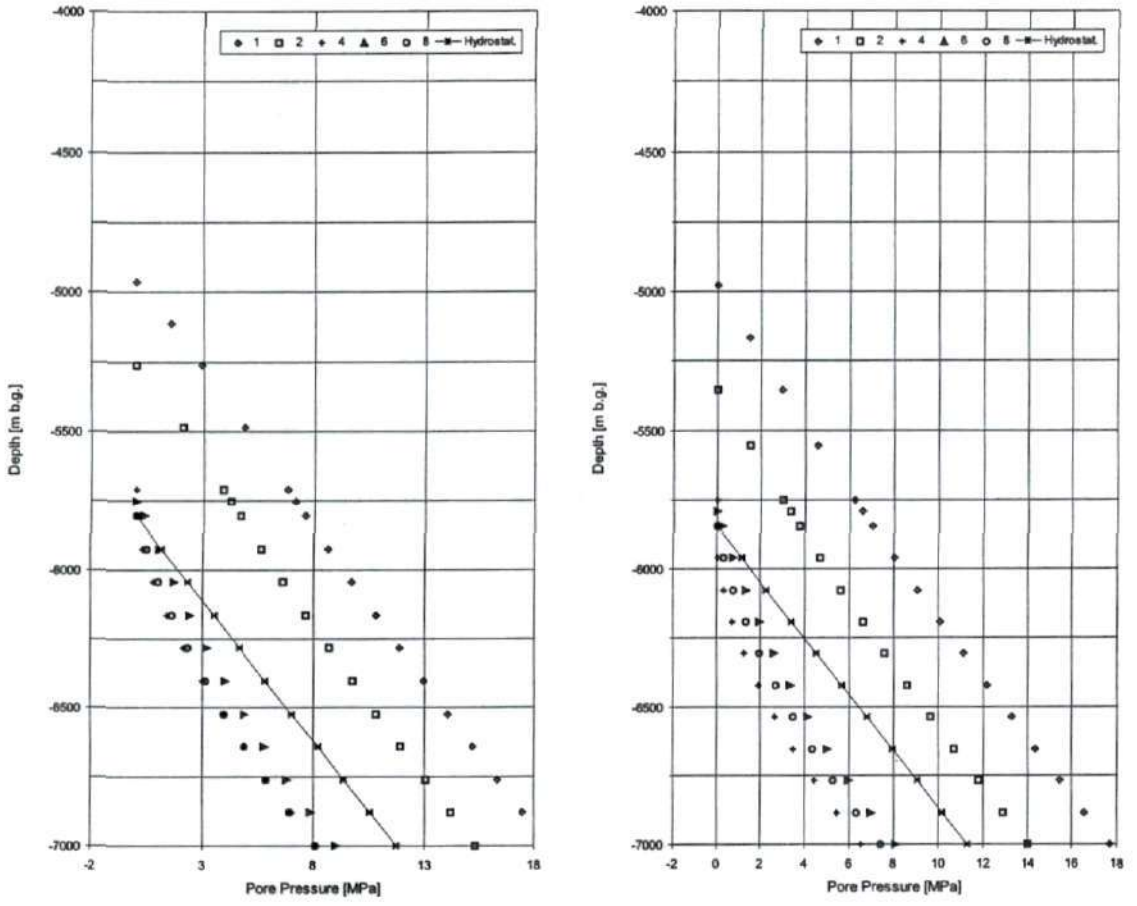

Fig. 10.5-3: Model scenario A: Pore pressure evolution along SB1 and SB3

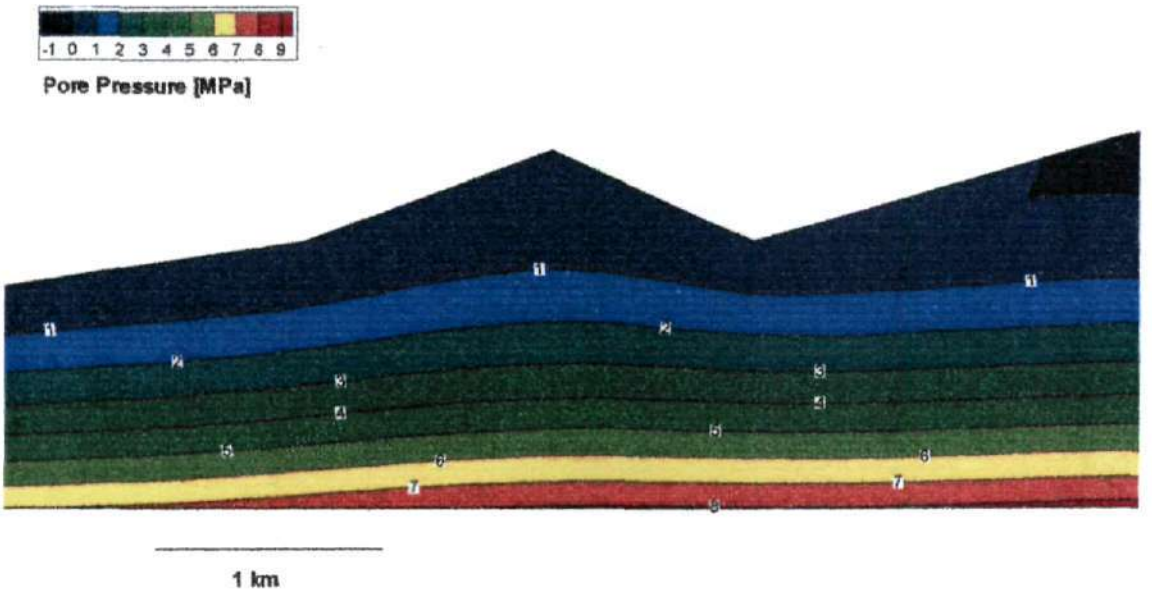

Fig. 10.5-4: Model scenario A, step X: Simulated pore pressure distribution in the model space

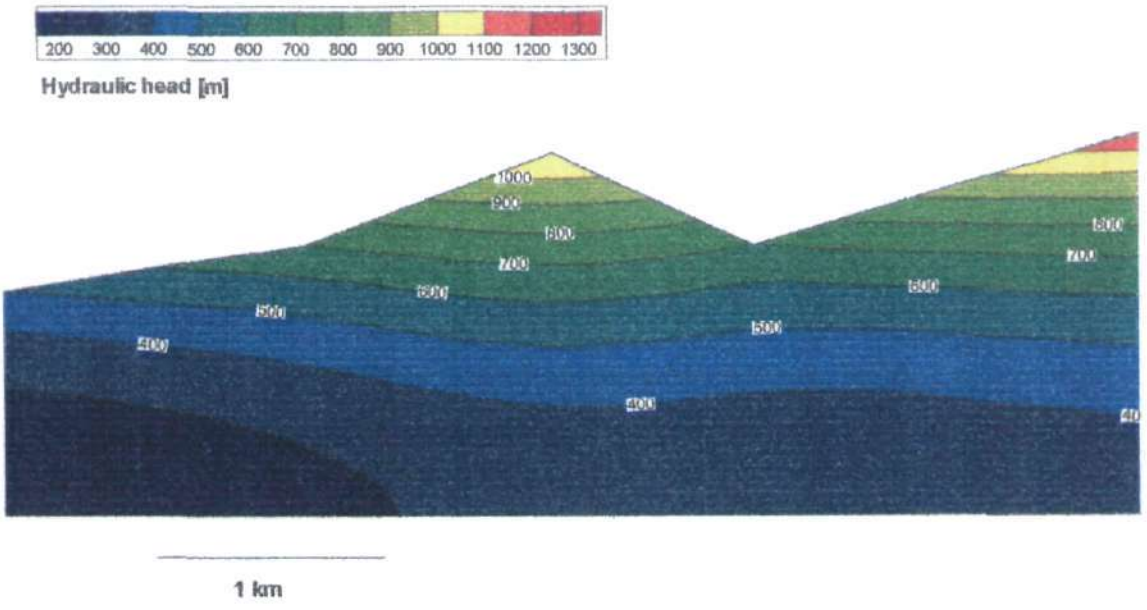

Fig. 10.5-5: Model scenario A, step X: Simulated head distribution in the model space

Fig. 10.5-4 shows that distribution of the UPZ which follows essentially the pattern of the K-model. The development of an UPZ below the Eggeligrat saddle is to be compared with the distribution of maximum and minimum principal stresses (Fig. 10.5-6). Each erosion step produces a decrease in octahedral stress, which affects also the regions under the Secklis Bach valley and under the Eggeligrat hill. Since octahedral stresses decrease more significantly below valleys than below hills, one would expect lower pore pressures under the valleys. The model, however, shows underpressures which are stronger below hills than below valleys. The reason for this apparent paradox is groundwater flow, which rises head conditions in topographic low areas (exfiltration zones) as illustrated by the head isolines in Fig. 10.5-5.

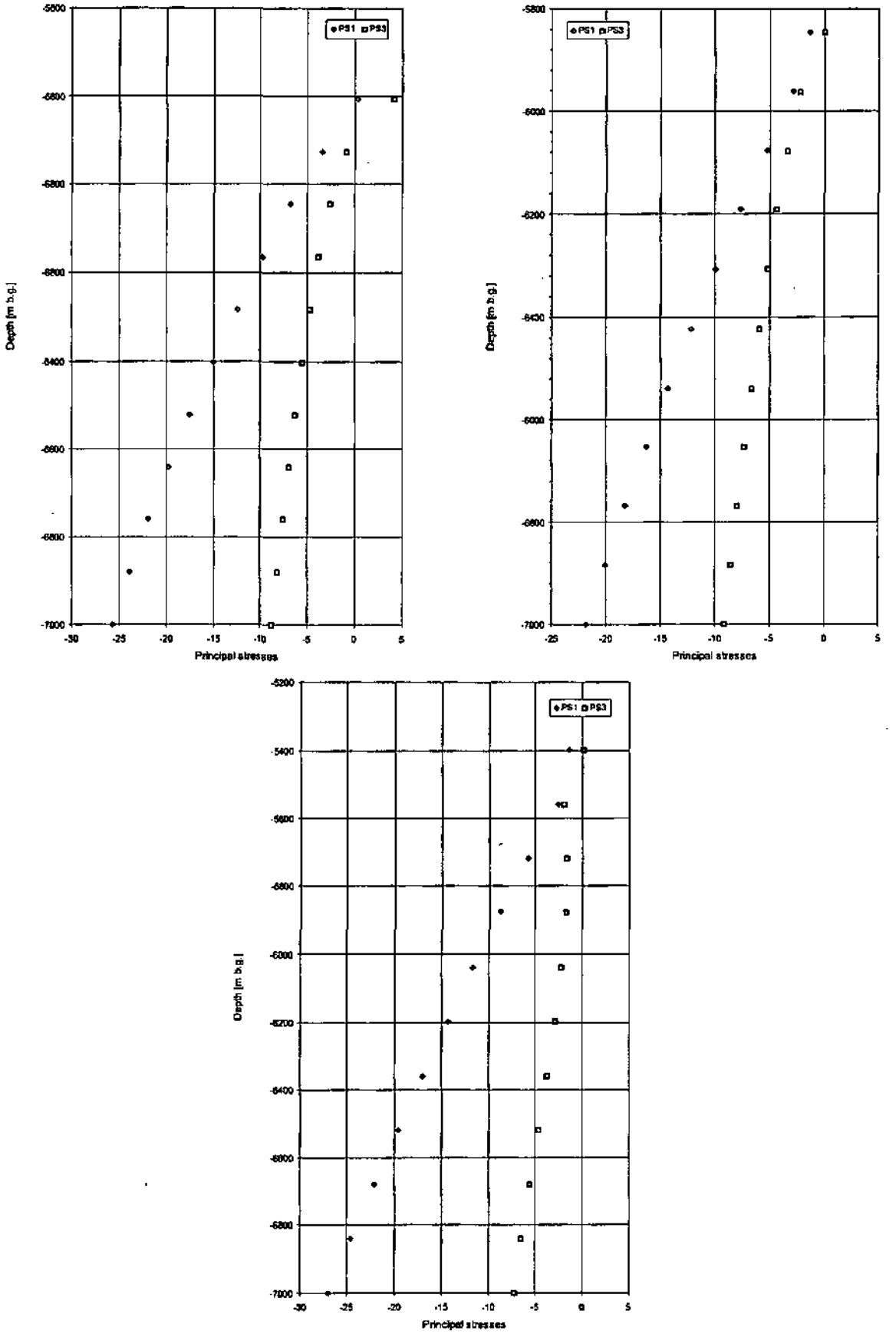

Fig. 10.5-6: Model scenario A: Principal stresses along SB1 (top left), SB3 (top right) and SBx (bottom)

10.5.4 Model scenario B

10.5.4.1 Objectives and setup

The only difference between model scenarios A and B is the discontinuous erosional activity in scenario B, for which erosion is constricted to specific time intervals. These time intervals correspond to interglacial and interstadial periods of significant duration. During these intervals, erosion is active, albeit of different rate from one erosion step to the next.

The ice-free periods correspond to temperate conditions during which slope instabilities provoked by the melting of glaciers are either briskly or progressively re-equilibrated by landslides, creep movements, etc. Scenario B is designed expressly to investigate glacier-driven erosion, whilst - intentionelly - ignoring glacier load changes due to built up and melting. As such, this scenario is similar to scenario Q1 (Sect. 9.4) where the specific contribution of the landslide event of Altzellen was highlighted with respect to the contribution of glaciers by deconvolution of this particular contribution. The main difference, however, is that in the latter case, short-term geomorphologic events were analysed in great detail, while in the present scenario, all types of erosional activity are "averaged" over a comparatively long ice-free period.

10.5.4.2 Results

Fig. 10.5-7 depicts the simulated pore pressure distribution along boreholes SB1 and SB3 at the end of the last erosion step ⑧. Figs. 10.5-8 and 10.5-9 illustrate the corresponding pore pressure and head distributions in the model domain. The simulated magnitude of current pore pressures is slightly lower than in scenario A. Erosion steps ④ and ⑥, which relate to those periods characterised by stronger erosional activity, exhibit temporarily stronger underpressures. However, this development of underpressures relates to enhanced erosion and not to concentrated erosion in defined time intervals as proven by comparison with scenario A. The head and pore pressure distributions of scenario B exhibit only a small increase in the UPZ with respect to scenario A. This fact is not necessarily related to discontinuous erosion and could result from numerical noise.

In summary, concentration of erosional activity on specific time intervals with respect to continuous erosion does not seem to have a noticeable impact on pore pressures. Note also that negative pore pressures result from step ④, which are - as commented in Sections 10.2 and 10.3 - unrealistic.

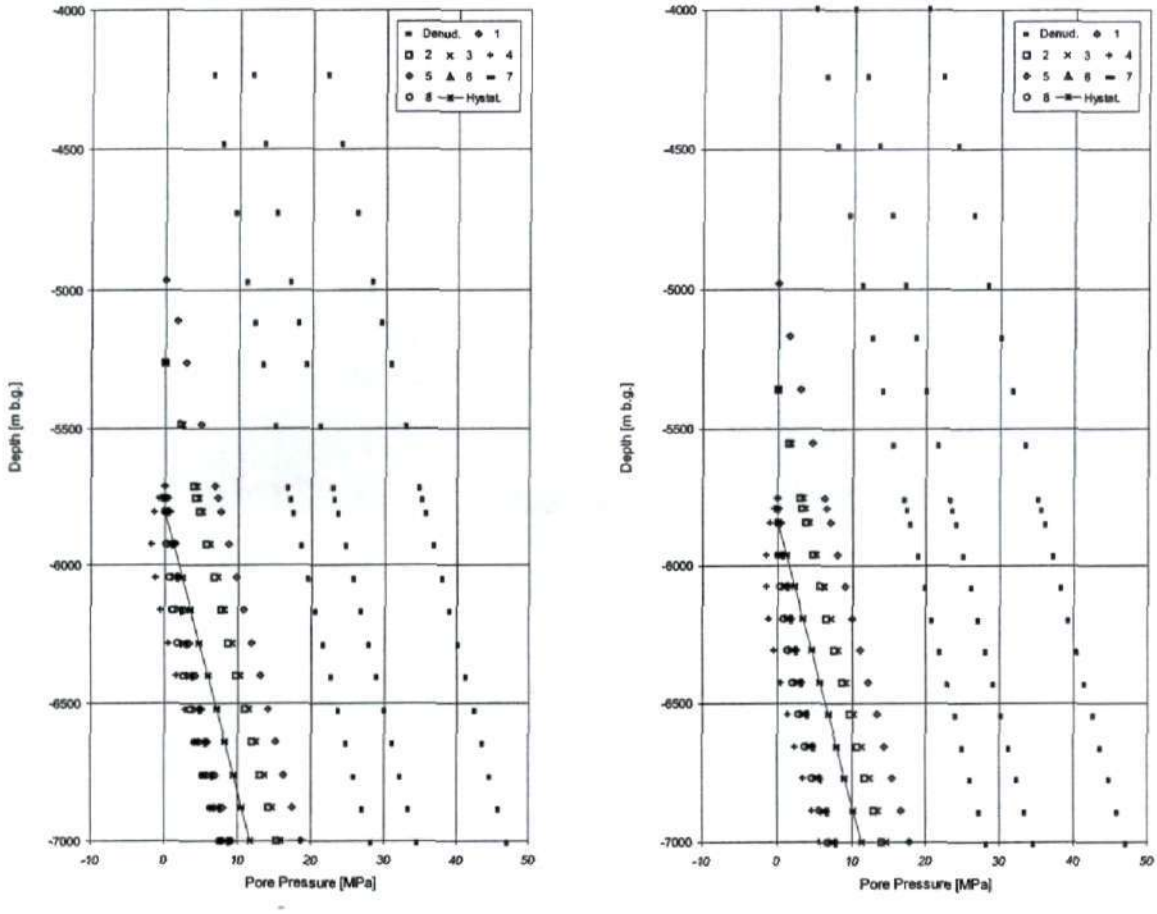

Fig. 10.5-7: Model scenario B: Evolution of pore pressure along SB1 (left) and SB3 (right)

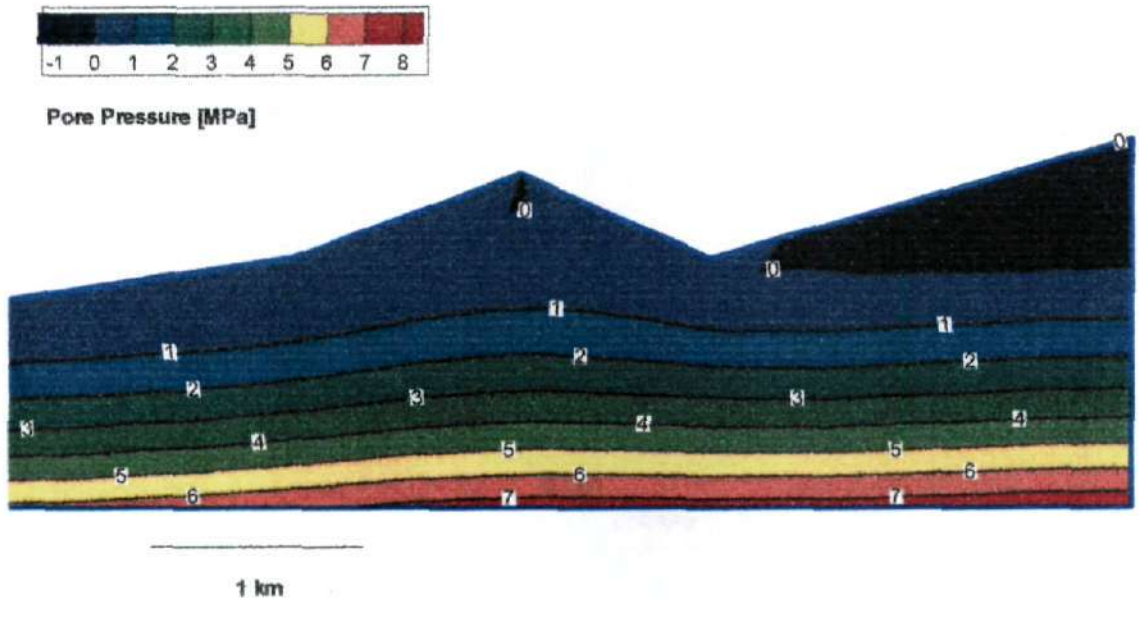

Fig. 10.5-8: Model scenario B, step X: Simulated pore pressure distribution in the model space

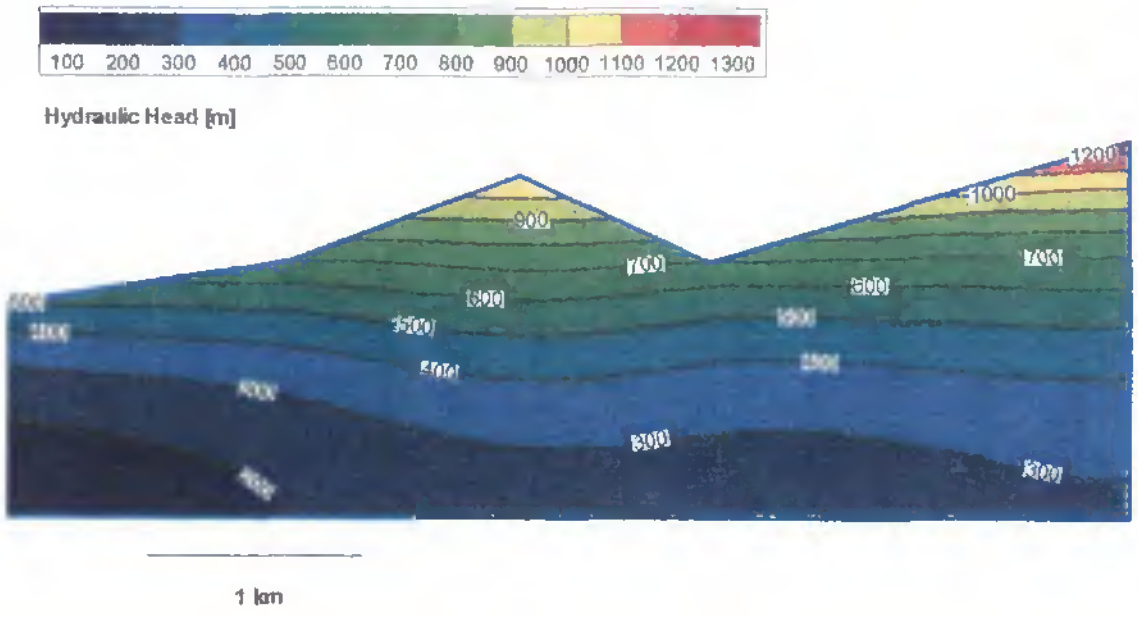

Fig. 10.5-9: Model scenario B, step X: Simulated head distribution in the model space

10.5.5 Model scenario C

10.5.5.1 Scope and setup

Among all four model scenarios, Scenario C represents the most plausible and comprehensive one, because it takes all potential mechanisms into account: denudation, differential erosion and loading-unloading glacier cycles. By comparison with the former models A and B, the specific role of ice load is highlighted.

10.5.5.2 Results

As learned from the studies in Chapter 9, the glacier loading-unloading cycles during the Quaternary era seem to play the governing role in the generation of underpressures. This is confirmed here since stronger underpressures are produced by this scenario. Like in scenario B, the chosen parameter set results in temporary negative pore pressures, which - albeit not realistic - clearly demonstrate that glacier rebound shall be considered by all means. Fig. 10.5-10 represents the evolution of the pore pressures in SB1 and SB3 respectively (plots concentrate on the differential erosion steps).

Although magnitude and orientation of the principal stress vectors are very similar for scenarios A, B and C, a tendency to higher principal stresses in scenario C with respect to B, and B with respect to A is noticeable by comparison of Fig. 10.5-11 with Fig. 10.5-6. With exception of the unrealistic suction pressures computed temporarily in models B and C, the overall pore pressure distribution in scenario C (Fig. 10.5-12) is in fairly good agreement with the observed pressure data. Moreover, all simulations predict stronger underpressures on the flanks of the valleys than below hills, in accordance with locations where the ice load was thickest. The effect of glacier rebound is not only noticeable in the magnitude of underpressures, but also in the characteristic shape of the UPZ (Fig. 10.5-13). Note also that in this simulation, the envelope of the UPZ (defined as H = 500 m) reaches altitude levels slightly above the Engelberger Aa valley level, corresponding therefore to the computed suction pressures (Fig. 10.5-12).

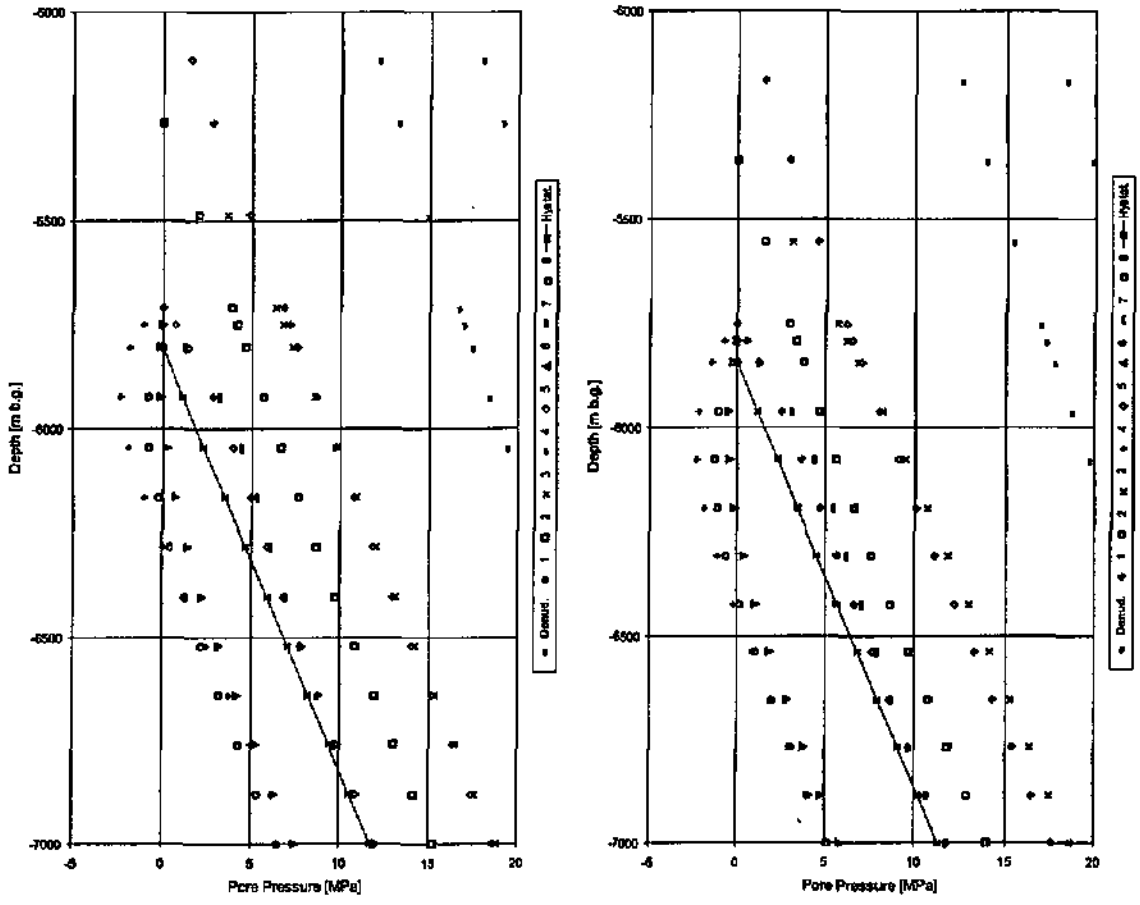

Fig. 10.5-10: Model scenario C: Evolution of pore pressures along SB1 (left) and SB3 (right)

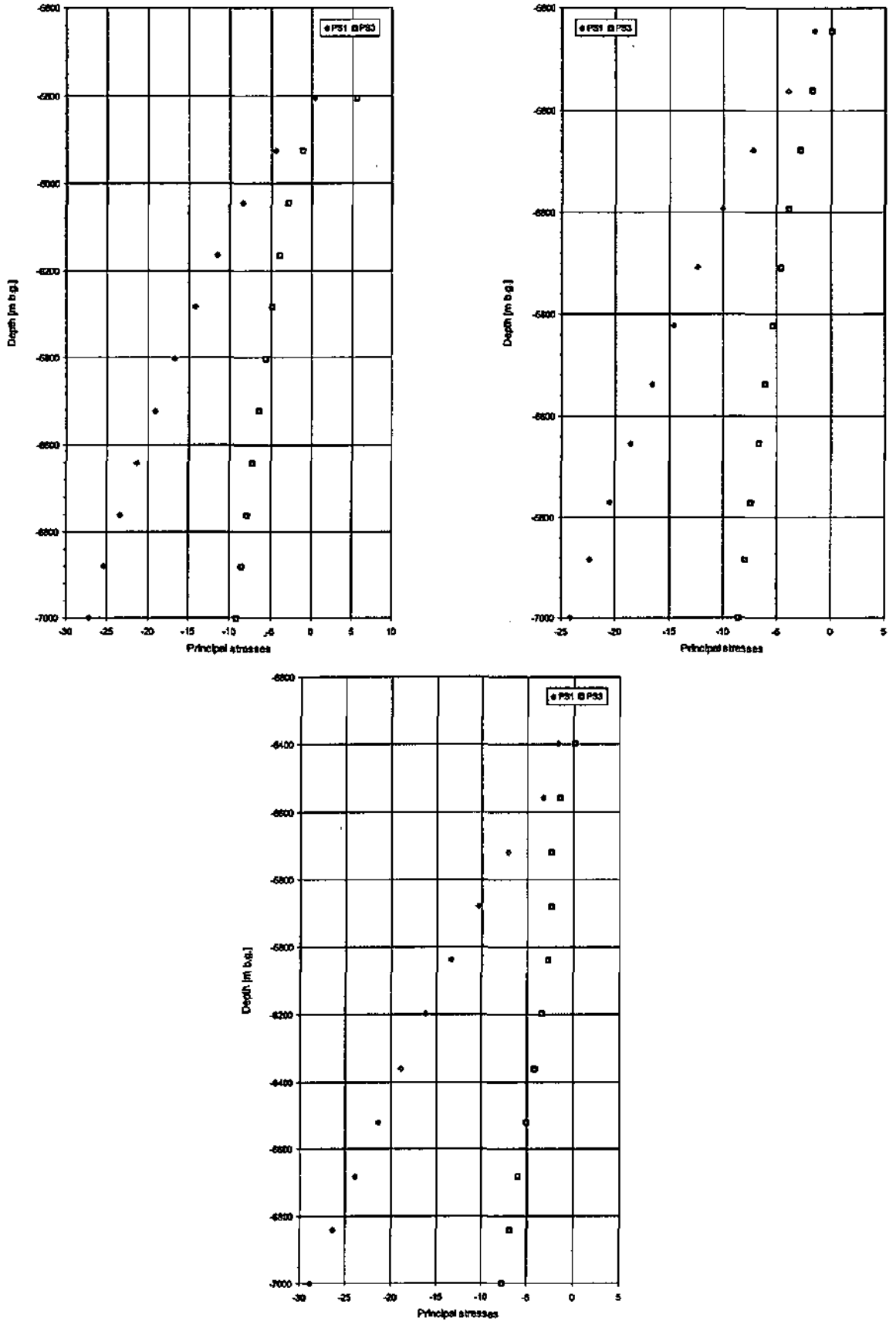

Fig. 10.5-11: Model scenario C: Principal stresses along SB1 (top left), SB3 (top right) and SBx (bottom)

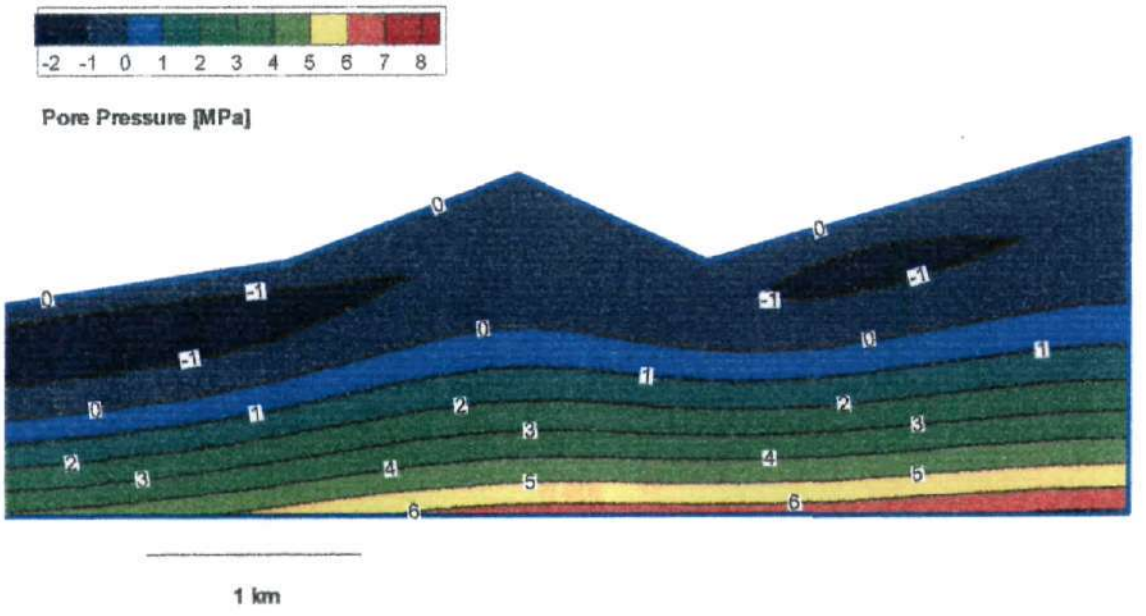

Fig. 10.5-12: Model scenario C, step X: Simulated pore pressure distribution in the model space

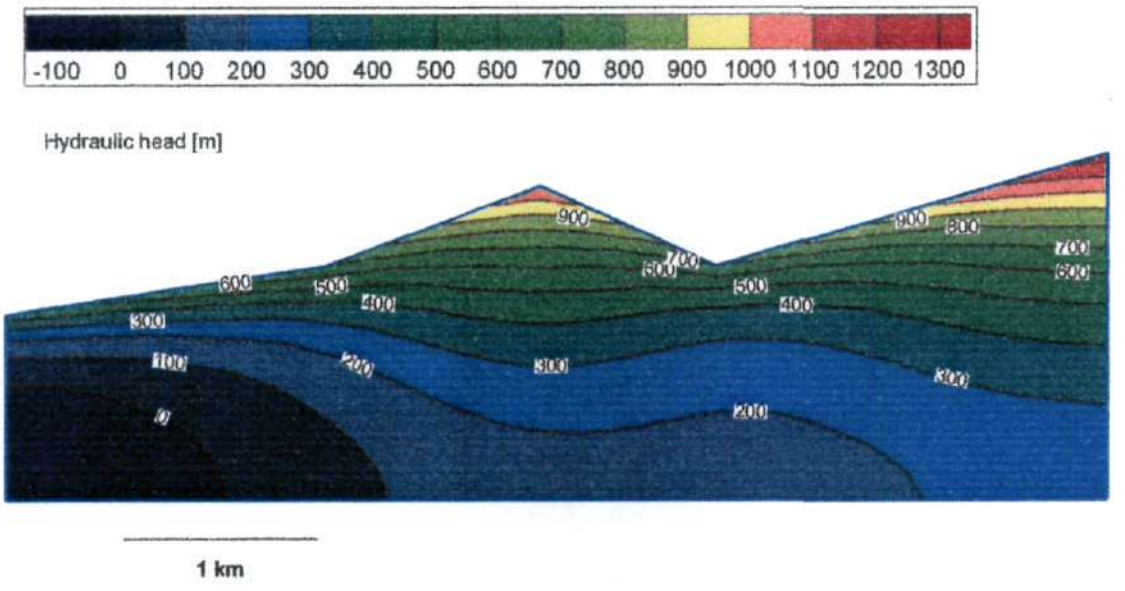

Fig. 10.5-13: Model scenario C, step X: Simulated head distribution in the model space

10.5.6 Model scenario D

10.5.6.1 Objectives and setup

Model scenario D devotes to the role of boundary conditions. Up to the end of erosion step

①, 700'000 a BP, the boundary conditions are identical to those of the former scenarios, i.e. no-flow on model bottom and lateral boundaries, atmospheric pressure on top. After step ①, however, all boundaries are open to flow up to today. This assumption is, obviously, not very realistic, since lateral drainage boundaries would be normal to the 2D model domain (limestone units) and discharge into the Engelberger Aa valley as well as towards the bottom is not very likely.

Therefore, this model configuration corresponds to a very conservative situation in terms of abnormal pressure decay. Dramatic events, as represented by instantaneous glacier loading and unloading, are expected to provoke strong pressure changes in the ground, including overpressures during glacier build up. The open boundaries play the role of extensive water-conducting fractures and of a highly permeable layer connecting directly the basement of the marl-shale aquitard with a discharge area (bottom boundary) at level 540 m a.s.l.

10.5.6.2 Reaults

Fig. 10.5-14 illustrates the evolution of the pore pressures from the situation before step ① (removal of upper 3'000 m, topographic level: 4'000 m a.s.l.), in which still almost hydrostatic pressures prevail at any reference point, over steps ① to ⑧, for which very contrasted pore pressures develop, leading sometimes to complex pressure patterns, i.e. to the coexistence of overpressures and underpressures (underpressures below the hill, overpressures in SB3 region). As usual, magnitude of underpressures must be considered with caution wherever values are below zero. Overpresseures of the order of 2.5 MPa develop locally as a result of glacier load (Fig. 10.5-15 for the situation after erosion step ⑤, i.e. at time step VII).

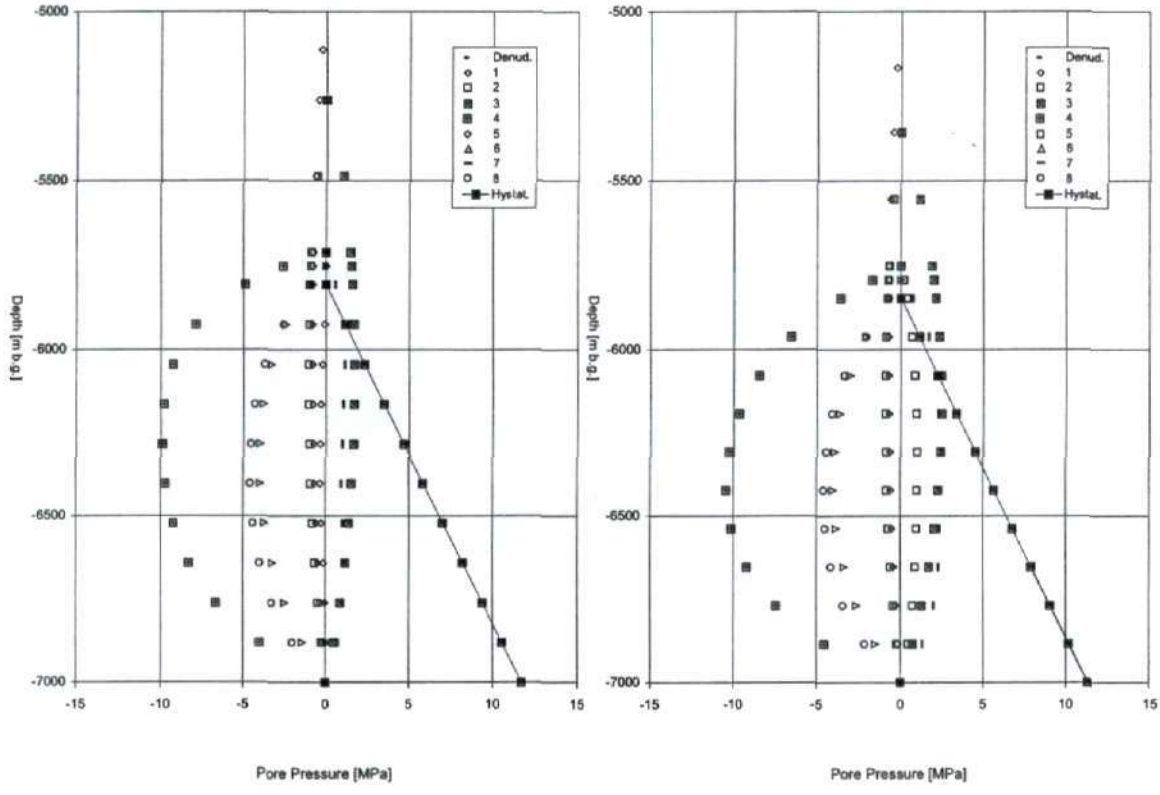

Fig. 10.5-14: Model scenario D: Evolution of pore pressures along SB1 (left) and SB3 (right)

Fig. 10.5-15: Model scenario D, step VII: Simulated pore pressure distribution in the model space

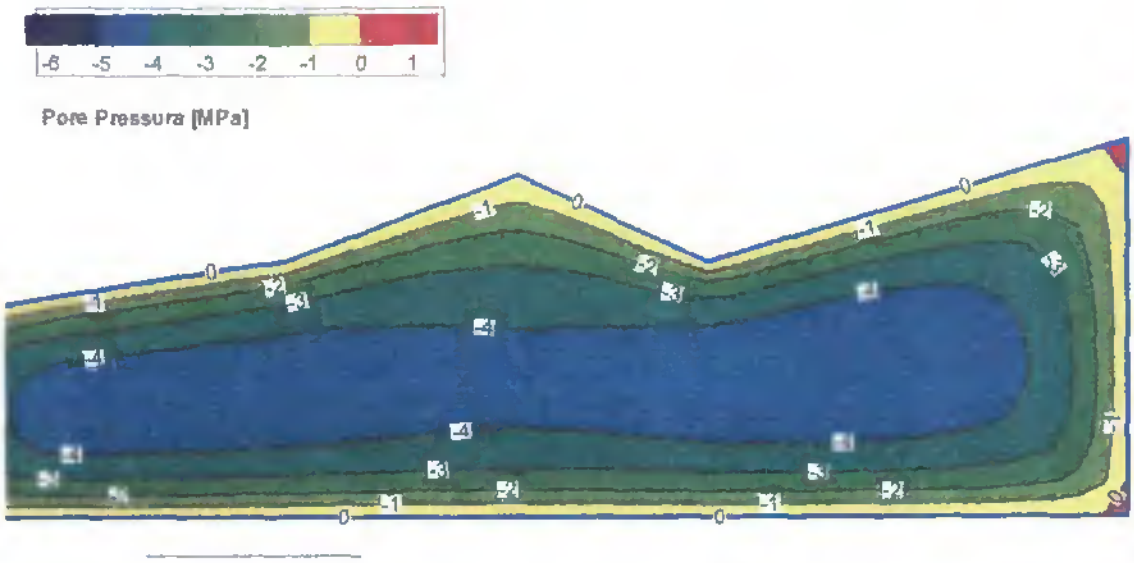

Fig. 10.5-16: Model scenario D, step X: Simulated pore pressure distribution in the model space

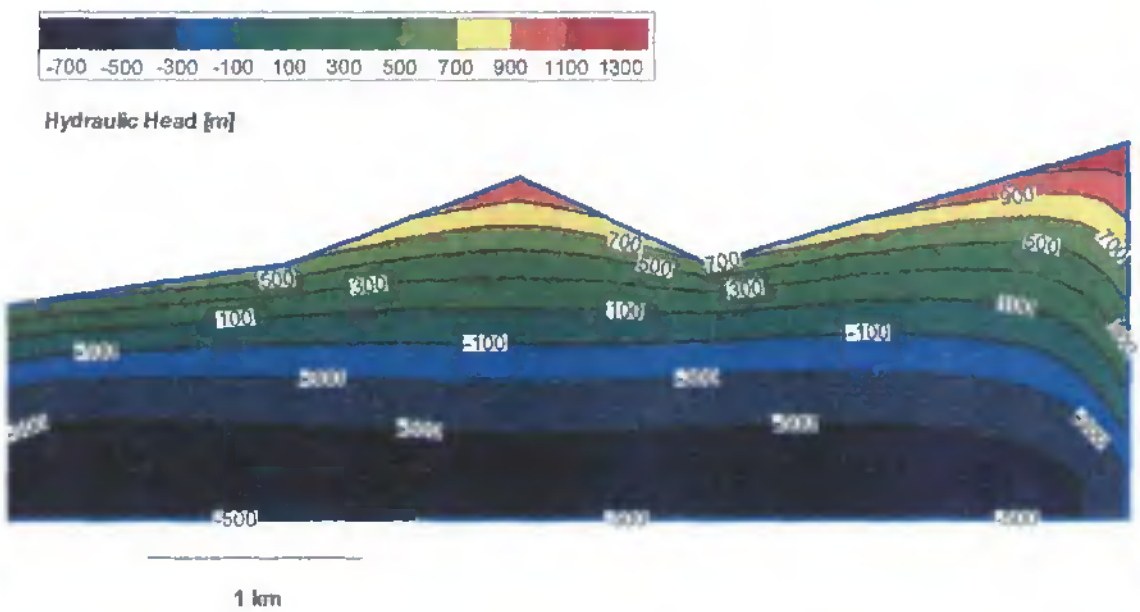

Fig. 10.5-17: Model scenario D, step X: Simulated head distribution in the model space

Typically, very low - and to some extent unrealistic - hydraulic pressures are computed for today (Fig. 10.5-16). After disclosing absolute negative pore pressures and concentrating on the overall pressure trend, the following lessons are provided by model scenario D:

1. Keeping strictly the same parameter values and the evolution scenario as model C, but changing only the boundary conditions, modifies considerably the path followed by pore pressures in the aquitard. However, the outcome as of today (Fig. 10.5-17) is only

marginally different from previous model scenarios.

2. Completely different causes can result in similar effects, i.e. completely different pressure evolutions may end up in similar pressure distributions. It is thus illusory to expect the ultimate explanation for the evolution of disequilibrium pressures.

If the shortest-term hypothesis for the generation of underpressures is considered as stand alone mechanism (i.e. glacier rebound), the potential temporary show-up of overpressures in the marl-shale aquitard cannot be disregarded. In this context, it is justified to question how far alternating pore pressure values are compatible with the isotopic evolution of the groundwaters.

10.5.7 Conclusions from scenarios A to D

Scenario A produces hydraulic underpressures at all reference points (SB1, SBx, SB3). In this case, the underpressures which developed on account of the stress re-arrangement under the Eggeligrat are stronger than those on the mountain flanks, which does not imply that it is the same for hydraulic head.

In scenario B, underpressures are in general slightly stronger as in scenario A. The question whether this situation stems from periods of high erosion or from numerical noise cannot be answered yet.

The results of model scenario C show, as expected, that the additional consideration of glacier rebound noticeably amplifies the magnitude of underpressures in such a way that realistic values are obtained.

Case D produces significant underpressures after each unloading step. Although open boundaries speed up the dissipation process, a noteworthy result is that computed underpressures still exist at the present time. Another remarkable outcome of this simulation is the periodic onset of strong overpressures in favour of glacier progradations (increase of glacier load).

11 SUMMARY AND CONCLUSIONS

11.1 Relevant results

At the end of this study, the probably most important statement is what NEUZIL wrote in his 1995 paper (NEUZIL, 1995): "the hydrodynamic disequilibrium is dominated by the most recent forcing as the fingerprint of geologic processes grows increasingly faint with time. This exacerbates a nonuniqueness that is introduced by uncertainty in system properties and geometry." All modelling studies, albeit different in simulated duration, geologic forcing and approach, *confirm the predominant role of the last mechanism potentially able to generate underpressure with respect to former ones.*

With respect to the nonuniqueness of solutions addressed by NEUZIL (1995), simulations documented in Chapters 8 to 10 show that completely different causes may result in similar effects. Therefore, it is a matter of interpretation to identify candidate geologic forcings and to exclude others, as for example transient gas flow. In return, *it can be affirmed that deformation of the rock skeleton is the most important mechenism leeding to subnormal pressure.* Hydraulic underpressures are generated because the fluid cannot accommodate rapidly the increase in pore space provided by rock decompaction. Changes in boundary conditions cannot explain head values reaching far below any possible exfiltration area.

Another important outcome of this study is that the driving force (geologic forcing) generating hydraulic underpressures is of coupled hydro-mechanical nature. *Potential effects of free ges ere deemed negligible beceuse of the small emount of free ges in the marl-shale aquitard and because low gas saturations do not impede mechanical rebound.* On the contrary, small amounts of free gas prolong the duration of disequilibrium pressure. Whatever non-darcian processes (osmosis, swelling) are considered, their impact on the currently observed underpressures are probably negligible because non-darcian processes (especially osmosis) would counteract the development of subnormal pressures.

The mechanical rebound of the marl-shale aquitard, which led to the currently measured subnormel hydreulic heeds, is predominantly generated by glacier retreat end more specifically by glacier melting at the end of the last glaciefion some 12'000 years ago. Consequently, *geologic forcing is probably inactive at present.* It will be reactivated when the next ice age begins. However, *possible contribution of erosion cannot be fully ruled out because of the poor understanding of the past geomorphologic evolution of the Wellenberg site and especially beceuse of the uncertainty associated with estimation of equiterd diffusivity.* Erosion is the ever active geologic forcing "par excellence" and its contribution might be underestimated yet. The importance of erosion being inversely proportional to the diffusivity ratio: the lower the assumed rock diffusivity, the stronger the potential importance of erosion with respect to glacial rebound.

Moreover, in agreement with the current understanding of geologic conditions and marl-shale aquitard deformation behaviour, it is probably correct to assume that the deformation obeys approximately linear-elasticity. It seems also that critical parameters and boundary conditions play a stronger role than the choice of a material model. This statement may need to be revised if additional piece of information on the long term deformation behaviour of the aquitard contradicts it (in situ experiments).

In comparison with the time ranges in the order of millions of years read in the literature for decay of head anomalies in large sedimentary basins, estimates for Wellenberg lay within a time range shorter by one or two orders of magnitude. Two reasons may explain this difference:

1. the marl is stiffer than most shales, and/or

2. the aquitard at Wellenberg is of a comparatively small scale with respect to large sedimentary basins, and thus the distance between the centre of the aquitard to drainage boundaries is much shorter than in large sedimentary basins. In other words, the equilibration process paces faster at Wellenberg than in large sedimentary basins.

Results of model scenarios show how far fingerprints from former unloading events or ages are almost completely irrelevant for the understanding of current disequilibrium pressure. In this context, and assuming that the governing driving force is glacier retreat, the importance of the duration of an ice age must be emphasised: the longer an ice age, the more overpressure due to the ice load can be dissipated in the ground during the presence of the ice itself. Observing the simulated head evolution over time, the analogy with an oedometer test response is striking. The lower the diffusivity, the longer the duration necessary to dissipate a given pressure perturbation. To describe head evolution for very low diffusivity values, the term "memory effect" has been used, which expresses that the aquitard system is still reacting to pressure perturbations that sometimes are remote. The term "time constant" is even more appropriate to describe the delay in pressure equilibration because - strictly speaking and owing to the linear-elastic approximation - there is no real memory effect in most of the applied models. A true memory effect implies plastic material (i.e. irrecoverable strain).

11.2 Robustness of the preferred hypothesis (mechanical rebound) and discussion of alternative mechanisms

11.2.1 Inferences from the existence of hydraulic underpressures at Wellenberg

Hydraulic head and residence time of groundwater are information about the flow conditions, not only in the vicinity of the tested borehole section but also for significantly larger fields around the observed or sampled borehole interval. Very long groundwater residence times and subnormal pressure conditions correlate positively at Wellenberg. This does not necessarily imply that there is a common origin for both phenomena, but rather that *conditions allowing the existence of quasi-stagnating groundwater may also prove suitable for the generation and preservation of underpressures*. The marl-shale aquitard seems therefore to fit into this scheme. As a rule, the water-conducting features characterised on core material and observed on outcrops carry only small amounts of water and form at best a sparsely connected network. Advective transport is probably limited to this network. Diffusion is the principal transport mechanism in the matrix and probably also in most sections of the water-conducting features.

Glacier effects play a stronger role than differential erosion in the generation and maintenance of subnormal pressure, especially when assuming that the stiffness of the marl-shale aquitard is just marginally lower for large blocks than for laboratory samples. However, this issue deserves further consideration, especially in the perspective of disposal of radioactive waste. Additional modelling work alone will not improve substantially the current level of knowledge. What is needed, in order to reduce uncertainty on the leading generation mechanism, is additional data from key locations in the ground. The relatively large parameter bandwidths and the inevitable uncertainties associated with reconstruction of past geological events do not allow one to fully exclude erosion as an important contribution to underpressuring, since the effects of both mechanisms are almost indistinguishable today.

The fact that underpressures could develop despite of the strong horizontal compression can be elegantly explained. Since horizontal stress is also decreased when vertical stress is decreased, *it is not the absolute magnitude of compressional stress that influences pore pressures but its decreasa*.

In spite of the above reservations, the modelling studies documented in this thesis supply important findings, which are considered to be generally valid:

1. It is most likely that the UPZ at Wellenberg is currently decaying, unless its maintenance is controlled by ongoing long term erosion. Its evolution is primarily dictated by the hydraulic diffusivity of the aquitard rock and the dimensions of the marl-shale aquitard.
2. Under assumption that statement 1) above is correct, reactivation of underpressures is dependent on a future glaciation.
3. At the lead of a new glaciation, pore pressures will rise in the marl-shale aquitard as a consequence of the applied ice load. Both magnitude and duration of the underpressures following ice melting depend on the ice load, the level of glacier erosion as well as on the duration of the current interglacial period and the one of the ice age, and of course on the rock properties.
4. The hydraulic underpressures observed today originated probably during the Quaternary era itself. Possible earlier contributions (Pliocene denudation) would have decayed long ago or would contribute only negligibly to today's pore pressures.

The arguments for and against an origin of the underpressures by glacier unloading and/or differential erosion are:

- The Quaternary evolution conceptual model is robust because glaciations are relatively well known with respect to former geological events and because both magnitude and position of subnormal heads, predicted by glacier models, correspond to the observation. However, the modelled scenarios require relatively high ice levels, which should not fluctuate strongly during glaciations.
- Differential erosion represents a valid alternative to the glacier rebound hypothesis. The process lasts over longer periods of time and does not provoke fluctuations of the pore pressures in the aquitard. This model is, therefore, more in accordance with the observed lengthy residence time of groundwaters in the marl-shale aquitard. However, the assumptions are considerably weaker with respect to the sequence of events and rates of erosion than in the case of the Quaternary conceptual model. For example, if scouring of the Engelberg Aa and Secklis Bach valleys had occurred significantly earlier than what is postulated, the contribution to underpressures stemming from erosion would become even weaker.

With respect to the parameters controlling generation and decay of abnormal hydraulic pressure, namely hydraulic conductivity and specific storage, the largest uncertainty is clearly associated with K. S_s is a parameter based on rock and fluid compressibility. Both compressibility terms can be considered, in a first approximation, as invariant from depth. Rock compressibility was fixed many million years ago when the aquitard was exposed to high overburden stress. Fluid compressibility depends also on temperature, which does not strongly vary for the observed depth and time ranges. In return, the definition of representative hydraulic conductivity is a ticklish task. Many factors ruling K_{eff} (fracture transmissivity distribution, fracture connectivity, channelling) are unknown at aquitard scale and could only be approximated by means of a series of geometric and parametric assumptions based on a variety of conceptual choices. Based on the current conceptualisation (fracture length) it is assumed that representative K-values can be determined at hectometre scale. Further work is needed to try to reduce uncertainty ranges for both K and S_s parameters. Among several possibilities, cross-hole interference packer tests at different distances may help to constrain uncertainties and to gain further insight into K-variability and possibly K-anisotropy.

Time-dependency of key parameters is an important issue, which still remains open. Evidently, both K and S_s have evolved through time, especially in the shallow part of the

marl-shale aquitard. This can be affirmed based on hydrochemical and isotopic data which show that "higher" K-values correlate with mixed groundwater types (meteoric water and highly saline formation water) and relatively short residence times. For different reasons (costs, time, level of difficulty), time-dependency was only marginally addressed in this contribution. This choice is probably justified at this level of investigation, where emphasis is on understanding key processes. However, it might be useful to take both depth-dependency and time-dependency into account for model simulations aimed at forecasting the evolution of hydraulic pressure. Not so much because it will strongly affect the model results, but because it may help to convince both scientists and the general public.

11.2.2 Uncertainties

Although the proposed abstraction schemes produce satisfactory results, i.e. are able to reproduce the observed UPZ in its magnitude and position pretty well, there are still many uncertainties. As stressed in Chapter 6, modelling studies are in essence suited for estimation of possible consequences of different hypotheses, but they cannot provide a genuine representation of the reality. Additionally, as discussed in Section 11.1, different mechanisms can lead to almost identical pressure responses. Their effects can even superimpose on each other, hindering from distinction of individual contributions.

Several issues in the field of hydraulic underpressure have not been addressed by the present mathematical models. Among them, there are three which may deserve further attention:

1. unsaturated conditions
2. density effects
3. temperature effects.

NEUZIL & POLLOCK (1983) show that absolute negative pore pressures may theoretically exist in an aquitard exposed to unloading. Several model outputs presented in this thesis tend to produce suction pressures. Although artificial, these suction pressures deserve further consideration. Clearly, the potential for absolute negative pore pressures must not be confused with free (methane) gas in the aquitard. Absolute negative pore pressures might result in a mixture of water and vapour or in a multiphase system including methane.

Both during build up and dissipation of underpressures, not only the envelope (defined as H = 500 m), but the entire UPZ, is affected as illustrated by various head evolution profiles along boreholes (e.g. Figs. 8.5-2, 9.4-3). Finally, as shown in NAGRA (1997), the uncertainty range around the minimum head value inferred from borehole SB3 reaches below 0 m a.s.l. Therefore, it is possible that unsaturated conditions exist inside the UPZ. Unfortunately, packer tests cannot reveal absolute negative pore pressures. In order to measure suction pressure in situ, a dedicated tool is necessary (psychrometer) which would have to be installed in isolated long term monitoring intervals. Unsaturated conditions imply two-phase flow conditions and therefore a similar situation to the one exposed in Section 8.5. Free gas will absorb a portion of the stress transmission and thus counteract the development of underpressures and, on the other hand, gas will contribute to reduce the mobility of the wetting phase, i.e. water, which macroscopically corresponds to reducing the relative permeability to water and therefore to prolonging the duration of disequilibrium pressure decay.

Consequences of negative pore pressures are difficult to estimate due to the counteracting trends summarised above. Whatsoever, the presence of suction pressure would require a dedicated approach based on codes solving two-phase flow equations. It is possible that taking suction into account, shifts prediction of the generation of underpressures to older times than currently assumed and longer duration abnormal pressure dissipation.

Density effects also have not been investigated in this study, but it is likely that they are negligible. Although hydrochemical sampling was restricted to the upper envelope of the UPZ, it is likely that the salinity, and hence density distribution in very low-K regions is fairly homogeneous.

Temperature effects have been discussed in Chapter 7. Cooling is expected to contribute to the generation of disequilibrium pressures by reducing the fluid pressure in the pores. However, this contribution is deemed negligible for the Quaternary era, since most of the cooling occurred long before, and since cooling would rather contribute to enhance underpressures (i.e. indistinguishable from rebound).

The preferred conceptual model of glacier rebound provides a satisfactory explanation for the head anomaly. However, simulated head evolution in the marl-shale aquitard over different time spans of the Quaternary reveal strong fluctuations associated principally with glacier progradations and retreats. In other terms, there are periods of overpressures followed by periods of underpressures and, assuming extreme boundary conditions, coexistence of overpressures and underpressures was even temporarily possible. The probability of oscillations of pore pressures might perhaps be tested by means of hydrochemical and/or isotopic methods. In any case, it would be an interesting avenue of investigation to set up and apply a method which uses hydrochemical and isotopic information as a discriminator.

Another open question is the role of the Engelberger Aa valley. In all regional-size models, the valley was considered as the boundary of the model, leading to exfiltration even of deep aquitard groundwater. It is, however possible, due to the lithologic continuity of the marl-shale aquitard across this valley, that it is not acting as an exfiltration zone for deep groundwaters. What impact such a situation would have on maintenance of underpressures has not be explored either, and would, possibly, be useful.

The present condition of governing driving forces is not only important for reconstruction of past conditions, but also for predictions of the future evolution. For instance, the contribution of differential erosion decreases at the same rate as valleys get more and more mature, i.e. achieve a topographically equilibrated profile. The Engelberger Aa valley, especially below the village of Grafenort has already reached a large degree of maturity. Therefore, it is expected that a future glaciation will cause only little erosion in the corresponding valley section, and hence will contribute only marginally to a next build up of negative pore pressure.

Erosion is an endless process which restlessly removes the surface of the marl-shale aquitard and thus increases hydraulic conductivity in progressively deeper sections as well as reduces the distance to exfiltration areas. Therefore, erosion – even if not necessarily the main driver of underpressures at Wellenberg – will have "le dernier mot" since by its action, underpressures in the future, even if periodically re-activated, will in the long run decrease step by step.

12 PERSPECTIVES: USE OF UNDERPRESSURES AS INVESTIGATION TOOL AND SAFETY CRITERION FOR UNDERGROUND REPOSITORY PROJECTS

One of the most challenging tasks is to derive a robust model of the in situ K-distribution based on sparse hydraulic testing data as it is required for performance assessment and siting. Problems associated with K-estimates begin with the interpretation of hydrotest data. Since hydraulic conductivity cannot be measured directly in tight rocks, its determination bases on extrapolations, which themselves base on ad hoc flow models. Additionally, the radius of visibility from the well into the formation, i.e. the volume of rock for which the inferred K-value is representative, is in aquitards restricted to the immediate vicinity of the well, which often does not exceed a few centimetres. Finally, upscaling from individual K-values to K-values representative of an entire hydrogeological unit represents, beyond doubt, a challenging work.

Various contributions address this issue and several sophisticated methods have been developed in the recent past in order to construct so-called "realistic K-distributions". The K-model applied to the Quaternary model scenarios Q2 and Q3 (Sect. 9.5), derives, for instance, from such an approach (NAGRA, 1997). The outcoma of this model is deemed representative of in situ conditions. In reality, it is essentially a clear representation of the (low) degree of knowledge of the hydrodynamic system. However, there is no other way to proceed, and the K-model bears the advantage of being evolutionary, i.e. to be able to flexibly taka additional data into account. This approach comprises also several inconveniences, which are:

1. Additional K-data will not necessarily improve the model as a whole, but only contribute to improve the model in the limited volume in which these data have been collected. The new information on K-variability and K-anisotropy is not necessarily representative for the whole aquitard.

2. Hydraulic conductivity is often considered in the waste management community as the only reliable criterion. Hydrogeologists often do not refrain from spending huge amounts of money in order to characterise the K-distribution and K-variability. Stacks of theses pile up, devoted to generation of fracture networks and geostatistically generated K-distributions. However, whatever fascinating and useful these studies may be, they fail to demonstrate that performance assessment criteria can be met.

Therefore, it might be worth to consider a complementary approach which consists of basing performance assessment on hydraulic head information as independent input. In the case of Wellenberg, where hydraulic underpressures clearly demonstrate large-scale and long-lasting isolation of the marl-shale aquitard, all subnormal pressure evidence is an additional proof of adequate rock properties for disposal of waste.

The lack of information is inherent to any site characterisation project. Obtain a representative set of K-values for a tight rock is not only impracticable, it is also extremely expensive and counterproductive since it implies destroying the natural barrier by drilling a larger set of boreholes.

As shown in NAGRA (1997), applying different K-realisations results in a wide range of dissipation durations and UPZ-geometries. If we would extrapolate these results back in time, even assuming the latest possible generation of underpressures some 12'000 a BP, we would notice that several of these K-realisations *are simply impossible*, unless soft rock properties are assumed. In other words, underpressure data can be used to constrain the statistically generated K-distributions.

Hydraulic head information has, like the chemical and isotopic composition of groundwater, the advantage, with respect to transmissivity data, of being representative of a larger volume of rock around the tested interval (VINARD & LAVANCHY, 1994). Various studies (e.g.

RIVERA & SENGER, 1993; VOBORNY et al. 1997) show conspicuously that water-conducting faults inside the UPZ and intersecting an investigation borehole are incompatible with the presence of an UPZ. This simply because the UPZ would have disappeared in the vicinity of such features. It is therefore a point of utmost importance to be able to define a so-called "distance of exclusion", i.e. a volume of aquitard rock inside the UPZ and around an observation point in which highly permeable features of any kind can be excluded. Unfortunately, there is no dedicated parameter sensitivity study available yet. Rapid inspection of simulated head patterns in the vicinity of implemented structural features or in the vicinity of highly permeable boundaries (e.g. Fig. 9.4-7) tends to show that a distance of exclusion of the order of few hectometres[10] may be defined. Therefore, head data from the UPZ can be directly used as spatially extended exclusion criteria for the existence of hydraulically hazardous features. Few additional boreholes at key-locations would suffice.

In essence, the basic idea drafted above is close to the elaborate "recharge area concept" advanced by TÓTH & SHENG (1996). Without pretending to enter the field of inverse modelling for estimation of hydraulic conductivity from head data, it would certainly make sense to consider the head anomaly at Wellenberg as indicative of overall low hydraulic conductivity. The idea of using head anomalies as exclusion criterion of high-conductivity flow-pathways is not new, and has been presented in a form or another in the recent past by TÓTH (1990), NEUZIL (1995) and VINARD & LAVANCHY (1994). Due to the complexity of the inverse problem (transience, consideration of various types of geologic forcings and possibly of two-phase flow leading to non-uniqueness of solutions), there is no (and will never be) an inverse technique, which fully acknowledges the variety of parameters. Therefore, a pragmatic and iterative process following summarily the following stages may be a suitable alternative:

1. work out conservative model scenarios in close co-operation between geologists, hydrogeologists and performance assessors
2. define evaluation criteria for the subset of scenarios which can be tested by means of hydrogeological methods
3. check the compatibility of each conservative scenario with the current knowledge of underpressures and eliminate impossible and unlikely scenarios by performing parameter sensitivity analysis (properties of WCF, background K_{eff}) in order to define K and S_s ranges suitable for the aquitard, based on possible geologic forcings
4. if it can be reasonably assumed that geologic forcing is inactive at present time, the problem reduces itself to a simple transient simulation.

In basing site characterisation on indirect information, and more specifically on disequilibrium pressure, a lot of costly and sophisticated investigations become superfluous while at the same time more reliable information is provided for performance assessment.

[10] this distance can be estimated if time is considered also (dissipation of disequilibrium pressure around a permeable feature)

REFERENCES

AESCHBACH, W. 1997: Kalte Vergangenheit - heisse Zukunft? Neue Erkenntnisse zum Klima der letzten Eiszeit. Neue Zürch. Zeit. Nr. 144, 73.

ARISTORENAS, G.V., EINSTEIN, H.H. 1993: WLB: Numerical investigation of underpressures occurring at Wellenberg (Final report). Unpubl. Nagra Internal Report Nagra, Wettingen.

BAYLY, B. 1992: Mechanics in Structural Geology. Springer Verlag, New York.

BEAR, J. 1972: Dynamics of Fluids in Porous Media. American Elsevier, New York.

BEAUMONT, C., WILLETT, S. FULLSACK, P., HAMILTON, J. 1994: Progress report on geodynamical modelling of crustal deformation in compressional orogens. Lithoprobe Alberta Basement Transects Workshop (Feb. 14-15), Univ. of Brithish Columbia, Canada.

BELL, J.S., McCALLUM, R.E. 1990: In situ stress in the Peace River Arch area, Western Canada. Bull. Canad. Petrol. Geol. 38A, 270-281.

BELITZ, K, BREDEHOEFT, J.D. 1988: Hydrodynamics of Denver Basin: Explanation of subnormal fluid pressures. Am. Assoc. Petrol. Geol. Bull. 72/11, 1334-1359.

BERNABÉ, Y., FRYER, D.T. 1995: On the use of small stress excursions to investigate the mechanical behaviour of porous rocks (technical note). Int. J. Rock Mech. Mins. Sci. & Geomech. Abstr. 32/1, 93-99

BETHKE, C.M. 1985: A numerical model of compaction-driven groundwater flow and heat transfer and ist application to the Paleohydrology of intracratonic sedimentary basins. J. Geophys. Res. 90/B8, 6817-6828.

BIOT, M.A. 1941: General theory of three-dimensional consolidation. J. Appl. Physics. 12, 155-165.

BIOT, M.A., WILLIS, D.G. 1957: The elastic coefficients of the theory of consolidation. J. Appl. Mech. 24/1, 594-601.

BLÜMLING, P. & GLAWE, U. 1996: WLB: Felsmechanik-Datensatz und Resultate der in situ Spannungsmessungen. Unpubl. Nagra Internal Report Nagra, Wettingen.

BOULTON, G., CURLE, F. 1997: Simulation of the effects of long-term climatic change on groundwater flow and the safety of geological disposal sites. European Commission, EUR 17793 EN, Brussels.

BOUR, O., LERCHE, J. 1994: Numerical modelling of abnormal fluid pressures in the Navarin Basin, Bering Sea. Marine and Petrol. Geol. 11/4, 491-500.

BRADLEY, J.S. 1975: Abnormal formation pressure. Amer. Assoc. Petrol Geol. Bull. 59, 957-973.

BRADLEY, J.S. 1985: Safe disposal of toxic and radioactive liquid wastes. Geology. 13/ May 1985, 328-329.

BREDEHOEFT, J.D. 1967: Response of well-aquifer systems to earth tides. J. of Geophysical Research. 72/12, 3075-3086.

BREDEHOEFT, J.D., HANSHAW, B.B. 1968: On tha maintanance of anomalous fluid pressures: I. Thick sedimentary sequences. Geol. Soc. Amer. Bull. 79, 1097-1106.

BREDEHOEFT, J.D. & COOLEY, R.L. 1983: Comment on "A note on the meaning of storage coefficient" by NARASIMHAN, T.N. & KANEHIRO, B.Y. 1980. Water Resour. Res. 19/6, 1632-1634.

BREDEHOEFT, J.D., WESLEY, J.B. & FOUCH, T.D. 1994: Simulation of the origin of fluid pressure, fracture generation, and the movement of fluids in the Uinta Basin, Utah. Amer. Assoc. Petrol. Geol. Bull. 78, 1729-1747.

BROMHEAD, E.N., DIXON, N. 1984: Pore-water pressure observations in the coastal clay cliffs at the Isle of Sheppey, England. Proceedings, 4th Int. Symp. on Landslides, Toronto. 1, 385-390.

BURGER, A., RECORDON, E., BOVET, D., COTTON, L. SAUGY, B. 1984: Thermique des nappes souterraines. Presses polytechniques romandes, Lausanne.

CARLSLAW, H.S., JAEGER, J.C. 1959: Conduction of Heat in Solids. Oxford Univarsity Press (2nd edition), London.

CLARK, S.P., JAEGER, E. 1969: Denudation rates in the Alps from geochronologic and heat flow data. Am. J. Sci. 267, 1143-1160.

CLOETINGH, S., VAN WEES, J.D., VAN DER BEEK, P.A. & SPADINI, G. 1995: Role of pre-rift rheology in kinematics of extensional basin formation: constraints from thermomechanical models of Mediterranean and intracratonic basins. Marina and Petrol. Geology, 12/8, 793-807.

CRYER, C.W. 1983: A comparison of the three-dimensional consolidation theorias of Biot and Terzaghi. Quart. J. Mech. and Appl. Math. XVI/4, 401-412.

CORBET, T.F. & BETHKE, C.M. 1992: Disequilibrium fluid pressures and groundwater flow in the Western Canada Sedimentary Basin. J. Geophys. Res. 97/B5, 7203-7217.

DEJU, R. A. 1973: A worldwide look at the occurrences of high formation pressure in petroliferous basins. Special publication of Gulf R&D Co., Pittsburgh.

DELANAY, P.T. 1982: Rapid intrusion of magma into wet rock: Groundwater flow due to pore pressure increases. J. Geophys. Res., 87/B9, 7739-7756.

DEMING, D. 1994: Factors necessary to define a pressure seal. Amer. Assoc. Petrol. Geol. Bull. 78/6, 1005-1009.

DE MARSILY, G. 1986: Quantitative hydrogeology. Groundwater hydrology for engineers. Chapter 8.6: Other (one-dimensional) solutions to the diffusion equation. Academic Press Inc., London/San Diego.

DETOURNAY, E., CHENG, A. H-D. 1988: Poroelastic response of a borehole in a non-hydrostatic stress field. Int. J. Rock. Mech. Min. Sci. & Geomech. Abstr. 25/3, 171-182.

DIAMOND, L.W. & MARSHALL, D.D. 1994: Fluid inclusions in vein samples from boreholes at Wellenberg, Switzerland. Unpubl. Nagra Internal Report Nagra, Wettingen.

DICK, K.A., GRAF, H.R., MÜLLER, B.U., HARTMANN, P. & SCHLÜCHTER, C. 1996: Das nordalpine Wasserschloss und seine eiszeitgeologische Umgebung. Eclogae, geol. Helv. 89/1, 635-645.

DICKEY, P. A., COX, W.C. 1977: Oil and gas in reservoirs with subnormal pressures. Amer. Assoc. Petrol. Geol. Bull. 61, 1539-1547.

DOMENICO, P.A. & PALCIAUSKAS, V.V. 1979: Thermal expansion of fluids and fracture initiation in compacting sediments. Geol. Soc. Amer. Bull. 90/I, 953-979.

DOMENICO, P.A. & SCHWARTZ, F.W. 1990: Physical and Chemical Hydrogeology. Chapter 8: Ground water in the Earth's Crust. John Wiley & Sons, New York.

EHRMINGER, B., JOHNS, R.T., VOBORNY, O. 1995: Hydrogeology of the Lägern-Weinland region of Northern Switzerland. Unpubl. Nagra Internal Report Nagra, Wettingen.

EINSTEIN, H.H. 1993: Significance of geomechanics in relation to radioactive waste repositories. Unpubl. Hand-out document to Nagra.

ENGELDER, T. 1993: Stress regimes in the lithosphere. Princeton Univ. Press, Princeton.

ENGLAND, L.A., FREEZE, R.A. 1988: Finite-Element Simulation of long-term transient regional ground-water flow. Groundw. 26/3, 298-308.

ERLOUGHER, R.C. 1977: Advances in well test analysis. Soc. of Petrol Eng. Monograph. 5, Dallas, Texas.

FENELLI, G.W., PICARELLI, L. 1990: The pore pressure field built up in a rapidly eroded soil mass (Note). Can. Geotech. J. 27, 387-392.

FERTL, W.H., CHAPMAN, R.E., HOTZ, R.F. (eds.) 1994: Studies in abnormal pressures. Elsevier, Amsterdam, The Netherlands, 472p.

FINSTERLE, S., MISHRA, S., VINARD, P. & VOMVORIS, S. 1992: Wellenberg: Regional gas depletion model - one-dimensional scoping calculations. Unpubl. Nagra Internal Report Nagra, Wettingen.

FINSTERLE, S. 1992: Wellenberg - One-dimensional stress-release model assuming two-phase flow conditions. Unpubl. Nagra Internal Report Nagra, Wettingen.

GIBSON, R.E. 1958: The progress of consolidation in a clay layer increasing in thickness with time. Géotechnique. 8. 171-182.

GIBSON, R.E., LO, K.Y. 1961: A theory of consolidation for soils exhibiting secondary compression. Pub. 41. 16. Norway Geotech. Inst., Oslo.

GIBSON, R.E., ENGLAND, G.L., HUSSEV, M.J.L. 1967: The theory of one-dimensional consolidation of saturated clays. Géotechnique. 17, 261-273.

GOY, L., FABRE, D., MENARD, G. 1996: Modelling of rock temperatures for deep alpine tunnel projects. Rock Mech. Rock Engng. 29/1, 1-18.

GREEN, D.H., WANG, H.F. 1986: Fluid pressure response to undrained compression in saturated sedimentary rock. Geophysics. 51/4, 948-956.

GRETENER, P.E. 1979: Pore pressure: Fundamentals, general ramifications and implications for structural geology. Educ. Course Note Ser. emer. Assoc. Petrol. Geol. 4.

GRETENER, P.E. 1993: Course Notes. Unpubl. Document. University of Calgary, Calgary, Alberta.

GRETENER, P.E. 1969: Fluid pressure in porous media - Its importance in geology: A review. Bull. of Canad. Petrol. Geology. 17/3, 255-295.

GRETENER, P.E., ZENG-MO, F. 1985: Three decades of geopressures - Insights and Enigmas. Bull. Ver. Schweiz. Petroleum-Geol. 51/120, 1-34.

GRINGARTEN, A.C. 1982: Interpretation of tests in fissured reservoirs and multilayered reservoirs with double porosity behavior: Theory and Practice. Soc. of Petrol. Eng. SPE Int. Petrol. Techn. Symp., Bejing, March 18-26.

GUBLER, E. 1991: Recent crustal movements in Switzerland - Vertical movements. Chap. 5: Geodynamics. In: Swiss Geodetic Commission (eds.): Report on the Geodetic activities in the years 1987 to 1991. SGC Rep., Zürich, presented to the XX General Assembly of the International Union of Geodesy and Geophysics in Vienna, August 1991.

GUDMUNDSSON, G.H. 1994: An order-of-magnitude estimate of the current uplift-rates in Switzerland caused by the Würm Alpine deglaciation. Eclogea geol. Helv. 87/2, 545-557.

HAEBERLI, W. 1994: Research on permafrost and periglacial processes in mountain areas – status and perspectives. Proc. 6th Int. Conf., South China University of Technology Press, Beijing, China, 2, 1014-1018.

HAEBERLI, W. 1994: Accelerated glacier and permafrost changes in the Alps. Mountain Environments in changing climates, M. BENISTON (ed.), London, 91-107.

HANSHAW, B.B., BREDEHOEFT, J.D. 1968: On the maintenance of anomalous fluid pressures: II. Source layer at depth. Geol. Soc. Amer. Bull. 79, 1107-1122.

HANTKE, R. 1961: Tektonik der helvetischen Kalkalpen zwischen Obwalden und dem St. Galler Rheintal. Vjschr. natf. Ges. Zürich 106/1.

HANTKE, R. 1980: Eiszeitalter. Band 2: Die jüngste Erdgeschichte der Schweiz und ihrer Nachbargebiete – Letzte Warmzeiten, Würm-Eiszeit, Eisabbau und Nacheiszeit der Alpen-Nordseite vom Rhein- zum Rhone-System. Ott Verlag AG, Thun.

HANTUSH, M.S. 1964: Hydraulics of wells. Proc. Amer. Soc. Civil Eng., 281-433.

HAXBY, W.F., TURCOTTE, D.L. 1976: Stresses induced by the addition or removal of overburden and associated thermal effects. Geology, 181-184.

HERB, R. 1988: Eozäne Paläogeographie und Paläotektonik des Helvetikums. Eclogae geol. Helv. 81/3, 611-657.

HERBERT, A. W., JACKSON, C.P., LEVER, D.A. 1988: Coupled groundwater flow and solute transport with fluid density strongly dependent upon concentration. Water Resour. Res. 24/10, 1781-1795.

HETTKAMP, TH. & RUMMEL, F. 1996: WLB: Erstellung eines Materialgesetzes zum Deformationsverhalten des Wirtgesteins am Standort Wellenberg. Unpubl. Nagra Internal Report Nagra, Wettingen.

HIBBIT, KARLSSON, SORENSEN (1995): ABAQUS textbook

HORSEMAN, S.T., ALEXANDER, J., HOLMES, D.C. 1991: Implications of long-term transient flow, coupled flow and borehole effects on hydrogeological testing in the Opalinus clay: Preliminary study with scoping calculations. Nagra Tech. Report NTB 91-16, Nagra, Wettingen.

HORSEMAN, S.T., HIGGO, J.J.W., ALEXANDER, J. & HARRINGTON, J.F. 1996: Water, Gas and Soluta Movement Through Argillaceous Media. Nuclear Energy Agency, NEA - OECD eds., Paris.

HORSEMAN, S.T. (1997): Possible role of interfacial phenomena in the underpressuring of the Valanginian Marl, Wellenberg, Switzerland. Unpubl. Draft report (Fluid Processes Series), Nagra, Wettingen.

HOTTMAN, C.E., SMITH, J.H., PURCELL, W.R. 1979: Relationship among Earth stresses, pore pressure, and drilling problems offshore Gulf of Alaska. J. of Petrol. Tech. Nov. 1979, 1477-1484.

HUANG, S.L., SPECK, R.C., WANG, Z. 1995: The temperature effect on swelling of shales under cyclic wetting and drying. Int. J. Rock. Mech. Min. Sci. & Geomech. Abstr. 32, 227-236.

HUBBERT, M.K. 1940: The theory of ground water motion. J. Geol. 40, 745-944.

HUBBERT, M.K., RUBEY, W.W. 1959: Role of fluid pressure in mechanics of overthrust faulting. I. Mechanics of fluid-filled porous solids and its application to overthrust faulting. Geol. Soc. Am. Bull. 70/2, 115-166.

HUBER, M. & HUBER, A. 1994a: WLB: Strukturgeologische Synthese und tektonisches Modell. Unpubl. Nagra Internal Report Nagra, Wettingen.

HUECKEL, T., TUTUMLUER, E. 1994: Modeling of elastic anisotropy due to one-dimensional plastic consolidation of clays. Comp. and Geotech. 16, 311-349.

HUNT, J.M. 1990: Generation and migration of petroleum from abnormally pressured fluid compartments. Amer. Assoc. Petrol. Geol. Bull. 74/1, 1-12.

HÜRLIMANN, W., JOB, D., SIEBER, Ch. 1990: Modellierung der Grundwasserströmungsverhältnisse am Wellenberg. Nagra Technical Report, NTB 87-18, Nagra, Baden.

JACOB, C.E. 1940: On the flow of water in an elastic aquifer. Eos Trans. AGU, 2, 574-586.

JÄCKLI, H. 1958: Der rezente Abtrag der Alpen im Spiegel der Vorlandsedimentation. Eclogae geol. Helv. 51/2, 354-365.

JAEGER, J.C., COOK, N.G.W. 1979: Fundamentals of Rock Mechanics. Chapman and Hall (3rd edition), London & New York.

JAQUET, O., VINARD, P. 1993: Geostatistics for improved geological confinement. Geoconfine 93, Amould, Barrès & Côme (eds.), Balkema, Rotterdam.

JAQUET, O., JEANNIN, P.-Y. 1994: Modelling the karstic medium: a geostatistical approach. M. Armstrong & P.A. Dowd (Eds.), Geostetistical simulations, 185-198, Kluwer Acad. Publ., London.

JAQUET, O., LANYON, B., MARSCHALL, P. & TAUZIN, E. 1997: The K-Model Wellenberg - A geostatistical model of the host rock hydraulic conductivity. Unpubl. Nagra Internal Report Nagra, Wettingen.

JAQUET, O., SCHINDLER, M., VOBORNY, O., VINARD, P. 1997: Modelling of groundwater flow at the Wellenberg Site using Monte Carlo simulations. Proc. 21st Int. Symp. Scientif. Basis for Nucl. Waste Manag. Sept. 28 - Oct. 3, Davos.

JEANRICHARD, F. 1972: Contribution à l'étude du mouvement vertical des Alpes. Boll. di Geodesia e Scienze Affini 31, 17-40.

JIAO, J.J., ZHENG, C., HENNET, R.J.-C. 1997: Analysis of underpressured reservoirs for waste disposal. Hydrogeol. J. 5/3, 19-31.

KAELIN, B., RYBACH, L. and KEMPTER, E.H.K. 1992: Rates of depostion, uplift and erosion in the Swiss Molasse basin, estimated from sonic - and density logs. Bull. Swiss. Assoc. of Petroleum Geol. And Eng. 58/133.

KEMPTER, E.H.K. 1991: Drucksiegel und abnormale Porendrücke in Weiach. Unpublished Aktennotiz.

KENNEDY, K.G. & DAVIDSON, L.M. 1989: Oberbauenstock (OBS) 1987: Results of the hydrogeological testing program OBS-1. Nagra Tech. Report NTB 88-03. Nagra, Wettingen.

KEMENY, J.M. 1991: A model of non-linear rock deformation under compression due to subcritical crack growth. Int. J. Rock Mech. Min Sci. Geomech. Abstr. 28, 459-467.

KIRALY, L. 1994: Groundwater flow in fractured rocks - Models and reality. Int. Proc. 14 th Min. Trop. Seminar. "Interpretationsmethodologie in Exploration und Produktion." Arnsberg-Meheim, 3-6.5.94, Ruhr Uni. Bochum, 195/1-195/21.

KLEMENZ, W. 1992: Wellenberg, Überblick über die hydrogeologischen Verhältnisse. Unpubl. Memorandum, Colenco Inc.

KLEMENZ, W. 1993: Erosionsszenarien Wellenberg. Nagra Tech. Report NTB 93-34. Nagra, Wettingen.

KLEMENZ, W. 1995: Quartäre Entwicklung des Standortes Wellenberg. Unpubl. Nagra Internal Report Nagra, Wettingen.

KLEMENZ, W. 1996: Differentielle Erosion im Gebiet Wellenberg. Unpubl. Colenco Memorandum, Baden.

KONIETZKY, H. 1996: WLB: Felsmechanische Modellierung. Unpubl. Nagra Internal Report Nagra, Wettingen.

KOPPULA, S.D., MORGENSTERN, N.R. 1984: Deficient pore pressures in an eroding soil mass. Can. Geotech. J. 21, 277-288.

KUHLMANN, U. 1992/1994: Inverse Modellierung in geklüfteten Grundwasserträgern. VAW-Mittailungen Nr. 120, ETHZ, Zurich and Nagra Tech. Report NTB 93-19. Nagra, Wettingen.

KUHLMANN, U. 1995: CASA - Calibration and Sensitivity Analysis in steady state and transient groundwater flow. Unpubl. Nagra Internal Report Nagra, Wettingen.

LAMBE, T.W., WITTMAN, R.V. 1979: Soil Mechanics, SI Version. John Wiley & Sons Inc.

LAVANCHY, J.M. & MARSCHALL, P. 1997: WLB: Hydrogeological interpretation of the Wellenberg borehole data (SB1, SB2, SB3, SB4, SB6, SB4a/v and SB4a/s). Unpubl. Nagra Internal Report Nagra, Wettingen.

LAW, B.E., NUCCIO, V.F., STANTON, R.W. 1989: Evaluation of source-rock characteristics, thermal maturation and pressure history, of the Upper Cretaceous Cameo Coal Zone, Deep Seam Well, Piceance Basin, Colorado. Proc. of the 1989 Coalbed Methane Symp. Univ. of Alabama, Tuscaloosa, 341-353.

LEFTWICH, J.T., ENGELDER, T. 1994: The characteristics of geopressure profiles in the Gulf of Mexico basin. "Basin Compartments and Seals, P.J. Ortoleva, ed., AAPG Memoir 61, Chap. 8, 119-129.

LIU, L., ZOBACK, M.D. 1992: The effect of topography on the state of stress in the crust: application to the site of the Cajon Pass scientific drilling project. J. of Geoph. Res. 97/b4, 5095-5108.

LÖW, S., GUYONNET, D. LAVANCHY, J.-M., VOBORNY, O. and VINARD, P. 1994: From field measurements to effective hydraulic properties of a fractured aquitard - A case study. Proc. Of the IAHR Symp. on Transp. and React. Proc. in Aquif., Dracos & Stauffer (eds.), A.A Balkema Rotterdam.

LUCKNER, L., VAN GENUCHTEN, M. Th., NIELSEN, D.R. 1989: A consistent set of parametric models for the two-phase flow of immiscible fluids in the subsurface. Water Resources Research, 25/10, 2187-2193.

MAGARA, K. 1981: Discussion of "Patterns of dynamic pressure increment of formation-fluid in large drainage basins, exemplified by the Red Earth Region, Alberta, Canada" by J. Tóth. Bull. of Canad. Petrol. Geol. 29/1, 134-142.

MARINE, I.W., FRITZ, S.J. 1981: Osmotic model to explain anomalous hydraulic heads. Water Resourc. Research. 17/1, 73-82.

MARSCHALL, P., VOMVORIS, S., JAQUET, O., LANYON, G.W., VINARD, P. 1997: The Wellenberg K-Model: A Geostatistical Descritption of Hydraulic Conductivity Distribution in the Host Rock for Site Characterization and Performance Assessment Purposes. Proc. 21st Int. Symp. Scientif. Basis for Nucl. Waste Manag. Sept. 28 - Oct. 3, Davos.

MAZUREK, M. M., WABER, H.N. & BLÄSI, H.-R. (eds.) (BALLENTINE, C.J., DIAMOND, L.W., EICHINGER, L., GAUTSCHI, A. & MARSHALL, D.D.) 1994: Geology, mineralogy and geochemistry of the Wellenberg. Unpubl. Nagra Internal Report Nagra, Wettingen.

MAZUREK, M. 1997: GDS II: WLB - Geologische Eigenschaften der wasserführenden Systeme. Unpubl. Nagra internal report. Nagra, Wettingen.

MEANS, W.D. 1976: Stress and Strain - Basic Concepts of Continuum Mechanics for Geologists. Springer Verlag, New York.

MILNES, A.G. & PFIFFNER, O.A. 1980: Tectonic evolution of the Central Alps in the cross section St. Gallen-Como. Eclogae Geol. Helv. 73/2, 619-633.

MICHEL, J.P., FAIRBRIDGE, R.W. 1980: Dictionary of Earth-Science, English-French, French-English. Masson publ. USA, New York.

MISHRA, S., PARTL, Q., SCHINDLER, M. & HÜRLIMANN, W. 1993a: Modelling gas-water flow at Oberbauenstock. Nagra Tech. Report NTB 93-35. Nagra, Wettingen.

MISHRA, S., VINARD, P., SCHRÖDER, U., JAQUET, O. & HÜRLIMANN, W. 1993b: WLB - 3-D Pilot-model, A simplified sub-regional groundwater flow model of the Wellenberg Region. Unpubl. Nagra Internal Report Nagra, Wettingen.

MOUCHET, J.P. & MITCHELL, A. 1989: Abnormal pressures while drilling. Origins – prediction – detection – evaluation. Elf Aquitaine Manuals Techniques 2, Boussens, France.

MÜLLER, B., ZOBACK, M.L., FUCHS, K., AMSTIN, L., GREGERSEN, S., PAVONI, N., STEPHANSSON, O. & LJUNGGREN, C. 1992: Regional patterns of tectonic stress in Europe. In: UNIVERSITÄT KARLSRUHE (ed.) 1992: Spannung und Spannungsumwandlung in der Lithosphäre (p. 725-767). Berbd. Sonder-forsch.bereich 108 für die Jahre 1990 - 1992 (Teil B) u. J. geophys. Res.

MULLIS, J. 1996: Fluideinschluss-Untersuchungen in Ankerit, Calcit und Quarz der Sondierbohrung SB4 am Wellenberg. Unpubl. Nagra Interner Ber. Nagra, Wettingen.

NAGRA 1988: Berichterstattung über die Untersuchungen der Phase I am potentiellen Standort Oberbauenstock (Gemeinde Bauer, UR). Nagra Technical Report, NTB 88-18, Baden.

NAGRA 1993a: Untersuchungen zur Standorteignung im Hinblick auf die Endlagerung schwach- und mittelaktiver Abfälle – Geologische Grundlagen und Datensatz zur Beurteilung der Langzeitsicherheit des Endlagers für schwach- und mittelaktive Abfälle am Standort Wellenberg (Gemeinde Wolfenschiessen, NW). Nagra Tech. Report NTB 93-28. Nagra, Wettingen.

NAGRA 1993b: Recherche sur l'aptitude des sites à accueillir un dépôt final de déchets faiblement et moyennement radioactifs à vie courte. Résultats des recherches effectuées sur le site potentiel du Bois de la Glaive (Commune d'Ollon, VD). Nagra Tech. Report NTB 93-29.

NAGRA 1996: Endlager für schwach- und mittelaktive Abfälle (Endlager SMA) – Zwischenbericht über die Untersuchungen 1994/95 am Standort Wellenberg (Gemeinde Wolfenschiessen, NW). Nagra Tech. Report NTB 96-03. Nagra, Wettingen.

NAGRA 1997: Geosynthese Wellenberg 1996 - Ergebnisse der Untersuchungsphasen I und II. Nagra Tech. Report NTB 96-01. Nagra, Wettingen.

NARASIMHAN, T.N. & WITHERSPOON, P.A. 1977: Numerical model for saturated - unsaturated flow in deformable porous media. I. Theory. Water. Resour. Res. 13, 657-664.

NARASIMHAN, T.N. & KANEHIRO, B.Y. 1980: A note on the meaning of storage coefficient. Water Resour. Res. 18/2, 423-429.

NEUMAN, S.P., WITHERSPOON, P.A. 1969: Theory of flow in a confined two aquifer system. Water. Resour. Res. 5/4, 803-816.

NEUZIL, C.E. 1985: Comment on "Possible Effects of Erosional Changes of the Topographic Relief on Pore Pressures at Depth" by J. Tóth and R.F. Miller. Water Resour. Res. 21/6, 895-898.

NEUZIL, C.E. 1986: Groundwater flow in low-permeability environments. Water resourc. Research. 22/8, 1163-1195.

NEUZIL, C.E. 1993: Low fluid pressure within the Pierre Shale: A transient response to erosion. Water Resour. Res. 29/7, 2007-2020.

NEUZIL, C.E. 1994: How permeable are clays and shales? Water Resour. Res. 30/2, 145-150.

NEUZIL, C.E. 1995: Abnormal pressures as hydrodynamic phenomena. Amer. J. of Science 295, 742-786.

NEUZIL, C.E. & POLLOCK, D.W. 1983: Erosional unloading and fluid pressures in hydraulically "tight" rocks. J. Geol. 91/2, 179-193.

OLSON, R.E. 1970: Mechanisms controlling compressibility of clays. J. of soil. Mech. and found. Division. 96/SM6, 1863-1878.

OLSON, R.E. 1977: Consolidation under time dependent loading. J. Geotech. Eng. Div., ASCE 103/GT1, 55-60.

ORR, E.D., KREITLER, C.W. 1985: Interpretation of pressure-depth data from confined underpressured aquifers exemplified by the Deep-Basin Brine aquifer, Palo Duro Basin, Texas. Water Resour. Res., 21, 533-544.

PALCIAUSKAS, V.V. & DOMENICO, P.A. 1979: Thermal expansion of fluids and fracture initiation in compacting sediments: Summary. Geol. Soc. Amer. Bull, Part I. 90, 518-520.

PALCIAUSKAS, V.V. & DOMENICO, P.A. 1982: Characterization of drained and undrained response of thermally loaded repository rocks. Water Resour. Res. 18/2, 281-290.

PALCIAUSKAS, V.V. & DOMENICO, P.A. 1989: Fluid pressures in deforming porous rocks. Water Resour. Res. 25/2, 203-213.

PARKS, K.P. & TÓTH, J. 1995: Field evidence for erosion-induced underpressuring in Upper Cretaceous and Tertiary strata, West Central Alberta Canada. Bull. Canad. Petrol. Geol. 43/3, 281-292.

PASQUIER, F. 1996: WLB: Interpretation of the long-term monitoring data from the Wellenberg boreholes SB1 to SB6 (1990-1995): Estimation of the steady state hydraulic heads and analysis of pressure fluctuations. Unpubl. Nagra Internal Report Nagra, Wettingen.

PAUL, A., BERGER, W.H. 1997: Modellierung der Eiszeiten: Klimazyklen und Klimaübergänge. Geowiss. 15/1, 20-27.

PEARSON, F.J. Jr. 1996: Ruminations on porosity and salinity in WLB marl. Unpubl. PSI Aktennotiz. Paul Scherrer Inst., Villigen.

PEARSON, F.J. Jr. 1997: What is the porosity of a mudrock ? In: APLIN, A.C., FLEET, A. and MACQUAKER, J. (eds.): Proceedings of a meeting on mudrocks at the basin scale: Properties, controls and behaviour. Geol. Soc. Special Publ. London.

PERRODON, A. 1983: Dynamics of oil and gas accumulations. Bull. des centres rech. Exploration-production, Elf-Aquitaine, Mem. 5, Pau, France.

PFIFFNER, O.A., SAHLI, S. & STÄUBLE, M. 1996: Compression and uplift of the external massifs in the Helvetic zone. In: PFIFFNER, O.A. et al.: Deep structure of the Swiss Alps (NRP 20). Birkhäuser Verl., Basel.

POWLEY, D.E. 1984: Pressures, normal and abnormal: AAPG Advanced Exploration Schools Unpubl. Lecture Notes (cited by Hunt 1990).

PRUESS, K. 1990: Numerical modeling of gas migration at a potential repository for low and intermediate level nuclear wastes at Oberbauenstock, Switzerland. Nagra Tech. Report NTB 89-28. Nagra, Wettingen.

PRUESS, K. 1991: TOUGH2 - a general-purpose numerical simulator for multiphase fluid and heat flow. Lawrence Berkeley National Laboratory-Report 29400.

RECORDON, E. 1986: Dynamique des eaux souterraines. Cours postgrade. Ecole polytechnique fédérale de Lausanne.

RICE, J.R., CLEARY, M.P. 1976: Some basic stress diffusion solutions for fluid saturated elastic porous media with compressible constituents. Rev. Geophys. And Space Phys., 14/2, 227-241.

RIVERA, A. & SENGER, R. 1993: WLB: Preliminary assessment of the observed underpressuring on the transient hydraulic regime. Unpubl. Nagra Internal Report Nagra, Wettingen.

SCHAER, J.-P., JEANRICHARD, F. 1974: Mouvements verticaux anciens et actuels dans les Alpes suisses. Eclogae geol. Helv. 67/1, 101-119.

SCHRÖDER, U., VOBORNY, O., SCHINDLER, M., VINARD, P. 1994: Projekt HYDROMOD: Aufbau des Standortmodells WLB, Vorgehen und Erfahrungen. Unpubl. Nagra Internal Report Nagra, Wettingen.

SCHLÜCHTER, CH. 1995: Wellenberg SB6: Quartärgeologie, Landschaftsgeschichte und Erosionsszenarien. Unpubl. Nagra Internal Report Nagra, Wettingen.

SCHLÜCHTER, CH. & RÖTHLISBERGER, CH. 1995: Gletscher im ständigen Wandel. Jubiläums-Symposium der Schweizerischen Gletscherkommission 1993 in Verbier (VS). "100 Jahre Gletscherkommission – 100'000 Jahre Gletschergeschichte". VDF Hochschulverlag AG an der ETH Zürich.

SCHLÜCHTER, CH. & MÜLLER-DICK, K.A. 1996: Das Eiszeitalter in der Schweiz - Eine schematische Zusammenfassung. Publ. des Geol. Inst. Univ. Bern, Komm. f. Quartärforsch. der Schweiz, Akademie der Naturwiss. u. IGCP-378, Hrsg. Stiftung Landschaft u. Kies, Ostermundigen.

SENGER, R.K., FOGG, G.E., KREITLER, C.W. 1987: Effects of hydrostratigraphy and basin development on hydrodynamics of the Palo Duro Basin, Texas, Appendix B. Bureau of Economic Geology, Report of Investigations No. 165, Univ. of Texas, Austin, USA.

SENGER, R.K., FOGG, G.E. 1987: Regional underpressuring in deep brine aquifers, Palo Duro Basin, Texas. 1. Effects of hydrostratigraphy and topography. Water Res. Research. 23/8, 1481-1493.

SENGER, R.K. 1993: Paleohydrology of variable-density ground-water flow systems in mature sedimentary basins: example of the Palo Duro basin, Texas, USA. J. of. Hydrol. 151, 109-145.

SENGER, R.K. 1997: WLB - Study of the effects of erosional decompaction under double-porosity two-phase flow conditions. Unpubl. Nagra Internal Report Nagra, Wettingen.

SHAO, J.F. 1997: A numerical solution for a thermo-hydro-mechanical coupling problem with heat convection. Int. J. Rock Mech. Min. Sci. 34/1, 163-166.

SHARP, J.M. 1983: Permeability controls on aquathermal pressuring. Am. Assoc. Of Petrol Geol. Bull. 67/11, 2057-2061.

SHARP, J.M., DOMENICO, P.A. 1976: Energy transport in thick sequences of compacting sediment (technical note). Geol. soc. of America Bull. Vol. 87, 390-400.

SMITH, J.E. 1971: The dynamics of shale compaction and evolution of pore-fluid pressures. Math. Geology. 3/3, 239-263.

SNOW, D.T. 1968: Rock fracture spacings, openings and porosities. J. Soil Mech. Found. Div. amer. Soc. Civ. Eng. 94 (SM1), 73-91.

SOLER, J.M., PERSON, F.J. 1997: Possible osmotic effects on Wellenberg underpressure. Unpubl. Aktennotiz, Paul Scherrer Institute, Switzerland.

SPECK, C.K. 1994: Änderungen des Grundwasserregimes unter dem Einfluss von Gletschern und Permafrost. VAW Mitteilungen Nr. 134. ETHZ, Zurich.

SPECK, C.K. 1995: Hydrothermisches Regime im Schweizer Mittelland während der Würm-Eiszeit. Geowissenschaften 13/1.

TACHER, L. 1994: Geological site model Wellenberg. Unpubl. Nagra Internal Report Nagra, Wettingen.

TACHER, L., PARRIAUX, A., VINARD, P. 1994: New geological infographic methods applied to civil engineering: Application to the nuclear waste underground disposal at Wellenberg (Switzerland). Proc. 7th int. Congress Int. Assoc. of Engineer. Geol., Balkema, Rotterdam.

TACHER, L., MAYORAZ, R. 1994: Geologische 3-D-Modellierung, Anwendung im Untertagebau. Schweiz. Ing. und Archit.

TERZAGHI, K. 1943: Theoretical soil mechanics. J. Wiley, New York.

TERZAGHI, K., FRÖHLICH, R.B. 1936: Theorie der Setzung von Tonschichten. Deuticke, Leipzig.

TIMOSHENKO, S.P., GOODIER, J.N. 1970: Theory of Elasticity, 3rd edition. McGraw-Hill.

TÓTH, J. 1963: A theroretical analysis of groundwater flow in small drainage basins. J. Geoph. Res. 68/16, 4795-4812.

TÓTH, J. 1979a: Pattems of dynamic pressure increment of formation-fluid flow in large drainage basins, exemplified by the Red Earth Region, Alberta, Canada. Bull. of Canad. Petrol. Geology, 27/1, 63-83.

TÓTH, J. 1979b: Cross-formational gravity-flow of groundwater: a mechanism of the transport and accumulation of petroleum (the generalized hydraulic theory of petroleum migration). Am. Assoc. Petrol. Geol. Bull., 121-167.

TÓTH, J. 1990: Hydraulic continuity in large sedimentary basins. Int. Conf. on Groundwater in Large Sedimentary Basins, Perth 1990.

TÓTH, J. 1990: Anomalous pore pressures as indicators of transient subsurface flow conditions, exemplified by the Alberta Basin, Western Canada. Memoires of tha 22nd Congress of IAH. XXII, Part 1, 730.

TÓTH, J. & MILLAR, R.F. 1983: Possible effects of erosional changes of the topographic ralief on pore pressures at depth. Water Rasour. Res. 19/6, 1585-1597.

TÓTH, J. & CORBET, T. 1986: Post-paleocene evolution of regional groundwater flow-systems and their relation to petroleum accumulations, Taber area, Southern Alberta, Canada. Bull. Canad. Petrol. Geol. 34/3, 339-363.

TÓTH, J. MACCAGNO, M.D., OTTO, C.J. ROSTRON, B. 1991: Generation and migration of petroleum from abnormally pressured fluid compartments: discussion. Amer. Assoc. Petro. Geol. Bull. 75/2, 331-335.

TRÜMPY, R. 1980: Geology of Switzerland – a guide book. Part A: An Outline of the Geology of Switzerland. Wepf & Co., Basel/New York, 104 pp.

VAUGHAN, P.R., WALBANCKE, H.J. 1973: Pore pressure changes and the delayed failure of cutting slopes in overconsolidated clay. Géotechnique 23/4, 531-539.

VERRUIJT, A. 1969: Elastic storage of aquifers. Flow through porous media, DE WIEST, R.J.M., Ed., 331-376.

VINARD, P. 1997: A comprehensive hydrodynamic modelling approach for the hydrogeological site characterisation and for deriving input to performance assessment. Proc. 21st Int. Symp. Scientif. Basis for Nucl. Waste Manag. Sept. 28 - Oct. 3, Davos.

VINARD, P. 1996: Evaluation of the impact of glaciation and erosion on the hydraulic pressure distribution in a tight marl-shale formation at Wellenberg, Central Switzerland. Workshop proceedings "Glaciation and Hydrogeology". SKI Report 97:13, A80-A81.

VINARD, P. 1998: WLB – Generation and evolution of hydraulic underpressures in the host rock (Pafris formation and tertiary shales). Unpubl. Nagra Internal Report Nagra, Wettingen.

VINARD, P., WILSON, W. 1994: Hydrogeologisches konzeptionelles Modell WLB, 1993. Vollständig Tabelle der Hypothesen. Unpubl. Nagra Internal Report Nagra, Wettingen.

VINARD, P., BLÜMLING, P., McCORD, J.P., ARISTORENAS, G. 1993: Evaluation of hydraulic underpressures at Wellenberg, Switzerland. Int. J. Rock. Mech. Min. Sic. & Geomech. Abstr. 30/7, 1143-1150.

VINARD, P. & McCORD, J.P. (eds.) 1991: Factors possibly affecting formation static pressure estimates at Wellenberg. Unpubl. Nagra Internal Report Nagra, Wettingen.

VINARD, P. (ed.) & McCORD, J.P. (Compilation) 1994: WLB: Compilation and critique of the external review committee comments and recommendations on NIB 91-34. Unpubl. Nagra Internal Report Nagra, Wettingen.

VINARD, P. & LAVANCHY, J.-M. 1994: WLB: Final results of the hydraulic testing Phase 1 and hydrogeological synthesis of the borehole data. Unpubl. Nagra Internal Report Nagra, Wettingen.

VOBORNY, O., SCHINDLER, M., JAQUET, O. & VINARD, P. 1997: WLB: Modellierung der grossräumigen Grundwasserströmungen basierend auf geostatistischer Modellierung des Wirtgesteins. Unpubl. Nagra Internal Report Nagra, Wettingen.

VOMVORIS, S., PEARSON, F.J. Jr., WABER, N., SCHOLTIS, A., VOBORNY, O., SCHINDLER, M., VINARD, P. & KUHLMANN, U. 1995: WLB: Geodatensatz-II prov.: Consistency of hydrochemical data and results of hydrodynamic modeling. Unpubl. Nagra Internal Report Nagra, Wettingen.

VOMVORIS, S., PEARSON, F.J., WABER, N., SCHOLTIS, A., SCHINDLER, M. & VINARD, P. 1997: Consistency of results of hydrodynamic modeling and hydrochemical data. Unpubl. Nagra Internal Report Nagra, Wettingen.

ZOBACK, M.L., ZOBACK, M.D., ADAMS, J., ASSUMPCÃO, M., BELL, S., BERGMAN, E.A., BLÜMLING, P., BRERETON N.R., DENHAM, D., DING, J., FUCHS, K., GAY, N., GREGERSEN, S., GUPTA, H.K., GVISHIANI, A., JACOB, K., KLEIN, R., KNOLL, P., MAGEE, M., MERCIER, J.L., MÜLLER, B.C., PAQUIN, C., RAJENDRAN, K., STEPHANSSON, O., SUAREZ, G., SUTER, M., UDIAS, A., XU, Z.H. & ZHIZHIN, M. 1989: Global patterns of tectonic stress. Nature 341/6240, 291-298.